UNIVERSITÀ DELLA CALABRIA

UNIVERSITA' DELLA CALABRIA

Dipartimento di Fisica

Dottorato di Ricerca in

Scienze e Tecnologie Fisiche, Chimiche e dei Materiali in convenzione con il CNR

CICLO

XXXI

Chemical characterization of atmospheric aerosols from natural and anthropogenic sources in the Mediterranean area

Settore Scientifico Disciplinare

CHIM/01 - Chimica Analitica

Coordinatore: Ch.mo Prof. Vincenzo Carbone

Supervisori: Dott.ssa Francesca Sprovieri

Dott. Attilio Naccarato

Dottorando: Dott. Sacha Moretti

Alla mia Famiglia

ed alla mia "Dolce metà"

Simona

"Non preoccuparti delle tue difficoltà in matematica; posso assicurarti che le mie sono ancora maggiori."

ALBERT EINSTEIN

INDEX

Abstract (EN)

The Mediterranean Sea basin constitutes a semi-enclosed area where atmospheric particles originating from natural and anthropogenic continental sources and gas-to-particle conversion processes are present at all times. The area is, in fact, located to the south of highly populated European countries characterized by industrial, semi-industrial, and rural economies, and to the north of Africa, which includes the Sahara desert. Detailed wind trajectory analysis reported in previous research studies show that more than 60% of air masses crossing the Mediterranean originate from the north-northwest sector, containing particles emitted or derived from industrial and urban sources, whereas 13–16% of air masses coming from the Sahara region carrying predominantly mineral dust. The transport of Saharan dust occurs mostly during the spring and summer seasons and causes sporadic crustal aerosol pulses to the Mediterranean area. On the other hand, aerosol scavenging by precipitation during the rainy season (from October to May) reduces aerosol concentrations. Summer is also characterized by low inversion layers and strong sunlight conditions, causing photochemical smog. Moreover, forest fires, which occur during the summer months in the Mediterranean region and in North Africa, increase black carbon and fine particle emissions. In this frame, it is clear enough that specific meteorological conditions result in high temporal variability of aerosol concentrations. There is strong evidence on the relationship between short-term and long-term exposure to atmospheric particles, with adverse health effects. Therefore, the study on atmospheric Particulate Matter (PM) (solid or liquid particles dispersed in the atmosphere which may persist for long times to undergo transport and diffusion phenomena), and the relative chemical composition of the two particle size fractions $PM_{2.5}$, (aerodynamic diameter $\leq$ 2.5 μm) and PM_{10} (aerodynamic diameter $\leq$ 10 μm), is essential to evaluate the effect of the PM on human health and environment.

The present work of thesis developed during the Ph.D. is focused on the chemical characterization of aerosol in the Mediterranean area through a monitoring program which has foreseen a number of oceanographic campaigns performed in the Mediterranean sea onboard the CNR-research vessel in the framework of the ongoing MEDOCEANOR measurements program as well as long-term measurements carried out on-land, specifically at the high altitude GAW observatory “Monte Curcio” of the CNR-IIA (1780 m a.s.l.), located on the Sila massif, Southern Italy, and thus able to intercept long-range transport air masses and across a number of monitoring sites (i.e., coastal, urban, rural sites etc.)

distributed in the south of Italy as part of the I-AMICA regional network. The concentration of aerosol size fractions and its chemical composition performed at permanent ground-based stations as well as during oceanographic measurement campaigns have been analyzed in order to assess a spatially and temporally consistent measurement data across Mediterranean basin, and to investigate the main natural and anthropogenic sources affecting the air quality using source apportionment techniques.

The seasonal oceanographic campaigns developed along different routes in the western sector of the Mediterranean Sea basin, and aimed to study the influence of natural and anthropogenic sources of PM and associated levels of pollutants. Chemical analysis assisted by the receptor models, identified, in particular, six main sources: crustal, volcanic, biomass burning, marine spray, industrial and vehicular traffic. The carbonaceous content in the PM sampled in Monte Curcio station shows seasonal trends for Organic Carbon (OC) and Elemental Carbon (EC) in both PM size fractions. The concentrations during the warm season are higher than those observed during the cold season and the annual levels of EC and OC were lower than those observed at the other four monitoring sites as part of the regional network "I-AMICA" distributed in southern Italy (Capo Granitola, Lamezia Terme, Lecce; Naples) due to different environmental conditions (eg, coastal/marine, suburban and urban) characterizing these sampling sites compared to "Monte Curcio" remote site.

In particular, both OC and EC average concentrations were minimal at Monte Curcio and increased in the following order: remote < coastal/marine < suburban < urban (i.e., Monte Curcio < Capo Granitola < Lamezia Terme < Lecce < Naples). The Secondary Organic Carbon (SOC) was mainly present in $PM_{2.5}$ at all sites, and higher SOC/OC ratios were observed at the urban and suburban site. Indeed, the yearly average SOC in Monte Curcio station has been estimated as 52% of OC in $PM_{2.5}$ and representing, on average, the major mass contributes to $PM_{2.5}$ during the cold season. Furthermore, the receptor models used shown differences among the possible sources of carbonaceous aerosol between different seasons. The cold season was characterized by aerosol mainly coming from the long-range transport, while during the warm season it is influenced by local and regional sources.

In the following Chapters, the results have been presented and discussed.

Abstract (IT)

Il bacino del Mar Mediterraneo costituisce un'area semi-chiusa in cui sono presenti in ogni momento particelle atmosferiche provenienti da fonti continentali naturali e antropogeniche e processi di conversione gas-particella. L'area è infatti situata a sud di paesi europei altamente popolati caratterizzati da economie industriali, semi-industriali e rurali, e nel nord dell'Africa, che comprende il deserto del Sahara. Analisi dettagliate della traiettoria del vento riportate in precedenti studi di ricerca mostrano che oltre il 60% delle masse d'aria che attraversano il Mediterraneo provengono dal settore nord-nord-occidentale, contenenti particelle emesse o derivate da fonti industriali e urbane, mentre il 13-16% delle masse d'aria provenienti dalla regione del Sahara che trasporta prevalentemente polvere minerale. Il trasporto di polvere sahariana avviene soprattutto durante la primavera e l'estate e causa sporadici impulsi di aerosol crostale nell'area Mediterranea. D'altra parte, l'abbattimento tramite le precipitazioni durante la stagione delle piogge (da ottobre a maggio) riduce le concentrazioni di aerosol. L'estate è anche caratterizzata da bassi livelli di inversione e forti condizioni di luce solare che causano lo smog fotochimico. Inoltre, gli incendi boschivi, che si verificano durante i mesi estivi nella regione mediterranea e nel Nord Africa, aumentano le emissioni di "black carbon" e di particelle fini. In questo contesto, è abbastanza chiaro che specifiche condizioni meteorologiche caratteristiche dell'area Mediterranea determinano un'elevata variabilità temporale delle concentrazioni di aerosol. Esistono forti evidenze sulla relazione esistente tra l'esposizione a breve ed a lungo termine all'inquinamento dell'aerosol atmosferico e gli effetti negativi sulla salute. In particolare, lo studio del particolato atmosferico [*Particulate Matter* (PM)], ovvero un agglomerato dinamico di particelle solide o liquide disperse in atmosfera e che possono persistere per tempi sufficientemente lunghi tale da subire fenomeni di trasporto e diffusione, e la relativa composizione chimica nelle due frazioni granulometriche $PM_{2.5}$, (particolato di diametro aerodinamico $\leq 2{,}5$ µm) e PM_{10} (particolato di diametro aerodinamico ≤ 10 µm), è fondamentale per valutare gli effetti di quest'ultimo sulla salute umana, sia sul breve che sul lungo termine.

Il presente lavoro di tesi di Dottorato è incentrato sulla caratterizzazione chimica dell'aerosol nella suddetta area attraverso un programma di monitoraggio che ha previsto una serie di campagne oceanografiche eseguite nel Mediterraneo a bordo della nave di ricerca del CNR nell'ambito del programma di misurazione MEDOCEANOR. Oltre alle misurazioni in mare sono state svolte anche campagne di misure a lungo termine effettuate a terra, in particolare presso l'Osservatorio di alta quota GAW di "Monte Curcio" del CNR-IIA (1780 m slm),

situato sul massiccio della Sila, nel Sud Italia. L'Osservatorio è situato in una posizione strategica in quanto in grado di intercettare le masse d'aria di trasporto a lungo raggio; pertanto, grazie alla sua posizione ed essendo anche parte della rete regionale I-AMICA nel sud del Mediterraneo, rete che comprende siti con caratteristiche diverse (ad es. siti costieri, urbani, rurali, ecc.), è stato effettuato lo studio della distribuzione spazio-temporale del PM nell'ambito di tale network. La concentrazione delle diverse frazioni dell'aerosol e la composizione chimica correlata eseguita presso le stazioni di terra e durante campagne di misurazione oceanografica sono state analizzate al fine di valutare i dati di misurazione coerenti spazialmente e temporalmente nel bacino del Mediterraneo e per indagare le principali fonti naturali e antropogeniche che influenzano la qualità dell'aria utilizzando tecniche di ripartizione della fonte ("source apportionment").

Le campagne oceanografiche stagionali effettuate nei diversi anni hanno infatti seguito delle rotte finalizzate allo studio dell'influenza di sorgenti naturali ed antropogeniche sui livelli degli inquinanti associati al particolato atmosferico campionato nelle due frazioni $PM_{2.5}$ e PM_{10} evidenziando diverse fonti di inquinamento. L'analisi chimica, coadiuvata dai modelli a recettore hanno identificato, in particolare, sei sorgenti principali: crostale, vulcanico, biomass burning, spray marino, industriale e derivante dal traffico veicolare.

Il contenuto carbonioso nel PM campionato nella stazione di Monte Curcio mostra trend stagionali sia per il Carbonio Organico (OC) che per il Carbonio Elementare (EC) in entrambe le frazioni $PM_{2.5}$ e PM_{10}. Le concentrazioni durante la stagione calda sono superiori a quelle osservate durante la stagione fredda ed i livelli annuali di EC e OC sono risultati inferiori rispetto alle concentrazioni osservate in altri quattro siti di campionamento facenti parte della rete Regionale "I-AMICA" distribuiti nell'Italia meridionale (Capo Granitola; Lamezia Terme; Lecce; Napoli) aventi una caratterizzazione ambientale diversa dal sito remoto di Monte Curcio (es., costiero / marino; suburbano e urbano). In particolare, le concentrazioni medie di EC e OC sono risultate minime nel sito remoto (Monte Curcio) ed aumentavano nel seguente ordine: remoto < costiero / marino < suburbano < urbano (es. Monte Curcio < Capo Granitola < Lamezia Terme < Lecce < Napoli). Il Carbonio Organico Secondario (SOC), in tutti i siti, è risultato presente principalmente nel $PM_{2.5}$ ed i rapporti SOC/OC più elevati sono stati osservati nel sito urbano e in quello suburbano. In effetti, il SOC annuale medio nella stazione di Monte Curcio è stato stimato come il 52% di OC nel $PM_{2,5}$ e rappresenta, in media, la maggior parte del contributo di massa nel $PM_{2,5}$ durante la stagione fredda. Inoltre, l'utilizzo di modelli a recettore ha evidenziato differenze nelle possibili fonti di aerosol carbonioso tra le diverse stagioni. La stagione fredda è caratterizzata

da aerosol carbonioso proveniente principalmente dal trasposto a lungo raggio, mentre durante la stagione calda è influenzato da fonti locali e regionali. I risultati e la discussione degli stessi sono riportati in dettaglio nei seguenti capitoli del presente lavoro di Tesi di Dottorato.

1. Introduction

During the Ph.D. course, I had the opportunity to deal with different research projects, most of them focused on the study of the chemical composition of aerosol in the central Mediterranean area which represents the main topic of this work. As semi-closed sea, the Mediterranean has a distinct combination of climatological, meteorological, geographical and geological characteristics, all factors that influence the air quality in this region (Sprovieri and Pirrone 2008a; Sprovieri et al. 2010). The high level of industrialization and dense population around the basin provides significant effects on the Mediterranean atmosphere which consists of a mixture of anthropogenic and natural contributions thus confirming this region to be a major crossroad of different air mass transport processes. Natural emissions occur through Saharan dust outbreaks (Querol et al. 2009), geologic processes, including volcanoes and geothermal activity, as well as through biogenic, biomass burning, marine emissions (G. Pace, A. di Sarra, D. Meloni 2006), and evasion from terrestrial and aquatic surfaces (Pirrone et al. 2010) that still remain not well quantified and as yet un-estimated (Sprovieri et al. 2010). In addition, anthropogenic emission in busy shipping lanes and large port cities (Gencarelli et al. 2014), as well as highly industrialized population centers surrounding the basin itself, are important sources of pollution plumes containing a wide range of particulate and gaseous pollutants (Bencardino et al. 2011). The contributions of both anthropogenic and natural components within the Mediterranean region depend on different factors such as the relative distance between sources and receptor sites and the meteo-climatological conditions. The high levels of solar radiation observed in the Mediterranean area in combination with several factors such as small cloudiness, thermally induced recirculation near the densely populated coast and frequent high pressure situations leading to subsidence, stability and clear sky (Gencarelli et al. 2014) favor enhancement in photochemical production (Sprovieri et al. 2010) and air pollutant accumulation (Bencardino et al. 2011). One of the major questions in the scientific community is to what extent the background air pollutant concentrations are related to sources within the Mediterranean basin and how much it results from long range transport emitted outside the basin itself. Since air pollutants are released to the atmosphere from a variety of natural and anthropogenic sources, their estimates are highly uncertain, and their relative contributions vary geographically and temporally. Moreover, it is well known that the European Union reviewed its environmental policy by setting up the Directives Air Quality given particular attention to those pollutants, like aerosols, ozone, and heavy metals,

which can have a significant impact both on human health and environment. Until now a large number of studies highlighted the relation between adverse health effects with short- and long-term exposure to atmospheric pollutants of main concern as atmospheric particulate fractions (Pietrodangelo A., Bencardino M., Cecinato A., Decesari S., Perrino C., Sprovieri F. 2010). Previous works on aerosol characterization observed at a number of monitoring sites across Europe were published (Putaud et al. 2010). However, only a few of these stations are located close to the sea and they do not cover the whole Mediterranean area that seems to be a unique area with the highest aerosol optical depths in the world (Hatzianastassiou et al. 2004).

In this context, the aim of the study conducted within my Ph.D. was to: (1) quantify ambient concentrations of $PM_{2.5}$ and PM_{10} and their composition in the Mediterranean sea basin both at *off-shore* sites, during oceanographic campaigns (see the Case study 1 in the following Chapters of the Thesis), and *on-shore*, across a number of monitoring sites distributed in the Southern of Italy (see the Case study 2 and 3 in the following Chapters of the Thesis) (2) investigate the relationship between $PM_{2.5}$ and PM_{10} and their elemental composition, (3) characterize the carbonaceous content of aerosol size fractions (4) analyze the influence of meteorological conditions on PM time-series, and (5) identify major emission source areas.

Since 2000 yr, the CNR-IIA in the framework of the on-going Med-Oceanor measurements program, performs seasonal cruise campaigns, across the Mediterranean Sea (Sprovieri et al. 2003; Sprovieri and Pirrone 2008; Sprovieri et al., 2010a,b; Gencarelli et al., 2014). The herein presented study introduces new insights gained from data collected during four research cruise campaigns across the Mediterranean Sea carried out in 2011, 2012, 2015, and 2017 to achieve the reported above specific objectives of the Thesis work (Case Study 1). In the first three cruise campaigns, I was involved in the chemical analysis and data treatment of all samples collected whereas in the 2017 cruise campaign I was completely involved from the measurements performed onboard the research vessel of the CNR to the samples analysis and data treatment. This latter steps of the work were carried out also in collaboration with Professor Querol's research group during my experience in Barcelona as a visiting Ph.D. student. The analytical approach used in this work of Ph.D. thesis was based on the employ of Inductively Coupled Atomic Emission Spectrometry (ICP-AES) for major elements identification while for trace elements analysis was chosen the Inductively Coupled Plasma Mass Spectrometry (ICP-MS); both analytical techniques in the scientific community represent the best solutions among the elemental analysis. Regarding the determination of soluble ion concentrations, the ion chromatography (IC) was used. The

obtained datasets were analyzed by using different approaches and data analysis tools, as the Enrichment Factors (EFs), the factor analysis (as PCA or FA) or the hybrid receptor models (as CWT or PSCF) for a source apportionment investigation on the aerosol sampled during the monitoring campaigns.

In addition to over-water measurements, the Ph.D. work foresaw a long-term measurements campaign for carbonaceous assessment of particulate fractions at the only high altitude GAW station of the CNR-IIA, "Monte Curcio" (Case Study 2) during which I fully involved in both monitoring and data analysis and treatment. The chemical characterization of carbonaceous fraction, which is composed by organic carbon (OC) and elemental carbon (EC), was performed by the thermo-optical transmittance (TOT) method using a Sunset Laboratory OC/EC analyzer. The obtained results were compared with those obtained from the MAAP (Multi-Angle Absorption Photometer) which provides information on the equivalent Black Carbon (eBC) that is comparable with the EC concentrations. For a better aerosol characterization, and considering that the Mediterranean basin is affected by local and long-range transport of marine, desert, and anthropogenic aerosols, in the framework of the regional network "I-AMICA", simultaneous measurements for carbonaceous assessment of particulate matter have been performed across different ground-based sites (from coastal, to mountain and urban) distributed in the Southern Italy, including "Monte Curcio" observatory, to investigate long-range transport vs. local emissions in conjunction with aerosol ageing processes. In this context, I was fully involved in the sampling campaign as well as in the samples analysis and data treatment related to the "Monte Curcio" site. The results obtained were related to the climatic and geographic conditions of the studied area to identify the possible factors affecting the concentrations of carbonaceous species, and to obtain more information using different tools for source identification and apportionment, which are still missing, particularly, in the south of Italy.

2. Atmospheric particulate pollution

The study of atmospheric chemistry can be traced back to the eighteenth century when chemists such as Joseph Priestley, Antoine-Laurent Lavoisier, and Henry Cavendish attempted to determine the chemical components of the atmosphere. Largely through their efforts, as well as those of a number of nineteenth-century chemists and physicists, the identity of the and major components of the atmosphere, N_2, O_2, water vapor, CO_2, and the rare gases were established. In the late nineteenth-early twentieth century focus shifted from the major atmospheric constituents to trace constituents, that is, those having mole fraction below 10^{-6} (1 part per million by volume). It is clear that the atmosphere contains a myriad of trace species, whose presence can be due to geologic, biological, chemical, and anthropogenic processes. Spectacular innovations in instrumentation since 1975 have enabled identification of atmospheric trace species down to levels of about 10-12 parts per part of the air, (1 part per trillion by volume) (Seinfeld and Pandis 2006).

The aerosol definition makes immediately understand what we are talking about:

"*Solid and /or liquid particles suspended in a gas*"

Particles in the atmosphere arise from natural sources, such as windborne dust, sea spray and volcanoes, and from anthropogenic activities such as combustion of fuels. Emitted directly as particles (primary aerosol) or formed in the atmosphere by gas-to-particle conversion processes (secondary aerosol), the atmospheric aerosol is generally considered as the suspension of particles with a diameter ranging from few nanometers (nm) to tens micrometers (µm). Once airborne, particles can change their composition by condensation of vapor species, by evaporation, by coagulation with other particles, by chemical reaction or by activation in the presence of water supersaturation to become fog and cloud droplets (Seinfeld and Pandis 2006).

The removal of particles from the atmosphere can occur by two mechanisms: deposition at the Earth's surface (dry deposition) and incorporation into cloud droplets during the formation of precipitation (wet deposition). According to particle size, dry deposition involves three sub-mechanisms, sedimentation and impaction for big particles and diffusion following the Brownian motion for smaller particles.

Atmospheric particles emitted from air pollution sources and formed by natural processes have a multitude of different shapes and densities. That is why in air pollution control, it is

necessary to use a particle size definition that directly relates to how the particle behaves in a fluid such as air. For this purpose, the aerodynamic diameter is defined as the diameter of a spherical particle having a density of 1g cm^{-3} that has the same inertial properties (i.e. terminal settling velocity) in the air as the particle of interest.

2.1 Size distribution

Depending on the physical and chemical processes involved in the formation and growth of the particles, the particles are conventionally divided into different size fractions, generally called "modes" (Fig. 2.1), which denomination mostly refers to how the particles are formed: nucleation, Aitken, accumulation and coarse modes (Whitby and Cantrell 1976).

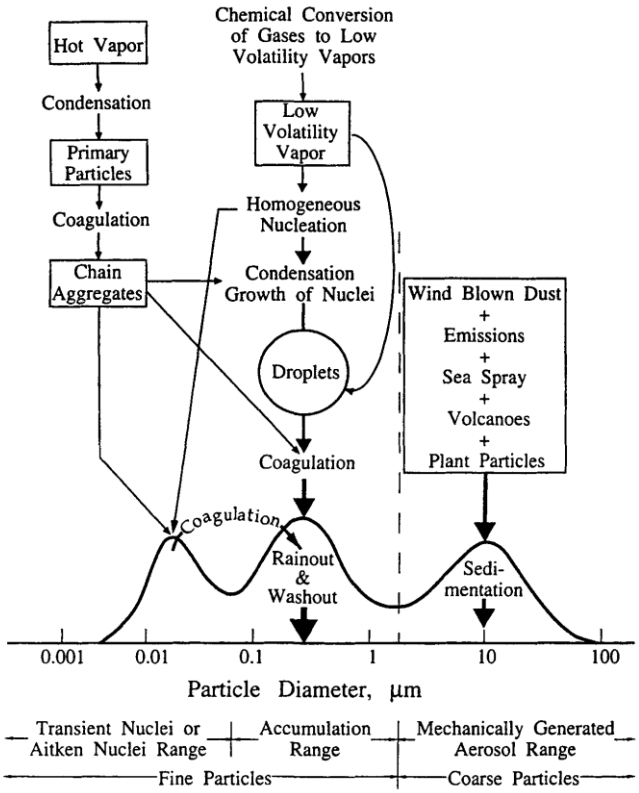

Fig. 2.1 Atmospheric aerosol typical polymodal size distribution. (Whitby and Cantrell 1976)

The *nucleation mode* exists in the range below 0.02 μm of particle diameter and usually presents its maximum number-density around 5-15 nm of particle diameter. New particles are formed by homogeneous nucleation from chemical conversion of gaseous precursors into low volatility vapors. These particles have hours lifetime in the atmosphere as they rapidly coagulate with larger particles or grow into larger sizes due to condensation. Classical

nucleation theory shows that the nucleation highly depends on the concentrations of the gaseous precursors, relative humidity and temperature. In particular, the nucleation is favored by a decrease in the temperature and/or increases in the relative humidity (Easter and Peters 1994).

Aitken mode particles range from 0.02 to 0.1 μm and originate from either primary particles (natural and anthropogenic) or by the growth of nucleation mode particles. It is likely that secondary Aitken mode particles are formed by coagulation of ultrafine particles, by condensation and by liquid phase reactions. A typical primary source that has a very large emission of Aitken mode particles is represented by combustion processes.

The *accumulation mode* covers the range between 0.1 and 1 μm. In the atmosphere, Aitken mode particles grow to accumulation mode particles mainly by coagulation and liquid phase reactions occurring in cloud droplets (Hussein et al. 2004).

The *coarse mode* includes particles greater than1 μm. Most of these particles are formed by mechanical processes, such as the erosion of the earth's crust (mineral dust) or other materials, or the bursting bubbles on the ocean surface (sea spray).

Coagulation processes do not affect the particle number concentration of coarse particles. The processes of formation and growth of particles in the range < 1 μm do not tend to produce particles > 1 μm. On the other hand, mechanical processes forming primary particles cannot easily reduce the particles size to diameters < 1 μm owing to energetic limitations. Thus, the transfer of particles from different modes of the size spectrum presents a barrier around 1 μm.

Coarse particles have sufficiently large sedimentation velocities that they settle out of the atmosphere in a reasonably short time. Because removal mechanisms are efficient at the small and large particle extremes of the size spectrum, the same mechanisms are inefficient in the accumulation range mode. Particles in the accumulation mode tend to have considerably longer atmospheric residence times than those in either the nuclei or coarse mode (Seinfeld and Pandis 2006).

The chemical fates of trace atmospheric species are often intertwined. The life cycles of the trace species are strongly coupled through the complex array of chemical and physical processes in the atmosphere. As a result of these couplings, a perturbation in the concentration of one species can lead to significant changes in the concentrations and lifetimes of other trace species and to feedbacks that can either amplify or damp the original perturbation.

Depending on their atmospheric lifetime, trace species can exhibit an enormous range of spatial and temporal variability. Relatively long-lived species have a spatial uniformity such that a handful of strategically located sampling sites around the globe are adequate to characterize their spatial distribution and temporal trend. As species lifetimes become shorter, their spatial and temporal distributions become more variable. Urban areas, for example, can require tens of monitoring stations over an area of hundreds of square kilometers in order to characterize the spatial and temporal distribution of their atmospheric components (Seinfeld and Pandis 2006).

2.2 Particulate sources

Atmospheric aerosol pollution and in particular the particulate matter could be emitted from anthropogenic and natural sources. Much of the air pollution that damages human health and the environment today is the result of human activities; but natural sources also emit air pollutants, contributing to the exposure of people and ecosystems to bad air quality.

2.2.1 Anthropogenic sources

The anthropogenic chemical pollution has no borders and no matter where the pollutants are released into the atmosphere will have an impact over the global environment. The most relevant sources are the incineration of fossil fuels to produce energy (heat and electricity), major industrial processes (like metallurgy industry or cement/construction industry) and transportation.

The production of electricity involves an environmental impact based on the nature of the used specific conversion technology. The main types of fuel used are oil and coal, which differ in their quantitative chemical composition, calorific value, and combustion products. The residues released into the atmosphere, both for fuel oil and coal plants, consist of gas and particulate. Most particles emitted by oil power plants have a diameter of less than 1 μm. The main element is carbon, while Ca, Si and Al are also characteristic. Regards coal-based power plants, about 35% of the mass of the particles emitted has a diameter smaller than 3 μm and are mostly formed by aluminum-silicates of Na, Mg, K, Ca, Ti, Fe. There are also carbonaceous particles with traces of elements such as Se and As.

The emissions due to the chemical, petrochemical, iron, and steel, metallurgical and cement industries depend on the type of plant. Generally, carbon particles (fumes, ash) are produced with impurities typical of the fuel used and of the production process; they can be carbon oxides, organic sulfur compounds, hydrocarbons, and nitrogen oxides.

Vehicular traffic causes the release of particles deriving from the direct emissions of the vehicles (exhaust particles), from the wear of the road surface, brakes and tires and other mobile parts of the vehicles (non-exhaust particles), which accumulate on the road surface and can be re-suspended by the action of the passage of the vehicles themselves. In urban areas, the emission from vehicular traffic is considered to be the main source of PM_{10}.

2.2.2 Natural sources

The major contributions of natural sources can be ascribed to sea spray, the wind blows of desert dust and volcanic emissions.

The action of the wind exerted on the sea surface causes the ejection of numerous small droplets of seawater in the atmosphere called "jet drops". These droplets, due to subsequent evaporation, leave particles of marine aerosol in the air. Moreover, due to the explosion of air bubbles on the surface of the sea, particles called “film drops” are introduced directly into the atmosphere (O’Dowd and de Leeuw 2007). These particles generally fall within the range of coarse mode. The chemical composition of marine aerosols is characterized by the presence of anions (chloride and sulfate), cations (sodium and magnesium), organic phosphorus and trace metals such as Ni, Cd, Pb, V, and Zn.

The major sources of mineral dust are arid and semiarid areas and in the case of Europe, arid zones in North Africa are the major source. In Europe, African dust may greatly increase ambient PM levels, especially in southern European countries, where it is a known source causing exceedances of the PM thresholds (Querol et al. 2009; Bencardino et al. 2011). The high contribution of African Dust in southern Europe in winter and summer derives from the high wind speed values and the dry climate, respectively.

The volcanic activity still occurs in some islands of continental Europe, such as the Canaries and Sicily. Fine ashes from these volcanoes could represent an important local source of PM in nearby areas. Emissions of sulfur dioxide (SO_2) from volcanoes can also contribute to the formation of secondary particles. For example, Etna provides a semi-permanent emission of SO_2 (2,400 tons/day) from its volcanic plume contributing to the formation of large quantities of secondary particulate (Calabrese et al. 2016).

2.3 Particulate matter types: urban, sub-urban, free tropospheric and marine aerosol sites

2.3.1 Urban Aerosol

Aerosol coming from an urban area is formed by a mixture of primary particulate emissions from industries, vehicular traffic, power generation, natural sources, and secondary material formed by gas-to-particle conversion mechanisms. The aerosol mass distribution (distribution of particle mass with respect to particle size, admitting that all the particles have the same density ρ_p (g cm^{-3})) in urban sites usually has two distinct modes, one in the sub-micrometer regime (referred to as the "accumulation mode") and the other in the coarse-particle regime (Fig. 2.2).

The aerosol size distribution is quite variable in an urban area. Extremely high concentrations of fine particles (less than 0.1 μm in diameter) are found close to sources (e.g., highways), but their concentration decreases rapidly with distance from the source (Fig. 2.3).

Close to a major road, there is approximately more than an order of magnitude of particles compared to the average urban concentration. However, the concentration of these particles decays rapidly because of dilution at a characteristic distance of roughly 100 m from the road (Zhu et al. 2002). The increase in mass concentration next to major roads is usually smaller, it represents about 10-20% of the urban background. Part of this mass increase in the Aitken and accumulation modes because of the fresh combustion particles, but a significant part can be in the coarse mode due to the re-suspension of dust particles from traffic (Fig. 2.4). The mass concentrations of the accumulation and coarse particle modes are comparable for most urban areas. The Aitken and nucleation modes, except for those areas close to combustion sources, contain negligible volume distribution (volume of particles per cm^3 of air having diameters in the range D_p to (D_p + dD_p), with D_p the diameter of the particles) (Fig. 2.2 and 2.4).

The sources and chemical composition of the fine and coarse urban particles are different. Coarse particles are generated by mechanical processes and consist of soil dust, sea salt, fly ash and tire wear particles. Aitken and accumulation mode particles contain primary particles from combustion sources and secondary aerosol material (sulfate, nitrate, ammonium, secondary organics) formed by chemical reactions resulting in a gas-to-particle conversion. The main mechanisms of particles transfer from the Aitken to accumulation mode are coagulation and growth by condensation of vapors formed by chemical reactions onto

existing particles. Coagulation among accumulation mode particles is a slow process and does not transfer particles to the coarse mode (Seinfeld and Pandis 2006).

Processing of accumulation and coarse mode aerosol by clouds can also modify the concentration and composition of these two modes. Aqueous-phase chemical reactions take place in cloud and fog droplets, and in aerosol particles at relative humidity approaching 100%. These reactions can lead to the production of sulfate and after evaporation of water, a larger aerosol particle is released in the atmosphere. This transformation can lead to the formation of the condensation mode and the droplet mode (Hering and Friedlander 1982; John et al. 1990; Meng and Seinfeld 1994).

Terms often used to describe the aerosol mass concentration include TSP (total suspended particulate matter) and PM_x (particulate matter with a diameter smaller than x μm). TSP refers to the mass concentration of atmospheric particles smaller than 40-50 μm, while $PM_{2.5}$ and PM_{10} represent the most commonly monitored fractions of particulate matter, which are smaller than 2.5 and 10 μm, respectively.

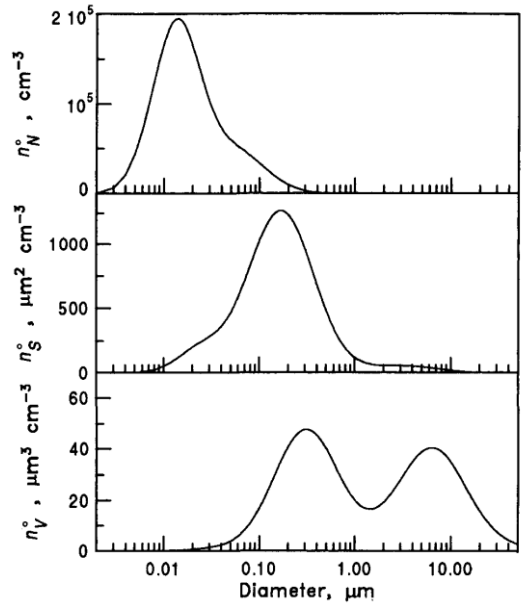

Fig. 2.2 Profiles of number, surface and volume distribution of a typical urban aerosol. (Seinfeld and Pandis 2006)

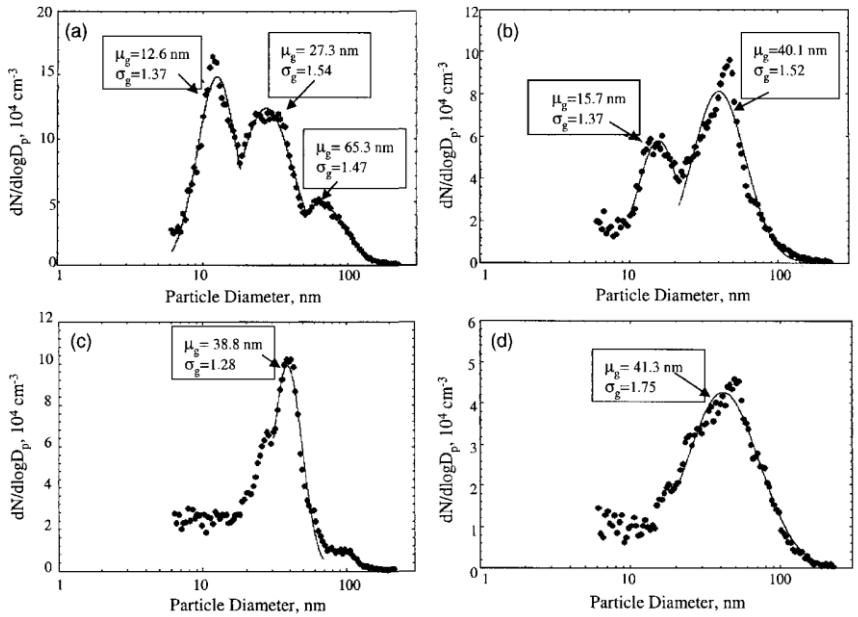

Fig. 2.3 Measured and fitted multimodal number distributions at different distances downwind from a major road in Los Angeles (a) 30 m downwind, (b) 60 m downwind, (c) 90 m downwind, and (d) 150 m downwind. Note the different scale for the y-axis (Zhu et al. 2002).

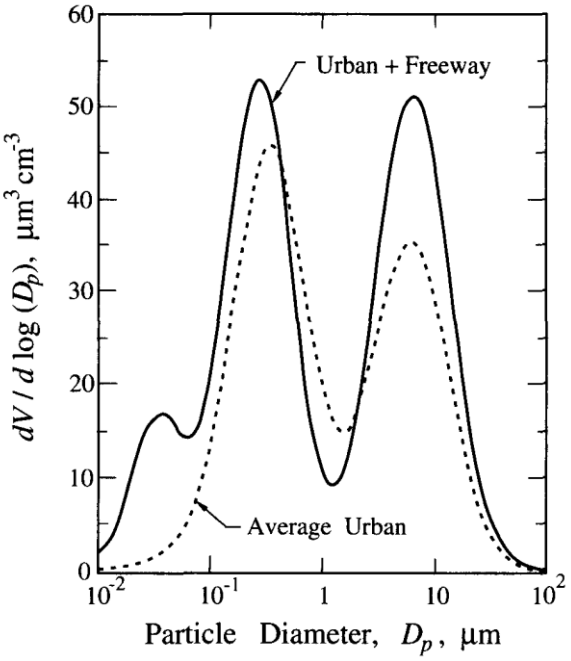

Fig. 2.4 Aerosol volume distribution next to a source, a freeway, compared to the average urban conditions. (Seinfeld and Pandis 2006)

2.3.2 Sub-urban aerosol

Aerosols in suburban areas are mainly of natural origin with a moderate influence of anthropogenic sources (Hobbs et al. 1985). The number distribution (number of particles per cm^3 of air having diameters in the range D_p to $(D_p + dD_p)$) is characterized by two modes

centered at diameters about 0.02 and 0.08 μm (Jaenicke 1993), while the mass distribution is dominated by the coarse mode centered at about 7 μm (Fig. 2.5).

The mass distribution of continental aerosol not influenced by local sources has a small accumulation mode and no nuclei mode. The PM_{10} concentration of sub-urban aerosols is about 20 μg m^{-3}.

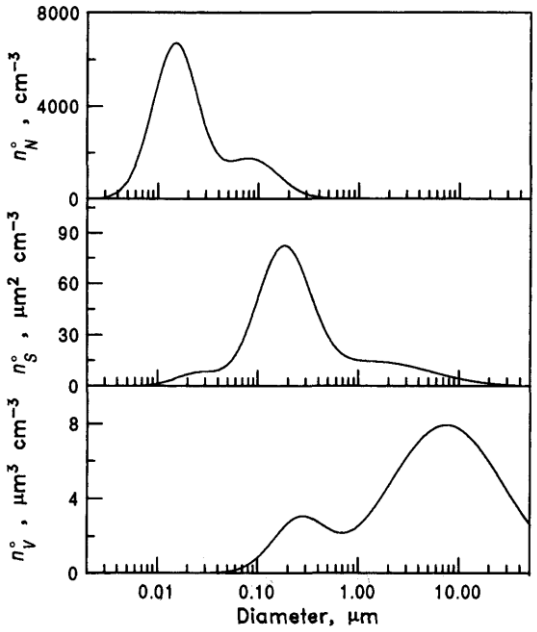

Fig. 2.5 Typical sub-urban aerosol number, surface, and volume distributions (Seinfeld and Pandis 2006).

2.3.3 Free Tropospheric Aerosol

In the most general terms, the atmosphere is divided into lower and upper regions (troposphere, stratosphere, mesosphere, and exosphere). The troposphere, can be divided into the *planetary boundary layer* (lower troposphere), extending from the Earth's surface up to about 1 km, and the *free troposphere* (which comprises mid and upper-troposphere) extending from about 1 km to the tropopause (about 10-15 km altitude depending on latitude and time of year).

The background free tropospheric aerosol is found in the mid- and upper troposphere above the clouds. The modes in the number distribution correspond to mean diameters of 0.01 and 0.25 μm (Jaenicke 1993) (Fig. 2.6). The middle troposphere spectra typically indicate more particles in the accumulation mode relative to lower tropospheric spectra, suggesting precipitation scavenging and deposition of smaller and larger particles (Leaitch and Isaac 1991). The low temperature and low aerosol surface area make the upper troposphere

suitable for new particle formation, and a nucleation mode is often present in the number distribution (Fig. 2.6).

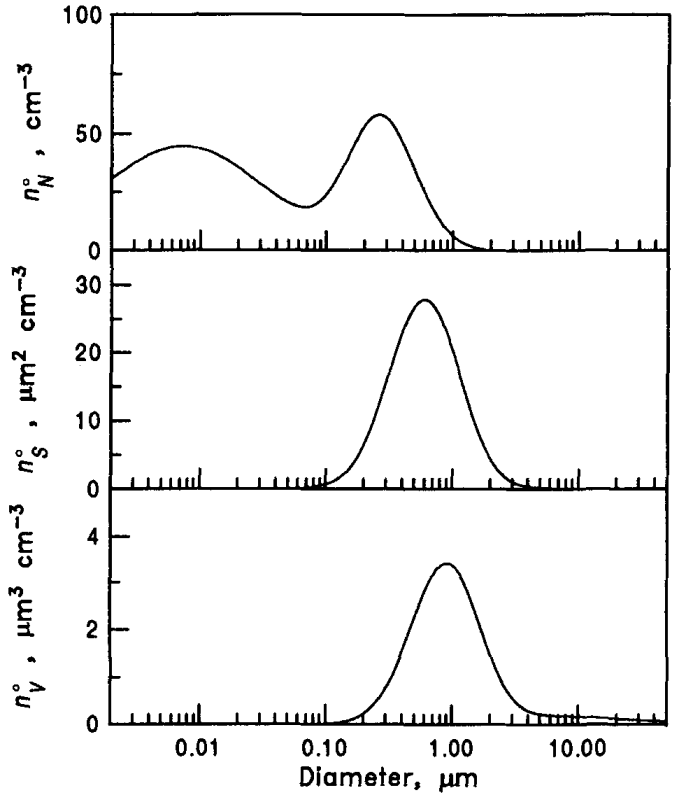

Fig. 2.6 Typical free tropospheric aerosol number, surface, and volume distributions (Seinfeld and Pandis 2006).

2.3.4 Marine Aerosol

In the absence of significant transport of continental aerosols, particles over the remote oceans are mainly of marine origin (Savoie and Prospero 1989). Marine atmospheric particle concentration is normally in the range of 100-300 cm^{-3}. Their size distribution is usually characterized by three modes (Fig. 2.7): the Aitken ($D_p < 0.1$ μm) the accumulation ($0.1 < D_p < 0.6$ μm), and the coarse mode ($D_p > 0.6$ μm) (Fitzgerald 1991).

Typically, the coarse-particle mode, which represents 95% of the total mass but only 5-10% of the particle number (Fig. 2.8), results from the evaporation of sea spray produced by bursting bubbles or wind-induced wave breaking (Monahan et al. 1983). Typical sea salt aerosol concentration in the marine boundary layer (MBL) is around 5-30 cm^{-3} (O'Dowd and Smith 1993). Lewis and Schwartz had thoroughly treated sea salt aerosols in their work (Lewis and Schwartz 2004), pay attention to the mechanism, methods, measurements, and models of sea salt aerosol production.

Figures 2.7 and 2.8 show number and volume aerosol distributions in clean maritime air measured by several investigators (De Leeuw 1986; Hoppel et al. 1990) and the modeled marine aerosol size distribution. The distributions of Hoppel et al. (1990) and De Leeuw (1986) were obtained at wind speeds of less than 5 m s^{-1} in the subtropical and North Atlantic, respectively. The distribution of Mészáros and Vissy (Mészáros and Vissy 1974) is an average of spectra obtained in the South Atlantic and Indian Oceans during periods when the average wind speed was 12 m s^{-1}. It is difficult to determine the extent to which the differences in these size distributions are the result of differences in sampling location and meteorological conditions such as wind speed (which affects the concentrations of the larger particles) or to uncertainties inherent in the different measurement methods.

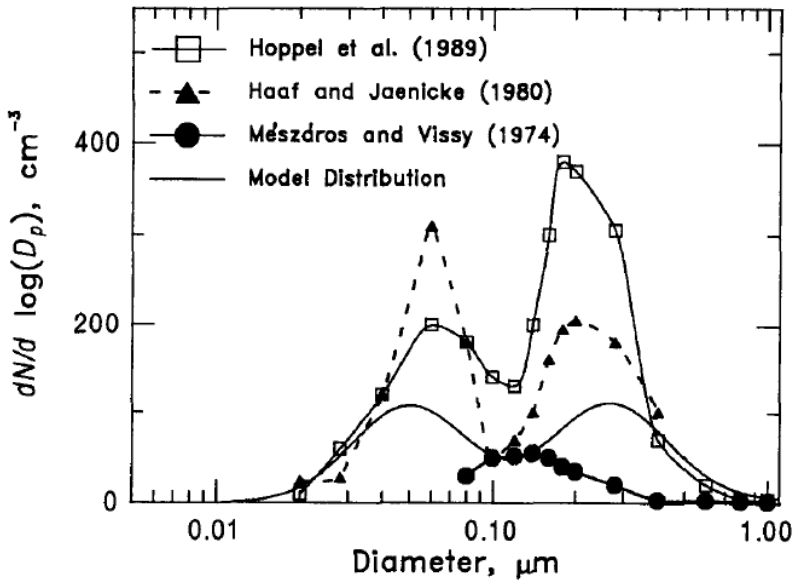

Fig. 2.7 Comparison of measured marine aerosol number distributions and modeled distribution used to represent average conditions (Seinfeld and Pandis 2006).

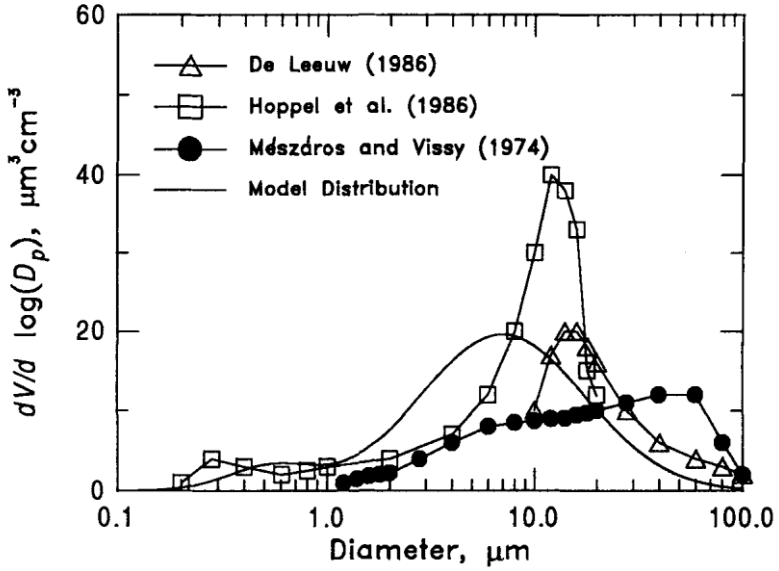

Fig. 2.8 Comparison of measured marine aerosol number distributions and modeled distribution used to represent average conditions (Seinfeld and Pandis 2006).

2.4 Chemical characteristic of Particulate Matter

The chemical composition of atmospheric particles depends on the type of emission source. Natural particles originate mainly from sea spray, volcanic emission, mineral dust (from long-range transport or erosion processes), wildfires and biogenic sources. Primary particles fraction of sea spray is mainly constituted by sodium chloride and some sulfates. Seaspray is produced via the bubble-bursting processes typically resulting from white cap generation, film production and jet drops, resulting in sea spray particles in the size range from sub-micrometers up to a few micrometers (O'Dowd and de Leeuw 2007). Volcanic emissions are sources of primary particles, but perhaps are also mainly secondary sulfur compounds sources from SO_2 emission, although the contribution of such events to bulk particle mass levels in ambient air is generally limited. Crustal and mineral dust could be subjected to regional variation as a function of the geology of the source areas, but in general, they are composed of silicates, carbonates, aluminum, iron, and trace metals. They are originated by erosion processes, e.g., caused by the wind, or transported from the desert region (e.g. Saharan dust outbreaks in South Europe). Forest fires are sources of both organic primary emission and gaseous precursor of particles. Biogenic sources emit vegetal debris, pollen, spores which have sizes extending into the coarse mode and minor amounts of micro-organisms (e.g. viruses, bacteria, fungi, protozoa or algae) contributing to particles in the size range < 2 μm. The natural secondary aerosol is prevalently constituted by sulfate, originated from the oxidation of SO_2 emitted by volcanoes, nitrate, originated from the

oxidation of NO_x from soil transpiration and lightning, and organic aerosol originated from organic gaseous precursors such us biogenic emission of large forested areas.

In an urban environment, primary particles are emitted as a result of traffic-related combustion processes, house heating, and industrial processes. Industrial activities such as building, mining, manufacturing of cement, ceramic and bricks, and smelters are typical sources of primary particles. Smelters produce mostly fine particles formed during condensation of hot vapors, with Ni, V, Mn, and Cu emitted together. The other industrial sources can mostly emit coarse mineral particles. Particles mechanically generated by road traffic, such as erosion of the pavement (road dust) and abrasion of break and tires, are coarse particles whereas particles emitted by vehicles exhaust are fine particles. Oxidation of SO_2 emitted by fossil fuel combustion and metal smelting (Charlson et al. 1992) produces sulfuric acid, which could be incorporated as sulfuric acid itself or neutralized by ammonia or by reaction with calcium carbonate or sodium chlorine. NO_x are emitted by traffic in an urban environment and by some industrial processes. After oxidation of NO_x, nitric acid is formed, which may be neutralized and then incorporated into the particle phase. Nitrate and sulfate size distributions mainly depend on the neutralizing agent. Therefore, ammonium nitrate and ammonium sulfate are present in the fine fraction while sodium nitrate and calcium nitrate and sulfate are in the coarse fraction. In large agricultural areas, combustion of biomass and fossil fuels are important sources of organic gaseous precursors of anthropogenic secondary aerosol. These vapors are mainly emitted by gasoline evaporation (fugitive emission) and combustion processes. Human activity may also generate anthropogenic bio-aerosols.

2.4.1 Heavy metals

More than 40 trace elements are routinely found in atmospheric particulate matter samples. These elements arise from dozens of different sources including combustion of coal, oil, wood burning, steel furnaces, boilers, smelters, dust, waste incineration, and brake wear. Depending on their sources, these elements can be found in either fine or coarse mode. Concentrations of selected elements together with the size mode where these elements are usually found are shown in Tab. 2.1. The concentration of these elements even for similar pollution levels varies over almost three orders of magnitude, indicating the strong effect of local sources. In general, elements such as lead, iron, and copper have the highest concentrations and are usually called “majority elements”, while elements such as cobalt, chromium, and antimony are characterized by low concentrations and are called “trace elements”.

Elements produced during combustion usually exist in the form of oxides (e.g., Fe_2O_3, Fe_3O_4, Al_2O_3), but their chemical form is in general uncertain.

Element	Mode[a]	Concentration (ng m^{-3})		
		Remote	Rural	Urban
Fe	F and C	0.6–4,200	55–14,500	130–13,800
Pb	F	0.01–65	2–1,700	30–90,000
Zn	F	0.03–450	10–400	15–8,000
Cd	F	0.01–1	0.4–1,000	0.2–7,000
As	F	0.01–2	1–28	2–2,500
V	F and C	0.01–15	3–100	1–1,500
Cu	F and C	0.03–15	3–300	3–5,000
Mn	F and C	0.01–15	4–100	4–500
Hg	—	0.01–1	0.05–160	1–500
Ni	F and C	0.01–60	1–80	1–300
Sb	F	0–1	0.5–7	0.5–150
Cr	F and C	0.01–10	1–50	2–150
Co	F and C	0–1	0.1–10	0.2–100
Se	F and C	0.01–0.2	0.01–30	0.2–30

[a]F = fine mode; C = coarse mode.

Tab. 2.1 Concentration (ng m^{-3}) and size distribution of various elements found in atmospheric particles (Schroeder et al. 1987).

Since some airborne trace metals such as As, Cd, Hg, and Ni are identified or suspected to have potent carcinogenic effects on human health, the European Union (EU) has set strict guidelines to monitor this trace metal species (Directive 2004/107/CE). However, not all the metals that may be released into the atmosphere have been regulated.

The trace metal content can vary according to the emission sources, and among the anthropogenic sources, the industrial emission generally provides the major contribution. Taiwo et al. (Taiwo et al. 2014) affirmed that the metal production by industrial processes is one of the major contributors to the emissions of total trace elements such as Cd, Cr, Cu, Hg, Ni, Se, V, and Zn in the UK in 2009 (Tab. 2.2). A study by Querol et al. (Querol et al. 2007) also showed a number of trace elements in airborne PM are associated with industrial emissions in Spain.

Analysis of airborne PM close to steel plants has shown that Fe, Mn, Zn, Pb, Cd, and K are associated with emissions from the steel and iron plants (Moreno et al. 2004; Ebert et al. 2012). Microscopic analysis of individual particles has confirmed the presence of individual Fe-rich particles close to steel plants. For example, Moreno et al. (Moreno et al. 2004) identified iron spherules in both fine and coarse PM fractions at a steelworks in Port Talbot, South Wales, UK; Erbet et al. (Ebert et al. 2012) observed a significant fraction of individual

iron oxides and iron mixtures in airborne PM near a steel industry in Duisburg, in the Rhine-Ruhr area of Germany.

	Total emissions (tonnes)	Industrial contribution %	Major sources
As	13	93	Treated wood for industrial combustion; metal production; public electricity and heat production
Cd	2	78	Non-ferrous metal production and iron and steel manufacture (as well as other forms of industrial combustion), energy production (include a significant proportion from waste combustion and fuel oil combustion for electricity generation)
Cr	26	89	Coal combustion, iron and steel production in integrated works and in electric arc furnaces and the production of chromium based chemicals
Cu	52	49	Metal production, combustion of lubricants in industry and coal combustion
Pb	60	87	Metal production and combustion of lubricants in industry
Hg	7	99	Iron and steel production processes, public electricity and heat production, waste incineration, the manufacture of chlorine in mercury cells, coal and other forms of industrial combustion
Ni	83	54	Combustion of heavy fuel oil
Se	31	92	Glass production and combustion for public electricity and heat production
V	477	21	Fuel oil combustion
Zn	339	72	Metal production and combustion in industry

Tab. 2.2 Contribution of each trace metal from industrial processes to total emissions and their major sources in the UK based on a 2009 United Kingdom National Atmospheric Emissions Inventory (Taiwo et al. 2014).

Among the natural sources (e.g., crustal and mineral dust), the emitted particulate by volcanoes contains several elements; however, most elements have extremely low concentrations (ppb-to-ppm level). The geological effects of such emissions are usually confined to the formation of fumarolic incrustations and the dissipation of element-containing aerosols in the environment. On the other hand, gas transport and deposition of elements in volcanic processes provide the opportunity to make direct observations. The volcanic emissions of trace elements are composed of volatile and aerosol fractions (e.g., Symonds and Reed 1993). The volatile fraction includes elements that escape from the

surface of the magma as gaseous species (they can later form condensation aerosols). Other elements leave the magma surface or conduit wall rocks as molten or solid rock particles.

2.4.2 Carbonaceous aerosols

The carbonaceous aerosol is composed by an organic fraction, named organic carbon (OC), and by a refractory light-absorbing component. The latter is generally referred to as elemental carbon (EC) if quantified using thermal-optical methods, or as Black Carbon (BC) if quantified using optical measurements. Major source categories of carbonaceous particles include open biomass burning (e.g., agricultural burning, wildfires, prescribed burning), mobile/transportation sources, electricity generating units and other power production sources, residential heating and cooking sources.

Due to some overlap among the refractory components of carbonaceous aerosol, it is common to use to measure the airborne EC as a surrogate measure of ambient air BC (Bond et al. 2013; Long et al. 2013). However, they are not measures of the same carbonaceous particle properties and should not be viewed as interchangeable; instead, BC and EC are both defined operationally by measurement methods (Salako et al. 2012). Climate scientists refer to BC as carbonaceous material meeting four physical properties: it strongly absorbs visible light, it is refractory with a vaporization temperature near 4000 K, it is insoluble in water and many organic solvents, and it is an aggregation of small carbon spherules (Bond et al. 2013). As traditionally used in the scientific literature, however, the term BC often refers to measurements of carbon particles meeting only some of these properties, in particular, light absorptive properties as measured via optical attenuation methods. Researchers have coined the term “equivalent BC” to describe estimates of BC mass based on optical measurement methods (Bond et al. 2013; Lack et al. 2014). The term “refractory BC” is used to indicate the refractory components of carbonaceous particles (i.e., components that maintain their form at high temperatures), as measured by laser-induced incandescence (Bond et al. 2013; Petzold et al. 2013). EC is operationally defined based on thermal properties rather than light absorbing properties; however, because EC measurements capture a major fraction of BC (i.e., EC particles include strongly light absorbing carbon particles), EC has been used as a surrogate measure of BC. Several papers including (Bond et al. 2013; Petzold et al. 2013; Lack et al. 2014) have proposed formal definitions and recommended terminology for the different fractions of carbonaceous aerosols, and they have also provided detailed descriptions of the various measurement methods, their uncertainties, and limitations.

While EC has a primary origin, OC can be both primarily emitted but also formed in the atmosphere through condensation to the aerosol phase of low vapor pressure compounds emitted as primary pollutants or formed in the atmosphere (Gentner et al. 2012). Because of this, the ratio OC/EC in aerosol fractions differ widely, both in space and seasonally, and is a useful diagnostic ratio that could give information regarding the typology of the sampling sites and emission sources, and regarding the processes occurring in the atmosphere which can lead to the formation of secondary organic compounds.

The generally used EC/OC carbon analyzer is based on a thermal-optical method, which corrects for charring that may otherwise overestimate EC. However, artifacts may also arise if samples contain brown carbon (BrC), which is a part of organic carbon that absorbs in the visible and ultraviolet spectral regions (Andreae and Gelencsér 2006). BrC can be volatilized over a broad temperature range and some of the BrC can be accounted for as EC, hence overestimating the EC concentration. Moreover, the combustion temperature of EC and BrC can be lowered in the presence of inorganic species, which are sampled on the filter and can catalyze the oxidation of EC and BrC (Andreae and Gelencsér 2006). This can result in misinterpretation of EC as OC and hence lead to an underestimation of the EC mass concentration.

2.4.3 Ionic species

Water-soluble ionic species account for a large fraction of atmospheric particle mass and are ubiquitous compounds, found in urban and rural areas. They are associated with adverse effects on human health, acidification, and eutrophication of ecosystems and visibility reduction (Grantz et al. 2003; Holmes 2007).

Ionic charge in particles can increase the formation of the larger particle as a result of the enhanced stability of the charge clusters and higher growth rates due to the electrostatic forces (ion-induced nucleation (IIN)). Until the 1990s, there was not enough data and model development to support the IIN. Since this decade, several models were developed in order to predict the rates of IIN with different levels of accuracy. There has been a gradual accumulation of observational evidence that ions contribute to nucleation under certain atmospheric conditions, confirmed by the development of models which attempt to simulate this nucleation process. However, field observations do not paint a clear picture of the impact of IIN and its role in the boundary layer is still uncertain (e.g. Laakso et al. (2007)).

Atmospheric ions originate both from primary, as marine (Na^{+}, Cl^{-}) or crustal (Ca^{2+}, Al^{+3}), and secondary sources, e.g. oxidation of organic compounds leading to products

characterized by low volatility. Spatial and temporal variations of ionic compounds in PM can be very significant since they are controlled by numerous factors, such as climatic and orographic features, emission rates of gaseous precursors or long-range transport of pollutants. Moreover, in Mediterranean countries, natural PM sources related to Saharan air mass intrusions contribute to increasing the levels of primary as well as secondary ions (Nicolás et al. 2009). Several studies have demonstrated that mineral dust particles and trace gases influence their concentrations each other: the formation of sulfate and nitrate is favored by the reactions of the corresponding oxides on mineral dust particles (Hien et al. 2005).
The composition of sea salt reflects the composition of seawater enriched in organic material (marine-derived sterols, fatty alcohols, and fatty acids) that exists in the surface layer of the oceans (Schneider and Gagosian 1985). Reactions on sea salt particles modify its chemical composition; for example, sodium chloride reacts with sulfuric acid vapor to produce sodium sulfate and hydrochloric acid vapor, leading to an apparent "chloride deficit" in the marine aerosol:

Eq. 2.1 $H_2SO_4\,(g) + 2\,NaCl \rightarrow Na_2SO_4 + 2\,HCl\,(g)$

Sulfuric acid has the lowest vapor pressure of all the available atmospheric inorganic aerosol constituents resulting as the most likely to nucleate from the gas phase. Ammonia can facilitate this process by forming stable acid-base complexes with sulfuric acid that have very low volatility. However, ammonia is not the only ternary agent of atmospheric importance. For example, organic species such as amines from primary emissions are more effective than ammonia in spite of having lower concentrations (Berndt et al. 2014). Moreover, oxidation products of biogenic and anthropogenic non-methane volatile organic compounds (VOC) emissions can have sufficiently low volatility and necessary functional group characteristics to contribute as ternary agents as well (Riccobono et al. 2014).

2.4.4 Organic Aerosol

Organic Aerosol (OA) is important for both air quality and climate perspectives. Measurements across the Northern Hemisphere (NH) mid-latitudes suggest OA represents between 18 and 70% of fine aerosol mass depending on the location and the atmospheric conditions (Zhang et al. 2007). Organic Aerosol can be emitted as a primary organic aerosol (POA) or formed as a secondary organic aerosol (SOA). In particular, SOA is formed from the oxidation products of volatile organic compounds (VOCs) and semi-volatile and

intermediate volatility organic compounds (S/IVOCs). Across the NH mid-latitudes, SOA accounts for 64, 83, and 95% of the submicron mass of observed surface OA in urban, urban downwind and remote environments, respectively (Zhang et al. 2007). Emitted from both natural and anthropogenic sources, SOA has an important climatic impact: it can perturb the energy balance of the Earth by absorption and scattering (aerosol-radiation interactions) and by altering cloud properties (aerosol-cloud interactions) (Forster, P. and Ramaswamy 2007). The identity of SOA precursors is critical to our understanding of the SOA budget and its life cycle; however, the dominant precursors of SOA remain highly uncertain in their magnitudes and spatial distributions. Biogenic volatile organic compounds (bVOCs) are considered important natural sources of SOA due to high emissions (Guenther et al. 2012) and fast reactivity. Laboratory and field studies suggest that monoterpene ($C_{10}H_{16}$) (Yu et al. 1999), isoprene (C_5H_8) (Ng et al. 2008), sesquiterpenes ($C_{15}H_{24}$) (Tasoglou and Pandis 2015) and the heterogeneous uptake of glyoxal (Volkamer et al. 2007) are all important biogenic sources of SOA. Isoprene and monoterpene are also emitted from phytoplankton (Yassaa et al. 2008) and even if the SOA production rates from marine VOCs is small, estimated at 5 Tg (SOA) a^{-1} by Myriokefalitakis et al. (Myriokefalitakis et al. 2010), marine SOA may be important from a climate perspective due to changes cloud-condensation nuclei.

Recent studies (Hodzic et al. 2016; Tsimpidi et al. 2016) affirm that the sum of the global SOA burden from anthropogenic and biomass burning precursors is dominated by S/IVOCs (72 and 69 %, respectively).

As previously mentioned, new particle formation by binary homogeneous nucleation of sulfuric acid (H_2SO_4) is one of the possible ways, with the gaseous sulfur compounds (sulfur dioxide, SO_2, and dimethyl sulfide, DMS) and VOCs that are oxidized forming low volatility gases, which irreversibly condense onto pre-existing aerosol. Indeed, in a polluted urban area, particle growth can be driven by rapid sulfuric acid formation (Wang et al. 2013, 2016). On the contrary, in unpolluted forest regions, such as the Hyytiälä station in Finland, different chemistry is involved and the extremely low volatile organic carbon (ELVOC) driven activation of cluster mode particles or organic nucleation and subsequent growth into the Aitken mode (Ehn et al. 2014) can dominate. Nucleation does not require sulfuric acid as ELVOC can nucleate under atmospheric conditions to form secondary organic aerosol (SOA) although ionization appears to be an essential contributing factor (Ehn et al. 2014). SOA can also nucleate on seed particles in the form of a secondary inorganic aerosol (SIA) and black or elemental carbon (BC) from primary emissions (Chu et al. 2012).

The particle-phase state may be another important factor for new particles formation but is poorly characterized, and is dependent on relative humidity, ambient temperature and SOA precursor (Shiraiwa et al. 2017).

It has been established since the 1960s that the presence of (VOCs) with NO_x and sunlight promote the formation of O_3 in the troposphere and the mechanism is now well understood (Jenkin and Clemitshaw 2000). The sunlight initiates the process by providing near ultra-violet radiation which dissociates certain stable molecules, leading to the formation of hydrogen-containing free radicals (HO_x) (Fig. 2.9).

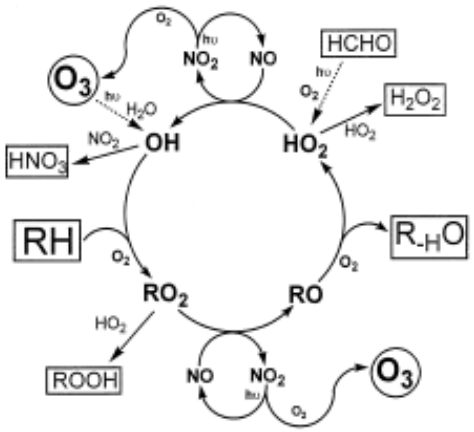

Fig. 2.9 Schematic representation of the free radical-catalyzed oxidation of a generic saturated hydrocarbon, RH, to its first-generation oxidized product, R_HO. The key role of the NO_x species in the chain-propagating process is also illustrated, which leads to the generation of O_3 as a by-product. The major sources and sinks of the free radicals are also shown (Jenkin and Clemitshaw 2000).

In the presence of NO_x, these free radicals catalyze the oxidation of VOCs, ultimately to carbon dioxide and water vapor. Partially oxidized organic species such as aldehydes, ketones, and carbon monoxide are produced as intermediate oxidation products, with O_3 formed as a by-product. An enormous variety of VOC classes may be emitted from numerous anthropogenic and biogenic sources and, depending on location, either or both categories can make a major contribution to photochemical ozone formation.

2.5 Environmental and human health effect

The aerosol particles, in particular those of fine size, play an important role among atmospheric pollutants due to their strong environmental impact. In fact, in the presence of suspended powders, phenomena are linked such as the formation of clouds and haze, the variation of the optical properties of the atmosphere with effects on the visibility and the

earth's energy balance, the contamination of water and soil through dry and wet deposition, the catalysis of chemical reactions in the atmosphere and the erosion of materials.

Air pollution in an urban environment is an important risk factor for human health, with documented effects on mortality and long-term morbidity. Among the numerous environmental pollutants, particulate matter, especially fine (under 4 microns in diameter), is recognized as one of the most dangerous agents and its effects have been reliably quantitatively estimated. The attributable damage to the inhaled particles is due to they have passed the natural barriers of the respiratory system, reaching the pulmonary alveoli, release toxic substances and can obstruct the alveoli themselves. The material that remains in the lungs can also have intrinsic toxicity, interfere with the elimination of other more dangerous materials, cause adsorption phenomena on the particles. The deposition of particles in the respiratory system is shown in Fig. 2.10.

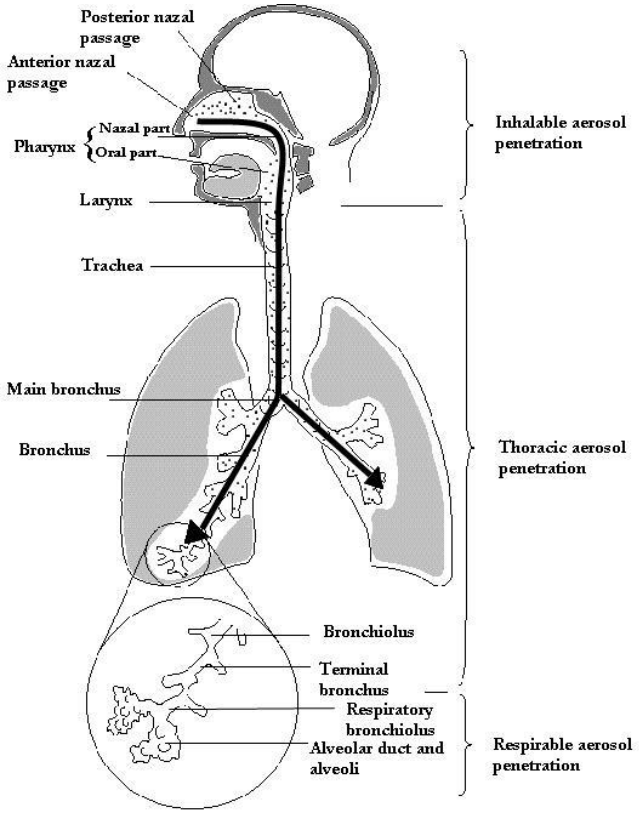

Fig. 2.10 Respiratory collection of particles (EPA 2012).

Basically, the smaller the particle is, the more likely it will penetrate deeper into the lung. Indeed, small particles, typically less than 4 μm, can interfere with oxygen gas-exchange in the lung alveolar region, while particles much greater than 100 μm are typically not inhaled.

Fig. 2.11. shows the penetration ability of particles into the lung, defined by commonly-used size-based particle terms (EPA 2012).

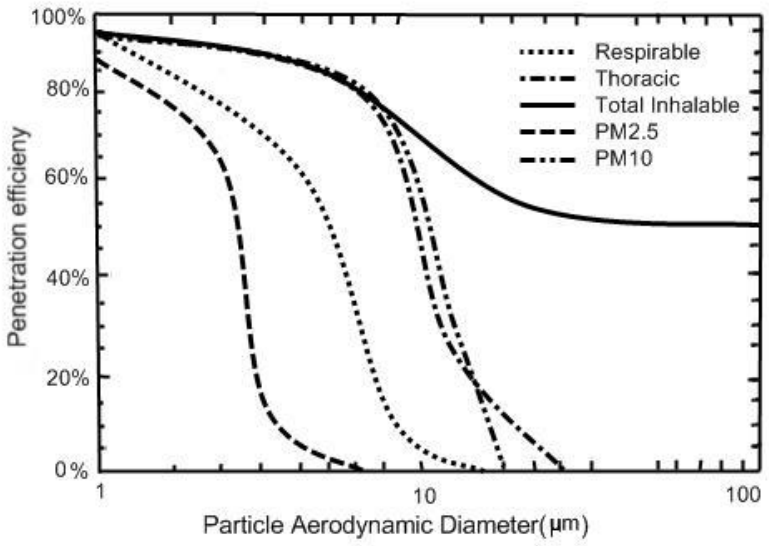

Fig. 2.11 Modeled lung deposition as a function of particle size. (EPA 2012)

Inhalable, thoracic, and respirable particles, which describe where particles are likely to deposit in the lung, are terms used more commonly in industrial hygiene (occupational-related PM exposures), while $PM_{2.5}$ and PM_{10} are terms used by Institutions such as the American Environmental Protection Agency (EPA) to describe particles up to 2.5 μm and up to 10 μm, respectively. These size fractions are also described with the terms ”coarse” (10 μm – 2.5 μm), ”fine” (< 2.5 μm) and “ultrafine” (< 0.1 μm). Exposure to large particles can cause coughing and sneezing, while smaller particles can bypass the body’s defense mechanisms and disrupt cellular processes (EPA 2012).

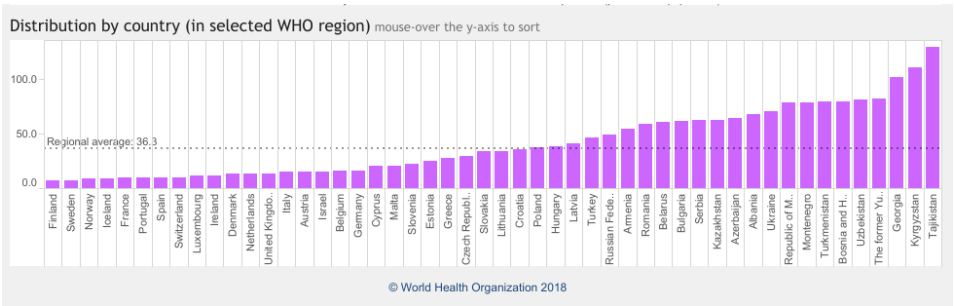

Fig. 2.12 European mortality distribution; WHO report for 2016.

This information makes easy to understand why clean air is considered to be a basic requirement for human health and well-being. However, air pollution continues to pose a significant threat to health worldwide. According to a World Health Organization (WHO) assessment of the burden of disease due to air pollution, more than 4.2 million premature death each year can be attributed to the effects of urban outdoor and indoor air pollution (WHO 2016). Air pollution is the contamination of indoor and outdoor environments by any chemical, physical or biological agent that modifies the natural characteristics of the atmosphere. Household combustion devices, motor vehicles, and industrial facilities are common sources of air pollution. Pollutants of major public health concern include particulate matter, carbon monoxide, ozone, nitrogen dioxide, and sulfur dioxide. Worldwide, ambient air pollution is estimated to cause about 16% of the lung cancer deaths, 25% of chronic obstructive pulmonary disease (COPD) deaths, about 17% of ischemic heart disease and stroke, and about 26% of respiratory infection deaths (Fig. 2.12; WHO 2016).

3. Sampling and analytical technique for particulate matter characterization

3.1 Sampling approaches for particulate matter

Atmospheric particulate is commonly sampled through pump-based devices, but none of them is able to collect all particles in the desired size range with 100% efficiency. For example, particle size selection devices, such as a Well Impactor Ninety Six (WINS) or Very Sharp Cut Cyclone (VSCC) used in $PM_{2.5}$ sampling, are designed to collect 50% of particles of 2.5 μm aerodynamic diameter size while allowing the remaining 50% to pass through the device (EPA 2012). The collection efficiency of these devices increases at particle sizes greater than 2.5 μm, while particles less than 2.5 μm pass through the device with greater penetration efficiency until finally collected on a collection plate or filter. $PM_{2.5}$ is then determined to be the mass concentration of particles collected on a filter that passed through the WINS or VSCC (collection plates and filters capture particles at ~100% collection efficiency).

Particulate sampling includes various collecting techniques including inertial collection, together with filtration, gravitational, and precipitation techniques. Inertial collectors are designed to give a size-representative sample of particles in the atmosphere using the principle that particles in a gas stream are denser than the fluid (air) in which they are suspended. A particle moving in an air stream with approximately the same velocity as the air stream has more momentum (mass x velocity) than the volume of air that it displaces because of its higher mass. The momentum, or inertia, possessed by a particle in a moving air stream will cause the particle to be deflected less than the air in the vicinity of the particle when the air stream undergoes a sudden change in direction. Such a deflection will occur when an obstacle is placed directly in the path of an aerosol stream. If the resulting deflection of the particle from the air trajectory around the obstacle is great enough (large angle of deflection), the particle will strike the obstacle. High incident velocities will increase the momentum of particles in the air stream, thereby enhancing their removal. High velocities can be attained by passing the air stream through an orifice (jet) prior to the stream striking the obstacle, as shown in Fig. 3.1 (EPA 2012). Examples of the inertial collectors are the two-stage impactor, Andersen cascade impactor, and automated cascade impactor.

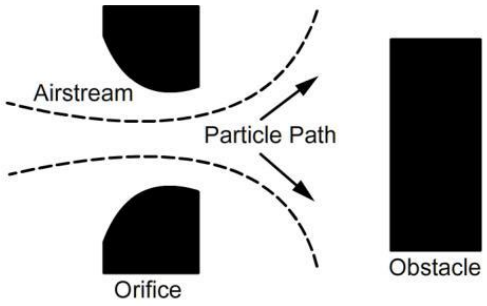

Fig. 3.1 Particle collection by impaction (EPA 2012)

Impingement devices differ from impactors because the jet and striking surface are immersed in a collecting fluid such as water. Impingers are most commonly used in collecting dust, mists, and fumes in the evaluation of occupational health hazards. In addition to collecting soluble gases and particulate matter, the Greenburg-Smith impinger efficiently collects insoluble particles that are greater than two μm in diameter.

Centrifugal separation is a variation of the inertial collection process in which particles are removed from an air stream by the centrifugal force created by moving an aerosol rapidly through a circular path. Several types of sampling devices employ the principle of centrifugal separation, among which the most commonly used is the cyclone sampler. The cyclone showed in Fig. 3.2 contains no moving parts and is designed so that air drawn through it moves in either a circular or a helical path of decreasing radius, thereby increasing its collection efficiency for small particles. As the gas stream surges through the cyclone, particles are separated at the inside surface of the cyclone's wall where the gas velocity approaches zero due to the created centrifugal force. In most cyclone samplers, the particles adhere to the wall or drop into a collection space below the cyclone's chamber.

Most cyclones are not efficient collectors of particles, having diameters less than 2 or 3 μm, depending on particle density. However, small cyclones can be designed to collect particles below one μm in diameter.

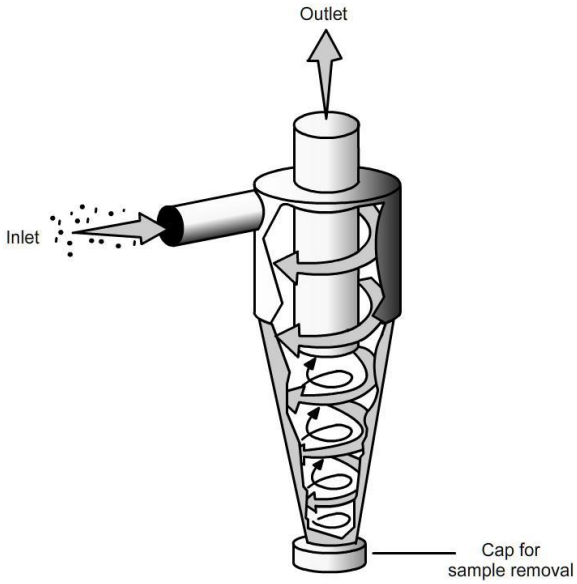

Fig. 3.2 Cyclone sampler (EPA 2012)

Filtration sampling, which is a combination of filtration/impaction sampling, is the most widely used approach for the collection of atmospheric particulates. Filter-based sampling methods are widely used since filters are relatively low in cost, easily stored, and used for subsequent simple and/or complex analyses of collected PM.

Filters capture particles from an air stream by a number of different mechanisms. These mechanisms include *inertial impaction, direct interception, diffusional deposition, electrical attraction,* and *gravitational attraction.* The predominant mechanism depends on the flow rate, the composition, and nature of the particles, particle size, and the type of filter media.

Filter sampling for particulate matter has several advantages over other methods. A primary one is a feasibility of handling large volume rates of flow. Also, after collection, the filtered sample is usually readily available for direct observation.

The number of sizes of filters available has proved to be another advantage. By changing the size of the filter media, the volume of air samples can be varied while maintaining the same linear flow rate through the filter. The selection of sizes also allows filter borders to be designed for use in a variety of situations. This is a definite advantage when the sampling space confines limit accessibility. The variability among filters extends beyond the matter of size alone. Exist different type of filters that are capable of sampling a wide range of environmental conditions of temperature, humidity, and dust loadings.

The use of filter media for sampling is not without its difficulties. One disadvantage is related to the variation in physical and chemical properties of filters in any given filter type. In the case of an impaction instrument, once its operating characteristics have been determined,

these should remain relatively fixed. On the other hand, in sampling with filters, the media is changed between each sample collection. Although filters that minimize the variability between individual filters of a specific type can be obtained, it is more common to find some differences in performance, particularly between different lots of filters.

3.2 PM weight strategies

The mass concentration measurements are the first routine measurements in networks addressing particulate ambient air pollution. As mentioned in the first chapter many epidemiological studies gave evidence that particle mass concentration is associated with adverse health effects. Indeed, given the possible health effect, the European Union set a guideline (2008/50/EG) to regulate the particle mass concentration inhaled by the European population. The PM mass concentration, often reported as $\mu g\ m^{-3}$, can be measured by:

- Gravimetric method
- Oscillating microbalance method (TEOM instrument)
- A method based on beta-absorption (Beta gauges)
- A method based on light scattering

Gravimetric methods of sampling and analysis are commonly used to measure quantities of airborne particulate matter collected in a sampling site. Such measurements are carried out to estimate occupational exposures to airborne particles and/or to evaluate the efficacy of air pollution control technologies. Gravimetric analysis of airborne particles is often complemented by other analytical methods which are employed to measure concentrations of specific chemical agents in occupational atmospheres. Examples of government-promulgated methods for gravimetric measurement of airborne particles in workplaces include those developed by the US National Institute for Occupational Safety and Health (NIOSH) and the European Committee for Standardization (CEN) (EN 12341:2014). These protocols, which are conceptually easy, entail the pump-based collection of airborne particles onto pre-weighed, weight-stable filters that are housed in a sample holder and placed to sample. After sampling, the filter is weighed in order to obtain the weight of the sampled particulate by difference. Accurate gravimetric analysis of air particles requires minimization of electrostatic effects, control of the sorption of moisture and/or other volatiles, control of the temperature stability and extreme care in sample handling (ASTM D6552). Possible systematic errors in PM mass determination, resulting from the use of different samplers, sampling heads, substrates, gravimetric analysis and positive or negative sampling artifacts for the various chemical compounds in particulate matter, are discussed

in the companion paper by (Putaud et al. 2004). The major source of uncertainty in the mass determination originates from positive and negative artifacts in the capturing of ammonium nitrate and semi-volatile organic compounds on filters or other substrates. The magnitude of these artifacts strongly depends on the actual chemical composition of the aerosols, as well as on meteorological conditions. Furthermore, the presence of particle-bound water during off-line gravimetric mass determination at 50% relative humidity can cause a positive artifact. This may be an important source of inconsistency between the PM mass concentrations determined according to the EN 12341 norm and that measured by TEOM (Tapered Element Oscillating Microbalance), instrument which provides continuous measurement of PM mass. Indeed TEOM dries the sampled air stream to limit the quantity of water associated with aerosol particles. Routine TEOM (Fig 3.3) heat the inlet at 50°C, whereas TEOM equipped with a sample equilibration system (SES) achieve RH 30% by sampling through a Nafion dryer, and heating at 30 °C only. Several studies, covering a range of ambient conditions have demonstrated that, because of these combined problems, routine TEOM underestimate PM_{10} measurements by up to 35%, when compared with the EN12341 reference method. This underestimation is more severe in winter than in summer, because in summer the ambient and instrument temperatures are more comparable. The advantage of using this method is the online measurement with long-term stability up to several months and the good agreement with filter samplers when used with appropriate RH control or correction. On the contrary, the disadvantages of the standard TEOM measurements are due to influence of the chemical composition of the aerosol particles, if used according to factory settings, and the impossibility of knowing the chemical composition of aerosol after sampling, as it is possible to do using the gravimetric method.

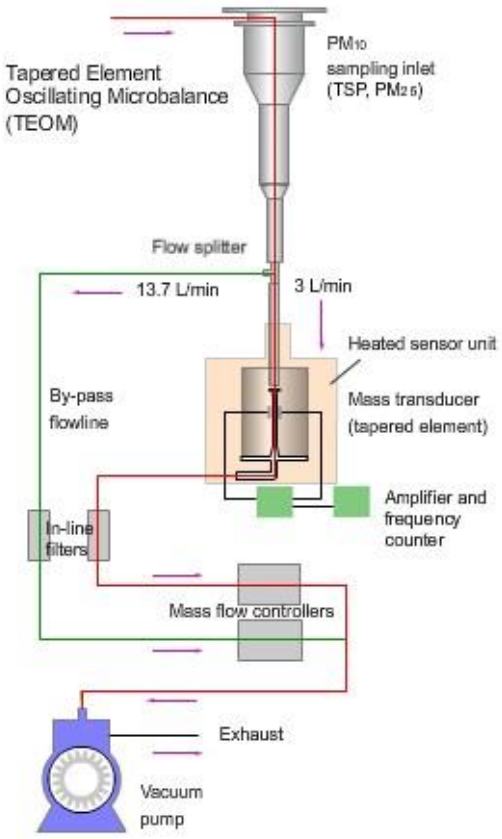

Fig 3.3 TEOM schematic diagram (QLD gov).

Beta gauge technology is used to determine the mass of atmospheric particulate collected on a filter by measuring the relative change in the β-particle intensity when passing through the clean filter and then loaded with the collected particle mass. Beta gauges have been used for mass determination for a long time. Such a system has been found useful for the measurement of aerosol mass concentration in the occupational environment.

The general design of a beta gauge is shown in Fig. 3.4. The system consists of a β source, a detector, and a filter holder. The radionuclide in the β source is normally chosen such that β-particle emission is the predominant mode of decay. Its half-life should be sufficiently long so that decay correction over the duration of a measurement can be disregarded and there is no need to frequently replace the source (Chueinta and Hopke 2001).

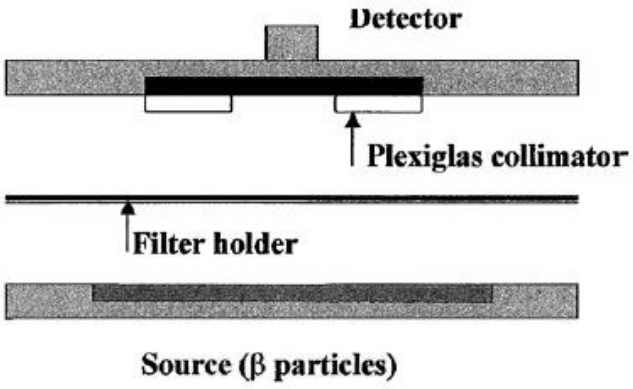

Fig. 3.4 Generalized schematic diagram of the beta gauge. (Chueinta and Hopke 2001)

The common β sources used in beta gauges are ^{14}C ($T_{1/2}$ = 5732 yr, E_{max} = 156 keV) and ^{147}Pm ($T_{1/2}$ = 2,62 yr, E_{max} = 225 keV). Both of these isotopes are practical sources for the measurement of an aerosol sample, which is generally a thin specimen in the 1 mg/cm^2 to 10 mg cm^{-2} range. The advantages of this method are the possible online measurement with the long-term stability of the source, up to one year, and the good agreement with the gravimetric method.

The instrument that uses the light-scattering physical principle to measure all PM fractions less than or equal to 10 μm on real-time basis devices is called aerosol spectrometer. This type of instrument assumes particles with a spherical shape and then calculates the PM_{10} and $PM_{2.5}$ mass from the obtained volume distribution. The aerosol spectrometer consists of a total aerosol inlet and an optical bench with an integrated laser in a chamber connected with a sampling pump at constant airflow. The sampled particles are measured by the physical principle of light scattering, as schematically shown in Fig. 3.5. The extent of light-scattering through the presence of particles in the sample air is measured by a photodetector. The signal of the photodetector is converted to a mass concentration by using a calibration constant. This calibration constant is pre-set in the factory using a specific calibration aerosol. Light-scattering devices are usually portable, have an internal pump, are equipped with a battery and data storage, and are able to provide continuous data. Some devices are able to determine several mass fractions (e.g., PM_{10}, $PM_{2.5}$, PM_1) at the same time or count the number of particles in a range of size channels.

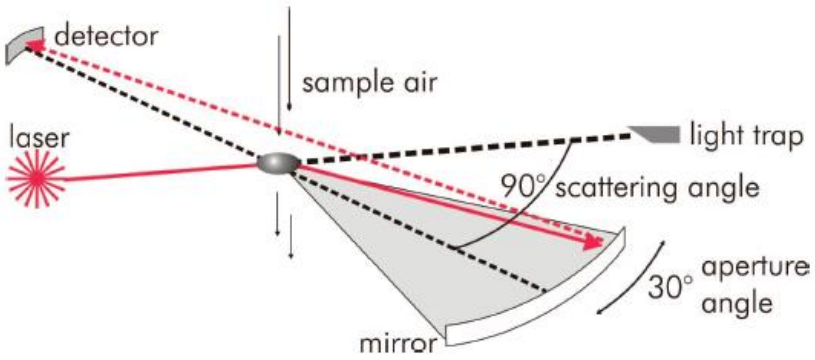

Fig 3.5 Measurement principle of the aerosol spectrometer (Grimm and Eatough 2009).

3.3 Microwave-assisted sample digestion for the element assay

Once the particulate matter has been sampled (usually on a filter media), a suitable choice of extraction technique is critical in sample preparation as it can affect the subsequent analysis of the sample. Most analytical instruments are unable to handle matrices directly and some forms of pretreatment are required to extract and to enrich the analytes, particularly in food and environmental samples, which are characterized by complex matrices and the presence of trace and ultra-trace amounts of analytes. The most frequently mentioned problems arising in preparing samples for analysis are usually the expense in terms of time and reagent consumption, loss of analytes and contamination. Ideally, sample preparation should be fast, accurate, precise, and environment-friendly.

For particulate matter filter samples, acidic digestion was the principal sample preparation method for elemental assay. The thermal digestion using a heated plate was the most widely used and recommended method by environmental protection agencies (such as EPA or EEA). For the past two decades, there has been steady progress in extraction technology, resulting in significant improvements to existing methods, as well as the development of new sample preparation techniques such as microwave-assisted extraction (MAE). A characteristic of this technique is the possibility of working at elevated temperatures and pressures to improve the overall extraction efficiency. With its advantages in terms of shorter extraction time, controllable temperature setting and high throughput capability, MAE became one of the most commonly used approaches for the sample digestion before the instrumental analysis.

3.4 Metal content determination

Toxic particles components are complex mixtures of solids or liquids with different characteristics (e.g., mass, size, shape, surface area, chemical composition, acidity, solubility). Heavy metals are a major source of environmental pollution caused by anthropogenic activities and are well known as a considerable risk to human health and wildlife. Studies about both single and mixed metal particles have shown that, due to the extensive industrial use, heavy metal pollution spans in many ecosystems and many aquatic, marine and terrestrial organisms are constantly exposed to complex metal mixtures and the associated toxicities (Daus et al. 2009). As regards the atmosphere, particulate matter is the carrier of metals reaching the internal lung structure and its content determines its potential health hazard.

Heavy metals (e.g., Cr, Mn, Ni, Cu, Zn, As, Cd, and Pb) have been used by humans for thousands of years. The International Agency for Research on Cancer (IARC) classified As, Ni, Cd, and Cr as class I carcinogenic contaminants. Human beings exposed to As via drinking water show excess risk of mortality due to lung, bladder, and kidney cancer, with the risk increasing the time of exposure. In addition, those exposed to As by inhalation, such as smelter workers, pesticide manufacturers, and miners in many different countries, consistently demonstrate an excess risk of lung cancer (Järup 2003). Cd exposure was reported to be related to chronic renal failure (Hellström et al. 2001), while Pb inorganics compounds were classified as class II (B) carcinogens (i.e., ‘possible human carcinogen'). Moreover, the risks of spontaneous abortion, the reduced fetal growth (preterm delivery, low birth weight), and reduced offspring neurobehavioral development may be related to high levels of parental Pb exposure (Bellinger 2005). Although Zn, Cu, and Mn were classified as non-carcinogenic contaminants, Zn, for example, as the major heavy metal in airborne $PM_{2.5}$, may cause damage to plasmid DNA.

Elemental chemical analysis of PM is performed using sensitive analytical techniques, mainly it was used the Atomic Absorption Spectroscopy (AAS) but in recent years, Inductively Coupled Plasma (ICP) atomic emission spectrometry (AES) and ICP Mass Spectroscopy (MS) have replaced the traditional AAS methods for the analysis of a wide range of trace elements in PM. Among which the most commonly used analysis of the metals on PM the x-ray fluorescence technique has taken hold in recent years.

3.4.1 ICP–MS and ICP–AES

Inductively coupled plasma-mass spectrometry (ICP-MS) and inductively coupled plasma - atomic emission spectrometry (ICP-AES) are widely used as routine techniques in analytical laboratories for multi-elemental determination at the trace and ultratrace level in liquid samples of a quite different matrix composition.

As a suitable ultratrace analytical technique, ICP-MS was developed by coupling an ICP source at ambient pressure with a quadrupole-based MS instrument by Gray and Date in 1975. At present, due to excellent limits of detection (LODs), ICP-MS is the most frequently used and very popular atomic spectrometric technique for a fast, sensitive multi-element determination at the trace and ultratrace concentration level for a wide variety of liquid samples. This is demonstrated by the rapid growth of ICP-MS installations worldwide, such as different types of quadrupole-based (Q) or double-focusing sector field (SF) instruments (Becker 2005).

Instrumental developments (e.g., SF instruments with multiple-ion collection, introduced 12 years before the insertion of collision and reaction cells in order to reduce disturbing isobaric interferences) improved the ultratrace analytical methods, also in combination with online and off-line separation techniques (high-performance liquid chromatography (HPLC) and capillary electrophoresis (CE)), routine capability, as well as decreasing price and user-friendly maintenance.

The introduction of the reaction/collision cell in ICP-MS instruments (e.g., from Micromass, Perkin Elmer Sciex, Agilent or Thermo Electron) is one of the most significant improvements in ICP-MS instrumentation for more sensitive trace and ultratrace analysis and more precise determination of isotope ratios in comparison to commercial quadrupole ICP-MS without collision cell. The ions collision-induced reaction, formed in the ICP, with molecules or atoms of the collision gas or gas mixture (e.g., He and/or H_2,O_2, Xe, CH_4 or NH_3) introduced into the collision or reaction cell, shows a reduction of the ions' spread energy (‘‘cooling’’) from some eV to <0.1 eV, also in dissociation with the molecular ions and neutralization of disturbing atomic ions of the noble gas used in the plasma (Ar contaminants) (Becker 2005). Tanner and co-workers reviewed collision-induced processes and reaction chemistry in a gas-filled collision cell, resolving interference problems in ICP-MS (Tanner et al. 2002).

In addition to all other atomic spectrometric techniques, ICP-MS also allows a precise, accurate isotope analysis of chemical elements at low concentration range. This outstanding capability of ICP-MS is of interest in trace and ultratrace analysis for the application of

isotope-dilution analysis (IDA), providing the possibility of absolute quantification for elements with two and more isotopes in any sample material, in order to obtain accurate trace-element concentrations. In IDA, one or two enriched isotope tracers of the element of interest (with well-known concentrations) are added to the sample. The determination of trace-element concentration is performed by measuring changed isotope ratios in the sample–spike mixture compared to those in the sample and highly enriched isotope tracer using the equation of IDA.

The ICP source is introduced into atomic spectro-chemistry for the excitation (ICP-AES) or ionization (ICP-MS) of analytes, whereby the plasma is formed in a stream of argon gas flowing through the plasma torch consisting of three concentric quartz tubes. The energy is transferred to the argon gas at atmospheric pressure by means of a cooled induction coil made of copper using a radio-frequency (RF) generator (Fig 3.6). ICP-based instruments mostly operate with 27 or 40 MHz at an RF power of 1–2 kW. In ICP-AES, the energy of electrons and excited argon atoms (via collisions with analytes) is used to convert the atoms and the molecules (formed after desolvation of aerosol and evaporation) into an excited state. If the excited electrons are returned to their ground state, the photons thus emitted are analyzed using an AES instrument. The atomic emission spectra obtained are very complex compared to ICP mass spectra.

In an ICP different types of charged analytes can be formed, such as positively single-charged and double-charged but also negatively charged ions and electrons. For analytical purposes in ICP-MS, only positively charged ions are applied for MS analysis. The double-charged ions (e.g., $^{56}Fe^{2+}$ on m/z = 28 in the determination of $^{28}Si^{+}$) and molecular ions (e.g., $^{40}Ar^{16}O^{+}$ on $^{56}Fe^{+}$) observed in ICP mass spectra in the low percent range can cause isobaric interference problems. The ions are extracted from the argon plasma (at ≈ 100 kPa) by means of an interface (at ≈ 130 Pa) between the sampler and the skimmer cones into the high vacuum of the mass analyzers [quadrupole, double- focusing SF or time-of-flight (TOF)-MS], where the ions are separated according to their mass-to-charge ratio (and energy-to-charge ratio in double-focusing SF instruments). The separated ion beams are detected by photomultiplier or Faraday cups. ICP-MS instruments with multiple-collector systems are advantageous for precise isotope-ratio measurements (e.g., for geochronology or for the study of fine isotope variations in nature) (Becker 2005).

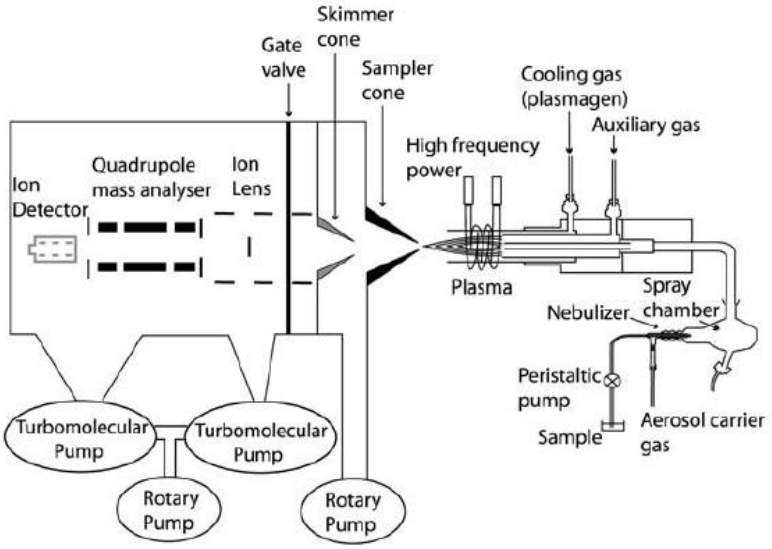

Fig. 3.6 Typical quadrupole ICP-MS scheme (Tyler 2001)

An interesting advantage of ICP-MS and ICP-AES, as multi-element trace analytical methods with a wide dynamic range, compared to other MS techniques with multi-element capability used for the trace analysis of solid samples (such as glow-discharge MS (GDMS) or spark-source MS (SSMS) (Mora et al. 2003)) is that the inductively coupled ion and/or excitation source works at atmospheric pressure. This feature of ICP techniques reduces the time for trace analysis and opens up the possibility of combined techniques for liquids (HPLC, CE and hydride generation (HG)), gases (gas chromatography (GC)- ICP-MS) and also fast trace analysis of solid samples (e.g., electrothermal vaporization (ETV)-ICP-MS and laser ablation (LA)-ICP-MS or LA-ICP-AES). The main advantage of using combined techniques (e.g., for speciation analysis) is that the argon-gas flow rate required for the chromatographic system (HPLC or CE) and also for the ICP can be adjusted accordingly using a suitable nebulization system. Furthermore, time-resolved transient signals of analytes can be measured within a short time.

ICP-MS detection limits are very impressive. Most detection limits are in the 1-10 part per trillion (ppt) range for solutions. ICP-AES has typically detection limits two or three orders of magnitude lower than ICP-MS, with a concentration of most elements in the 1-10 part per billion (ppb) range.

Recently, an ICP-AES spectrometer has shown impressive detection limits in the sub-ppb region for some elements using a high-resolution monochromator with a radially viewed plasma. Other spectrometers have been able to get improvements using an axially viewed ICP, although this view has problematic matrix interferences.

It should be noted, however, that ICP-MS detection limits (1-10 ppt) are for simple solutions having low levels of other dissolved material. For detection limits related to concentrations in the solid, the advantage for ICP-MS can be degraded by up to 50 times because of the poorer dissolved solids capability. Some common lighter elements (e.g., S, Ca, Fe, K, and Se) have severe interferences in ICP-MS, which considerably degrade the detection limits.
ICP technology coupled with other detection systems can be useful for different applications. An example is represented by the use of ICP-MS/MS to determine Pd, Pt, and Rh in the deposited particulate matter on moss samples (Suoranta et al. 2016). Reliable measurements were obtained, either on-mass (^{103}Rh) or by employing a mass-shift approach using NH_3 as a reaction gas (measurements performed at masses 159 for Pd, 171 for Rh and 229 for Pt). Elemental recoveries were quantitative, within stated certified ranges, when test portions of IRMM CRM BCR 723 (road dust) were analyzed. Furthermore, results for moss samples were in agreement with data derived from a more laborious preparatory procedure involving cloud point extraction (CPE) and measurement by quadrupole ICP-MS. Moreover, an electrothermal vaporization (ETV) ICP-MS method for simultaneous determination of halogens (Cl, Br, and I) in airborne inhalable particulate matter (PM_{10}) without any sample preparation was proposed by De Gois et al. (De Gois et al. 2016). Using this method De Gois and coworkers achieved good detection limits with value 0.02 mg g^{-1} (30 ng m^{-3}) for Cl, 0.1 μg g^{-1} (0.1 ng m^{-3}) for Br, and 2 ng g^{-1} (0.003 ng m^{-3}) for I, which are suitable for the analysis of PM_{10} samples.

3.4.2 XRF

Alternative techniques, such as energy dispersive X-ray fluorescence (EDXRF), offer the possibility of direct analysis and may overcome the above-mentioned disadvantages. X-ray based analysis techniques have been intensively implemented for the determination of elements in several environmental matrices such as air filters (Canepari et al. 2009; Öztürk et al. 2010). However, the use of these techniques presents some drawbacks related to potentially complex sample preparation procedures, mainly based on wet chemistry methods to achieve the most complete sample solubilization possible. These types of procedures are quite expensive and time-consuming and may present some limitations for PM analysis, as has been shown for the microwave digestion method (Wang et al. 1996).
Analysis of particles on filters using EDXRF is typically carried out under vacuum for optimal performance, particularly for low Z (atomic number) elements, but this can result in loss of volatile species so hindering further analysis of filter samples by other techniques,

e.g., ion chromatography. Yatkin et al. (Yatkin et al. 2012) demonstrated that operation in an alternative He or air mode gave generally comparable data and that method performance met the data quality objectives of the European Directive for Air Quality for the determination of As and Pb but not of Cd or Ni. This was most likely due to the low loadings of these elements in typical PM_{10} filter samples and the insensitivity of XRFS for measuring Cd. Analysis of size-segregated metal-containing aerosols involved sampling using a nano-MOUDI and pXRFS analysis of the particles collected on the impaction targets. Test aerosols were created from stainless steel substrates using a spark discharge system and impaction targets analyzed both directly and quickly using pXRFS and by ICP-MS following digestion. Data correlated well for the two elements studied, Cr (R^2 = 0.84) and Fe (R^2 = 0.91). This XRFS approach was deemed useful for mass loadings on targets of >2.5 μg. The performance of a commercially available XRFS system (Furger et al. 2017) for in-situ measurement of elements in PM_{10} particles was compared to the analysis obtained on filter samples in the laboratory by ICP-AES and ICP-MS. Filter samples were collected over 24 h using a PM_{10} air sampler located alongside this instrument at the sampling site. To allow direct comparison, the hourly XRFS data were aggregated to 24 h averages. Regression analysis for Ba, Ca, Cu, Fe, K, Mn, Pb, S, Ti, and Zn had an excellent correlation (R^2 > 0.95) although slope values ranged between 0.97 and 1.8 (average 1.28). The authors suggested that the differences were due to factors such as different PM_{10} sampler inlet characteristics, XRF beam attenuation due to particle size effects, the relative effectiveness of the filter digestion method for different elements, and perhaps micro-spatial sampling heterogeneity i.e., the distance between the two sampling inlets.

Total Reflection XRF (TXRF) is a highly sensitive surface elemental analysis based on a particular geometrical setup of XRF that allows the detection of ultra-trace elemental levels in or below the ppb range. In this condition, an enhancement of the fluorescence signal of the sample occurs when a properly prepared sample is placed onto the surface of an X-ray reflector, which is impinged with an X-ray beam at an extremely grazing incidence angle, typically below the critical angle of the reflector in order to minimize the background. Its fluorescence signal is then efficiently collected by a detector placed at 90°, a few millimeters above the reflector surface (Klockenkämper and von Bohlen 2014). TXRF has recently emerged as a good alternative analytical technique in the environmental field, and it has been applied so far to assess pollution levels in air (Borgese et al. 2011; L. Borgese, M. Salmistraro, A. Gianoncelli, A. Zacco, R. Lucchini, N. Zimmerman, L. Pisani, G. Siviero, L.E. Depero 2012). Different sample preparation procedures can be used to analyze PM

composition following TXRF, most of which include a solubilization step to obtain the conventional liquid residue that is then deposited onto the sample carrier. Most of the commercial TXRF spectrometers do not allow performing direct filter measurements due to a high risk of detector damage (contamination on the entrance windows, saturation, etc.). Recently, (Borgese et al., 2011, 2012) proposed an alternative procedure to prepare filter samples for their measurement in TXRF spectrometers and demonstrated its suitability to analyze PM collected on PTFE membrane filters. This sample preparation method allowing for direct analysis leads to easier handling and storage of delicate and thin samples including membranes. The key advantages are simplicity and rapidity of use. X-ray analysis is faster and usually cheaper than ICP-MS because it does not require any sample pre-treatment, producing results comparable to ICP-MS (Yatkin et al. 2012). Moreover, X-Ray Fluorescence does not involve the destruction of the samples being analyzed. This is the greatest advantage, since it allows the subsequent determination of ions or organic contents from the same sample, using other techniques, such as ion chromatography (IC) or gas chromatography. To avoid this problem, ICP-MS is performed by using only one half of the sampling filter, leaving the other half for successive analysis, since the instrumental LOD of ICP is in the order of tens of ppt.

Both the ICP and the XRF techniques can give excellent accuracy and precision. Both techniques have potential problems as any analytical method does. EDXRF and/or Wavelength XRF suffer from matrix and inter-element interference issues, as ICP (AES and MS). With XRF, the standard and sample must be matrix matched with respect to both the matrix and the particle size. In addition, it has been seen that different chemical forms can cause problems such as alkyl Si versus Si oxides in an organic matrix, i.e. the elemental composition is similar, yet results for the methyl silicon are much lower than oxygenated silicon due to scattering. Furthermore, the analyte emission intensity is enhanced by matrix elements lower in atomic number and suppressed by analytes higher in atomic number.

3.5 Elemental and Organic Carbon determination

Although most countries that routinely measure air quality have established standards related to the mass of particulate matter below a diameter of 10 µm or 2.5 µm, very few countries have regulations related to acceptable levels of elemental carbon (EC). It is interesting to note that the European Union has had a requirement to monitor EC in $PM_{2.5}$ at selected rural background sites since mid-2010 (Directive 2008/50/EC 2008). There is a technical report

(CEN/TR 16243, 2011) on thermal optical transmittance/reflectance methods for measuring EC and OC, wherein thermal protocols (i.e. NIOSH-like, NIOSH 5040, IMPROVE, and EUSAAR 2) are recommended. These methods generally measure the same amount of total carbon (TC), whereas TC discrimination into OC and EC is operationally defined with large differences in the amount of OC and EC measured by different methods (e.g. Schmid et al. 2001; Seung et al. 2005). IMPROVE and NIOSH have been the most widely used thermal-optical protocols in the atmospheric science community. Traditionally, the IMPROVE protocol (Chow et al. 1993) has been applied to samples from non-urban background sites in the US IMPROVE network; in 2005, the IMPROVE network started to apply the IMPROVE a protocol, an only slightly modified version of IMPROVE thanks to refined measures of the sample temperature (Chow et al. 2007). The EPA/NIOSH (or STN) protocol (Peterson and Richards 2002) has been applied to samples from urban sites in USA-EPA's Speciation Trends Network. These protocols differ in temperature set points higher for EPA/NIOSH (e.g. the highest temperature in He is 900 °C) than for IMPROVE (e.g. the highest temperature in He is 550/580 ◦C) and in the residence times at each temperature step typically longer for IMPROVE than for EPA/NIOSH. Moreover, the IMPROVE protocol uses the reflectance method to correct for charring, while the EPA/NIOSH protocol has adopted the transmittance method.

For the thermal optical transmittance (TOT) method with the Sunset analyzers (Birch and Cary 1996), a punch (typically 1 or 1.5 cm^2) of a quartz fiber filter sample is placed in the quartz oven of the instrument. In the initial phase of the analysis, which takes place in a pure He gas stream, the filter punch is heated in different series of steps (according to the different temperature protocols, as reported in Table 3.1). The desorbed carbonaceous vapors are catalytically oxidized into CO_2 (by a MnO_2 catalyst), which is then transformed into CH_4 (in a Ni-firebrick methanator oven, see Fig. 3.7) and subsequently measured with a flame ionization detector (FID). Ideally, all OC would desorb in the inert gas stream while EC would combust in the oxidizing atmosphere at high temperature. In reality, thermally unstable organic compounds pyrolysis in the He-mode forms pyrolytic carbon (PC) which then usually desorbs off the filter in the oxidizing atmosphere, like native EC. Incorrectly accounting for PC formation can significantly bias the discrimination between OC and EC (e.g. Schmid et al. 2001; Schauer et al. 2003). To correct for pyrolysis, the optical properties of the sample are monitored before and during the analysis with a laser beam. Laser light of 670 nm is passed through the filter punch and the light transmission is continuously measured in order to correct for pyrolyzed OC. In the second phase, which takes place with

a 98% He / 2% O_2 mixture as a carrier gas, the filter punch is further heated, and the CO_2 evolved is measured by FID in the form of CH_4 (as in the first phase). When the light transmission through the filter punch equals that seen at the beginning of the first phase, the OC / EC split is set to correct for pyrolytic carbon (PC); the CO_2 measured in the first phase and during the second phase prior to the split is considered OC (including the PC), whereas the CO_2 measured after the split is considered the "original" EC. After the end of the second phase, while still in a He / O_2 mixture, a known amount of CH_4 gas is injected through a loop for internal calibration.

The function of the laser transmittance/reflectance is to correct for pyrolysis/charring of OC to PC, which can take place when OC is heated in the first phase of the analysis. Not correcting for charring leads to an underestimation of OC and a corresponding overestimation of EC. This correction is made by continuously monitoring the reflectance and/or the transmittance of the punch, which is largely dominated by PC and EC. As charring takes place (i.e. PC is formed), the reflectance/transmittance drops, whereas it increases when EC and/or PC oxidized. Hence, the correction is made by determining the amount of carbon oxidized in the second phase that is necessary to return the reflectance/transmittance back to the initial value before charring started. This approach assumes either that PC oxidizes before the original EC in the second phase, or that the light extinction/reflection per unit mass of PC generated during the analysis is the same as the light extinction/reflection per unit mass of the original EC, at least until the reflectance/transmittance regains its initial value. Such assumptions are unlikely to be met and therefore, there is inherent uncertainty in the split point between EC and OC. In any case, despite the problems, thermal optical transmittance is the main method used for the scientific community.

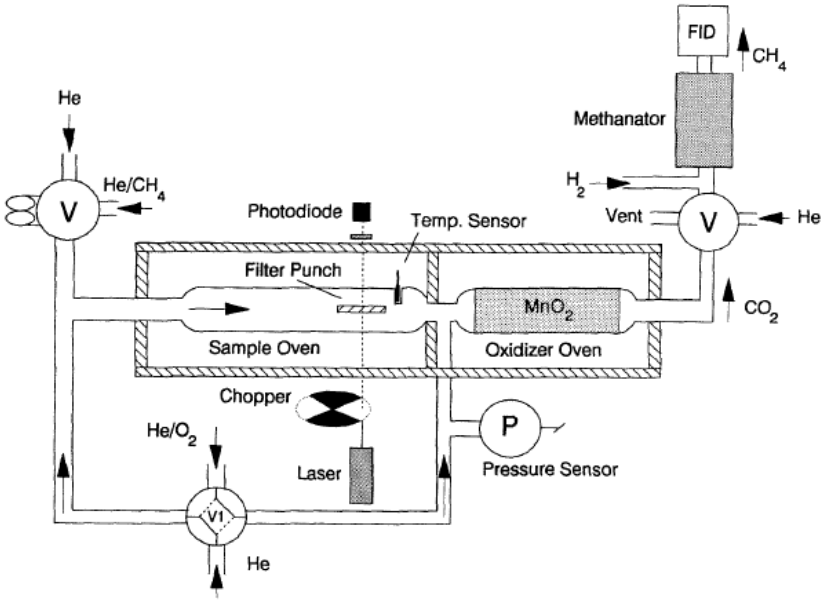

Fig. 3.7 Schematic of thermal-optical instrumentation. (Birch and Cary 1996)

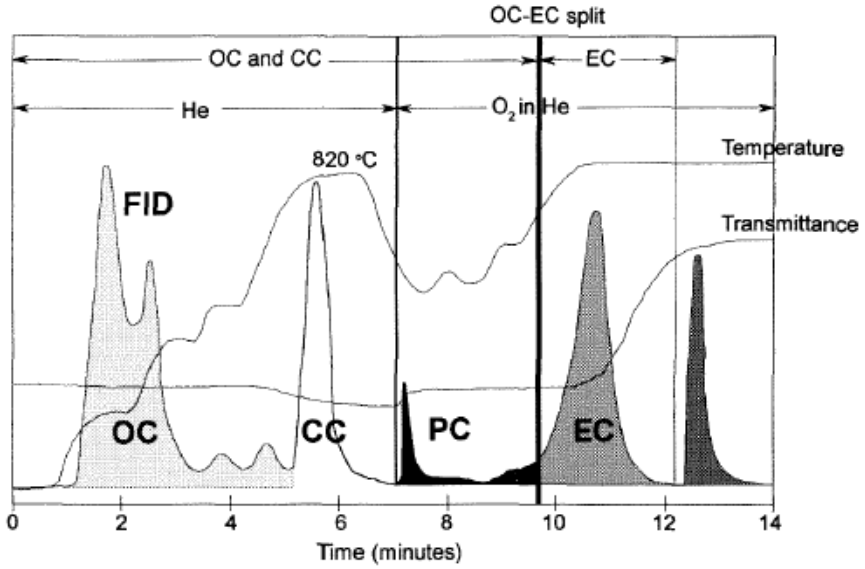

Fig. 3.8 Example of a thermogram for a sample containing rock dust (carbonate source) and diesel exhaust. Peaks correspond to organic (OC), carbonate (CC), pyrolytic (PC), and elemental (EC) carbon. The final peak is a methane calibration peak (Birch and Cary 1996).

	EPA/NIOSH[b]	NIOSH 5040	IMPROVE[c]	EUSAAR_1 short	EUSAAR_1 Long	He4-550	He4-750	He4-850	EUSAAR_2
STEP	*T*, duration °C, s	*T*, duration °C, s	*T*, duration °C, s	*T*, duration °C, s	*T*, duration °C, s	*T*, duration °C, s	*T*, duration °C, s	*T*, duration °C, s	*T*, duration °C, s
He1	310, 60	250, 60	120, 150–580	200, 120	200, 180	200, 180	200, 180	200, 180	200, 120
He2	475, 60	500, 60	250, 150–580	300, 150	300, 240	300, 240	300, 240	300, 240	300, 150
He3	615, 60	650, 60	450, 150–580	450, 180	450, 240	450, 240	450, 240	450, 240	450, 180
He4	900, 90	850, 90	550, 150–580	650, 180	650, 240	550, 240	750, 240	850, 240	650, 180
He/$O_2$1[a]	600, 45	650, 30	550, 150–580	550, 240	550, 300	550, 300	550, 300	550, 300	500, 120
He/$O_2$2	675, 45	750, 30	700, 150–580	850, 150	850, 180	850, 180	850, 180	850, 180	550, 120
He/$O_2$3	750, 45	850, 30	800, 150–580						700, 70
He/$O_2$4	825, 45	940, 120							850, 80
He/$O_2$5	920, 120								

[a] A mix of 2% oxygen in UHP helium.
[b] The temperature program for the EPA/NIOSH method is reported in Peterson and Richards (2002).
[c] The residence time at each temperature in the IMPROVE protocol depends on when the flame ionization detector (FID) signal returns to the baseline to achieve well-defined carbon fractions.

Table 3.1 Temperature protocols used to analyze samples in the Cavalli et al. work: temperature set point and residence time are reported. EUSAAR 2 protocol temperature set points and residence times are also reported (Cavalli et al. 2010).

When determined by optical methods, the refractory carbon is usually referred to as black carbon (BC). Amongst atmospheric aerosols, BC is considered the most efficient light-absorber in the visible spectrum (Bond et al. 2013; and reference therein) with a weak dependence on wavelength. As discussed in Bond et al. (Bond et al. 2013), there is not an established standard method for measuring BC and each BC measurement method is associated with biases and uncertainties. Therefore, the measurement method is one important factor to consider when comparing BC source apportionment results. Refractory BC is measured using laser-induced incandescence and equivalent BC mass (an estimate of BC mass) is measured using optical absorption methods (Bond et al. 2013). The Single Particle Soot Photometer (SP2) provides real-time measurements of the refractory BC content of individual particles by heating particles to vaporization temperatures and detecting refractory BC mass via incandescence; one of the limitations of this instrument involves its lack of detection of particles with diameters smaller than about 80 nm (Bond et al. 2013). Several of the common instruments that provide measurements of equivalent BC (eBC) mass, including the aethalometer, Particle Soot Absorption Photometer (PSAP), and Multi-angle Absorption Photometer (MAAP), use optical absorption methods for the analysis of PM collected on filters.

3.6 Chromatography approaches for ions and organic compound assay

A major challenge in atmospheric chemistry studies is to elucidate the sources, structure, transformation, formation processes, and the fate of the ubiquitous yet poorly understood organic atmospheric compounds. This requires detailed characterization of the size-

dependent chemical composition of the aerosols, which is not a simple task because of the complexity of the molecular composition of organic aerosols.

Ambient PM contains many inorganic elements in the form of ions (sulfate, SO_4^{2-}, nitrate, NO_3^-, chloride, Cl^-) and trace metals, as well as elemental carbon (EC) and a wide variety of organic compounds (organic carbon, OC) and water. The fine fraction is mainly composed of SO_4^{2-}; NO_3^-, OC, and EC. Whereas SO_4^{2-} and NO_3^- are produced within the atmosphere via oxidation of SO_2 and NOx, OC is mainly produced by oxidation of volatile organic compounds (VOCs). Particles larger than 2.5 μm typically contain elements from soil and sea salt (Finlayson-Pitts and Pitts 2000; Zhang et al. 2000; Jacob and Winner 2009). Actually, from the inorganic point of view, atmospheric aerosols can be seen as mixtures of many components including especially inorganic acids (e.g., H_2SO_4 and HNO_3), their salts [e.g., $(NH_4)_2SO_4$, $(NH_4)HSO_4$, Na_2SO_4, NH_4NO_3, $NaNO_3$, NaCl, KCl], and water (Charlson et al. 1978; Finlayson-Pitts and Pitts 2000). Inorganic ions such as NH_4^+; SO_4^{2-}; and NO_3^- are major components of ambient particulate matter and ion chromatography (IC) has become one of the most widely used analytical methods for the determination of ionic concentrations in ambient particles.

Ion chromatography is the most precious technique used in the off-line mode in order to determine concentrations of water-soluble ions in stabilized aqueous extracts of sampled atmospheric aerosols (chloroform is usually added as a biocide to inhibit bio-decomposition processes). The coupling of ion-exchange columns with the suppression of eluent conductivity allows the development of analysis methods for a variety of analytes, (Small et al. 1975) including Li^+, Na^+, K^+, Rb^{2+}, Cs^{2+}, NH_4^+, Ca^{2+}, Mg^{2+}, F^-, Cl^-, Br^-, I^-, NO_3^-; NO_2^-; SO_4^{2-}; SO_3^{2-}; PO_4^{3-}, and many amines, quaternary ammonium compounds, and organic acids. Especially for certain critical species such as SO_4^{2-}; NO_3^-, and Cl^-, sampling artifacts during particulate matter collection can be quite severe. In such cases, it is quite difficult to show conclusively the existence of an inorganic species in a specific form (Finlayson-Pitts and Pitts 2000) and the analysis by ion chromatography of the water-soluble ionic constituents of atmospheric aerosols becomes challenging. (Mulik et al. 1976) were among the first to undertake a successful application of ion chromatography to the off-line analysis of total water-soluble SO_4^{2-} and NO_3^- in ambient aerosols. More recently, a system facilitating direct on-line analysis of collected atmospheric aerosol samples has been developed and improved (Orsini et al. 2003).

The technique is known as PILS-IC and consists of an ion chromatograph (IC) coupled to a particle-into-liquid sampler (PILS). Proper selection of columns and elution phases allows

the separation of 9 major inorganic species (Na^+, NH_4^+, K^+, Ca^{2+}, Mg^{2+}, Cl^-, NO_3^-; NO_2^-; SO_4^{2-}) in 3.5–4 min, while acetate, formate, and oxalate can also be analyzed in 15 min. The collection efficiency of the PILS unit, for particle diameters between 0.03 and 10 mm, is higher than 97%. In the most recent papers dealing with the ion chromatographic analysis of water-soluble ionic constituents of atmospheric aerosols, the main reported cations are Na^+, NH_4^+, K^+, Ca^{2+}, and Mg^{2+}. The most often identified and quantified anionic species consist of inorganic anions, such as F^-, Cl^-, Br^-, NO_3^-; NO_2^-; SO_4^{2-}; SO_3^{2-} and PO_4^{3-}, and of organic anions present as mono- (formate, Fo^-, acetate, Ac^-, propionate, Pr^-), di-(oxalate, Ox^{2-}, malonate, Ma^{2-}, succinate, Sc^{2-}, glutarate, Gt^{2-}), and keto- (pyruvate, Py^-) carboxylate forms. The analysis of mono-, di-, and ketocarboxylic anions deserves special attention because these compounds are ubiquitous chemical constituents of the troposphere and contribute to both the acidity of precipitation and to the particulate organic carbon budget. They may also act as condensation nuclei (CN) and cloud condensation nuclei (CCN) (Matsumoto et al. 1998; Yu 2000).

Organic aerosol components are considered to account for a large (sometimes even the dominant) fraction of air particulate matter. The composition of the organics is very complex, with hundreds of compounds being detected in air particulate matter, even in remote areas with very little contributions from combustion processes (Finlayson-Pitts and Pitts 2000). Many organic constituents may influence the physical and chemical properties of the aerosol particles and thus affect the atmosphere and climate through interaction with reactive trace gases, water vapor, clouds, precipitation, and radiation. Among the organic compounds in the most comprehensive investigation, organics usually identified include organic acids (e.g., capric acid, palmitic acid, stearic acid, oleic acid, linoleic acid), aliphatic hydrocarbons (e.g., n-alkanes in the C10–C35 range), polar compounds (e.g., coumarin, xanthone, anthrone, flavone, carbazole), volatile organic compounds, VOCs, (e.g. 1-pentene, m,p-xylene, styrene, trichloroethylene) and polycyclic aromatic hydrocarbons, PAHs, (e.g., naphthalene, acenaphthylene, acenaphthene, fluorene, anthracene, chrysene, benzopyrene).

Polycyclic aromatic hydrocarbons are a group of over 1,000 compounds, a few of which occur in considerable amounts in the environment and food (Fig. 3.9). PAHs comprise fused aromatic rings and do not contain heteroatoms or carry substituents. PAHs containing up to four fused benzene rings are known as light PAHs and those containing more than four benzene rings are called heavy PAHs. Heavy PAHs are more stable and more toxic than light ones. PAHs are lipophilic in nature; nevertheless, some of them can dissolve quite well in water. Most PAHs in the environment derive from incomplete burning of carbon-containing

materials, such as oil, wood, garbage or coal. A maximum amount of PAHs is formed when materials burn at temperatures in the range 500–700 °C, as in wood fires or cigarettes.

In the Directive 2004/107/EC and subsequently in the Directive 2008/50/EC on ambient air quality and cleaner air for Europe, the European Council regulated the maximum concentration of some PAHs in the PM, setting target values in 1 ng m^{-3} in one year with the aim of minimizing harmful effects on human health, paying attention to sensitive populations, and the environment as a whole.

The European Committee for Standardization (CEN) Working Group (TC264 WG21), which developed and wrote the reference method for benzo[a]pyrene measurement in the air (the PAH subject to target-value assessment in Europe), found relatively little difference in performances between a number of solvents tested for their extraction ability. Indeed, most solvents and solvent mixtures are allowed by the standard method, as long as they achieve satisfactory recoveries when analyzing NIST Standard Reference Material 1649a. However, based on the extraction technique that is used, the standard method recommends the following "preferred solvents":

(1) Extraction under reflux: toluene

(2) Soxhlet extraction: toluene, dichloromethane, 1:1 hexane:acetone mixture

(3) Microwave extraction: 1:1 hexane:acetone mixture

(4) Accelerated solvent extraction: toluene, dichloromethane, 1:1 hexane: dichloromethane mixture

(5) Ultrasonic extraction: toluene, dichloromethane

In order to estimate health effects of different pollutants, the toxicity equivalency factor (TEF) methodology was developed by the U.S. Environmental Protection Agency (EPA) and adapted for PAH compounds (Nisbet and LaGoy 1992). TEF represents the toxicity of an individual PAH compound relative to the reference chemical—benzo(a)pyrene (BaP). Benzo(a)pyrene is the most studied PAH for carcinogenic properties (Collins et al. 1991) and, for this reason, it was selected as the reference compound. To calculate the toxicity potential of a specific PAH, its concentration is multiplied by the determined TEF value. The total potential carcinogenic potency of PAH mixtures in air samples is determined by summing up concentrations of individual PAHs, which are multiplied by the determined TEFs of individual PAHs (Nisbet and LaGoy 1992). The International Agency for Research on Cancer (IARC) classifies PAHs by their toxic potencies as probable (2A) and possible (2B) carcinogens (IARC Working Group on the Evaluation of Carcinogenic Risks to Humans 2010) and the following PAHs have been highlighted: benzo(a)pyrene,

dibenzo(a,h)anthracene, benz(a)anthracene, chrysene, benzo(b)fluoranthene, benzo(k)-fluoranthene, benzo(g,h,i)perylene, and indeno(1,2,3-c,d)pyrene. BaP is also regarded and recommended as a marker in Air Quality Standards. However, the uncertainties surrounding the use of BaP as a marker for carcinogenic PAHs has also been a subject of concern regarding the occurrence of carcinogenic PAHs in ambient air. With this intent, several states such as the UK, the United States, and Europe have therefore also recommended covering more PAHs than BaP in the analyses.

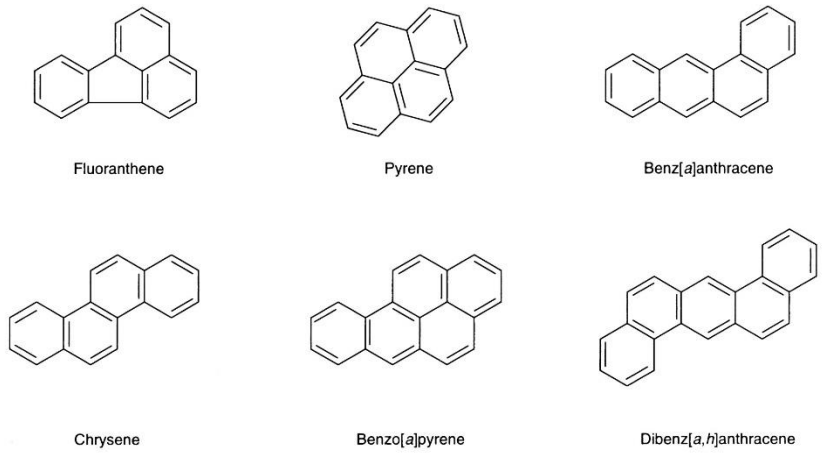

Fig. 3.9 Some example of PAH molecules.

Several methods have been used for sampling and analysis of aerosol particles, from online to on-site and off-line analyses. The off-line analysis relies on separate sampling and analysis. Several methods can be used for sampling, the most common ones being sampling on filters. For the analysis of organic compounds, such as VOCs and PAHs in the air, gas chromatography (GC) has been the most common analytical separation approaches in combination with several sampling and sample-preparation methods. The preference for GC over other systems (e.g., liquid chromatography (LC)) has been demonstrated by such factors as its greater selectivity, resolution, and sensitivity (Poster et al. 2006). To improve selectivity and ensure the robustness of sample identification and quantification, GC is often used in combination with mass spectrometry (MS) to produce very powerful GC-MS coupled techniques, which are able to yield even lower limits of detection (LODs) than GC alone.

Derivatization is typically required before analysis of polar compounds, such as alcohols, carboxylic acids, and amines. Typical derivatization methods include silylation, the formation of carbamates with isobutyl chloroformate or O- benzylhydroxylamine. Some of

the derivatization methods can even be incorporated in the sampling step or carried out during the thermal extraction. The conventional methods are, however, performed after solvent extraction (and evaporation of solvent). Modern instruments enable derivatization to be performed automatically in the autosampler unit, thus minimizing manual steps and improving the reliability of the procedure.

Solvent-based extraction is the most common sample preparation method for GC analysis, but thermal desorption methods have also been widely used. TD-GC–MS methods have been used, e.g., for determination of PAH and alkanes (Ho et al. 2008), of semi-volatile organic components (Falkovich and Rudich 2001), and of more polar compounds including alcohols, ketones, aldehydes, and organic acids (Ho and Yu 2004; Tobias et al. 2007). The latest commercial thermal desorbers enable quantitative recollection of split flow (both tube and trap desorption split flow) for repeat analysis and have built-in internal-standard-addition capabilities. Thus, the main challenges of TD-GC methods, i.e. one-shot analysis and quantitation with internal standards, are avoided.

In most applications, a single-quadrupole system with electron ionization (EI) has been used. The GC–EI-MS spectrum is highly useful in the identification of organic compounds because of the large commercial spectral libraries for EI-MS spectra. However, if the compound spectrum is not found in the spectral libraries identification is a challenge because, as a result of the heavy fragmentation, the molecular ion is often not detected. Soft ionization using chemical ionization (CI) enables detection of molecular ions and, therefore, for identification purposes a combination of GC–EI-MS and GC–CI-MS data, particularly with HRMS systems, is a powerful tool, combining the information of the fragmentation and the molecular ion.

On-site measurements for aerosol analysis have mainly been based on two different approaches, TD-GC and particle-into-liquid-sampler-LC systems (PILS-LC). The GC-based systems have been used for relatively broad characterization of semivolatile compounds in aerosols, whereas the PILS-LC systems are used mainly for targeted analysis of specific water-soluble compounds, for example, carboxylic acids and ionic species. The GC-based approach has been used for the analysis of semivolatile organic compounds in aerosol particles. The approach is based on a combination of collection by particle impaction with analysis by thermal desorption and GC–MS (thermal-desorption aerosol gas chromatograph, TAG) (Williams et al. 2006).

In the TAG system, ambient atmospheric particles, typically PM2.5 or PM1, are collected by means of humidification and inertial impaction. The sample is then thermally desorbed,

and analyzed by GC–MS. The sample collection is done concurrently with the analysis of the prior sample, with sampling time typically approximately 60 min (Worton et al. 2011). A sophisticated version of the TAG includes GC × GC instead of a single GC (Fig.3.10) (Goldstein et al. 2008; Worton et al. 2012).

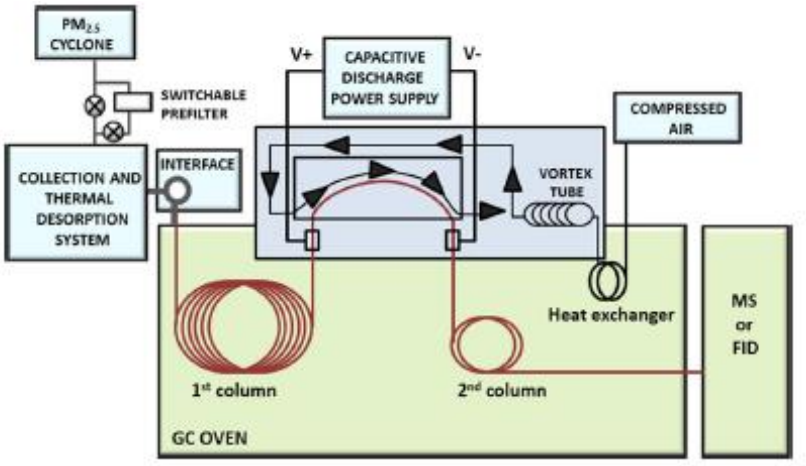

Fig. 3.10 TAG-GC × GC–MS system (Parshintsev et al. 2010)

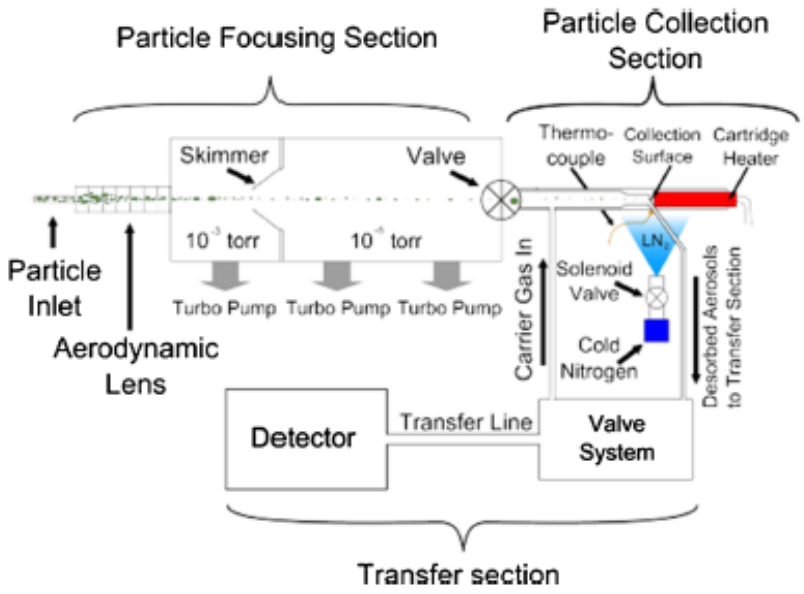

Fig. 3.11 Schematic of ACM instrument with three main sections: aerodynamic lens and the vacuum system, the particle-collection section, and the transfer section (Pratt and Prather 2012).

A recent study presented a novel type of sampling system connected on-line with GC–MS (Fig.3.11) (Hohaus et al. 2010). The collection is achieved by a high-vacuum environment on a collection surface (max. −165 °C). After sampling, the analytes are thermally desorbed in a flow of carrier gas and transferred into the GC–MS for analysis. The system has been

used for the collection and analysis of particles in the size range of 70-500 nm. The results have been in good agreement with offline measurements.

4 Receptor modeling methods for source apportionment

In the field of atmospheric sciences, source apportionment (SA) models aim to re-construct the impacts of emissions from different sources of atmospheric pollutants, e.g., particulate matter (PM), based on ambient data registered at monitoring sites.

There are three key approaches for source apportionment including the use of emission inventories and dispersion models, receptor models and monitoring data (Viana et al. 2008). Dispersion models are often used for estimation of a source's impact on air quality in an area/region and use emission rates and dispersion factors together with local topography and meteorology for estimation of source impacts (Cooper and Watson 1980; Henry et al. 1984). Receptor models (RMs) are used to estimate the contribution of different sources to ambient PM concentrations based on measurements and subsequent chemical analysis.

The fundamental principle of receptor modeling is that mass conservation can be assumed and a mass balance analysis can be used to identify and apportion sources of contaminants in the atmosphere. The approach to obtaining a data set for receptor modeling is to determine a large number of chemical constituents such as elemental concentrations in a number of samples. Once obtained this information, a mass balance equation can be written to account for all *j* chemical species in the *i* samples as contributions from *k* independent sources:

Eq. 4.1 $$x_{ij} = \sum_{k=1}^{p} g_{ij} f_{kj}$$

where x_{ij} is the j^{th} chemical species concentration measured in the i^{th} sample, f_{kj} is the concentration of the j^{th} species in material from the k^{th} source, and g_{ik} is the airborne contribution of material from the k^{th} source contributing to the i^{th} sample. This basic conceptual model can then be fitted to the various kinds of available data.

Therefore, receptor models can be defined as models that utilize physicochemical speciation data to quantify source contributions based on the principle of mass balance. RMs use the information on chemical composition at receptor sites and in source emissions to reconstruct the observed ambient concentrations and apportion the mass to different emission sources (Henry et al. 1984; Hopke 1991a). Such models form a subset of SA techniques and apportion the pollutant concentrations based on the measured ambient air data and the knowledge about the composition of the contributing sources (Henry et al., 1984). Gordon (Gordon 1988) and Hopke (Hopke 1991b) provide a historical perspective of the development of the RMs. The key outputs of the RMs are the percentage contributions of

different sources to pollutant concentration. These models have been used for identification of sources and their respective contributions to airborne particulate matter across the world (Harrison et al. 1997; Kumar et al. 2001; Stone et al. 2010; Kong et al. 2010; Clements et al. 2014). Such models provide relevant information for the development of air pollution management and control programs, validation of dispersion models and are particularly helpful in cases where complete emissions inventories are not available (Hopke 1991a; Watson et al. 2012).

The chemical mass balance (CMB) model assumes knowledge of the composition of the emissions for all relevant sources. If changes of the source profiles between the emitter and the receptor may be considered minimal, CMB can be considered as the ideal receptor model. However, these requirements are almost never completely fulfilled; therefore, pure CMB approaches are often problematic. One important characteristic of CMB is that secondary aerosols must be included not as the components of emission source profiles but as specific, single chemical compounds. This absence of mixture with other tracer elements is often regarded as a limitation and may lead to misinterpretation of results.

Principal component/factor analysis, e.g., principal component analysis (PCA), positive matrix factorization (PMF) or UNMIX model, attempts to apportion the sources on the basis of observations (internal correlations) at the receptor site alone. These are commonly used tools because the software to perform this type of analysis is widely available and detailed prior knowledge of the sources and source profiles is not required. The choice of the model dimension and the search for non-negative solutions by axis rotations can be based entirely on mathematical criteria. Nevertheless, it has been suggested that factor analysis attempts to get more information out of atmospheric data than is really there (Henry 1987). Furthermore, it is a common problem that the resulting components or factors may represent mixtures of emission sources, as opposed to clearly independent source profiles. Source signatures that change with time are a limitation for this and other types of receptor models.

To combine the advantages and reduce the disadvantages of CMB and factor analysis hybrid models have been developed. Examples are confirmatory or target transformation factor analyses, which offer some control of the solutions by "fixing" or "freeing" specific parameters, set according to the theoretical expectation of the researcher (Hopke 1988; Gleser 1997). With a constrained physical receptor model such as COPREM (Wåhlin 2003), an initial profile matrix with the main characteristics of known sources as columns is used, and a priori knowledge about the character of the sources can be used to achieve a solution with a sufficient number of sources. The multilinear engine (ME) (Paatero 1999), can solve

multilinear problems with the possibility of implementing many kinds of constraints using a scripting language.

The main objective of receptor models is, therefore, to identify the possible sources of PM (if not assumed already from the source profiles) and to obtain data on their contributions to the bulk PM mass. Even human exposure to these pollution components has been evaluated to assess their health effects and risks (Watson et al. 2002; Hopke et al. 2006; Ilacqua et al. 2007). Furthermore, policy-makers require sound scientific knowledge of the PM sources and their contributions to atmospheric PM levels and associated health risks for the development and implementation of policies to protect human health and the environment. Thus, the information provided by receptor models is fundamental to the design of effective mitigation strategies on the local scale and mesoscale.

A number of receptor models are used for source apportionment including semi-qualitative methods, such as the enrichment factor (EF) analysis and the diagnostic ratio analysis, quantitative methods, such as Chemical Mass Balance (CMB) model, multivariate statistical models, such as Principal Component Analysis (PCA) and Positive Matrix Factorization (PMF), Multilinear Engine (ME), Constrained Physical Receptor Model (COPREM), and UNMIX and hybrid models, such as Target Transformation Factor Analysis (TTFA).

4.1 Chemical mass balance model

CMB, as described by. Watson et al. (Watson et al. 1997), uses an effective variance least squares (EVLS) approach to solve Eq. 4.1 on the basis of known source profiles (f_{kj}) and measured receptor species concentrations associated with ambient PM (x_{ij}). In the effective variance least square, the weighting is inversely proportional to the square of the uncertainty in the source profiles and ambient data for each species according to Eq. 4.2:

Eq. 4.2
$$(W_e)_{jj} = \frac{1}{\sigma_j^2 + \sum_{k=1}^{p} \sigma_{jk}^2 g_k^2}$$

where σ_j is the uncertainty of the measured ambient concentration, x_i, and σ_{jk} is the measurement uncertainty of species *j* emitted by source *k*. The accuracy of CMB modeling results strongly relies on the availability of source profiles, which ideally must be from the region where the receptor is located and that should be contemporary to the underpinning ambient air measurements.

The CMB modeling procedure requires:

1) identification of the contributing source types;
2) selection of chemical species or other properties to be included in the calculation;
3) estimation of the fraction of each chemical species which is contained in each source type (source profiles);
4) estimation of the uncertainty in both ambient concentrations and source profiles;
5) solution of the chemical mass balance equations.

The CMB is implicit in all factor analysis and multiple linear regression models that intend to quantitatively estimate source contributions. These models attempt to derive source profiles from the covariation in space and/or time of many different samples of atmospheric constituents that originate in different sources. These profiles are then used in a CMB to quantify source contributions to each ambient sample

Because of CMBs sensitivity to collinearity of the source profiles, which impedes the mathematical solution of the mass balance, often it is necessary to merge sources into groups of source types in order to produce composite profiles. This exercise automatically builds in intrinsic assumptions into the CMB model. Thus, it is useful to characterize the sensitivity of the produced source contribution estimations to the lumping of sources and to the selection of receptor compounds by running a series of scenarios. In compensation for the requirement of source profiles as input, CMB can be carried out for a limited number of samples. However, small datasets may not fully characterize the source-receptor relationships at a given site.

A compilation of measured volatile organic compound (VOC) and particulate matter chemically speciated source profiles is available from the EPA in the SPECIATE database (US EPA, OAR). However, very few comparable data are available for other locations around the world. There have been some profiles developed in Europe, including for motor vehicles (El Haddad et al. 2009), metal smelting (El Haddad et al. 2011b), metallurgical coke production (El Haddad et al. 2011a), and shipping/heavy fuel oil combustion (El Haddad et al. 2011b). Few or no profiles have been measured in developing countries, and there has been a tendency to apply U.S. profiles. Although profiles can be selected to provide an acceptable fit to the data, profiles that do not properly reflect the actual compositions of the emissions can lead to serious errors in the resulting source apportionment.

The CMB model assumes that each measured profile has a fixed composition that has been measured at the source with some given measurement error. The EVLS model requires an uncertainty estimate for each of the ambient and source profile concentrations and propagates those errors into an iterative solution that calculates the contribution values and

their associated uncertainties. However, several aspects of the data used in this model have had only limited consideration in CMB analyses (Hopke 2016).

For example, secondary inorganic species are typically used in the model as pure ammonium sulfate and ammonium nitrate. However, it exists evidence on the formation of secondary organic aerosol (SOA) attributed to catalysis from the acid surface of acidic sulfate particles (George et al. 2015). Thus, it could be anticipated that there would be organic carbon associated with the secondary inorganic compounds through heterogeneous chemistry either on the surface of the particle or in cloud or fog water where the acidity catalyzed the formation of lower volatility organic species that remained with the inorganic material after the evaporation of the liquid water (Blando and Turpin 2000; Lim et al. 2010). Therefore, the gas-to-particle process can be considered as a "source" that gives rise to both inorganic and organic species in the particulate matter.

Source profiles are not readily available for most receptor sites. Thus, multivariate models that on the contrary of CMB do not require experimental source profiles as input (eigenvalue analysis and factor analysis) are widely popular and will be described below. It is a common misunderstanding that such methods require less a priori knowledge of the modeled receptor sites. Indeed, the determination of the optimal number of factors, the assessment of rotational ambiguity, and the interpretation of factors as potential sources are issues that require not only a good command of the software tool but also a profound qualitative understanding of emissions in the study area.

4.2 Multivariate methods

In the multivariate methods, the used model remains the mass balance outlined in Eq. 4.1. However, the number and nature of the sources are unknown and have to be derived from the ambient data. The approach of these methods can be visualized by looking at the scatter plots of two of the measured variables, as shown in Fig. 4.1 (Hopke 2016). The shown values are for samples collected in Gates of the Arctic National Park as described by Polissar et al. (Polissar et al. 1996). These plots illustrate the basis for a geometrical interpretation of multivariate analysis using "edges" as outlined by (Henry 2003). In Fig. 4.1a, the values of Si and Fe lie along a single line, suggesting that only one source contributes to their concentrations, with the obvious source being suspended soil. However, in Fig. 4.1b and 4.1c, it can be observed that there is a spread in the data with an edge showing a source with high K and relatively low Fe and Si. This source would likely be wildfires. There is an edge

near the K and Fe axes that is not denoted by a line, showing that there is K in the soil, but that most of the K in the $PM_{2.5}$ is contributed by the fires. Thus, the points in the space between the edges show samples that are a mixture of soil- and fire-derived particles. In Figure 4.1d, two distinct sources can be observed with very few samples representing mixtures of the two. The high-S source represents long-range transported particles coming from the Soviet Union during the late winter to early spring (Polissar et al. 1996, 1998), while the fires occurred mostly in the late spring and summer.

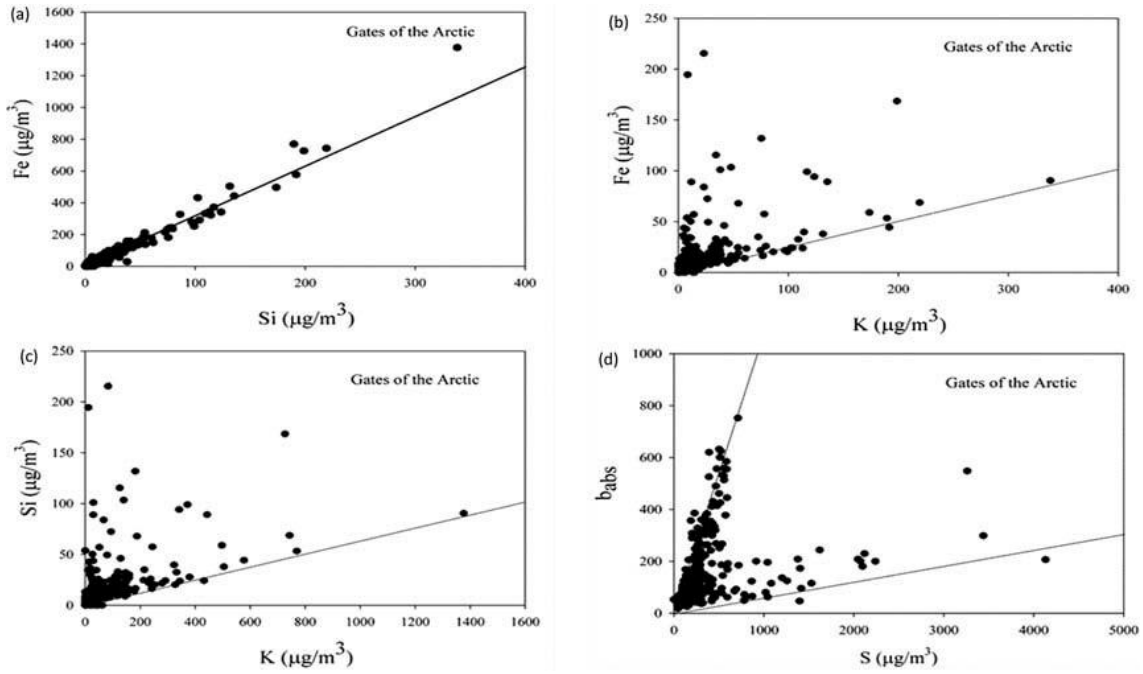

Fig. 4.1 Scatter plots of elemental concentrations or light absorbance measured in particle samples collected in Gates of the Arctic National Park: (a) Fe vs. Si, (b) Fe vs. K, (c) Si vs. K, and (d) b_{abs} vs. S (Hopke 2016).

Thus, these two sources were relatively independent of one another. Such separation is not common but illustrates how the source contributions can be graphically illustrated. In more complex systems, additional sources could contribute to those same chemical species and not necessarily form an edge. To be separable from other sources, there have to be points for which the contributions of a specific source are zero. If there are a sufficient number of such points, the solution will be unique (identifiable) (Anderson 1984). However, there are no published reports of such air quality data sets having been identified.

Thus, the objective of the multivariate methods is to estimate these variable relationships that define the edges and then use them to apportion the quantity of interest (e.g., PM mass, particle number concentration, total VOC concentration) to these identified source types. It

is up to the user of these techniques to put labels on the profiles based on prior experience on what is known about the nature of various kinds of emission sources. As noted earlier, a variation appears in particle compositions or organic constituents (particle or vapor), so these methods allow identifying the profiles of the sources at the receptor site, whereas the CMB uses the profiles measured at the source.

There are a number of different methods based on factor analysis including PCA, UNMIX, and PMF. Such methods do not require a priori information about source emission characteristics and are useful in cases where relevant source profiles are not available (Hopke 2003; Viana et al. 2008).

4.2.1 Principal component analysis (PCA)

In principal component analysis (PCA), the mass balance equation is solved using eigenvector analysis or single value decomposition. The availability of stand-alone software or plug-ins has contributed to the popularity of this method for source assignment.

The main objective of PCA is to convert a set of observations of possibly correlated variables into a set of values of linearly uncorrelated variables, called principal components (PCs), which are subsequently interpreted by the user of the model as potential source profiles. PCA uses proper orthogonal decomposition in such a way that the first principal component accounts for as much of the variability in the data as possible, and each succeeding component, in turn, has the highest variance possible under the constraint that it is uncorrelated with the preceding components (Roscoe et al. 1982). PCA is sensitive to the relative scaling of the original variables and is based upon the intrinsic assumption that the dataset jointly is normally distributed, which is not always the case for environmental concentration data. The artificial positioning of variance into the first few components can be partially solved by orthogonal rotations (e.g., varimax).

The most critical step of using PCA for SA is the interpretation of the PCs and their assignment to potential emission sources. PCA does not perform explicit data uncertainty treatment. Therefore, noise deriving from the uncertainty structure of the datasets, which often include heteroscedastic receptor species, is incorporated by PCA into the PCs (Paatero and Hopke 2003). Moreover, the basic assumption for PCA, the orthogonal component does not reflect the structure of real-world data (many source profiles have a degree of collinearity). Overall, this may lead PCA to produce solutions with collinear source profiles lumped into PCs or partially split into more PCs.

4.2.2 UNMIX

UNMIX model is a form of factor analysis, in which the problem is expanded to the solution of the source profiles and contributions over a set of samples. Thus, the basic equation in matrix form is:

Eq. 4.3 $$X = GF'$$

UNMIX is based on an eigenvalue analysis. The UNMIX model is another type of multivariate receptor model based on the principal component analysis (PCA). The model uses a new transformation method based on the self-modeling curve resolution (SMCR) techniques. Since a unique solution is not possible (Henry 1987), the SMCR technique restricts the feasible region of the real solution into a small region with explicit physical constraints, such as source compositions must be greater than or equal to zero. Explicit physical constraints form linear inequality constraints in the space spanned by the eigenvectors, and these constraints form the feasible region in eigenvectors' space. UNMIX is designed to resolve the most important sources contributing to the measured mass concentrations.

The major identified source categories are motor-vehicles, crustal, secondary sources and marine sources. The factor analysis (FA) or PCA model cannot distinguish spatially and temporally correlated sources. From the FA or PCA standpoint, spatially and temporally correlated sources are perceived as a single source because they often impact the receptor site at the same time. Although these are not a single source, they can be assumed as a pseudo-single composite source. The motor vehicle and road dust sources are spatially and temporally correlated as the road dust is resuspended in the air when the motor vehicle passes over the road.

4.2.3 Positive Matrix Factorization (PMF)

Positive matrix factorization takes a very different approach to the factor analysis problem. All of the other methods use an eigenvector analysis based on a singular value decomposition (SVD). The X matrix can also be defined (Hopke 2003):

Eq. 4.4 $$X = USV' = \overline{USV'} + E$$

where U and V are the first p columns of the U and V matrices. The U and V matrices are calculated from eigenvalue - eigenvector analyses of the XX' and X'X matrices, respectively. It can be shown (Lawson and Hanson 1987) that the second term on the right-hand side of Equation 4.4 estimates X in the least-squares sense that it gives the lowest possible value for

Eq. 4.5 $$\sum_{i=1}^{m}\sum_{j=1}^{n} e_{ij}^2 = \sum_{i=1}^{m}\sum_{j=1}^{n}\left(x_{ij} - \sum_{p=1}^{P} g_{ip}f_{pj}\right)^2$$

Thus, an eigenvector analysis is an implicit least-squares analysis in that it is minimizing the sum of squared residuals for the model. Paatero and Tapper (Paatero and Tapper 1993) showed that in PCA, there is a scaling of the data by column or by row and that this scaling will lead to distortions in the analysis. They further showed that optimum scaling of the data would be to individually scale each data point so as to obtain precise data with high influence on the solution rather than points with higher uncertainties. However, they showed that point-by-point scaling results in a scaled data matrix that cannot be reproduced by a conventional factor analysis based on the singular value decomposition. Thus, PMF takes the approach of an explicit least-squares approach in which the method minimizes the object function:

Eq. 4.6 $$Q = \sum_{i=1}^{m}\sum_{j=1}^{n}\left(\frac{x_{ij} - \sum_{p=1}^{P} g_{ip}f_{pj}}{s_{ij}}\right)^2$$

where s_{ij} is an estimate of the `uncertainty' in the j^{th} variable measured in the i^{th} sample. The factor analysis problem is then to minimize Q(E) with respect to G and F with the constraint that each of the elements of G and F is non-negative. Over the past few years, several approaches to solving the PMF problem have been developed.

Initially, PMF2 was developed (Paatero 1997) to provide a rapid solution to the model presented in Eq. 4.1. PMF2 was initially applied to data sets of major ion compositions of daily precipitation samples collected over a number of sites in Finland (Juntto and Paatero 1994) and samples of bulk precipitation (Anttila et al. 1995) in which they are able to obtain considerable information about the sources of these ions.

Polissar et al. (Polissar et al. 1998) re-analyzed an augmented set of Alaskan data and proposed an approach to uncertainty estimation that has now been widely used in PMF applications. It should be noted that the rules of thumb provided to estimate the uncertainties

were derived by extensive testing to find an approach that could provide useful results. It has no statistical basis, and other approaches to error estimation may provide superior results.

In the late 1990s, a need was identified to be able to solve more complex problems because not all mass balance problems are represented by the bilinear model in Eq. 4.1. For example, data obtained from a series of samples collected with a cascade impactor as a function of time are a three-way data tensor (size, composition, time). Information is lost if the data are combined to produce a matrix for analysis. Thus, a more flexible solver was needed, and (Paatero 1999) developed the multilinear engine that can solve any problem that can be expressed as a sum of product terms.

These two algorithms have a number of differences in how the solutions are obtained. One of the most important is the approaches to apply nonnegativity constraints (Kim and Hopke 2007). In PMF2, the objective function in Eq. 4.6 is augmented with "penalty" functions that increase as the solution values approach zero (Paatero 1997). Alternatively, EPA PMF uses traditional nonnegative least-squares constraints similar to those described in (Lawson and Hanson 1987; Wang and Hopke 1989). Therefore, the PMF2 nonnegativity constraints force solutions toward the center of the feasible region of the solution and away from the boundaries where factor values would approach zero. However, the EPA PMF approach would permit any factor value as long as it is nonnegative, and the solution space will be searched closer to the periphery of the feasible region.

PMF has now become the most widely used receptor model, with more than 1000 papers reporting its application. It has been applied to apportionment of airborne particulate matter e.g. (Polissar et al. 1996; VanCuren and Gustin 2015), precipitation e.g.,(Juntto and Paatero 1994; Anttila et al. 1995), VOCs (Kim et al. 2005), and Aerosol Mass Spectrometry (Zhang et al. 2011) data with a sharp rise in its use after the release of the EPA version of PMF (US EPA, ORD).

The most recent release of EPA PMF (V5.0) incorporates substantially improved error estimation methods (Paatero et al. 2014) that attempt to estimate the errors arising from the inherent uncertainties in the measured data as well as the rotational ambiguity in the solution. Aerosol chemical composition data for $PM_{2.5}$ samples collected during the period from 1988 to 1995 at Underhill, VT, were analyzed by Polissar et al. (Polissar et al. 2001). An 11-factor solution was obtained. Sources representing wood burning, oil combustion, the coal combustion emissions plus photochemical sulfate production, metal production plus municipal waste incineration and the emissions from motor vehicles were identified. Emissions from the smelting of non-ferrous metal ores, arsenic smelting, soil particles and

particles with high concentrations of Na were also identified by PMF. The results by Polissar et al. show an interesting feature of factor analysis solutions (Polissar et al. 2001). In particular, two sulfur-dominated factors were identified. The first S factor also has the highest loadings of Se (Fig. 4.2, top) suggesting emissions from coal-fired power plants. The factor has an annual cycle with maxima during the winter/spring season and minima in the summer (Fig. 4.3, top). It is thus denoted W-Coal. The second S factor has the opposite annual cycle with the summer maxima (Fig. 4.3, bottom). It has a much higher S/Se ratio (Fig. 4.2, bottom). It is suggested that the second S factor represents the photochemically enhanced sulfate production from SO_2 in the summer (S-Coal). Sources related to the second S factor provide the highest fine particulate matter mass concentrations. It is likely that the two S factors represent the same coal-fired power plants with the differences between the factors representing the extremes of photochemical production of sulfate from the emitted SO_2. Figure 4.3 shows the Se/S scatter plot for Underhill. Se is generally an important tracer for coal combustion. The slope for the linear regression for the winter subset of the data points is higher than that for the summer data while the corresponding correlation coefficient is higher for summer. Thus, although there is a single source type, two factors are required to reproduce the variability in the source profile arising from the differences in seasonal atmospheric processes. It is this type of variability that makes receptor modeling different from the standard mixture resolution problem in chemometrics.

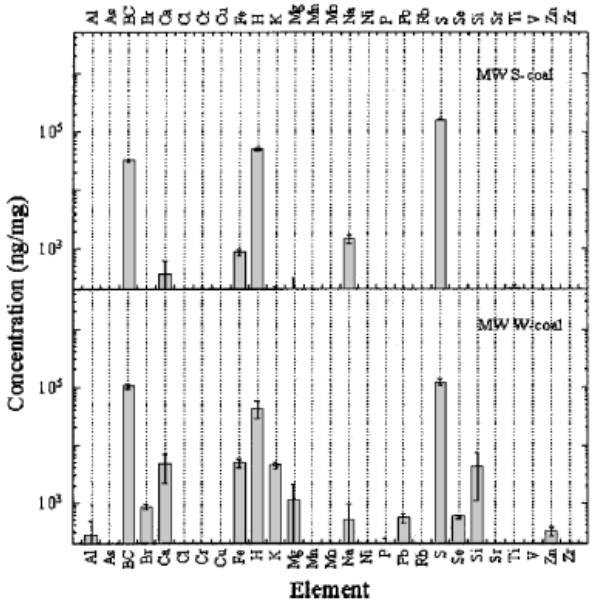

Fig 4.2 PMF-derived source profiles for the sulfur factors from Underhill, VT taken from (Polissar et al. 2001) in summer (top) and winter (bottom).

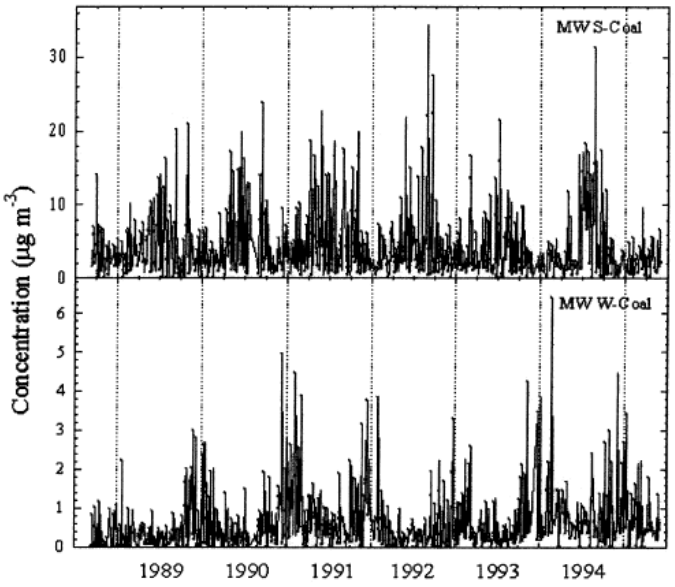

Fig 4.3 Yearly PMF-derived source contributions for the sulfur factors from Underhill, VT taken from Polissar et al. (2001). Top, summer coal-fired power plants; bottom, winter coal-fired power plants.

4.3 Hybrid receptor models

To obtain detailed information on pollutant concentrations and source of emission an effective management strategy was developed called Hybrid Receptor Model (HRM). Two categories of hybrid methods have been used for SA of PM: 1) constrained or expanded receptor models; 2) trajectory-based receptor models. The latter category utilizes pollutant concentrations and wind speed/direction measured nearby the receptor site or backward trajectories generated with a Lagrangian model.

These methods combine estimates of the motion of the air backward in time with concentrations measured at a sampling location. Examples of these hybrid receptor models include residence time analysis (RTA) (Ashbaugh et al. 1985; Poirot and Wishinski 1986), potential source contribution function analysis (PSCF) (Zeng and Hopke 1989; Gao et al. 1993; Hopke et al. 1993), concentration weighted field (CWT) (Seibert et al. 1994) and residence time-weighted concentration (RTWC) (Sthol 1996).

These models have been used to identify pollutant sources hundreds of kilometers from the receptors. They all involve counting the frequency of back trajectory segment endpoints in grid cells that make up the geographical domain of interest for the receptor site.

The dwelling time of air parcels over PM emission source areas is a critical parameter related to potential atmospheric transport impacts (Salvador et al. 2010; Chalbot et al. 2013). Slow moving airflows, corresponding to short range trajectories, can more effectively incorporate

airborne particulates and transfer them to distant regions, whereas rapid air streams are associated with atmospheric dispersion and physical losses of PM due to various exchange and mixing processes (Fleming et al. 2012).

4.3.1 Residence time analysis (RTA)

In RTA, a gridded array is created around the sampling location. Trajectories are a sequence of segments, each of which represents a fixed amount of time. Thus, each endpoint can be considered to be an indication that the air parcel has spent a given time within that grid cell. The total `residence time' that air spends in the given cell would be the total number of endpoints that fall into that cell. These values can be plotted over a map. The residence time values associated with high or low concentration can be plotted to examine likely directions from which contaminated or clean air is transported to the sampling site.

The problem with this method is that all of the trajectories begin at the receptor site, hence the residence time is maximum in the cells surrounding the sampling location.

Poirot et al. (Poirot et al. 2001) performed an RTA analysis of the source contributions to particles collected at Underhill, VT estimated with both UNMIX and PMF. Fig. 4.4 compares the RTA upwind incremental probability fields for the highest 10% of daily source contributions for the seven similar sources identified independently by the UNMIX and PMF models. The strong similarities in the incremental probability plots for the `similar sources' identified by PMF and UNMIX are not surprising, considering the strong correlations between the modeled source contributions.

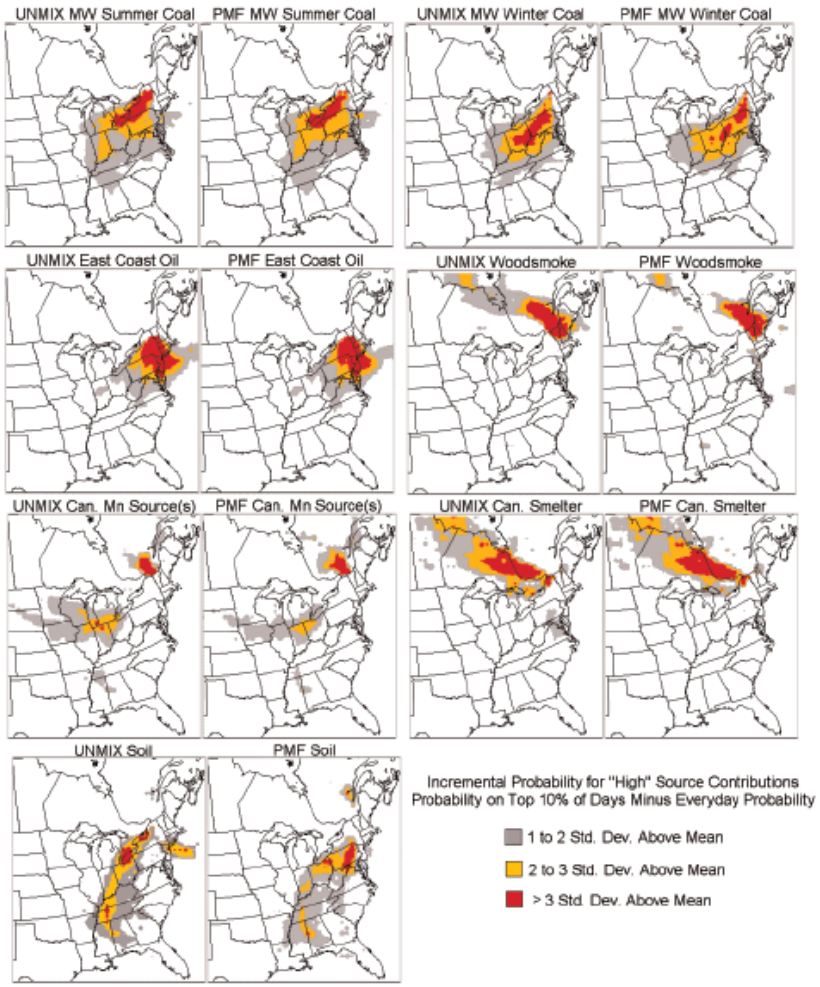

Fig. 4.4 RTA incremental probability fields for the top 10% of daily UNMIX and PMF source contributions (Poirot et al. 2001).

4.3.2 Potential source contribution function (PSCF)

The potential source contribution function (PSCF) receptor model was originally developed by Ashbaugh et al. (Ashbaugh et al. 1985). It has been applied in a series of studies over a variety of geographical scales (Cheng et al. 1993b, a; Gao et al. 1994, 1996).

Ashbaugh et al. (Ashbaugh et al. 1985) calculated the accumulated residence times of all trajectories within cells of a grid which they superimposed to the domain of the trajectory computations. This was done separately for a subset of high pollutant events (resulting in a partial residence time t) and for the whole data set (resulting in a residence time T). The spatial distribution of t/T provides information on source areas. Trajectories passing over grid cells with high t/T are more frequently associated with high pollutant concentrations at the receptor site than those passing over grid cells with low t/T.

Air parcel back trajectories ending at a receptor site are represented by segment endpoints. Each endpoint has two coordinates (latitude, longitude) representing the central location of

an air parcel at a particular time. To calculate the PSCF, the whole geographic region covered by the trajectories is divided into an array of grid cells whose size is dependent on the geographical scale of the problem so that the PSCF will be a function of locations as defined by the cell indices *i* and *j*.

Air parcel backward trajectories are related to the composition of the collected material by matching the time of arrival of each trajectory at the receptor site. The movement of an air parcel is described as a series of segment endpoints defined by their latitude and longitude. PSCF values for each grid cell were calculated by counting the trajectory segment endpoints that terminate within the grid cells. The number of endpoints that fall in the ij^{th} cell is $n(i, j)$. The number of endpoints for the same cell when the corresponding samples show concentrations higher than an arbitrary criterion value is defined to be $m(i, j)$. The PSCF value for the ij^{th} cell is defined as

Eq. 4.7 $$PSCF(i,j) = m(i,j)/n(i,j)$$

In the PSCF analysis, it is likely that the small values of $n(i, j)$ produce high PSCF values with high uncertainties. In order to minimize this artifact, an empirical weight function $W(n_{ij})$ proposed by Zeng and Hopke (1989) is commonly applied when the number of the endpoints for a particular cell was less than about three times the average values of the endpoints per cell.

Although the trajectory segment endpoints are subject to uncertainty, a sufficient number of endpoints should provide accurate estimates of the source locations if the location errors are random and not systematic. Cells containing emission sources would be identified with conditional probabilities close to 1 if trajectories that have crossed the cells effectively transport the emitted contaminant to the receptor site. The PSCF model thus provides a means to map the source potentials of geographical areas. It does not apportion the contribution of the identified source area to the measured receptor data.

4.3.3 Concentration-Weighted Trajectory (CWT)

A problem in the structure of PSCF method is that slight and extreme exceedances of the threshold concentration value are all treated in the same way, thus limitations in distinguishing moderate sources from strong ones may occur (Hsu et al. 2003).

A method of weighting trajectories with associated concentrations (concentration weighted trajectory (CWT)) was developed by Seibert et al. (Seibert et al. 1994) and used and implemented by Hsu et al. (Hsu et al. 2003). In this procedure, each grid cell gets a weighted concentration obtained by averaging sample concentrations that have associated trajectories that crossed that grid cell as follows:

Eq. 3.8 $$C_{ij} = \frac{1}{\sum_{l=1}^{M} \tau_{ijl}} \sum_{l=1}^{M} C_l \tau_{ijl}$$

C_{ij} is the average weighted concentration in the grid cell (i, j). C_l is the concentration of pollutants, τ_{ijl} is the number of trajectory endpoints in the grid cell (i, j) associated with the C_l sample, and M is the number of samples that have trajectory endpoints in a grid cell (i, j). Similar to the other models, a point filter is applied as the final step of CWT to eliminate grid cells with few endpoints. Weighted concentration fields show concentration gradients across potential sources. This method helps determine the relative significance of potential sources.

3.3.4 Residence time-weighted concentration (RTWC)

Stohl (Sthol 1996) improved the Seibert et al. procedure with a concentration redistribution method. Seibert et al. equally distributed concentration to each segment of the related trajectory, whereas sources of air pollutants are often concentrated in ‘‘hot spots’’ (Sthol 1996). This method starts with the first guess concentration field based on Eq. 4.9 developed by Seibert et al.

Eq. 4.9 $$\overline{C}_{ij} = \frac{1}{\sum_{l=1}^{M} \tau_{ijl}} \sum_{l=1}^{M} \log(C_l) \tau_{ijl}$$

Eq. 4.9 is similar to the CWT method (Eq. 4.8) described above, except that Eq. 4.9 uses logarithmic concentrations and statistically smooths the concentration field with a ‘‘9-point-operator’’ within the 95% confidence interval of the mean concentration in each grid cell. Logarithmic concentrations were used in the methods of Seibert et al. and Stohl because the concentration of particulate sulfate used in their studies followed an approximately log-normal distribution. The ‘‘9-point-operator’’ statistically smooths the concentration field to have weight distribution of a 3x3 matrix (0.06, 0.10, 0.06, 0.10, 0.36, 0.10, 0.06, 0.10, 0.06). With the first guess concentration field from the Seibert et al. procedure, sample

concentrations are then redistributed along the trajectories based on the weights from the concentration field. The equation for redistributing concentrations along trajectory *l* is

Eq. 4.10 $$C_{kl} = C_l \frac{X_{kl} N_l}{\sum_{j=1}^{N_l} X_{jl}} = C_l \frac{X_{kl}}{\overline{X}_l}, \quad j = 1, N_l$$

where X_{kl} are the mean concentrations of the grid cells which are hit by segments k = 1; N_l of trajectory *l* and $\overline{X}_l = (\sum_{j=1}^{N_l} X_{jl})/N_l$ is the average of the mean concentrations of the grid cells transected by the N_l segments of trajectory *l*. After the redistribution is finished for all trajectories, a new concentration field is computed with the equation

Eq. 4.11 $$\overline{C}_{ij} = \frac{1}{\sum_{l=1}^{M} \sum_{k=1}^{N_l} \tau_{ijkl}} \sum_{l=1}^{M} \sum_{k=1}^{N_l} \log(C_{kl}) \tau_{ijkl}$$

where τ_{ijkl} is the residence time of segment *k* of trajectory *l* in a grid cell (*i*, *j*). Eq. 4.11 is similar to Eq. 4.9, but the redistributed concentrations C_{kl} are used instead of the measured concentrations C_l. With this new concentration field, a second redistribution of the concentrations along the trajectories is performed, which in turn leads to a new concentration field. This procedure is repeated until the average difference between the concentration fields of two successive iterations is below 0.5%. RTWC is better at estimating the gradients of the concentration field (Stohl, 1996). Backward trajectories start at different heights traverse different distances and pathways. For longer range transport (>24 h), trajectories started at different heights may vary significantly. If this occurs, PSCF modeling results might also be different.

The NOAA HYSPLIT trajectory model and meteorological data are usually used to calculate air parcel back-trajectories for hybrid receptor modeling.

5 Case Study 1: Aerosol characterization in the Mediterranean Sea Basin during Oceanographic campaigns

5.1 Introduction

Atmospheric aerosol pollution and in particular the particulate matter could be emitted from anthropogenic and natural sources, as already saw in previous chapters. The Mediterranean Basin is among the most interesting semi-enclosed area in the world, as it is under intense anthropogenic pressure, surrounded by highly industrialized and populated centers, but also with different natural sources that impact on air quality in this area. In this context has been performed different campaigns within the on-going Med-Oceanor project, which is actively involved since 2000 in regular cruise measurement campaigns, across the Mediterranean Sea (Sprovieri et al. 2003; Sprovieri and Pirrone 2008b). During 2011, 2012 and 2015 have been conducted, onboard the CNR (National Reseach Council) research vessel, monitoring campaign to evaluate the chemical content of particulate matter and relative impact on air quality off-shore and near coastal sites. The sampling was carried out by my colleagues who participated in the campaigns each of which covered different areas of the Central and Western Mediterranean Sea, while I carried out the analytical part which includes sample preparation and then the analysis of the filters. Meanwhile, during the summer of 2017, I was involved and dealt also with the PM sampling on board of research vessel, in one of the research campaign carried out in the project Med-Oceanor. As with previous campaigns, this campaign was also carried out to assess the chemical contribution of particulate matter in the Mediterranean Basin, with a certain focus on the natural sources, in particular volcanoes and fumaroles, covering a smaller area of the Mediterranean with respect to the campaigns previously made it. Starting from the last campaign mentioned is already know that much of the air pollution that damages human health and the environment today is the result of human activities; but natural sources also emit air pollutants, contributing to the exposure of people and ecosystems to bad air quality. The major natural emissions in terms of mass are sea spray (84%), and mineral dust (13%), with other sources such as biological primary organic aerosols (POA), volcanic emissions, biogenic secondary organic aerosols (SOA), and volcanic and biogenic sulfate particles. Anthropogenic aerosols contribute with only 2% to global emissions, mainly in the form of anthropogenic sulfate (49%) and industrial dust (40%), with additional emissions of anthropogenic nitrate and SOA, and fossil fuel-derived POA. On the global-scale, primary aerosols are clearly dominant over secondary species

(98% vs. 2%) (Viana et al. 2014). On the local scale, this scenario is reversed. Indeed the quantification of source contributions on the local scale is more complex and it may differ from one region to another given that it is strongly affected by a broad spatial variability.

Natural contributions to PM levels and speciation in Europe have been characterized using different tools and approaches by numerous works in the literature (Querol et al. 2009; Masson et al. 2010; Beuck et al. 2011; Viana et al. 2014; Bencardino et al. 2014; Aleksandropoulou et al. 2015; Liora et al. 2016). Among the main natural sources of atmospheric aerosol that impact on the Mediterranean, and in general European countries, there is the wind-blow African dust. The major sources of mineral dust are arid and semiarid areas. In the case of Europe, arid zones in North Africa are the major source. In Europe, African dust may greatly increase ambient PM levels, especially in southern European countries, where it is a known source causing exceedances of the PM thresholds (Querol et al. 2009; Masson et al. 2010; Bencardino et al. 2011; Pey et al. 2013). The high contribution of African Dust in southern Europe in winter and summer derives from the high wind speed values and the dry climate, respectively. Another important natural pollutant source is derived from the finely dispersed PM emitted from the sea surface (sea spray). Seaspray is produced via the bubble-bursting processes typically resulting from white cap generation, producing film and jet drops, resulting in sea-spray particles in the range of sub-micrometers size up to a few micrometers (O'Dowd and de Leeuw 2007). Carbonaceous aerosol derived from wildfires is considered another natural source. Wildfire is caused by the burning of forests and other vegetation, strictly through natural processes. In Mediterranean countries, during summer the emissions from these fires have special relevance because the weather is usually drier and hotter, and fire outbreaks are commonly fanned by strong winds. In the last few years, the interest of researchers has increased to the biogenic aerosols, which are the primary and secondary particles emitted by vegetation (Kourtchev et al. 2008; Aleksandropoulou et al. 2015). Previous studies have already highlighted biogenic aerosol influences on a global scale, as biogenic volatile organic compound (BVOC) emissions were estimated to be 10 times higher than those of anthropogenic VOCs (Tsigaridis and Kanakidou 2003). Seismic activities and volcanic emission derived from the eruption are other natural sources of PM in the atmosphere. The main compounds emitted from volcanic eruptions include water vapor, ash, CO_2, SO_2 and HCl (von Glasow 2010). Volcanic ash emissions may have an impact at a global scale due to the fact that those emissions may be injected into the stratosphere, while it could be a regional impact because of the same emissions but injected into the troposphere. The identification of natural events affecting air

quality is a complex task which requires the combination of tools such as data on PM levels and chemical composition, aerosol maps, back-trajectory analysis, and dispersion and receptor modeling, among others.

5.2 Oceanographic Campaigns: sites description

Aerosol levels were performed during the 2017 cruise measurements campaign, named "Efesto 2017" on-board of the research vessel "Minerva Uno" of the Italian National Research Council (CNR) from 19th August to 4th September 2017. Aerosol mass sampling was performed with a time resolution of about 24h at each selected station fixed along the established route in the south-western Sector of the Mediterranean Sea, and particularly in the Tyrrhenian sea, with the aim to study the influence of natural emission sources (i.e., volcanic and fumaroles plums) located in this area of the Basin on the aerosol chemical composition (Fig. 5.1). In order to examine in detail the data obtained during the cruise, the sampling route was divided into two different areas: volcanic, including Mount Etna, Stromboli Island, and Marsili Seamount Volcanoes, and fumarole including Campi Flegrei, Vulcano and Ischia Islands, and finally, Panarea submarine fumarole. Below, a brief description of these sites has been also reported.

- Mount Etna covers an area of about 1250 km^2 and reaches an altitude of about 3340 m (37.754193N, 14.978929E). It is one of the most active volcanoes in the world, with frequent paroxysmal episodes separated by passive degassing periods. The edifice consists of a lower shield unit overlain by a stratovolcano (Chester et al. 1986). The stratovolcano is truncated at 2800–2900 m of altitude by the Ellittico caldera and Cratere del Piano, while the upper part of the volcano culminates with a large summit cone at the top of which four active craters (Bocca Nuova, Voragine, Northeast, and Southeast Craters) are located. The general atmospheric circulation over the Etna area is predominantly westerly to northwesterly. The sampling station selected across the route in this area was in front of Acireale and Acicastello town coasts, at a distance that allows sampling considering these wind directions.
- Stromboli (926m a.s.l; 38.7891N, 15.2131E) has been characterized for at least the last 2000 years by quasi-permanent activity consisting of mild intermittent explosions and continuous gas emissions from K-rich basalt (Barberi et al. 1993). Although Stromboli does have a significant hydrothermal system (Finizola et al. 2003), its magma also degasses directly into the atmosphere (i.e., at very high temperature, >1000 °C) from lava-filled vents. Such systems are often described as

"open- conduit" volcanoes, and many seem able to degas very large quantities of unerupted magma (e.g., Francis et al. 1993). In this point, the sampling vessel stayed for three days with three different points around the island of Stromboli.

- Marsili Seamount (Fig. 5.1) is about 60 km long and 20 km wide, rising about 3000 m from the seafloor at over 3500 m water depth (39.236276N, 14.369875E). Recent stratigraphic and geochemical studies suggest that in historical times, two submarine explosive eruptions occurred at MS. This is the first evidence of explosive volcanic activity at a significant water depth (500–800 m) in the Mediterranean Sea (Iezzi et al. 2014). Geophysical and morphological observations linked the hydrothermal activity in the Marsili to the post-volcanic activity (D'Alessandro et al. 2009; Caratori Tontini et al. 2010). The possible existence of a very large underwater explosive volcano together with some encouraging clues that point to MS as an important and possible long-lasting-renewable energy resource (Italiano et al. 2014) has reinforced research and exploitation efforts. The existence of an active magmatic chamber at about 2.5 km below the summit was proposed on the basis of petrologic studies of basalts (Trua et al. 2002) and it is compatible with gravimetric and magnetic data modeling (Caratori Tontini et al. 2010), as well as geochemical observations on the summit (Dekov et al. 2006).
- Solfatara, a crater located within the Campi Flegrei (458m a.s.l.; 40.8271N, 14.1391E), a Quaternary volcanic complex near Naples (Fig. 5.1), is renowned for its vigorous, low-temperature degassing. Indeed the term solfatara is applied to many similar manifestations found in other volcanic regions of the world. The hottest fumaroles at Solfatara reach temperatures of only 140 –160 °C. Previous studies indicate that gas emissions are dominated by H_2O, followed by CO_2 and H_2S (Chiodini et al. 2003). SO_2 is virtually absent.
- Vulcano is situated to the north of Sicily (Fig. 5.1). Vulcano and Panarea islands both belong to the Aeolian volcanic arc, related to subduction beneath the Tyrrhenian Sea. Following the last eruption of Vulcano (500m a.s.l.; 38.4041N, 14.9621E) in 1888–1990 a vigorous fumarole field developed in the summit crater, known as La Fossa. Numerous geochemical investigations have focused on Vulcano, especially since increases in gas fluxes and temperatures were observed in the 1970s. Like Solfatara, Vulcano does not have magma at the surface but its fumaroles do reach significantly higher temperatures, well in excess of 300 °C at some vents. The chemistry of their

fluids indicates mixing between hydrothermal and magmatic end-members (Mather et al. 2004).

- Ischia is the westernmost active volcanic complex of the Campania area and belongs to the Phleagrean volcanic district, which also includes Campi Flegrei. At Ischia, the last eruption took place in AD 1301 (Vezzoli 1988). Since that time, several earthquakes affected the island. The most recent and energetic earthquake occurred at Casamicciola in 1883 and caused damages and numerous causalities. Thermal manifestations characterize Ischia: thermal waters and fumaroles are well known since Roman times and are the main economic resource of the island at the present. Most of the fumarolic activity is concentrated along the faults affecting Mt. Epomeo, a resurgent block located in the central part of the island.
- Panarea Island (Aeolian Archipelago, southern Italy) lies in the western sector of a submarine, 120 m deep platform (Fig. 5.1) constituting the 56 km^2 wide summit of an ~2000 m high seamount (Gabbianelli et al. 1990; FavalliM et al. 2005). In the eastern sector of the platform, about ~1.5 km East of Panarea Island, a group of islets (Dattilo, Panarelli, Lisca Bianca, Bottaro, Lisca Nera and Le Formiche) forms an archipelago that surrounds a submerged area, characterized by relatively shallow depth (<35 m), hosting gas and thermal water discharges whose occurrence is known since the Roman Age. Geochemical studies of fluids from the submarine fumarolic field of this area started in the early 1990s (Italiano and Nuccio 1991) and increased after the gas burst event that occurred on the 3rd of November 2002 (Caracausi et al. 2005)

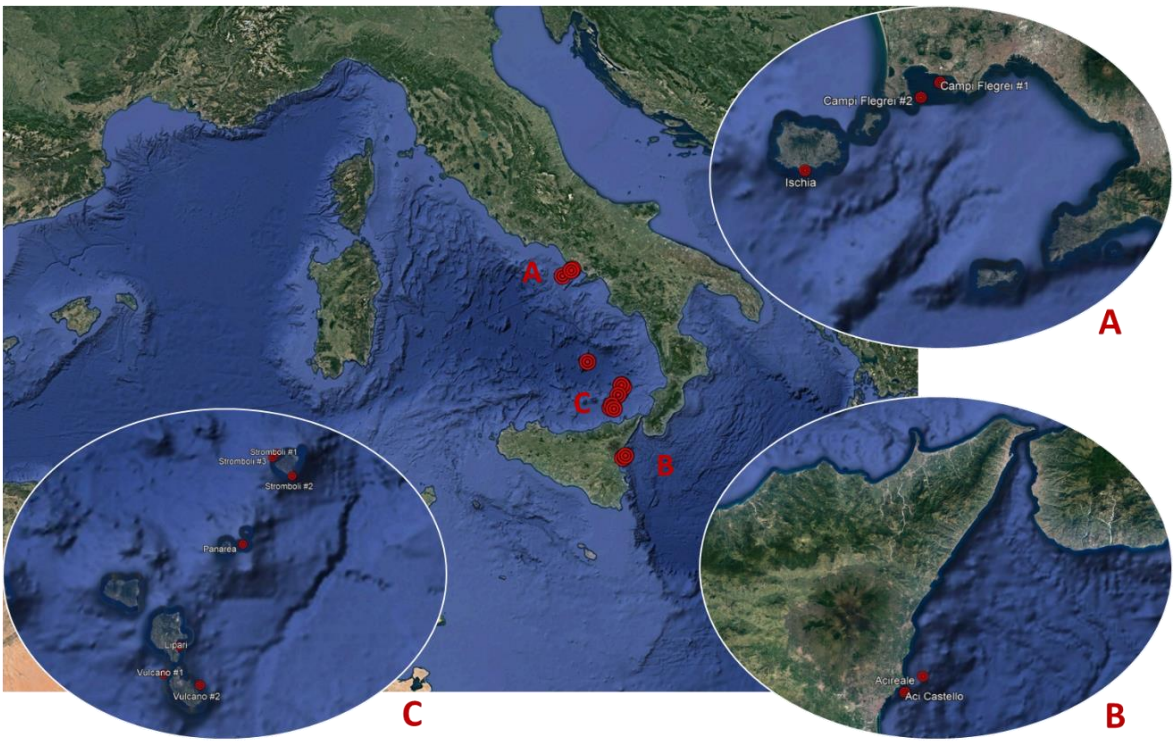

Fig. 5.1 Map of Efesto Campaign sites

5.3 Experimental and Data Treatment

The measurements equipment was fixed on the roof of the ship, to avoid contamination from the ship exhaust, on a deck about 30 m above the sea level. Daily 24-h ambient PM_{10} and $PM_{2.5}$ samples were collected on quartz fiber filters (2500 QAT-UP, Pallflex ®, CT, USA, 47mm in diameter) using a low volume sampler (Tecora Echo PM) for a total of 28 samples. The filters were conditioned and weighed in Rende before and after sampling to determine concentrations of both the fractions by standard gravimetric procedures. Once the gravimetric determination was completed the filters were treated and analyzed for the determination of the chemical composition.

The carbonaceous fraction of aerosol (TC = OC + EC) was analyzed cutting 1 cm^2 portion of each filter by a thermal-optical transmission technique exploiting a Sunset Laboratory OCEC Analyzer using the EUSAAR-II temperature protocol (Cavalli et al. 2010) in the CNR-IIA laboratory in Rende. The elemental and ions analyses were carried out in the laboratories of CSIC-IDAEA (Professor Querol research group), in Barcelona, where I had an experience abroad as a visiting Ph.D. student. Half of each filter was acid digested ($HF:HNO_3:HClO_4$, with a mixture of 2.5:1.25:1.25 mL, kept at 90 °C in a Teflon reactor for 14 h, driven to dryness and re-dissolved with 1.25 mL HNO_3 to make up a final volume of 25 mL with water) for the subsequent chemical analysis. The digested filters were analyzed

by means of Inductively Coupled Atomic Emission Spectrometry for major elements (Al, Ca, Na, Mg, K, Fe, P, S) and Inductively Coupled Plasma Mass Spectrometry for trace elements (Li, Ti, V, Cr, Mn, Co, Ni, Cu, Zn, As, Se, Rb, Sr, Cd, Sn, Sb, Ba, La, Ce, Hf, Pb, Bi, Th, U, among others). The remaining part of each filters was water leached in 20 mL sealed PVC bottles (14 h at 60 °C), preceded by an ultrasound bath during 15 minutes, for the determination of soluble ion concentrations by ion chromatography (sulfate, nitrite, nitrate, fluoride, bromide, chloride and phosphate) and ion selective electrode (ammonium). The chemical components of the PM were grouped as (a) sea salt (ss); (b) mineral dust; (c) organic matter and elemental carbon (OM + EC); (d) secondary inorganic aerosols, (SIA); and (e) trace elements. Each of these components can derive from a variety of sources, though they are often dominated by few sources. Mineral dust, for example, does not include OM that might be associated with engine exhaust or bio-aerosols deposited onto roadways or agricultural soils. These would be included in the OM fraction. Similarly, some fugitive dust sources include salts, but these would be accounted for in the salt fraction; sulfates and nitrates that react with salt would be accounted for in the inorganic ion fraction.

Six major ions make more than 99% of the mass of salts dissolved in seawater: four cations, sodium (ss-Na^+), magnesium (ss-Mg^{2+}), calcium (ss-Ca^{2+}), and potassium (ss-K^+); and two anions, chloride (ss-Cl^-) and sulfate (ss-SO_4^{2-}). The reaction of NaCl with sulfuric and nitric acid, present in atmosphere as fine particles, leads to the subsequent volatilization of HCl. As a consequence, the HCl volatilization will not make possible the use of [NaCl] to describe [sea salt]. For this reason, sea salt concentrations will be calculated in the following from the equation (Eq. 5.1) :

Eq. 5.1 $[\text{Sea salt}] = [\text{ss-}Na^+] + [Cl^-] + [\text{ss-}Mg^{2+}] + [\text{ss}-K^+] + [\text{ss-}Ca^{2+}] + [\text{ss-}SO_4^{2-}]$

Based on the seawater composition, the sea salt sulfate [ss$-SO_4^{2-}$] is calculated as [ss-Na^+] times 0.2509, sea salt Calcium [ss-Ca^{2+}] calculated as [ss-Na^+] times 0.038, sea salt Potassium [ss$-K^+$] as [ss-Na^+] times 0.037, and sea salt Magnesium [ss-Mg^{2+}] calculated as [ss-Na^+] times 0.1187. To calculate the sea salt Sodium [ss-Na^+] the value of non-sea salt Sodium was subtracted from the total Sodium value ([ss-Na^+] = [Na] – [nss - Na^+]).

Minerals have been expressed by (Macias et al. 1981) as the sum of the oxides of Al, Ca, K, and Fe, assuming the common oxide forms of Al_2O_3, CaO, K_2O, and Fe_2O_3, respectively. Dust content in both fractions was estimated multiplying the concentration of major elements

that make up the dust (as Al, Fe, Ca, Ti) with conversion factors to obtain the contribution of each to total dust.

Eq. 5.2 $[Dust] = [Al_2O_3] + [CaO] + [MgO] + [K_2O] + [Fe_2O_3] + [P_2O_5] + [TiO_2]$

To account for the unmeasured H, O, N, and S in organic compounds, a conversion factor (or multiplier) is used to transform OC to OM, i.e.,

Eq. 5.3 $OM = \boldsymbol{f} \times OC$

The ***f*** multiplier is not site or time specific. Depending on the extent of OM oxidation and secondary organic aerosol (SOA) formation, values for ***f*** vary from 1.2 for fresh aerosol in urban areas (Chow et al. 2002) to 2.6 for aged aerosol (Turpin and Lim 2001; Robinson et al. 2010; Roy et al. 2011). The conversion factor ***f*** is usually taken in the range from 1.4 for urban aerosols to 1.8 for remote aerosols. Turpin and Lim (2001) revisited these conversion factors and proposed values of 1.6 ± 0.2 and 2.1 ± 0.2 for urban and non-urban aerosols, respectively. Indeed in this work, the ***f*** =2.1 value was used. To establish the carbon contribute in each sample the value of OM obtained as explained above was added to the value of elemental carbon obtained through thermal-optical transmission method.

The secondary inorganic aerosol is composed of ions SO_4^{2-}, NO_3^- and NH_4^+. The sulfate possesses components in both sea salt and non-sea-salt deriving from the atmosphere. In our case study given the marine environment, the non-sea-salt sulfate (i.e., $nssSO_4^{2-} = [SO_4^{2-}] - 0.25094\ [Na^+]$, based on $[SO_4^{2-}] / [Na^+]$ molar ratio in seawater) can be estimated. Summed $nssSO_4^{2-} + NO_3^- + NH_4^+$ has been applied to estimate contributions from secondary inorganic ions (Querol et al. 2001; Mkoma et al. 2009; Cheung et al. 2011).

The last contribution at the PM mass deriving from trace elements is the simple sum of concentrations coming from the ICP-MS analysis of trace elements.

The addition of the above determinations accounted for 85 and 87 percent of the PM_{10} and $PM_{2.5}$ averages masses. The remaining undetermined mass is attributed to the structural and adsorbed water that was not removed during the sample conditioning. Relative analytical errors were estimated using a small amount (15 mg) of the NIST-1633b (fly ash) reference material loaded on a ¼ quartz fiber filter. Individual uncertainties were calculated following the procedure described by Amato et al. (2009) and Escrig et al. (2009), taking into account

the analytical uncertainty as well as the standard deviations of species concentrations in the blank filters.

In order to characterize the daily atmospheric scenarios with incidence on PM levels and also to interpret the different source regions of air masses in the study area, a number of complementary tools which included the back-trajectories calculated by HYSPLIT4 model (Draxler and Rolph 2010) were used. The occurrence of African dust outbreaks was also detected with these same tools, coupled with the information obtained by the NAAPS aerosol maps from the Marine Meteorology Division of the Naval Research Laboratory, USA (NRL) (http://www.nrlmry.navy.mil/aerosol) and the BSC-DREAM dust maps (http:// www.bsc.es/projects/earthscience/DREAM/; Pérez et al. 2006).

The methods used to carry out the source apportionment of this campaign was the Enrichment Factors (EFs) and factor analysis (FA). Enrichment Factors (EFs) are useful to rank the enrichment degree of an element compared to a known source; in this case, the Aluminum concentration was considered as the basis for comparison. EF is defined as the ratio of a given element to the concentration of an element in a sample, normalized to the same ratio in the earth's crust. For each element, the EF was calculated according to Eq. 5.4 to evaluate the contribution of volcanoes in the samples:

Eq. 5.4

$$EF = \frac{E_{sample}/Al_{sample}}{E_{volc}/Al_{volc}}$$

Where E is the elemental concentration and *volc* refer to concentration value in the volcanic stream.

In this study, the enrichment factors in Etna's plume were calculated for each element using average Etnean basalt (Calabrese et al. 2011) as reference material, and Al as the normalizing element, as well as for Stromboli's plume the EFs were calculated using average Stromboli basalt (Allard et al. 2000) as reference material, and Al as normalizing element.

Factor analysis is widely used for source identification and apportionment of particulate air pollutants at receptor sites and it was chosen even if we know that it could not distinguish spatially and temporally correlated sources. From the FA standpoint, spatially and temporally correlated sources are perceived as a single source because they almost always impact the receptor site at the same time (Hopke 2003). The FA was performed using Statistica software and Varimax tool.

5.4 Results and discussion

Sea level pressure composite means and anomalies over the Mediterranean basin was used according to the NCEP/NCAR Reanalysis (Kalnay et al. 1996) to achieve information on the weather conditions during the campaign (see Fig. 5.2). While in August, the synoptic conditions were characterized by the expansion towards the Mediterranean of the Azores Anticyclone, in line with seasonal climatology (there are no anomalies, Fig 5.2), on September 2 (Lipari stop) the situation was changed. In this case, the anticyclonic system was confined over the Atlantic Ocean and North of Europe, favoring the development of low-pressure systems across Eastern Europe and the Mediterranean Basin, where a strong negative pressure anomaly can be seen.

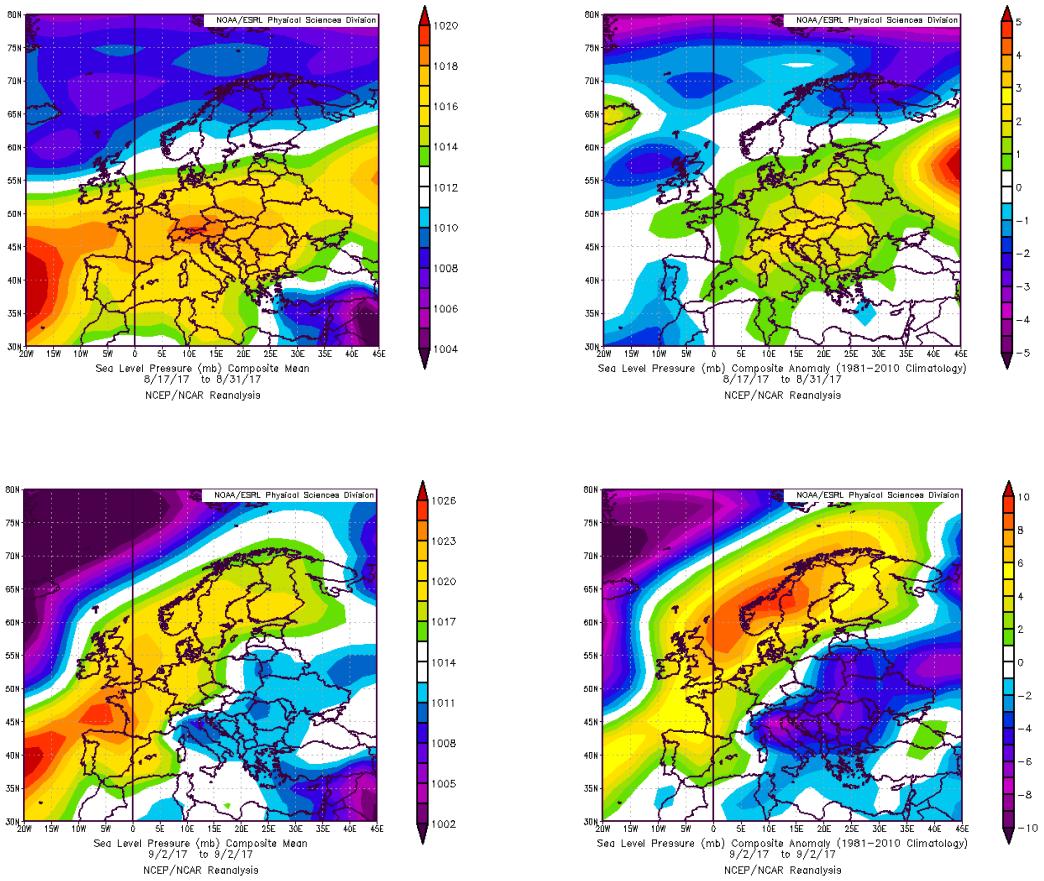

Fig 5.2 NCEP/NCAR reanalysis maps (mean and anomaly) of August (up) and September 2 (down)

The chemical percentage composition of the PM samples collected during the cruise in 2017, calculated as discussed in the previous paragraph, is shown in Fig 5.3. For the PM_{10} mass, the prevalent contributes derived from carbonaceous (OM + EC) and dust portions that

varied during the whole campaign. The maximum value of dust was reached at the Acireale stop, with Saharan dust contribute confirmed by NAAPS, BSC-DREAM and back trajectories maps (Fig. 5.4) while the average value was 27.8 %. The carbonaceous fraction was constantly higher than 20 % (Putaud et al. 2010) in the whole campaign except in Lipari where was found the lower value(14.3 %). This minimum probably attributable to the peculiar meteorological condition occurred in that sampling day, as discussed above; the maximum value, detected in Campi Flegrei (1) (38.4 %), could be due to the presence of very high vehicular traffic near the sampling area, indeed the highest value of EC (0.95 μg m^{-3}) and OC (3.64 μg m^{-3}) of the whole campaign was registered. The SIA component had an average mass contribution on a PM_{10} fraction of 19.7 % with the maximum in Stromboli (2) and the minimum always in Lipari stop (probably due to the same reason as the minimum of the carbonaceous fraction). Tracer elements and sea salt are those that contribute less to the mass, with tracers that contribute only about 1% on average and sea salt about 10%. The latter value in the marine environment is relatively low probably due to the more stable condition encountered for almost the whole campaign, with the maximum in correspondence of heavy sea and strong blow wind occurred during Lipari (36.6%) and Vulcano (2) (23.3%) stops.

Even in the $PM_{2.5}$ fraction, the prevailing average component was the carbonaceous portion with the 42.9 % and the maximum value obtained in the Campi Flegrei area (66.8 % in Campi Flegrei (1) and 51.5% in Campi Flegrei (2)). This result supports the previous thesis attributable to vehicular traffic. In this case, the SIA component reached 31.3 %. Indeed the SIA components (SO_4^{-2}, $NH_4^{+,}$ and NO_3^-) are prevalently recorded in fine fraction (Querol et al. 2001; Mather et al. 2004). The dust contributes to the $PM_{2.5}$ mass (19.7%), lower than the 27.8% found in PM_{10}, is the highest in Vulcano (1) (44.8%), Stromboli (2) (43.2%) and Campi Flegrei (2) (32.7%). The trace elements are more consistent in $PM_{2.5}$, even if on average they reach similar values to those for PM_{10} (1.4%), with the highest values recorded in Campi Flegrei (1) and Campi Flegrei (2) (with 1.7 and 2.1 %, respectively) and 1.7 % in Stromboli (1) stop.

Fig. 5.3 Chemical percentage composition of PM_{10} and $PM_{2.5}$.

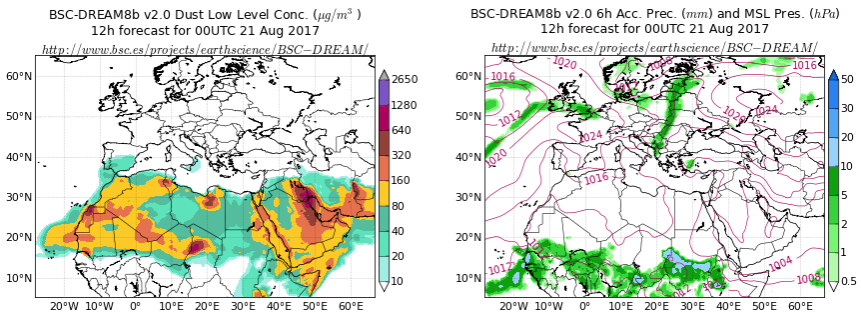

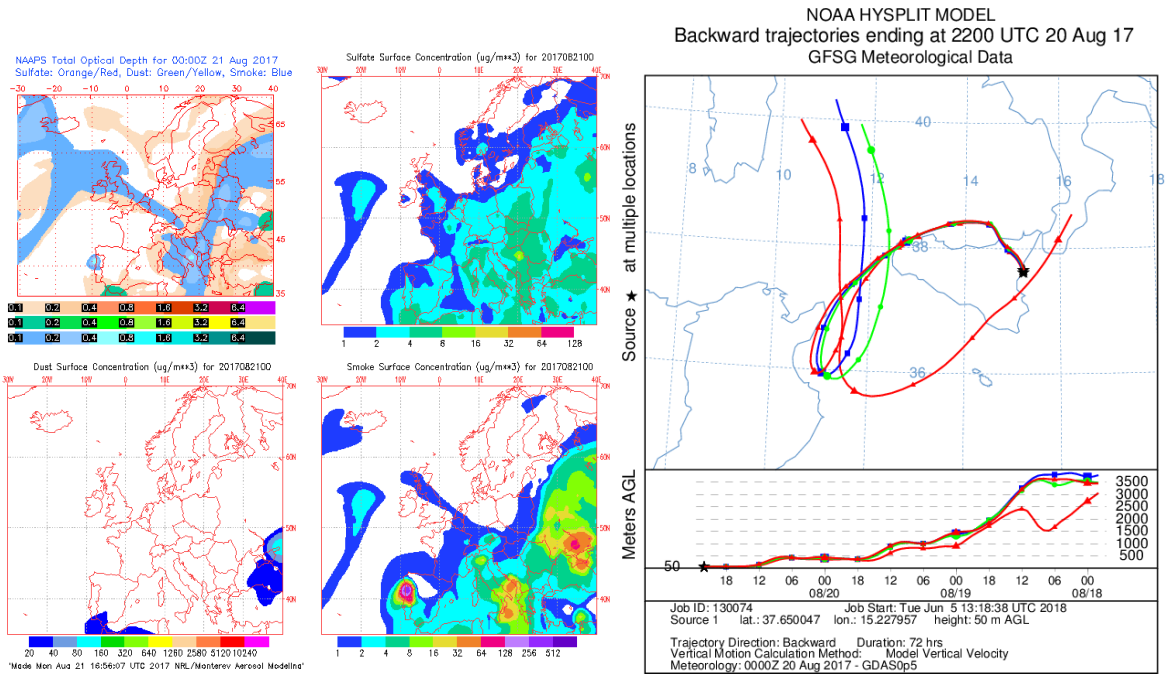

Fig. 5.4 Acireale maps NAAPS, back trajectory, and BSC-Dream.

It is no doubt that volcanic emissions are important sources of metal-bearing gases and particles into the atmosphere, as demonstrated by metal output inventories evaluated for a number of volcanoes, including Etna (Aiuppa et al. 2003; Allen et al. 2006; Bagnato et al. 2007) and Stromboli (Allard et al. 2000; Mather et al. 2004). Previous research has revealed a dual source history for volcanogenic trace metals, including the atmospheric release of 1) volatile elements, which are volatilized from the silicate melt during magma degassing, and later dispersed in atmospheric plumes as sub-micron sized volcanic aerosols, and 2) poorly volatile (refractory or lithophile) elements, transported via coarse volcanic ash fragments (Calabrese et al. 2011).

The volcanic area covered during the campaign, as discussed above, includes Etna and Stromboli that are sub-aerial volcanoes with a significant part of their structure under the sea, while the Marsili Seamount is submerged, and its activity is still open to debate. At the Marsili stop, in effect, in all classes of chemical components constitutive of PM, the lowest values were obtained. Some elements are particularly representative of terrestrial crust and were chosen to discriminate if the sampled PM in the different location were similar to the elements coming from that volcano; the elements chosen to obtain this information were Al, Ca and Fe. In the attempt to evaluate which of the samples was more similar to the volcanic plume, the average elemental concentrations in lava and ash, in the Etna case were obtained from literature data reported by Calabrese et al. (2011), while Stromboli composition of ash

and basalt obtained from Allard et al. (2000) work was used. In Fig. 5.5 are shown the ternary plot obtained for both volcanoes. The Acireale and Acicastello values are very similar to the Etna's values both in the lava and in the ashes, giving an indication of the successful sampling even at a considerable distance from the source. The values obtained from the ternary plot for Stromboli also show a good relationship between the basalt values found in the literature for samples Stromboli 2 and Stromboli 3, while the Stromboli 1 sample is closer to the ash values.

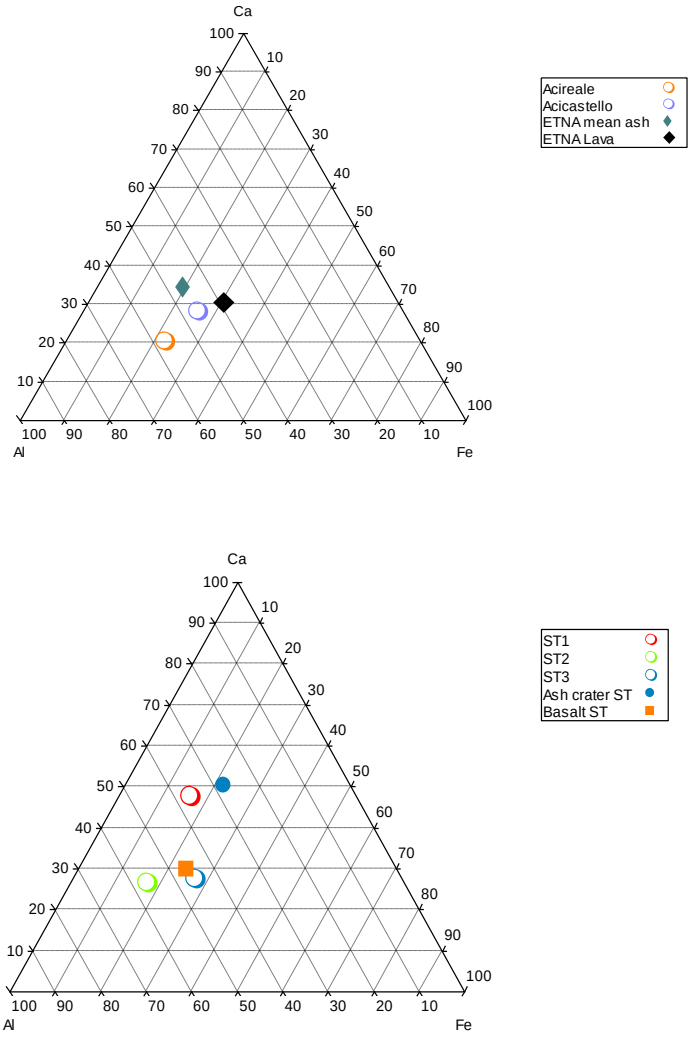

Fig. 5.5 Ternary plot for a) Etna samples (Acireale, Acicastello) and b) Stromboli samples (ST1, ST2, ST3)

Additional comparisons between sampled PM fraction and plume aerosol chemical properties can be achieved, by means of calculation of the enrichment factor (EF), which is a useful tool to highlight the enrichment or depletion degree of a given element in a geochemical medium relative to reference material. Although the use of enrichment factors

could hide serious flaws, such as the variable composition of the reference material, or inadequate choice of the element used to normalize the data (Reimann and De Caritat 2000), it provides first-order insights on elements mobility. The EF, calculated as explained above, allows assessing the extent to which any given element is enriched in PM relative to a reference element (Al). An EF close to unity indicates there is essentially no enrichment occurring for a given element in sampled PM relative to the expected abundance in basalt. Since Al is a poorly volatile element at magmatic conditions, and also one of the most immobile elements during the weathering of basalts (Aiuppa et al. 2000), EFs far exceeding unity characterize volatile (enriched in the plume because of their affinity for the magmatic vapor phase) and/or mobile elements.

Fig. 5.6 suggests that EFs for both volcanoes are overall consistent and that there exist three distinct groups of elements with different degrees of enrichment with respect to the basalt (Stromboli) and lava (Etna). The *strongly enriched* elements have EFs >100 in volcanic aerosols and are the most mobile (volatile and/or soluble) species (such as Sb, Se). The *enriched elements* have EFs ranging from 1 to 100, while the *depleted elements* such as Co, Fe, Sr, Mn, and Ti have with EF <1. Overall, volatile species (Tl, Se, Cr, and Sn) are enriched by two to three orders of magnitude in magmatic plume emissions of both volcanoes relative to non-volatile elements. Among the most enriched elements in Etna samples, the Cr and Mo were higher than the Stromboli's samples. The difference between the enriched elements in the two volcanoes can be noted in the presence of Sm and As in the Stromboli's samples while they are totally absent in Etna's samples. The case of the Tl, present among the elements enriched in the samples of Etna, is not a coincidence since also Calabrese et al (Calabrese et al. 2011) reported its presence among the most enriched elements in their work.

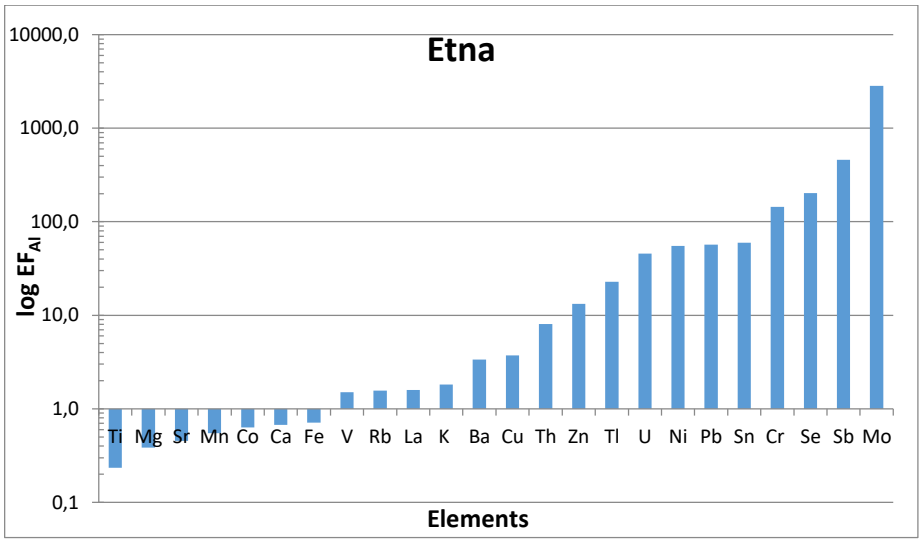

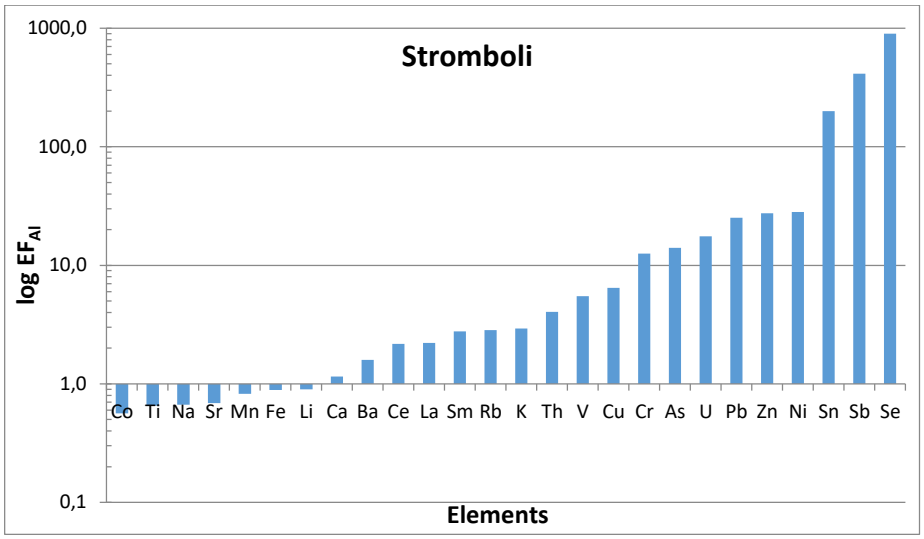

Fig. 5.6 Enrichment Factor for Etna (Acicastello sample) and Stromboli (Stromboli 3 sample).

The fumaroles area in this study includes Campi Flegrei, Ischia and Aeolian area (Vulcano, Panarea). The fumaroles plume may carry out a double action: 1) alteration of the pyroclastics by direct interaction between the acid fumarolic aerosol and rocks; 2) condensation of the acid gases such as SO_2 (whose disproportionation in water produces H_2SO_4 and H_2S), HCl and HF in dew and in meteoric waters, resulting in acid surface fluids. The results in this investigation indicate a high correlation between acid aerosol concentrations in PM samples and the natural emissions of sulfur-rich geothermal sources. These findings are shown in Fig. 5.7, in which can be noted clearly correlation of the SO_2 and SO_4^{-2} concentrations in both fractions, with R^2= 0.74 for $PM_{2.5}$ and R^2=0.76 for PM_{10}. Eliminating the Vulcano (2) sample, the R^2 coefficients for both PM fraction increase up to 0.95 and 0.94 for $PM_{2.5}$ and PM_{10} respectively, this may be associated with the atmospheric conditions of the day of sampling different from the previous ones, in which there were still rough seas and gusts of wind.

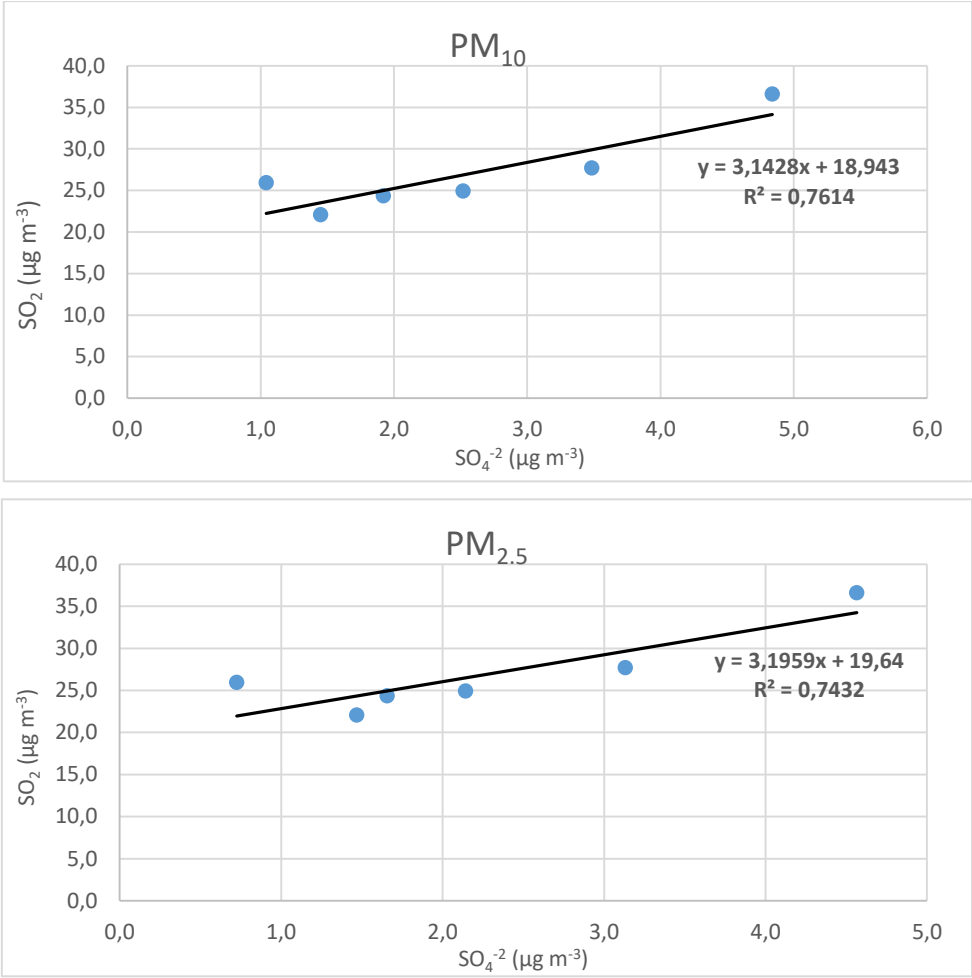

Fig. 5.7 Correlation between SO_2 and SO_4^{-2} in both fraction, PM_{10} and $PM_{2.5}$.

In support of this thesis, in Fig. 5.8 spatial SO_4^{-2} and SO_2 concentrations are reported, with higher concentrations of SO_4^{-2} in Vulcano (1) sample and the lower in Vulcano (2). The latter is probably due to the difficult interception of the wind with the pollutants, given the sudden change in direction of the wind itself.

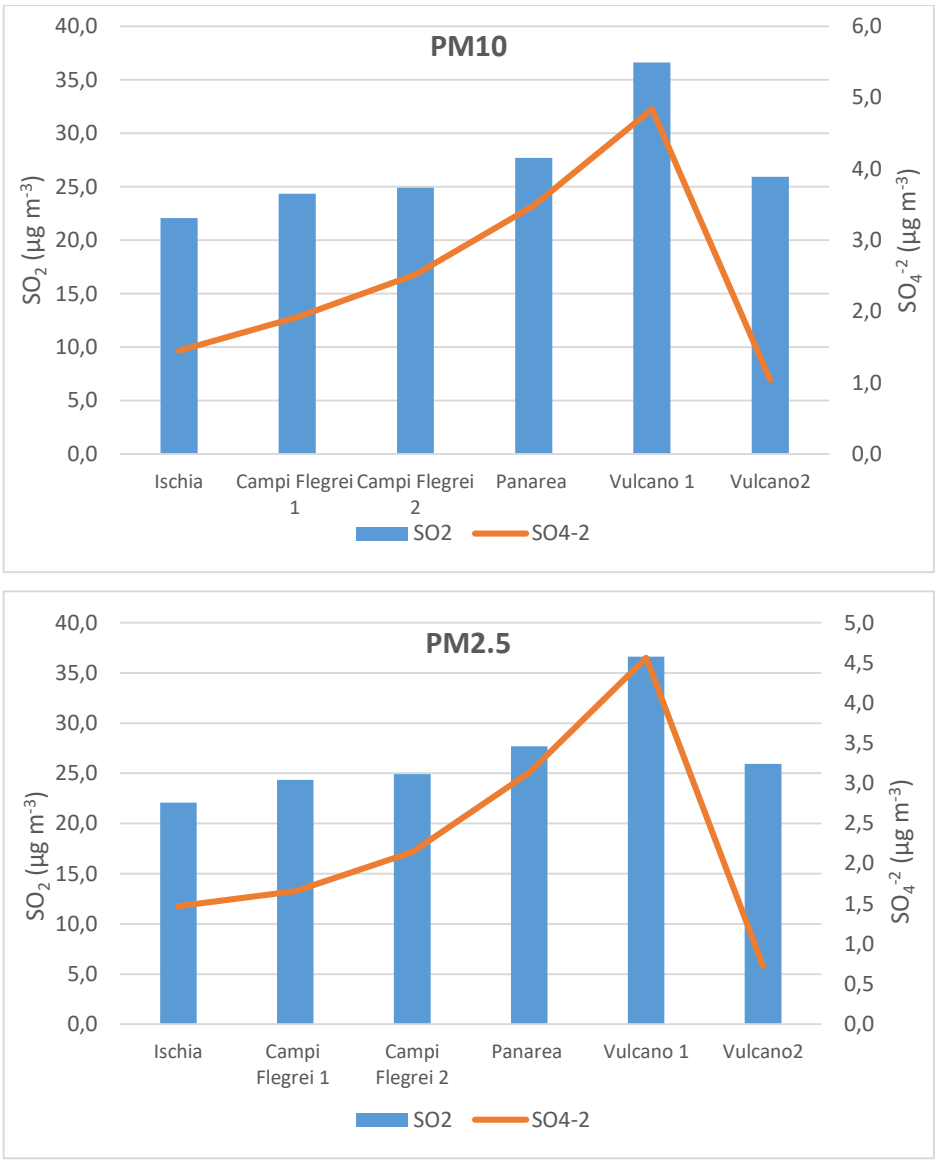

Fig. 5.8 Concentration of sulfur dioxide and sulfate ions in fumarolic area.

Factor analysis, a tool for source identification and apportionment of particulate air pollutants, was used to characterize the different sources of aerosols during the whole campaign. The dataset was subjected to Varimax Rotated Factor Analysis using Statistica software identifying six factors with Eigenvalues greater than one (Table 5.1). Loadings greater than 0.5 are shown in bold in the table. The six factors together explain more than 93% of the total variance of our dataset.

Variable	Factor1	Factor2	Factor3	Factor4	Factor5	Factor6
PM_x	0,4	**0,6**	0,3	0,2	**0,5**	-0,3
OC	**0,7**	**0,6**	0,2	0,2	0,0	0,2
EC	**0,9**	0,0	0,2	-0,1	-0,1	0,0
NH_4	0,0	**0,8**	-0,2	0,1	-0,4	-0,1
Al	-0,1	0,2	**0,8**	0,3	0,2	-0,3
Fe	0,3	0,1	**0,8**	0,2	0,3	0,0
Na	0,0	-0,2	0,2	0,0	**1,0**	0,0
Ca	0,1	0,0	0,3	**0,9**	0,2	0,0
Mg	0,0	-0,1	0,4	0,1	**0,9**	-0,1
P	0,0	0,1	0,1	**0,9**	0,0	0,0
Tot SO_4^{-2}	0,1	**1,0**	0,2	0,2	0,0	0,0
V	0,2	**0,9**	0,1	-0,1	-0,2	0,2
Cr	0,1	-0,1	**0,8**	-0,1	0,3	0,2
Mn	0,4	0,2	**0,7**	0,3	0,1	0,2
Zn	0,1	0,1	0,0	**0,9**	-0,1	0,2
As	**0,9**	0,1	-0,2	0,2	0,1	0,1
Sb	**0,9**	0,0	0,2	0,0	0,0	0,2
Ce	0,2	-0,1	0,2	0,1	0,0	**0,9**
Pb	**0,7**	0,4	0,2	0,1	0,0	**0,5**
Zr	0,1	0,1	-0,2	0,1	-0,1	**0,9**
Eigenvalue	4,0	3,4	3,4	3,0	2,4	2,4
% of Var.	20,1	17,1	17,1	14,9	12,1	11,8
Cum. %	20,1	37,2	54,2	69,1	81,2	93,0

Table 5.1 Varimax Rotated Factor Loadings for the whole data set of Med-Oceanor 2017 campaign.

- The first factor with high loadings for carbonaceous material (EC, OC) and As, Sb and Pb can be attributed to anthropogenic sources, which affected the part of the campaign. This result could support the thesis proposed above, according to which the intensive vehicular traffic observed during those days for the stop in the Campi Flegrei area influenced the result.
- The second factor, with high loadings of total SO_4^{-2}, NH_4^+ and V can be attributed at the shipping emissions, considering also the values of OC and PM. Indeed, as previously reported, the V element is used as a tracer of shipping emission.
- The third factor, with high loadings for Al, Fe, Cr, and Mn can be associated with mineral sources; these elements are common in the crust and basalt of volcanoes.
- The fourth factor, with high values of Ca, P and Zn is most probably linked with the stop in the harbor (Lipari); these elements are constitutive of fertilizer as $Ca(H_2PO_4)_2$ and in particular, Zn is used to micronutrients.
- The fifth factor is the simplest to detect, because the high values of Na and Mg associated with the value of 0.5 of the PM, indicate that it is associated with the sea salt aerosols.

- The sixth factor, with high loadings of Zr, Ce, and Pb, is probably due to Zircon compounds, that confirm the geogenic origin.

In the previous years, three cruise campaigns have been performed in the western sector of the Mediterranean Sea basin by the CNR-IIA researchers. In particular, two of them, during 2011 and 2015, followed a route in the Tyrrhenian Sea, and the last one, during the 2012 year the cruise developed a route covering the largest area of the western Mediterranean and crossing the Strait of Gibraltar (see Fig. 5.9). The three monitoring campaigns have been conducted with the purpose to evaluate the impact on the PM chemistry of both anthropogenic and natural emission sources, therefore the monitoring sites fixed along the routes were selected considering off-shore areas, and near coastal sites. Particularly, during the 2015 cruise campaign, a number of fixed sites (i.e., close to the Aeolian arc area) were overlapped with some of selected during the 2017 cruise. In order to perform a deep characterization of the Particulate matter in the Mediterranean Sea Basin, my contribution in this work was to analyze all samples collected during the past three cruises and compare the results with those obtained in 2017. Two size fractions of particulate matter (PM_{10} and $PM_{2.5}$) were collected. The mass of the particulate was determined gravimetrically while the analysis of the multielement profile for both fractions has been performed by Inductively Coupled Plasma Mass Spectrometry (ICP-MS), for both major and trace elements, differently to the 2017 campaign. These datasets were analyzed by using the Enrichment Factors (EFs) and the Principal Component Analysis (PCA) for a source apportionment investigation on the aerosol sampled during the campaigns.

In this case, for EFs determination the concentration of Fe in the Upper Continental Crust (UCC) concentrations were chosen, similarly to saw above with the Al element. Then, EF is defined as the ratio of a given element to the concentration of a crustal element in a sample (in our case iron), normalized to the same ratio in the earth's crust. For each element, the EF was calculated according to Eq. 5.5:

Eq. 5.5

$$EF = \frac{EC_{Sample}/Fe_{sample}}{EC_{UCC}/Fe_{UCC}}$$

Principal Component Analysis (PCA) was used to identify the principal emission sources of the sampled aerosol on the Western Mediterranean Sea. PCA is a basic tool for data analysis in order to visualize samples in the bidimensional plot, to reduce the dimensionality of the data, eliminate unnecessary information, and to find possible correlations between variables.

The PCA analysis was performed on the data matrix obtained using the concentration values in PM_{10} samples and was performed in the R framework using the package FactoMineR (Lê et al. 2008). Missing values in the dataset were imputed before to apply the PCA by using the R package MissMDA (Josse and Husson 2016).

To simplify the identification of the stops during each campaign a notation was chosen. For example, 12s3 indicates 2012 as the year of the campaign, in this case, Fenice 2012; the last number identifies the number of the stop in chronological order while "s" simply stands for "stop".

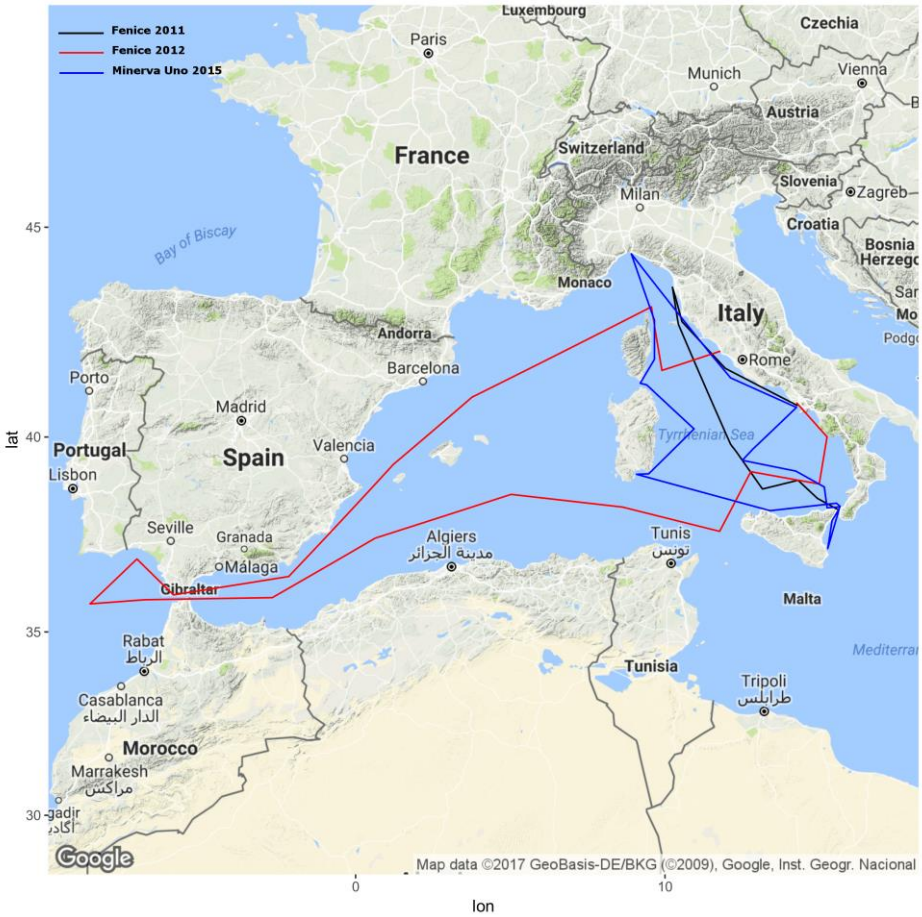

Fig. 5.9 Map of the routes. Fenice 2011 (black route), Fenice 2012 (red route), Minerva 2015, (blue route).

The campaigns were performed in different season as well as in different years, in fact Fenice 2011 campaign has been performed during the autumn (from October 28th to November 7th), while the other two campaigns have been performed in summer, with Fenice 2012 during August 14-28th and Minerva 2015 from June 28th to July 12th. Generally, during all the three

campaigns, a high-pressure area persisted for the whole routes, as confirmed by the sea level pressure maps, according to the NCEP/NCAR Reanalysis (Fig. 5.10).

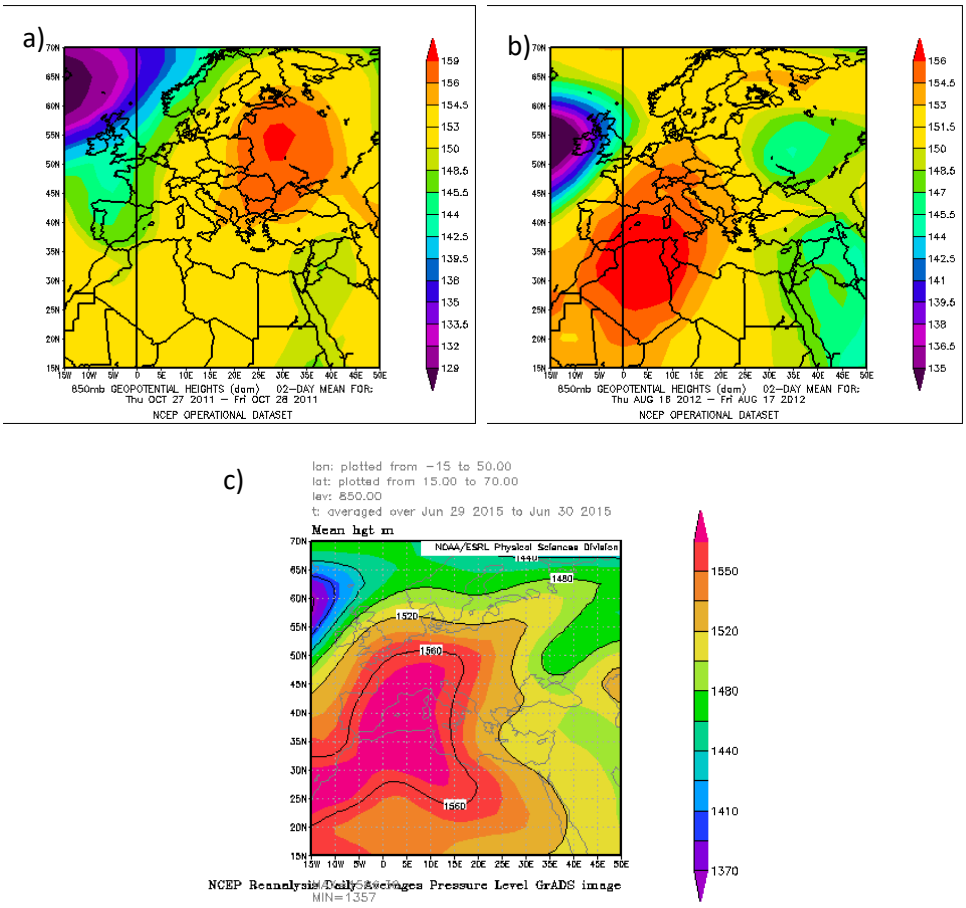

Fig. 5.10 NCEP Reanalysis maps for the three campaign: a) Fenice 2011, b) Fenice 2012 and c) Minerva 2015.

In particular, for the Fenice 2011 campaign, an anticyclone coming from Eastern Europe run into the Mediterranean Sea (Fig. 5.10a), recovering the RV's route, with an exception for the last two days (November 6-7th), when the anticyclone moved toward the North-East of Europe. On the other hand, for both summer campaigns, Fenice 2012 (Fig. 5.10b) and Minerva 2015 (Fig. 5.10c), an anticyclone coming from the Atlantic Ocean persisted in the Mediterranean Sea for the whole cruise. Wind speed and direction are important meteorological parameters, which strongly affect the motion of the air masses, the sea conditions, and thus plays an important role during the sampling of particulate matter. Minerva 2015 was the campaign with the lightest wind speed, (mean ± standard deviation, 2.7 ± 1.9 m s^{-1}) blowing mainly from W-NW and S-SE whereas Fenice 2012 was the campaign with the stronger wind (mean ± standard deviation, 9.4 ± 5.0 m s^{-1}) blowing from all the directions with a peak value of 32.5 m s^{-1}. Fenice 2011 was characterized by wind

blowing from E-NE and E-SE with speed between those of the other two campaigns (mean ± standard deviation, 6.0 ± 3.8 m s^{-1}).

The spatial variability of PM_{10} and $PM_{2.5}$ for each campaign are illustrated in Fig. 5.11.

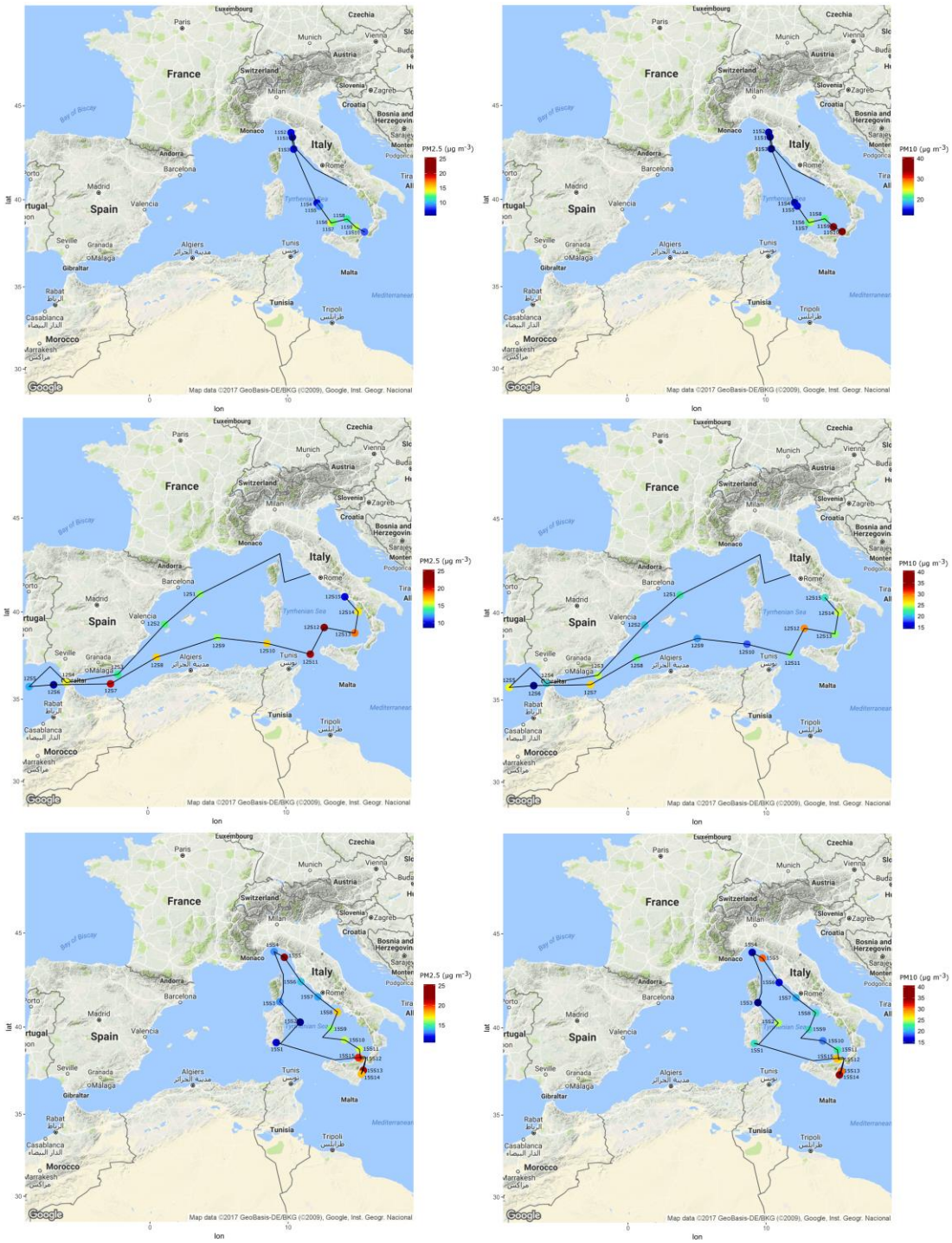

Fig. 5.11 Campaign routes and spatial variability of PM_{10} and $PM_{2.5}$.

As regards $PM_{2.5}$, analysis of variance (ANOVA) on the mass values shows that the recorded values during the three campaigns are statistically different ($p<0.05$). The lower average values for $PM_{2.5}$ were measured during Fenice 2011, the only cruise campaign carried out in autumn (about 10 µg m^{-3}). On the other hand, the other two summer cruises, Fenice 2012 and Minerva 2015, showed closer values of $PM_{2.5}$ mass, i.e., 17 and 19 µg m^{-3}, respectively. As concern the PM_{10} fraction, ANOVA shows that there is no statistically significant difference ($p<0.05$) among the values obtained during the three campaigns. Indeed, mean values of about 20 µg m^{-3} were found for the three campaigns (20.8 µg m^{-3} for Fenice 2011, 22.6 µg m^{-3} for Fenice 2012, and 23.5 µg m^{-3} for Minerva 2015).

As regards the Fenice 2011 cruise campaign, the lowest values for both $PM_{2.5}$ and PM_{10} were recorded and then increased along the route reaching the highest values, close to Sicily (11s9 and 11s10) due to the influence of Saharan dust as will be discussed below.

During Fenice 2012, fluctuant values were obtained, as can be seen in Fig. 5.11. The lowest value of $PM_{2.5}$ and PM_{10} was in the proximity of the Strait of Gibraltar (12s6), instead of the highest value for both fractions were recorded offshore (12s12), with back trajectory which show the possible intrusion of wildfire smoke from near land (Sicily) and sea salt due to high values of Na, K and Mg. Similarly to Fenice 2011, also during Minerva 2015 an increasing trend for both $PM_{2.5}$ and PM_{10} was recorded with the lowest values for both fractions close to the Sardinia whereas the highest values were registered close to the Sicily.

The percentage ratio between $PM_{2.5}$ and PM_{10} can be used to identify dust episodes. Low values of the ratio $PM_{2.5}/PM_{10}$ may be associated at an intrusion of air masses including Saharan dust, wildfires smoke or marine spray, generally characterized by a coarser size (Querol et al. 2004; Pérez et al. 2010). In Fig. 5.12 the ratio for each campaign is plotted. During the Fenice 2011 campaign, the lower ratios between $PM_{2.5}$ and PM_{10} were observed in the samples 11s9 and 11s10. The NAAPS maps, BSC-DREAM and the backward trajectories (Fig. 5.13) for this days confirm the intrusion of air mass from North Africa that can transport Saharan Dust and with the associated presence of high concentration of sodium, probably coming from sea spray for both sampling days due to unstable weather. As concern the Fenice 2012 campaign, based on the $PM_{2.5}/PM_{10}$ ratio, five hot spots were identified: 12s3, 12s5, 12s6, 12s14 and 12s15. A closer evaluation of the NAAPS maps, BSC-DREAM, and the backward trajectories revealed the presence of Saharan dust intrusions in the 12s3, 12s5, 12s6 and 12s14 samples while for the 12s15 sample no Saharan dust outbreak was found and probably the contribution is a mix between sea spray and anthropogenic with air masses coming from central-western Europe (FIG. S1). During the

Minerva 2015 campaign, two other events (15s2 and 15s14) with low $PM_{2.5}/PM_{10}$ ratio were reported. Both of them were characterized by the high value of sea salt (Na, Mg, and K) due to air masses that had dropped to sea level before reaching the sampling site confirmed by back trajectories (FIG S2).

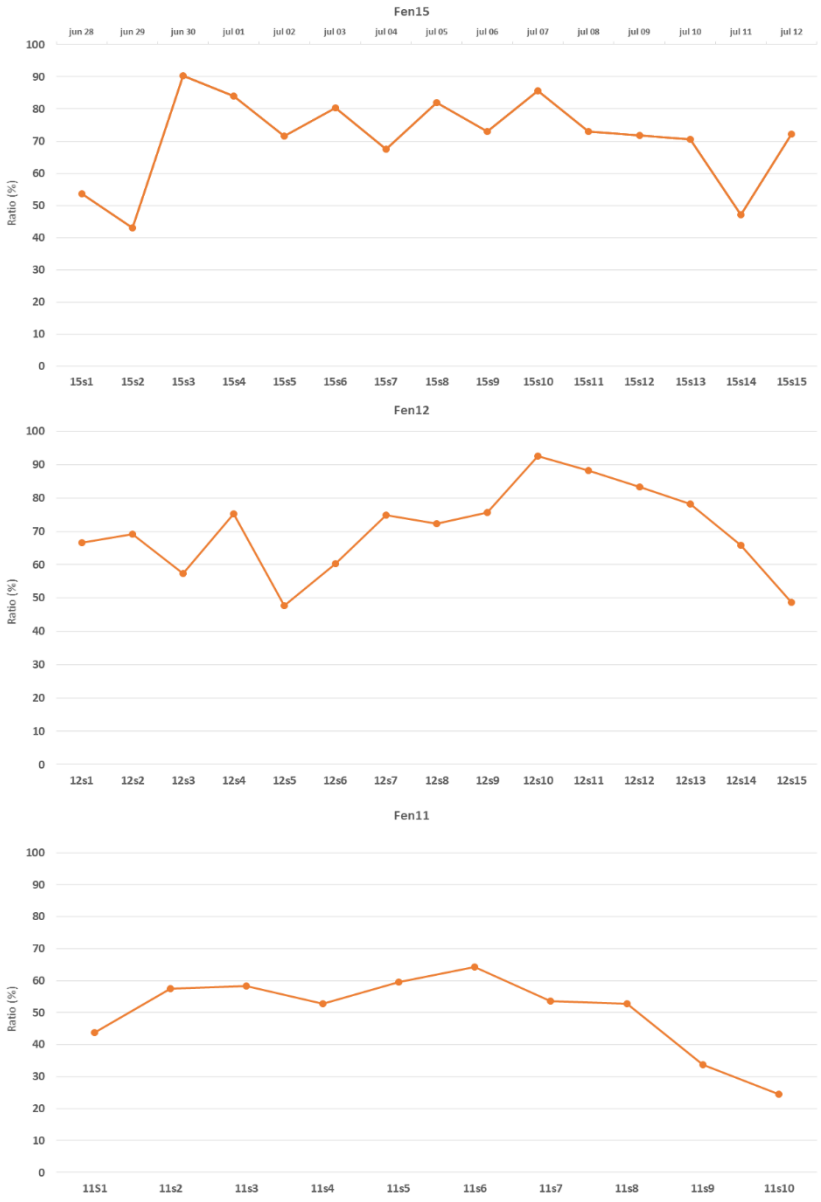

Fig 5.12 $PM_{2.5}/PM_{10}$ percentage ratio for each campaign.

a)

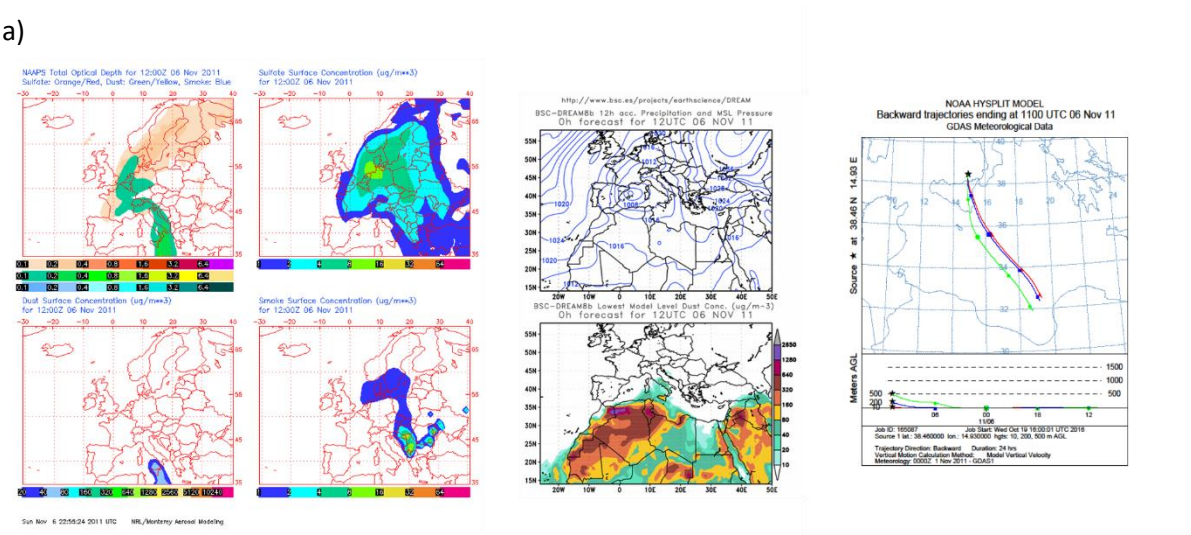

b)

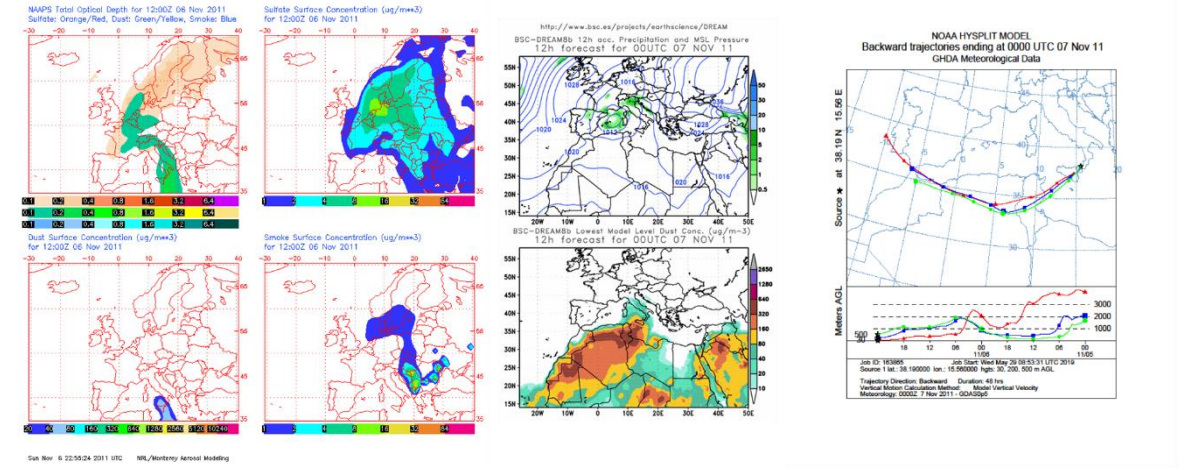

Fig 5.13 NAAPS, BSC-DREAM and back trajectory maps for Fenice 2011 campaign: a) 6 November (11s9) and b) 7 November (11s10) dust intrusion events.

Differently to the previously used approach, in this case, it has been researched the frequency of investigated elements, reported in Fig. 5.14; observing this figure it is possible to notice an interesting variability among the elements. Na, Mg, V, Mn, Sr, and Sb were detected in all PM_{10} samples whereas V, Mn, and Sb were detected in all the $PM_{2.5}$ samples. Other elements, i.e., Be, U, and Ag, were not found in both fractions during all the three campaigns. For both PM fractions, the elements can be grouped under three headings, according to the frequency in the samples (Fig. 5.14). One group includes the elements found in every campaign with almost equally percentages (these elements are Na, V, Mn, Fe and Sb for both fractions, and in addition, Mg, Al, K, Ca, Sr, Ba, Ce, and Nd for PM_{10}). In the second group there are elements with an increased frequency discrepancy between the campaigns but still observed in all the cruises. The last group includes the elements not detected in all

the campaigns, i.e., Co, As, Cd, Tl, Li, Cs, Tm for PM_{10} fraction and Eu, Dy, Ho, Er, Th, Yb, Sm, Cr, Co, As, Cd, Tl, Cs, Tm for $PM_{2.5}$. The elements that show the greater frequency variability are the most interesting because their presence in the particulate matter can be related to the route of the cruise and, as a consequence, to the encountered emission sources. A closer comparison of the frequencies between the two PM fractions allows to infer the elements that mainly characterize the coarse particulate fraction: Mg, Al, K, Ca, Sr, Ba, Ce, and Nd, probably due to sea salt and dust contribute. Indeed, since these elements have a higher frequency in PM_{10} compared to $PM_{2.5}$ they are mainly present in the coarse portion of the PM_{10} samples.

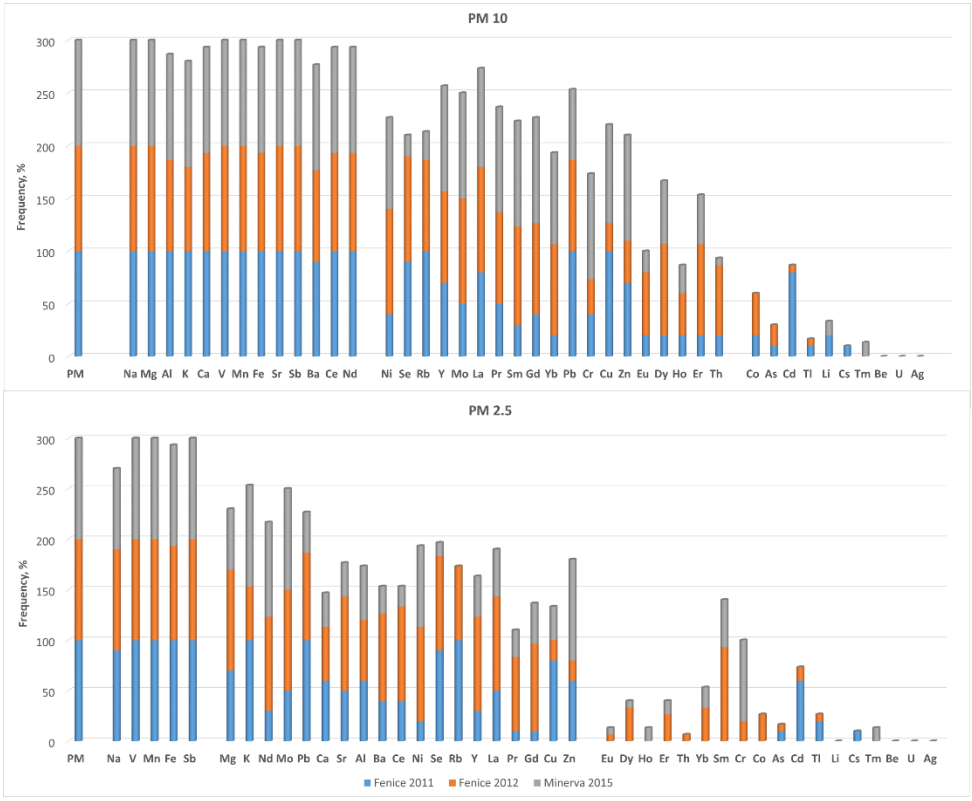

Fig. 5.14 Frequency of investigated elements in all the campaigns

Shipping emissions are usually accounted for by using the V/Ni ratio as a tracer of these sources. Vanadium and nickel may originate from a different source; however, a typical V/Ni ratio for shipping traffic ranges between 2.5 and 3.5 (Viana et al. 2009; Pandolfi et al. 2011). Consequently, their value was calculated for every sample so as to investigate the contribution of shipping traffic to the sampled particulate matter. During Fenice 2011 the V/Ni ratio showed a clear influence of shipping emissions for the samples collected in open sea route (11s4, 11s5, 11s6) and, in the last day of the campaign, close to the Strait of

Messina (11s10) (Fig. 5.15). A similar scenario was found during Fenice 2012 when the research vessel sampled close to the Strait of Gibraltar and in Minerva 2015 for the stretch of the route close to Sardinia and the Strait of Messina area. These results confirmed the massive contribution of shipping emissions for this area, due to the intense shipping traffic for commercial and touristic purpose. Indeed, also in the 2017 campaign, the contribution of shipping emission was found in Aeolian and strait of Messina area confirming this results.

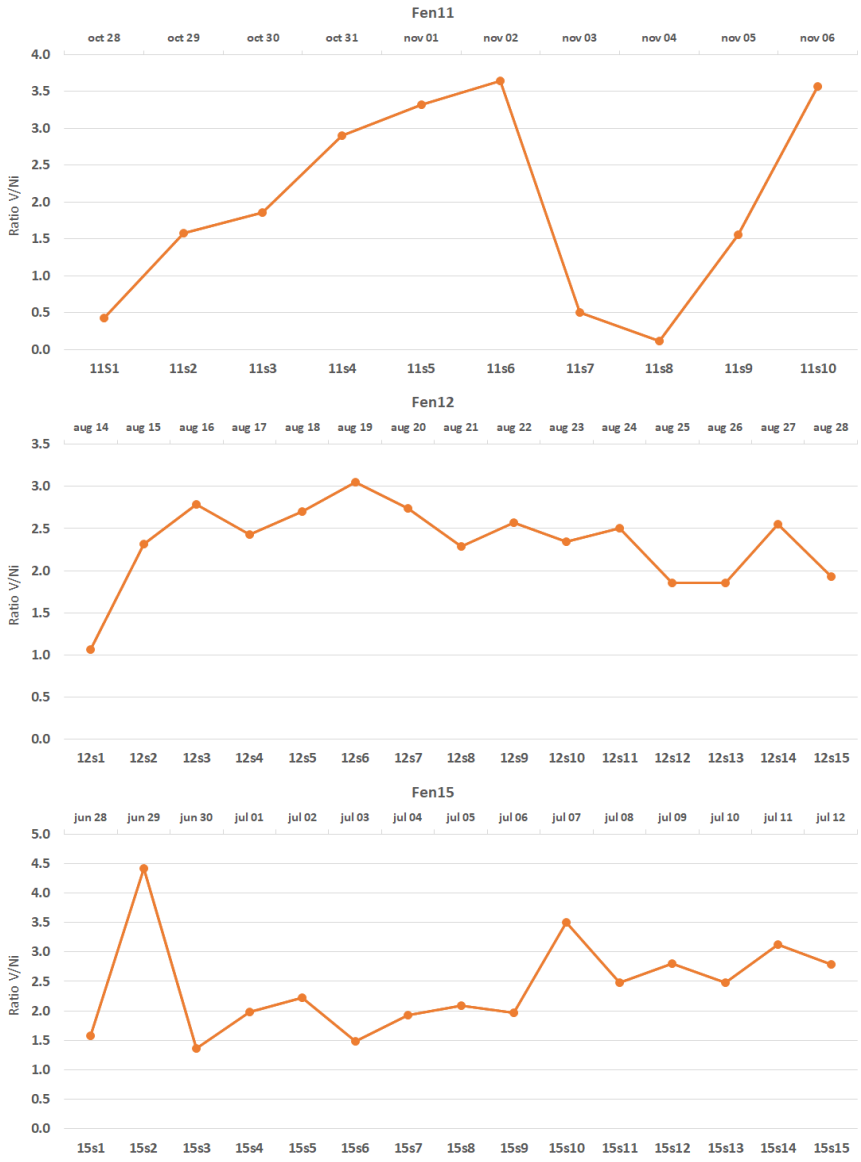

Fig 5.15 V/Ni ratios

Enrichment Factors are a common first approach for estimating the extent of anthropogenic contributions to measured concentrations of a given element, particularly in the context of inferring atmospheric aerosol composition (Lai et al. 2017). The choice of reference element is of great importance during enrichment factor analysis. Usually, Al, Ti, Fe or Si is used as

the reference element, as these elements have stable chemical properties and are influenced little by human activities. In this study, iron was selected as reference element while the abundance of elements in the earth's crust (UCC) was taken from Wedepohl (Hans Wedepohl 1995). The EF was computed for the elements with a concentration above the detection limit in at least 50% of the samples; the results are reported on a logarithmic scale in Fig. 5.16. Since the EF provide only qualitative information because of the wide variation of the element concentrations throughout the upper crust, EF=20 was selected as the threshold of significance. Therefore, elements with EF higher than 20 can be considered as significantly affected by the anthropogenic emissions; elements with EF lower than 10 can be mainly considered of crustal origin, and elements with EF between the two thresholds can be considered of mixed origin (crustal and anthropogenic) (Contini et al. 2010).

For Fenice 2011 Cd, Se, Sb, Cu, Pb, and Mo are enriched in both PM fractions whereas Zn and V can be considered enriched only in $PM_{2.5}$. In the case of Fenice 2012, the same six elements (Se, Sb, Ni, V, Pb, Mo) can be considered enriched in PM_{10} and $PM_{2.5}$. Similarly, for Minerva 2015, Sb, Mo, Ni, V, and Zn are enriched elements in both fractions; however, Pb and Cu show a moderate enrichment only for PM_{10} fraction. Comparing the results obtained with the 2017 campaign can be noted the persistent enrichment of elements highly volatile as Sb and Se but also Pb and Zn probably due to industrial activity in this case study.

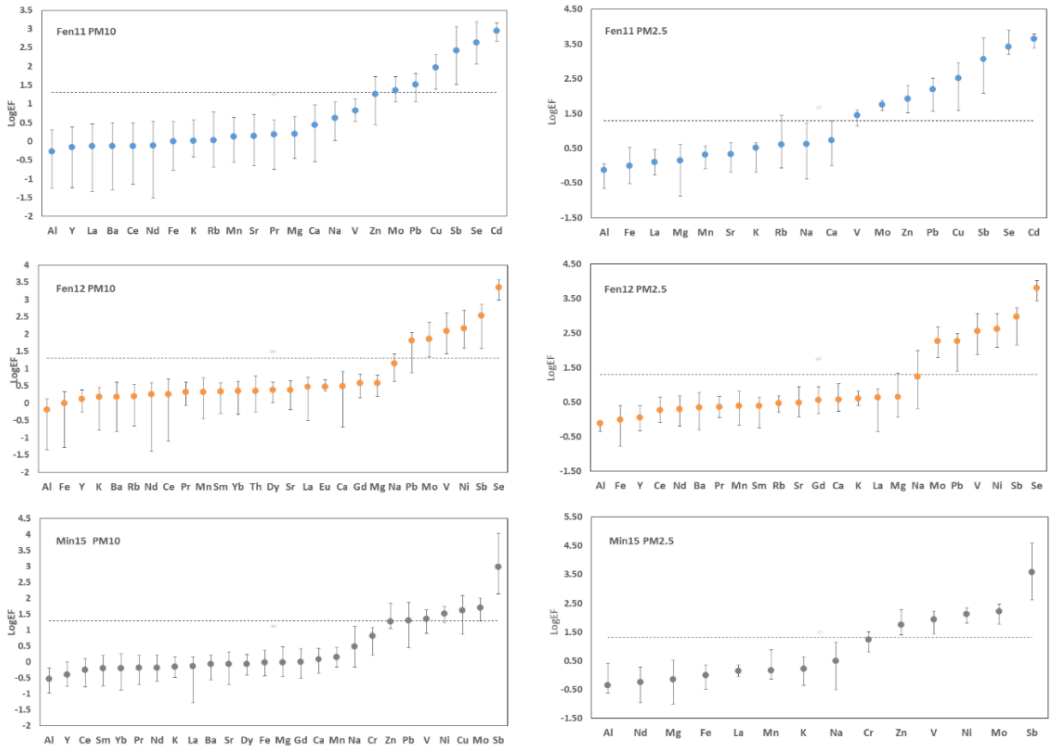

Fig. 5.16 Crustal enrichment factor (EF) for the different elements.

Principal Component Analysis (PCA) similar to FA previously used, was chosen to identify the principal emission sources of the sampled aerosol on the Central and western Mediterranean Sea during the three campaigns. Only the principal components (PC) with eigenvalues over one were considered obtaining 4 PCs which explain the 85.3% of the total variance.

- The first component (PC1), which explained about the 51% of the total variance, is loaded by Sr, Al, Mn, Fe, K, Ca, and Mg which are elements principally related to natural sources, mainly due to mineral dust (Querol et al. 2004; Cesari et al. 2016a).
- To the second component (PC2) the elements that contribute was Na, Mg, Cu, V, Ni, and Pb. This component, which explains about the 20% of the total variance, cannot be associated with a single source, instead, it seems to be a mix of marine spray due to the importance of sodium and magnesium (Moreno et al. 2010; Pandolfi et al. 2011) and other anthropogenic sources. A closer inspection of the factor loadings allows for understanding the presence of two different anthropogenic contributions: heavy oil combustion mainly due to the shipping traffic because of the positive correlation for V and Ni; road traffic because of the negative correlation for Cu, Zn and Pb (Cesari et al. 2016a).
- The third component (PC3) is driven by Sb. This PC explain about the 8% of the total variance and, given the route of the cruise, may be associated with the emission from the encountered volcanic sources (Shotyk et al. 2005).
- The fourth component (PC4) is a mixture of emission from industries and shipping traffic because of the high loading values, all in positive correlation, for Ni, Pb, V, and Zn (Cesari et al. 2016a).

The first principal component allowed the identification of different Saharan Dust intrusion event from all three campaigns. The identification of these events is confirmed by the NAAPS, BSC-DREAM and backward trajectory maps which shows the movement of the dust belt from Northern Africa in the Mediterranean basin. The second principal component identified some hot spots that can be related to intense shipping traffic during the three campaigns. In Fenice 2011 a noteworthy episode was recorded close to the Strait of Messina, the last day of the campaign (November 7th, sample 11s10); during Fenice 2012 in proximity of the Strait of Gibraltar on August 16-17th (12s3 and 12s4) and observed again at the same area during the way back to Italy on August 20th (12s7); during Minerva 2015, close to the Strait of Messina area (July 11th , sample 15s14). The PC3 highlighted an event of aerosol

degassing by Volcano Island that was intercepted on July 10th (sample 15s13) during the route to the Est coast of Sicily. The PC4 allowed to identify an episode of industrial emissions in Minerva 2015 (15s5), when the research vessel was close to an industrialized area in Tuscany. Moreover, as already pointed out by the PC2 scores and the V/Ni ratio, PC4 scores confirmed the significant influence of shipping emissions on the particulate matter sampled during the navigation close to the Strait of Messina and Strait of Gibraltar.

6 Case study 2: Carbonaceous aerosol assessment at high altitude GAW station of "Monte Curcio"

6.1 Introduction

Carbonaceous aerosols have atmospheric lifetimes of about few weeks; hence, they can be transported over long distances (Aruna et al. 2013), contributing not only to local but even to global air quality and potentially influencing global climate. This is in part due to highly variable temporal and spatial concentrations in the troposphere, caused by dispersion or turbulent mixing and in part due to undiscovered atmospheric transformations, such as heterogeneous oxidation or cloud seeding. In the atmosphere, aerosols become photochemically aged through complex mechanisms lead to the formation of secondary aerosols (Seinfeld and Pandis 2006).

In the last decade, the scientific community has paid much attention to the carbonaceous fraction of particulate matter (PM). These compounds account for an important fraction of atmospheric PM, generally contributing between 20 and 45% of PM with aerodynamic diameter ≤ 2.5 μm ($PM_{2.5}$), and between 20 and 35% of PM with aerodynamic diameter ≤ 10 μm (PM_{10}) in many European urban areas (Putaud et al. 2010).

The carbonaceous aerosol is composed by an organic fraction, named organic carbon (OC), and by a refractory light-absorbing component generally referred to as soot (as explained in chapter 1). Briefly, soot is generated by incomplete combustion of organic material from traffic, residential heating, industrial activities, and energy production using heavy oil, coal or biofuels. Depending on its empirical determination, soot is reported as elemental carbon (EC) or equivalent black carbon (eBC). Indeed, EC is quantified by thermal-optical transmittance methods, while eBC is derived from optical measurements. Particularly, eBC particles play an important role in the Earth's radiative budget by absorbing visible solar radiation and heating the atmosphere. The direct radiative forcing at the top of the atmosphere by BC particles has been estimated to be in the range +0.2 to 0.6 W m−2 (IPCC 2013). Elemental carbon is emitted directly into the atmosphere and has a long photochemical life which makes it a good indicator for primary anthropogenic air pollution (Kim et al. 2011; Xiao et al. 2011). As regards organic carbon, it originates from a variety of processes. It can be released into the atmosphere from anthropogenic (fossil fuel combustion, domestic heating and cooking, biomass burning), and biogenic sources (vegetation, wind-lifted biological particles, fires, emissions from marine environments), as

primary OC, or produced within the atmosphere by photochemical reactions through gas-to-particle conversion of volatile organic compounds, as secondary OC.

The investigation of carbonaceous aerosol has been performed in several European sites characterized by different anthropic impact (Rodríguez et al. 2007; Viana et al. 2007). These studies focus on the concentration levels, seasonal trends, and sources apportionments, thereby supporting the hypotheses that fossil fuel combustion is the dominant environmental carbonaceous source on a local scale in most seasons. Similarly, other studies focused on the rural, background, and village sites showed that biomass burning contributes the most to the formation of eBC as a result of the wood-burning for residential heating (Briggs and Long 2016; Glasius et al. 2018). As regards the OC and EC seasonal trends at traffic and urban sites, it has been reported that their concentrations reach the highest levels during the winter, whereas the OC concentration increases at rural sites during the warmer period (Querol et al. 2013; Crenn et al. 2017).

In Italy, one of the first studies on carbonaceous aerosol was performed in Rome during the period May 1999 – February 2000 (Avino et al. 2001) using the thermal method to determine the EC and OC concentrations. The temporal trends of particulate matter, total carbon, elemental carbon, and organic carbon have been interpreted using the measurements of the concentrations of natural radioactivity as a tracer of the dynamic properties of the planetary boundary layer. Recently Sandrini et al. (Sandrini et al. 2014b), reported a large-scale investigation of the OC and EC concentrations measured across the peninsula, exploring their spatial and seasonal variability for the period 2005–2012 in different sampling sites (i.e., industrial, traffic, urban, semi-rural, rural and remote locations). Another recent study carried out by Cesari et al. (Cesari et al. 2018) reported a three years measurement campaign for the determination of OC and EC in $PM_{2.5}$ and PM_{10} and an inter-comparison of EC and eBC in an urban background station in Apulia region, South Italy. This study confirms the seasonal trends for OC and EC in both PM size fractions, with higher concentrations during the warm season than those observed during the cold season. These findings support that the presence of a larger occurrence of stable atmospheric conditions during the warm months (unfavorable to the dispersal of pollutants) enhances the production of secondary organic aerosol.

The main objects of this work were to fill the gap, improving the knowledge of carbonaceous aerosol distribution, seasonal trends, main sources and correlation with a circulation of air masses. Indeed, this studies show in the first part the results obtained from the first long-term dataset in a high altitude remote site in South Italy, representative of the central

Mediterranean Sea and the possibility of detecting long-range transport, and in second part an interesting intensive measurement campaign conducted from November 2015 to January 2016 at five different sites of Southern Italy, to investigate and compare the characteristics and the relative contributions of carbonaceous species (OC and EC) to the PM_{10} and $PM_{2.5}$ mass.

6.2 Site description

Measurements were taken at the Monte Curcio Observatory (39° 18'57.2"N 16° 25'23.6"E; 1780 m a.s.l.), located in a strategic position within the Sila National Park in the Calabria region (South Italy, Fig. 6.1).

Fig 6.1 Map of Monte Curcio Observatory location.

It is a high altitude and remote monitoring station located on a southern Apennine mountain peak with a completely free horizon, thus allowing atmospheric monitoring measurements with large spatial representativeness. Due to its elevation and position in the middle of the Mediterranean basin, around 30 km far from the Tyrrhenian Sea and 60 km from the Ionian Sea, the Monte Curcio station is particularly able to intercept dust plumes from the Saharan desert as well as volcanic ashes and gases from the Stromboli and Mt. Etna volcanoes, located at around 120 km south-easterly and 220 km south-south-easterly from the atmospheric monitoring site, respectively.

6.3 Experimental and Data treatment

Consecutive nine months campaign was performed between April and December 2016 in which I was involved in sampling, and the analysis of the filters and the results. Daily (starting at midnight) $PM_{2.5}$ and PM_{10} samples were simultaneously collected, on quartz fiber filters (Pall LifeSciences, 47mm in diameter), using a dual channel sampler (SWAM, Fai Instruments) with on-line detection of particulate matter concentration based on β-ray attenuation. Since May 2016, simultaneous eBC concentrations, only in PM_{10} fraction, were measured using a Multi-Angle Absorption Photometer (MAAP Thermoscientific, mod. 5012). Light absorption coefficients and eBC concentration were recorded every 1 min at a wavelength of 670 nm. During the sampling period, meteorological data, including ambient temperature, relative humidity, wind velocity, and wind direction were also recorded using automatic equipment (LSI Lastem).

The concentration of the carbonaceous species was determined on one punch (area: 1 cm^2) cut from the quartz fiber filters employed for collecting the 24-h PM_{10} and $PM_{2.5}$ samples. The analysis of OC and EC was performed by the thermo-optical transmittance method using a Sunset Laboratory OC/EC analyzer (Sunset Laboratory, Tigard, OR, USA), implementing the EUSAAR-II temperature protocol (Cavalli et al. 2010). The European Standards CEN/TR 16243, suggest to pre-fire the quartz filters before collecting the samples to remove any residual carbon contamination before the sampling. In this work, prior to sampling, all the filters were pre-fired for 2h at 700°C. Blank filters were also analyzed for correcting the measured concentrations. EC concentrations observed in blank filters were negligible (<0.1 μg cm^{-2}); however, contamination was observed for OC. The corrected OC concentrations were obtained by subtracting the average value of the blank filters obtained from the OC measured in each exposed sample.

Given the know incidence on the air quality in Mediterranean country and to exclude its impact on the evaluation of seasonal and daily trends, the PM exceedance due to SDO (Saharan Dust Outbreaks) has been evaluated using the following methods:

- Interpretation of the daily weather conditions by analyzing the back-trajectories of air masses, with HYSPLIT model (Hybrid Single-Particle Lagrangian Integrated Trajectory) developed by National Oceanic and Atmospheric Administration, USA (NOAA), (Escudero et al. 2006). HYSPLIT accomplishes a wide range of simulations related to atmospheric transport and dispersion of pollutants using meteorological archived data and forecasts, provides information on the trajectories of air masses that can carry particulate.

- Application of BSC-DREAM model (Dust REgional Atmospheric Model) developed by Barcelona Supercomputing Center, (Pérez et al. 2006). The model predicts, every six hours, the life cycle in the atmosphere of the particulate eroded from desert areas, providing information on the concentration to the ground and at high altitude.
- Application of NAAPS model (Navy Aerosol Analysis and Prediction System), developed by Naval Research Laboratory (http://www.nrlmry.navy.mil/aerosol/). The model is capable of estimating concentrations of mineral aerosols, defining the origin as a function of the atmospheric optical thickness (AOT), NAVY, US., (2003). Greater is optical thickness for a wavelength, shorter is the amount of light of that wavelength that reaches the earth's surface. This model provides, for each day analyzed with an hourly resolution of six hours, the evolution of any clouds of mineral aerosols.

The exceedance of daily limit value (DLV) has been attributed to the Saharan dust transport exclusively in the case in which the three models were in agreement with each other, for the day in question, deleted from the dataset. During May 2016 an important contribution was observed in two different periods, from 10th to 12th and from 27th to 30th May. In the first period, the higher peak of the whole campaign was recorded on 11 May with 163.1 µg m^{-3} of PM_{10} and 42.3 µg m^{-3} of $PM_{2.5}$. In Fig 6.2 are reported the agreement between the three models used in this specific case, with the DREAM model that shows concentration in the range between 160 and 320 µg m^{-3}. In June only one contribute of Saharan dust was found in 18th June while in October and November it was recorded in 25th and 26th October and from 6th to 8th November (data not shown).

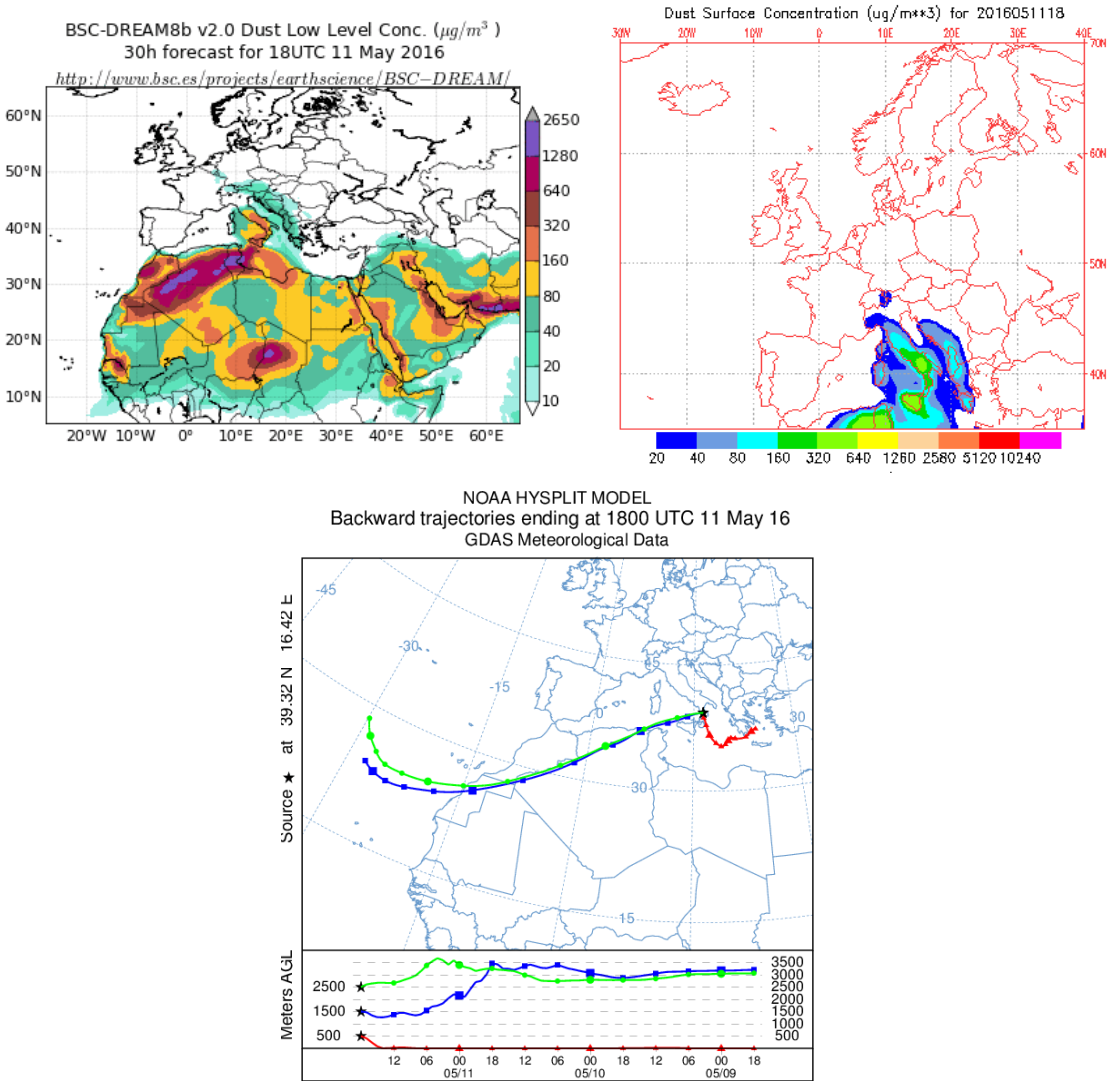

Fig 6.2 Graphs related to the exceeding of the threshold value of 11 May 2016; a) BSC-DREAM, b) NAAPS model graph and c) HYSPLIT back-trajectory model.

In the first chapter, we have seen that the EC is only emitted from primary sources, while the OC can be both primarily emitted (as primary organic carbon, POC), but also formed in the atmosphere through condensation to the aerosol phase of low vapor pressure compounds emitted as primary pollutants or formed in the atmosphere (called secondary organic carbon, SOC). In this work, I had chosen to estimate POC and SOC deploying two different methods. The first method is those proposed by Pio et. al. (Pio et al. 2011) by which the SOC concentration is estimated from the OC/EC minimum ratio ($(OC/EC)_{min}$) according to the following equation:

Eq. 6.1 $$SOC = OC - EC * (OC/EC)_{min}$$

In this approach, a critical point is represented by the choice of the ratio $(OC/EC)_{min}$. In this study, it was determined with two strategies in order to compare their performance. The first method was graphically looking at the minimum slope of the OC and EC correlation (Fig. 6.3) while in the second method (Pio et al. 2011) the data were ordered by the OC/EC ratio value and the lower 5% values were chosen as a subset. The median samples determined of these subsets were chosen to represent the minimum OC/EC ratio.

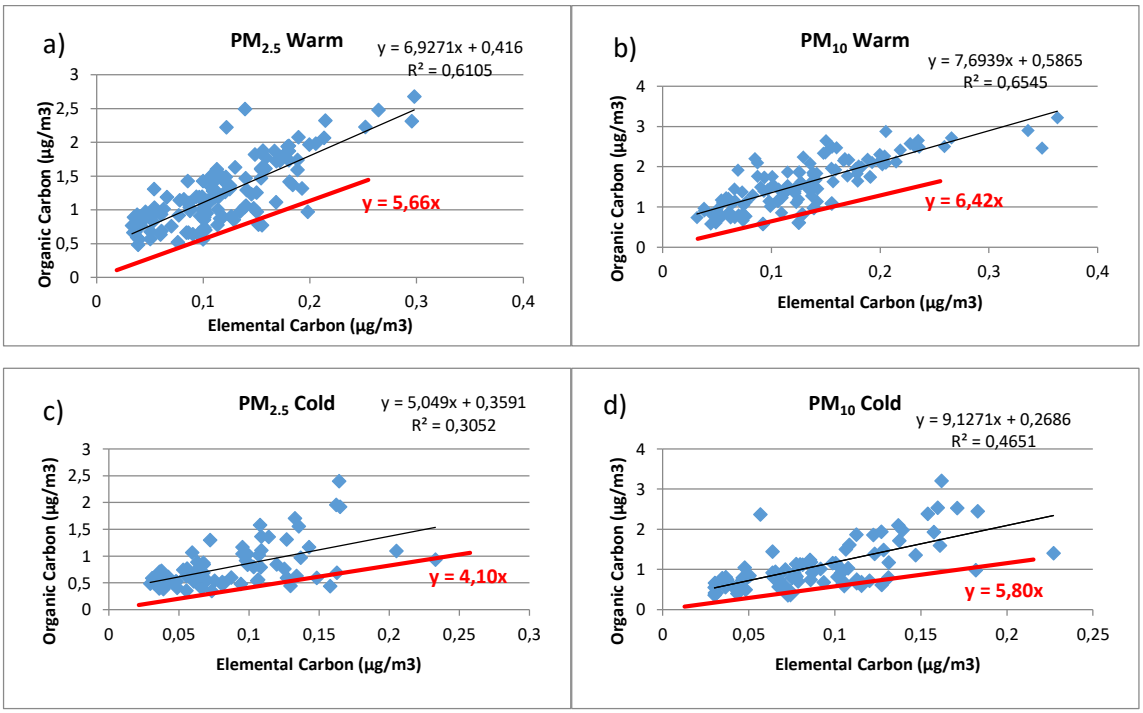

Fig. 6.3 Correlation between OC and EC concentrations in $PM_{2.5}$ and PM_{10} separating warm (a, b) and cold seasons (c, d). Red thick lines have the slopes corresponding to the minimum ratios $(OC/EC)_{min}$.

The third method recently proposed by (Wu and Yu 2016) in accordance with the EC tracer method rather than OC/EC minimum ratio method used for others. The key step in the EC tracer method is to determine an appropriate OC/EC ratio that represents primary combustion emission sources (i.e., $(OC/EC)_{pri}$) at the observation site. For this purpose (Wu and Yu 2016) proposed a SOC-EC correlation minimization method, providing a clear, quantitative criterion for $(OC/EC)_{pri}$ estimation with the best performance. Briefly, the method determines the actual $(OC/EC)_{pri}$ ratio by generating a series of $(OC/EC)_{pri}$ and SOC pairs followed by exploring the minimum correlation coefficient value between SOC and EC. This method requires the assumptions that EC is emitted from primary sources and both EC and SOC are independent variables. At first, a range of potential $(OC/EC)_{pri}$ values was

generated. Then for each generated $(OC/EC)_{pri}$ value, the concentrations of SOC were calculated according to:

Eq. 6.2 $$SOC = OC - [EC * (OC/EC)_{pri}]$$

Thereafter the SOC vs. EC correlation coefficient (R^2) was derived. The SOC vs. EC correlation coefficients can then be plotted against the corresponding assumed $(OC/EC)_{pri}$ values as exemplified in Fig. 6.4. The actual $(OC/EC)_{pri}$ ratio is finally determined based on the "assumed" $(OC/EC)_{pri}$ that corresponded to the minimum SOC vs. EC correlation coefficient.

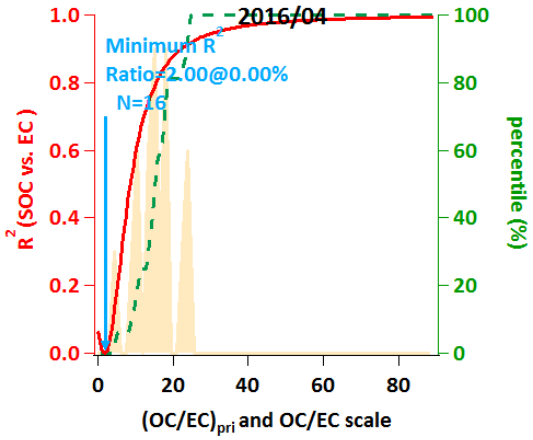

Fig 6.4 Example of graphic obtained using the method proposed by Wu and Yu 2016.

6.4 Results and discussion

The monthly averages of meteorological parameters (wind velocity and prevalent direction, temperature, relative humidity) including the interquartile ranges (25th and 75th percentiles) are reported in Table 6.1. The prevalent wind direction was found from the sector SSE-SE; it was mainly observed during the whole campaign except in the month of December where the prevailing wind direction was coming from the NE sector. The average wind velocities decreased during summer months (minimum reached in August, 3.3 m s^{-1}) before increasing again in autumn (maximum reached in November, 5.7 m s^{-1}). On the contrary, the temperatures showed a specular trend and had their higher values in the summer months (maximum reached in July, 16 °C). The relative humidity trend did not show a particular trend linked to seasonal variation. The lowest values were recorded in April. In summer, values around 70% can be attributed to the particular exposure of the site to air masses

coming from the Mediterranean, but also to the concomitant presence of higher temperatures and to the presence of lakes at few kilometers from the site. On the contrary, the values found during the autumn months can be attributed to the increase in rainfall during this season.

	Temperature (C°)	Relative Humidity (%)	Wind velocity (m s^{-1})	Prevalent wind direction
April	8.3 (4.5-11.7)	53.6 (25.6-91.3)	5.5 (2.9-7.4)	SE
May	7.7 (3.6-11.3)	74.1 (53.1-99.98)	5.3 (2.9-7.5)	SE
June	13.0 (9.9-16.1)	67.6 (53.4-82.7)	4.4 (2.5-5.8)	SE
July	16.0 (14.3-18.3)	65.5 (52.7-78.1)	3.4 (2.0-4.3)	SSE
August	14.4 (12.3-16.8)	71.0 (58.4-86.9)	3.3 (2.1-4.1)	SSE
September	10.3 (8.2-12.0)	82.0 (69.7-98.8)	3.5 (1.9-4.4)	SSE
October	8.7 (6.1-11.0)	77.7 (60.9-98.4)	5.6 (3.4-7.3)	SSE - SE
November	4.1 (2.3-6.5)	82.8 (75.3-99.3)	5.6 (3.4-7.2)	SSE – SE
December	-0.1 (-2.3-2.7)	69.2 (46.5-93.8)	4.5 (2.6-6.1)	ENE - NE - SSE

Table 6.1 Monthly averages of meteorological parameters (temperature, relative humidity, wind velocity, and prevalent wind direction). In parenthesis, the inter-quartile ranges (between 25th and 75th percentiles) are reported.

In Fig. 6.5 the monthly average of EC and OC concentrations in PM_{10} and $PM_{2.5}$ is reported. As shown in the figure, the carbonaceous compounds are mainly segregated in the $PM_{2.5}$, potentially caused by the contributions of combustion sources which affect mainly the fine fractions of atmospheric aerosols.

The trend of the OC and EC concentration in PM_{10} and $PM_{2.5}$ fractions are similar, with the highest concentrations observed during the warm period (April-August), while during the coldest months (September-December) lower carbon levels are observed. For PM_{10} the maximum recorded values were 1.97 μg m^{-3} and 0.17 μg m^{-3} for OC and EC, respectively; while in $PM_{2.5,}$ the maximum concentrations were 1.59 μg m^{-3} for OC and 0.15 μg m^{-3} for EC. The lowest concentrations were obtained in November for both fractions. In particular,

OC concentration was 0.66 μg m^{-3} in PM10 and 0.54 μg m^{-3} in $PM_{2.5}$, while EC value was 0.089 μg m^{-3} in PM_{10} and 0.095 μg m^{-3} in $PM_{2.5}$. The t-Student test was performed to investigate whether these differences were statistically significant. Results indicated that seasonal variability was significant for both species (OC and EC) ($p < 0.01$) which indicated that the variability was significant for both species, OC and EC. This trend was observed also in other high altitude remote sites in Italy (Sandrini et al. 2014a) and could be explained considering that during the cold period they are decoupled from the Planetary Boundary Layer, where emission sources are located, hence representative of the free troposphere. Indeed, dispersion and transport of lower atmospheric pollutant depend largely on the local planetary boundary layer structure, and the turbulence is the dominant mechanism mixing particulate matter (PM) and ambient air. By acting as a lid to the pollution vertical mixing extent, planetary boundary layer height is one of the important factors affecting pollution concentration and large-scale transport (Coulter 1979). The correlation between EC and OC in PM_{10} and $PM_{2.5}$ was studied to seek useful information regarding the origin of carbonaceous aerosols (Turpin and Huntzicker 1995). In this study, a good correlation was observed between EC and OC both in PM_{10} (Pearson 0.79, $p < 0.01$) and in $PM_{2.5}$ fraction (Pearson 0.74, $p < 0.01$). It confirms that, at this high altitude rural site, most of the carbonaceous species are transported by long-range air masses and that the time series of EC and OC concentrations are modulated by synoptic and local meteorology, increasing in this way the correlation between the two chemical species.

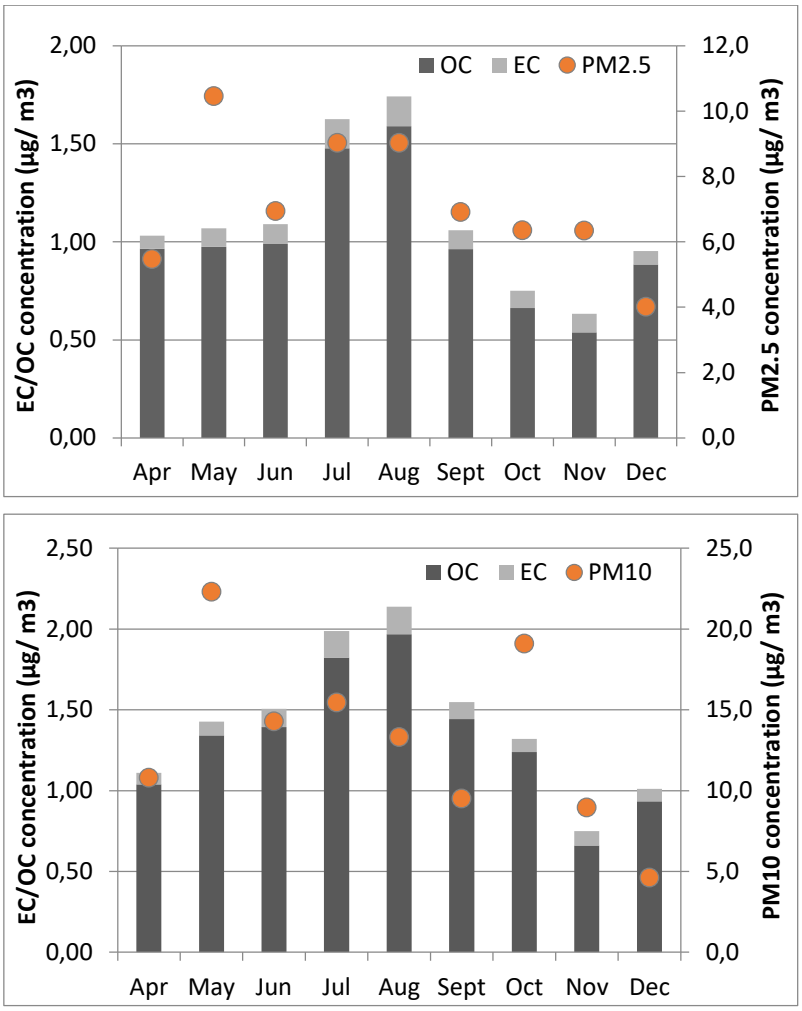

Fig. 6.5 Monthly averages of EC and OC concentrations in $PM_{2.5}$ (a) and in PM_{10} (b).

The distribution of carbonaceous species in the fine and coarse fractions are parameters that could help in discriminating between sources of carbon in the atmosphere. In Fig. 6.6 the monthly ratio between OC ($PM_{2.5}$)/OC (PM_{10}) is between 0.62 and 0.94, with the minimum in October and the maximum in April. The monthly EC ($PM_{2.5}$)/EC (PM_{10}) ratio was observed around 0.90 for whole campaign suggesting that elemental carbon is predominantly in the fine fraction whereas the contribution of OC to $PM_{2.5}$ is variable through the covered period. Both fractions are higher than the $PM_{2.5}/PM_{10}$ ratio (ranging from 0.44 to 0.86) highlighting that the fine fraction of aerosols is richer in carbon than the coarse part except in September and December. In December, the value of the three ratios was comparable to each other while in September the values of the ratios between OC ($PM_{2.5}$)/OC (PM_{10}) and $PM_{2.5}/PM_{10}$ are similar (0.66 and 0.76, respectively) and only EC ($PM_{2.5}$)/EC (PM_{10}) contribute to the predominance of carbon in the fine fraction. A seasonal trend is shown in Fig. 6.6b, where the OC/EC ratio in both fractions is reported. The OC/EC ratio is an

important parameter that helps the discrimination between sources and the high values (up to 15) indicates the cleanest remote locations where EC is very low. In this study, the OC/EC values ranged from 6.7 to 16.8 in $PM_{2.5}$ and 7.8 to 15.9 in PM_{10}. These values are in accordance with those found in other high altitude sites (Sandrini et al. 2014a). In $PM_{2.5}$, the ratio decreased during the warm period until around 10, with a minimum during November at 6.7. In the same way, the ratio OC/EC in PM_{10} decreased during the warm period, but increased in the months of September and October, with a minimum also in November as in $PM_{2.5}$. The increasing of December ratios shown in Fig. 6.6a and Fig. 6.6b, demonstrate the major presence of OC associated at $PM_{2.5}$ due to the decoupling from the planetary boundary layer and representative of free troposphere conditions. Another important evidence that emerges from Fig. 6.6b is the gap between the OC/EC ratio recorded in $PM_{2.5}$ and PM_{10} in May, September, and October, thus suggesting the major presence of OC in coarse fraction.

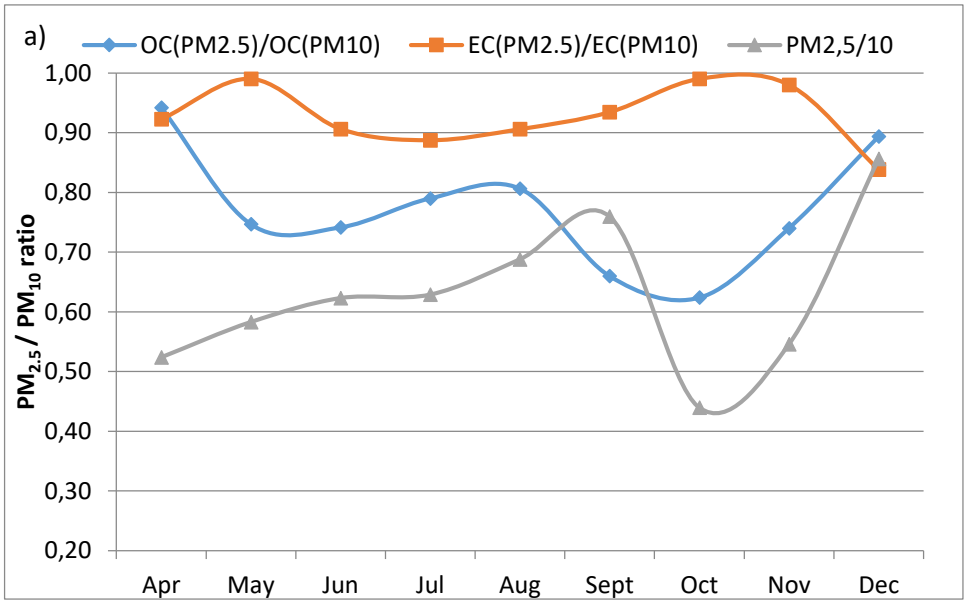

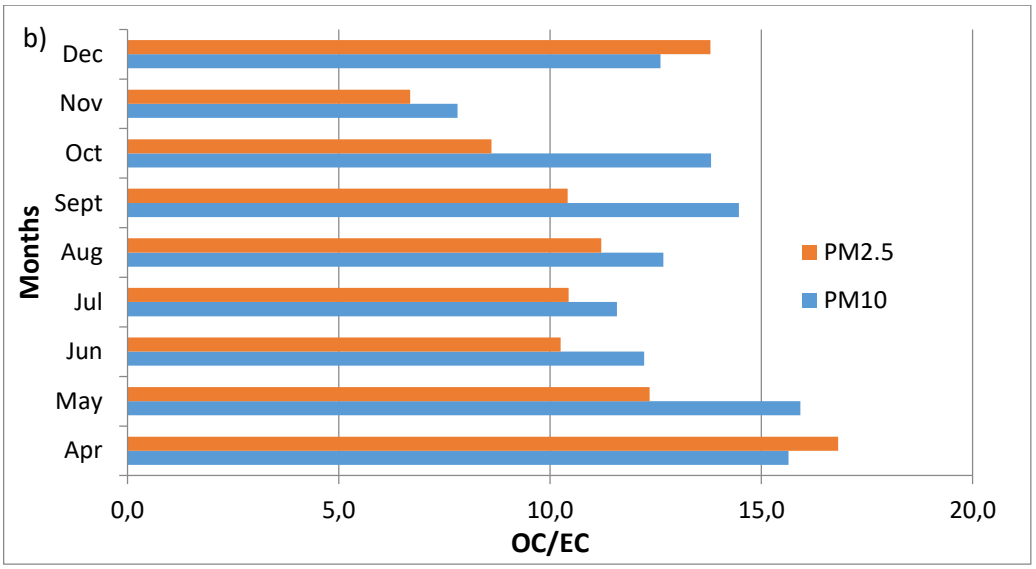

Fig. 6.6 (a) Monthly average ratios OC($PM_{2.5}$)/OC(PM_{10}), EC($PM_{2.5}$)/OC(PM_{10}), and $PM_{2.5}$/PM_{10}. (b) Monthly average ratios OC/EC in $PM_{2.5}$ and PM_{10}.

The quantification of primary and secondary organic carbon is quite difficult since no direct analytical methods are available. In the literature, different methods are proposed for the estimation of POC and SOC; in this work, we used the three methods described in the previous paragraph so as to show not only the found values but also to compare the results obtained with the different strategies. Using the first method (Pio et al. 2011), during the warm season, OC/EC minimum ratio was 5.66 and 6.42 for $PM_{2.5}$ and PM_{10} respectively while in the cold period, the ratios were 4.10 and 5.80. Using the second method, the OC/EC minimum ratios during the warm period were 5.41 and 6.70 for $PM_{2.5}$ and PM_{10} respectively; during the cold season, the minimum ratios become 3.71 and 5.42. The values obtained with the third method (Wu and Yu 2016) differ from those obtained with the other two methods, which are instead similar to each other, probably because the dataset used is small compared to other works as those of Xu and Bian (Xu et al. 2017; Bian et al. 2017) and could be affected by greater error. Using the OC/EC minimum ratio proposed by Pio et al. (Pio et al. 2011) the SOC concentration in warm period ranged between 0.44 and 0.77 μg m^{-3} in $PM_{2.5}$ while in PM_{10} ranged from 0.57 and 0.84 μg m^{-3}. In the cold period, the SOC concentration ranged from 0.2 to 0.63 μg m^{-3} in $PM_{2.5}$ and between 0.19 and 0.87 μg m^{-3} in PM_{10}.

In Fig. 6.7 the SOC/OC ratio is reported with an important decrement during the warm period in both fractions; in $PM_{2.5}$ decrease from 62% in April to 45% in July while in PM_{10} from 54% in April to 40% in July, as well as the OC/EC ratio which means an increase in the contribution of EC, therefore an increase in POC probably due to wildfire, more common in this part of Italy during summer and other incomplete combustion sources in local area. In

September, the SOC/OC ratio return to increase from 63% to 71% in $PM_{2.5}$ during December. However, in Fig. 6.7 it can be noted a minimum for both fractions during November, which supports the hypothesis before explained, according to which the POC was originated from Volcanoes or anthropogenic local sources, helped by poor rain and snow.

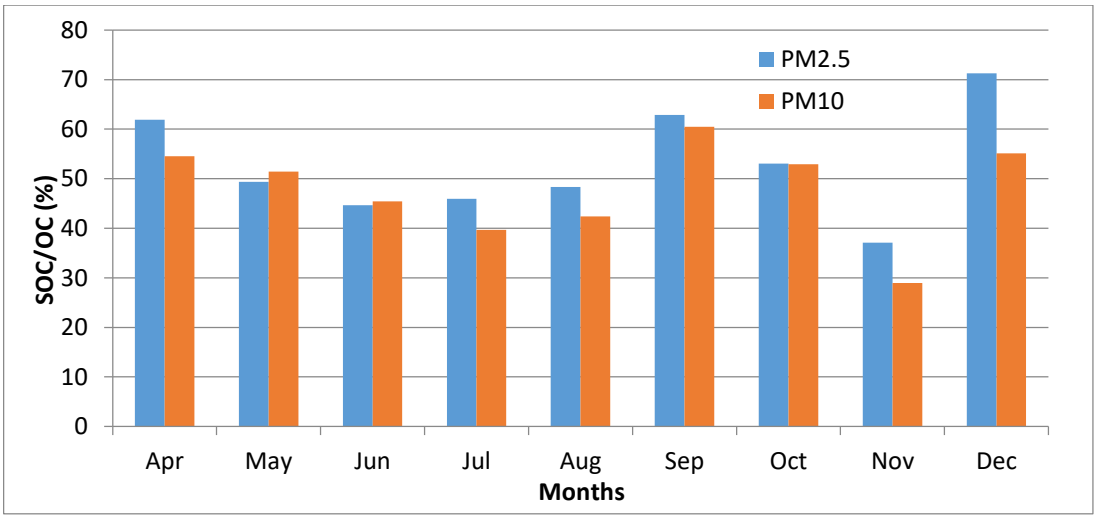

Fig. 6.7 Monthly average of secondary organic carbon in PM_{10} and $PM_{2.5}$.

As previously seen, the EC and eBC coming from the same sources, and is common uses of airborne EC measurements as a surrogate measure of ambient air BC. Therefore, in this case study, the EC subset data was compared to eBC data measured from May to December 2016. The monthly average concentration of EC and eBC are compared in Fig. 6.8. and show a high Pearson correlation coefficient (0.84, $p < 0.01$) and similar trends with larger concentrations during the warm period (Summer), confirmed by the t-Student test ($p < 0.05$). However, on average the daily concentration was higher than EC concentration, for both warm and cold season (Fig 6.8). The data can be compared with the work reported by (Cesari et al. 2018) in their urban background station (Apulia region) and it can be noted that our data are one order of magnitude lower than those.

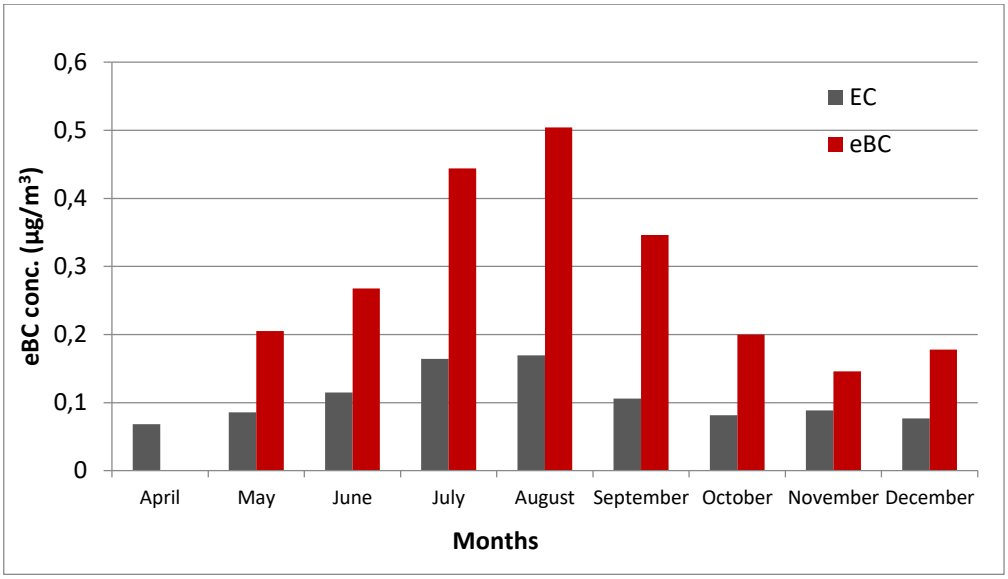

Fig 6.8 Monthly average concentration of EC (gray) and eBC (red)

Measured eBC were larger than EC of an average factor of 2.75 (± 0.97 standard deviations) with a growing trend during the warm period from 2.39 of May to the maximum value, 3.26 during August, falling again between September and December when the value becomes again at 2.32 with a relative minimum in November of 1.65. These values are relatively similar were also obtained by (Kanaya et al. 2008) who compared Sunset thermal EC measurements, following the NIOSH 5040 and IMPROVE protocol, with eBC measurement by MAAP (at 670 nm), finding a ratio eBC/EC around 2, consistent with the magnitude observed in this work. Differences between the two typologies of measurements are expected since the eBC and EC concentrations are based on two different measurement techniques (Massling et al. 2015). In addition, some of the recent studies have found that some types of OC can absorb light in UV–visible ranges and these types of OC are termed brown carbon (Andreae and Gelencsér 2006; Feng et al. 2013) which includes polycyclic aromatics, atmospheric humic-like substances, and bioaerosols comes from, for example, the biomass burning (Andreae and Gelencsér 2006) that could increase optically measured eBC with respect to chemically determined EC. Field measurements suggest that brown carbon may contribute approximately 10–30% of the total absorption by carbonaceous aerosols at a near-UV wavelength and approximately 10% at a wavelength of 550 nm (Lack et al. 2012; Washenfelder et al. 2015). The presence of brown carbon limits the assumption that the absorption coefficients measured by the MAAP are ascribed to eBC. Then, even if in this study the possible contribution of dust has been eliminated, this contribution could be added in small part to the possibility of biomass burning in the studied area. Especially during the

warm season where the planetary boundary layer was high, this could occur, being the station included in the planetary boundary layer itself.

The weekly pattern of eBC in the two different seasons are reported in Fig. 6.9 that shows a higher concentration of eBC during the warm season, compared with the cold season, and different weekly patterns. Throughout the cold season, particular weekly pattern (values are more similar to each other) was not evident, whereas in warm season higher concentrations were observed during the weekends compared to working days. This is likely due to the higher road traffic emissions during weekends (touristic site downstream of the sampling station site), and possible sources of biomass burning and wildfire that during summer can occur, being associated with prevalent calm wind (Table 6.1). The average daily pattern of hourly eBC concentrations, separating warm and cold seasons, is reported in Fig. 6.10. Concentrations of eBC during cold period show a minimum early in the morning (5 am) and grew up until 1 pm and then decrease again. This could be explained by the increase in temperature in the central hours of the day, with a consequent increase of PBL due to the diurnal cycle of planetary boundary-layer height. This involves the possibility of intrusion of pollutants. Indeed in the warm period, there was not an evident hourly pattern.

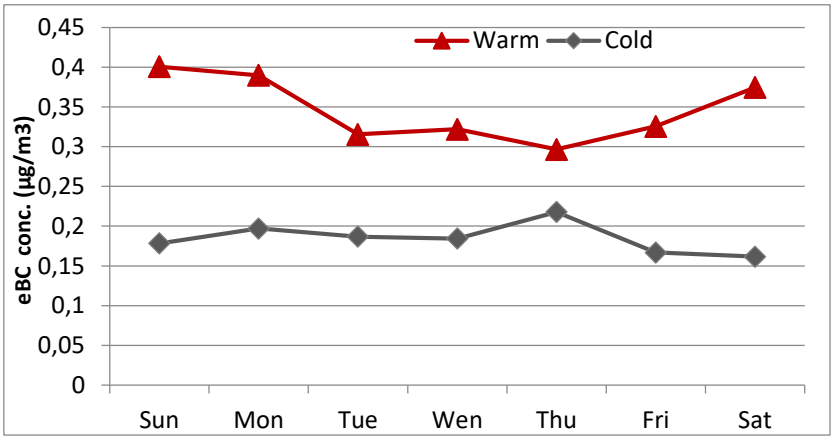

Fig. 6.9 Weekly average concentration of eBC during cold (gray) and warm (red) period.

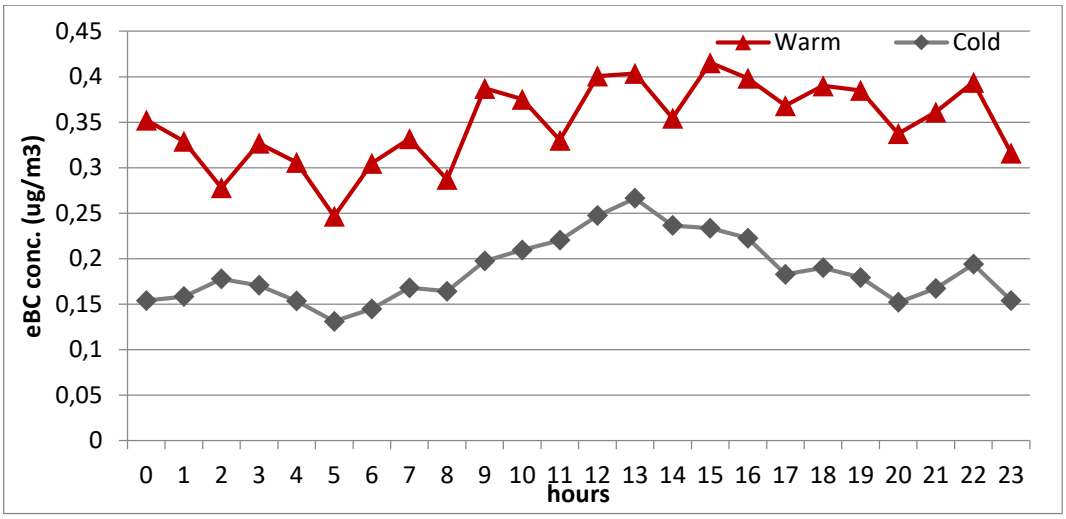

Fig. 6.10 Hourly average concentration of eBC during cold (gray) and warm (red) period.

Determining potential sources contributing to EC and OC concentrations at a particular site requires data analysis and modeling. One of the most common receptor models is back trajectory modeling. The latter, used in conjunction with atmospheric carbonaceous concentrations measured at the receptor site and are commonly referred to as Hybrid Receptor Models (HRM). As seen in chapter three, among the HRM potential source contribution function (PSCF) and concentration weighted trajectory (CWT) exist. Here, the CWT approach was chosen since it is suitable to quantify long-range transported aerosol (Jeong et al. 2011). The CWT method is based on back-trajectory analysis and, in each grid cell, a weighted concentration is obtained by averaging sample concentrations that have associated trajectories crossing that grid cell. In this work, I computed the data using Openair package for R (Carslaw 2015). Back-trajectories of air masses were computed by the Hybrid Single-Particle Lagrangian Integrated Trajectory (HYSPLIT4) model. In order to have a good compromise between synoptic scale and positional errors, 3-days (72 h) back-trajectories were computed (Squizzato et al. 2017) starting at a height of 1780 m above ground level (a.g.l.) at the measurement site.

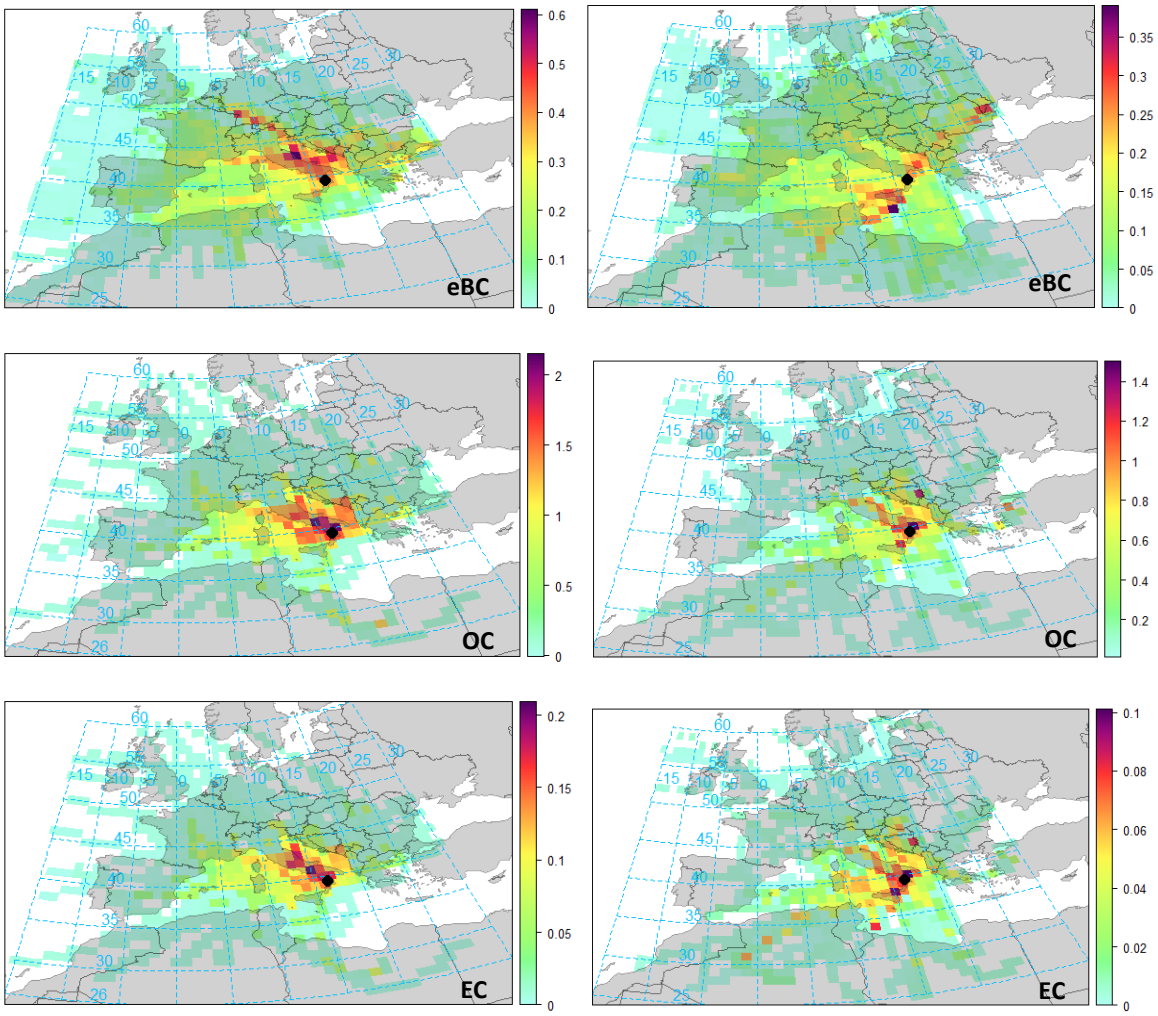

Fig 6.11 Results of CWT for eBC, EC, and OC in PM10 separating cold (right panel) and warm (left panel) seasons.

Fig. 6.11 shows CWT, separating warm and cold seasons, for eBC, OC, and EC in PM_{10} fraction. Results show differences in the possible sources of carbonaceous aerosol between the different seasons. Carbonaceous aerosol mainly comes from long-range transported aerosol during the cold season, while during the warm season is affected by regional sources. The pattern of eBC and EC are similar in both season, this because they are both mainly primary pollutants having essentially the same sources. The pattern of OC is similar to EC only during the warm season, probably because the formation of secondary organic aerosol (SOA) is influenced also by the circulation of air masses and could induce the differences observed in the CWT of EC and OC.

6.5 Case Study 3: Carbonaceous aerosol characterization in the framework of "I-AMICA" Regional network

In order to improve our knowledge on the carbonaceous aerosol distribution, seasonal trends and correlation with circulation of air masses in the Southern Mediterranean, a pilot study was performed in the framework of I-AMICA Regional Network started in 2015 as overall goal achieved during the PON-project "Infrastructure of High Technology for Integrated Climate and Environmental Monitoring". In particular, an intensive measurement campaign was conducted from November 2015 to January 2016 at five monitoring sites of Southern Italy, including Monte Curcio Station, to investigate and compare the characteristics and the relative contributions of carbonaceous species (OC and EC) to the PM_{10} and $PM_{2.5}$ mass. This area is affected by local and long-range transport of marine, desert, and anthropogenic aerosols (Dinoi et al. 2010; Contini et al. 2014), due to the geographical location. Thus, the comparison among different sites (from coastal to mountain and urban) within the same geographical region would be a useful tool for exploring long-range transport versus local emissions in conjunction with aerosol aging processes. The results obtained were related to the climatic and geographic conditions of the study areas to identify the possible factors affecting the concentrations of carbonaceous species. This work was conducted in collaboration with other research groups of the CNR (National Research Council) and the University of Naples. In this framework, I was involved in the sampling campaign and related carbonaceous fraction analysis for Monte Curcio Station (Dinoi et al. 2017).

Fig. 6.12 Map of observation sites: Naples (urban), Lecce (suburban), Lamezia Terme and Capo Granitola (coastal), Monte Curcio (remote).

6.6 Sites Description

Daily 24-h PM2.5 and PM10 samples were simultaneously collected at the following monitoring sites: Lecce, Lamezia Terme, Capo Granitola, Monte Curcio, and Naples. The first four sites are regional stations of the Global Atmosphere Watch Program (GAW-WMO), dedicated to monitoring the climate and the environment within the Mediterranean Area. Fig. 6.12 shows the geographical location of the sampling sites: urban (Naples), suburban (Lecce), two coastal sites (Lamezia Terme, and Capo Granitola) and the remote site (Monte Curcio). The sites were classified on the basis of their distance from pollution sources, according to criteria proposed by the European Environment Agency (European Environment Agency). Since Monte Curcio Observatory has already been illustrated previously, here are illustrated the other four sampling sites involved in this inter-comparison exercise:

- Lecce Observatory (ECO, 40.3°N 18.1°E; 36 m a.s.l.) is located inside the University Campus at about 4 km (W-SW) from the urban area of Lecce and about 15 km from South Adriatic Sea. The site is not strongly influenced by local sources, rather by the integrated contributions of traffic inside the University Campus and by diffused emissions of the town of Lecce and near towns, and sometimes by industrial emissions of Taranto (about 80 km in the NW direction) and Brindisi (about 30 km in the NNW direction).
- Naples-San Marcellino Observatory (40.5°N, 14.0°E; 53 m a.s.l.) located in the center of Naples, is a site within a restricted traffic area, close to the marina, but not distant (about 0.5 km) from very busy roads. This site is influenced by different sources, e.g., vehicular traffic, port emissions, and biomass combustion. It is also likely that emissions by numerous pizza restaurants located nearby (using wood burning) as well as by garbage accumulation in the town could influence measured PM concentrations. Although the site is within a restricted traffic area, Naples is an urban area strongly influenced by road traffic.
- Capo Granitola Observatory (CGR, 37.6°N 12.6°E; 5 m a.s.l.) is located only 5 m from the coastline, towards the Strait of Sicily and it is representative of the background conditions of the western Sicily/central Mediterranean basin. It is located in the Torretta Granitola hamlet, Campobello di Mazara municipality, 12 km from Mazzara del Vallo.
- Lamezia Terme Observatory (LMT, 38.8°N 16.2°E; 6 m a.s.l.) is located about 10 km from the urban city, 600 m inland from the Tyrrhenian coastline where the breeze

system plays a major role in defining local meteorology and natural and anthropogenic air mass transport. Its long and narrow shape creates a complex interaction of breezes which develops perpendicularly to the coast, determining an atmospheric circulation variability and the development of vertical structures of the coastal planetary boundary layer. The site is at the end of a natural channel between Thyrrenian and Ionian Seas (respectively W and E directions). The area experiences some pollution coming from the transport sector (airport, cruises from/to Gioia Tauro and local traffic mainly for E-NE direction), houses, and agriculture.

6.7 Experimental and Data treatment

At all the sites, 24-h PM_{10} and $PM_{2.5}$ samples were simultaneously collected, from 25 November 2015 to 1 January 2016. Mass concentration measurements were performed by the β-ray attenuation method, using low volume samplers (2.3 m^3 h^{-1}) with two channels for automatic sampling and monitoring, one for PM_{10} and one for $PM_{2.5}$ (SWAM 5a Dual Channel Monitor-FAI Instruments). Due to some technical problems occurred at both Capo Granitola and Monte Curcio Stations, the sampling period covered the first two weeks of the campaign. The number of samples considered in this work, are reported in Table 6.2.

The analysis of carbonaceous fraction was performed for all sites as already described in this chapter by the TOT method using a Sunset Laboratory OC/EC analyzer (Sunset Laboratory, Tigard, OR, USA) and the meteorological data during the sampling period, including ambient temperature, pressure, relative humidity (RH), wind velocity, and wind direction were also recorded by using automatic weather stations (Vaisala) for all the monitoring sites except for Monte Curcio, at which different types of equipment were used (LSI Lastem). In addition, at the four sites of the Global Atmosphere Watch program, particle concentration measurements were performed also using optical particle counters (OPC FAI Multichannel Monitor) which classifies particles in 22 size intervals, from 0.28 to 10 μm.

6.8 Results and discussion

6.8.1 PM_{10} and $PM_{2.5}$ Concentrations

The temporal variability of the PM_{10} and $PM_{2.5}$ average daily concentrations measured during the campaign at all sites is plotted in Fig. 6.13, while the statistics of the concentrations are shown in Table 6.2 which reports the average values (±standard deviation), minimum (Min), maximum (Max), $PM_{2.5}/PM_{10}$ average ratio, and the number of samples (N). The highest PM_{10} and $PM_{2.5}$ mass concentration values were observed in the

urban site of Naples (50.8 ± 21.7 and 37.8 ± 18.0 μg m^{-3}), followed by Lecce (32.7 ± 13.0 and 25.7 ± 11.6 μg m^{-3}), Capo Granitola (23.2 ± 8.6 and 10.4 ± 2.6 μg m^{-3}), Lamezia Terme (10.1 ± 3.8 and 7.2 ± 3.5 μg m^{-3}) and Monte Curcio (3.4 ± 1.4 and 3.0 ± 1.2 μg m^{-3}) with minimum values recorded in Monte Curcio as expected since it is the only remote site.

Sites	PM_{10} (μg/m³)				$PM_{2.5}$ (μg/m³)				$PM_{2.5}/PM_{10}$
	N	Avg ± Std	Min	Max	N	Avg ± Std	Min	Max	
Naples	37	50.8 ± 21.7	13.5	132.1	38	37.8 ± 18.0	10.1	102.5	0.74
Lecce	38	32.7 ± 13.0	7.4	64.9	36	25.7 ± 11.6	4.4	56.6	0.77
Lamezia Terme	38	10.1 ± 3.8	2.5	16.1	38	7.2 ± 3.5	1.4	13.8	0.68
Capo Granitola	14	23.2 ± 8.6	14.5	45.1	14	10.4 ± 2.6	6.1	14.6	0.50
Monte Curcio	31	3.4 ± 1.4	1.1	6.5	31	3.0 ± 1.2	1.2	6.1	0.82

Table 6.2 Number of samples, AVG and STD, MIN and MAX concentrations for PM_{10} and $PM_{2.5}$ fraction together with $PM_{2.5}/PM_{10}$ ratios measured during the campaign in each observation site (Dinoi et al. 2017).

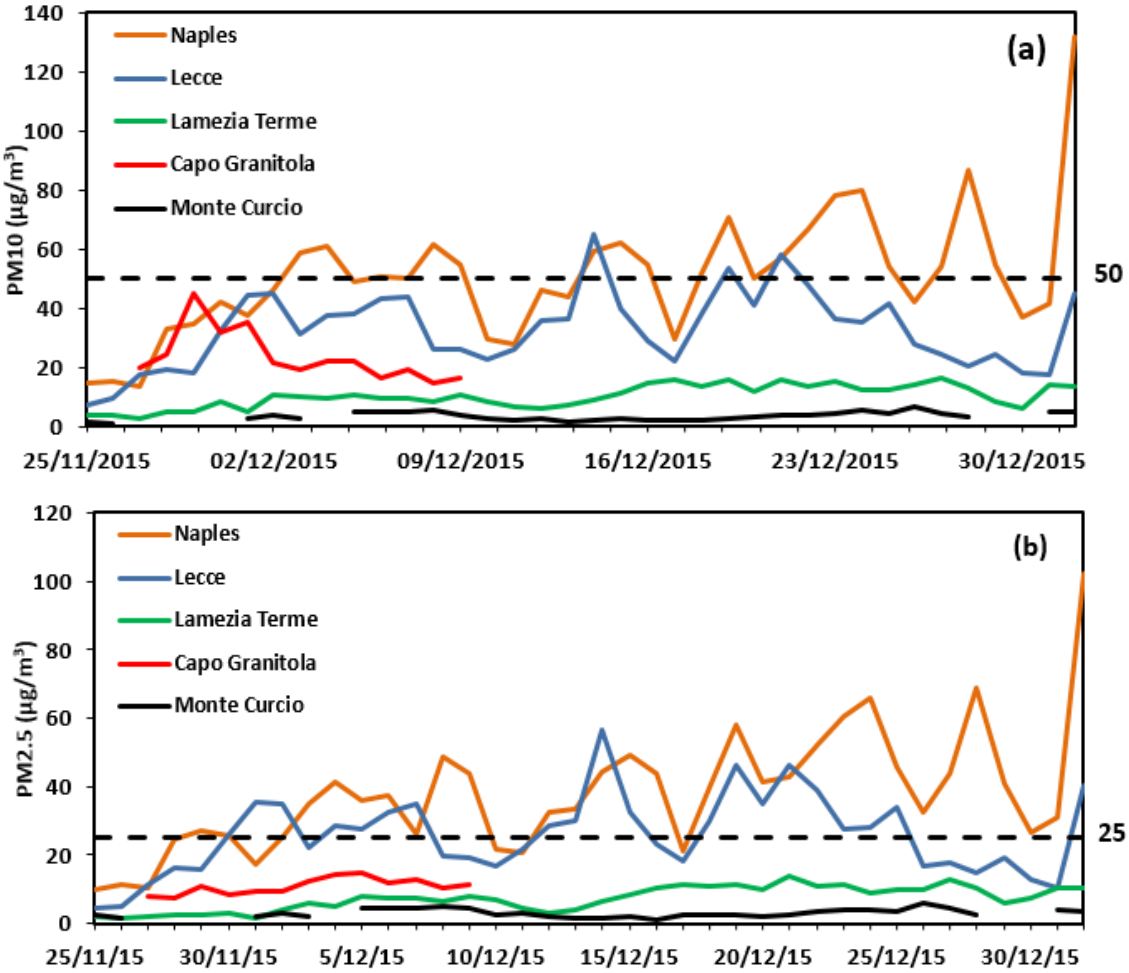

Fig. 6.13 Temporal variability of PM_{10} (a) and $PM_{2.5}$ (b) mass concentrations during measuring campaign at Naples, Lecce, Lamezia Terme, Capo Granitola and Monte Curcio sites. Horizontal dashed lines represent the legislative thresholds (Dinoi et al. 2017).

Fig. 6.13 shows that there have been several exceedances of the daily limit value (μg m^{-3}) for PM_{10} concentrations at the urban site (Naples) and at the suburban site (Lecce); instead, no exceedances were observed during the measurement period at the coastal/marine and remote sites. This confirms that Southern Italy continues to be one of the most problematic areas, especially in urban environments, with numerous exceedances. Results also suggest that local emissions and meteorological conditions have a role in determining some of these exceedances. It is interesting to observe the high PM mass concentrations recorded on 1 January 2016 at Naples. The PM_{10} and $PM_{2.5}$ daily levels were 132.1 μg m^{-3} and 102.5 μg m^{-3}, respectively, almost 3 times larger than the mean average values registered during the whole sampling campaign. The high PM levels could be due to the burning of fireworks that are traditionally used to celebrate New Year's Day.

Different studies have revealed that high PM concentrations can be due not only to increased emissions but also to atmospheric circulation and to typical conditions of the winter season, characterized by stagnant weather with a relatively low planetary boundary layer (PBL) height, which leads to accumulation of pollutants and aerosol formation processing (Durant et al. 2010). By acting as a lid to the pollution vertical mixing extent, PBL height is one of the important factors affecting pollution concentration and large-scale transport (Coulter 1979).

At the same time, the lowest PM concentrations observed in Lamezia Terme and Monte Curcio can be due to the lower anthropogenic emissions and favorable meteorological conditions (such as turbulence, high wind velocity, vertical thermal gradient leading to unstable atmospheric conditions) that promote atmospheric dispersion and dilution of pollutants. In particular, the Lamezia Terme site is characterized by prevalent circulation coming from the sea (western direction) with clean air mainly influenced by sea spray that could potentially contribute to high PM concentrations but lower OC (and especially low EC) concentrations. Monte Curcio site, being at 1780 m a.s.l. and far from pollution sources, is located for most of the time above the mixing layer. Therefore, it can be considered representative of free troposphere conditions.

The $PM_{2.5}/PM_{10}$ average ratios were found in the range between 0.68 and 0.82, as shown in Table 6.2, and they show that more than 68% of the PM_{10} is in the form of $PM_{2.5}$. The concentrations of two PM fraction were well correlated at three sites (Fig. 6.14a), Lecce (R^2 = 0.98), Naples (R^2 = 0.95) and Lamezia Terme (R^2 = 0.88), with a slope varying from 0.81 to 0.88. These results indicate that the two fractions are driven by similar sources and controlled by common processes of transport and dispersion. At the Monte Curcio site, a

slightly lower correlation (R^2 = 0.77) was found, where the high $PM_{2.5}/PM_{10}$ average ratio of 0.82 shows the predominant contribution of the fine fraction probably due to long-range transport since no local sources are present nearby this high altitude site. Fine aerosol, could come from industrial areas of continental Europe, and with its long persistence in the atmosphere can be transported over a large distance, as already observed in other remote sites (Moroni et al. 2015).

In Capo Granitola, the dataset is more limited compared to the other sites; however, some information could be obtained from the data in Fig. 6.14. At first glance, the two fractions seemed completely uncorrelated (R^2 = 0.01); instead, the points are distributed in two distinct periods, from 25 November 2015 to 2 December 2015 and from 3 December 2015 to 9 December 2015 (Fig. 6.14b), with different slopes: 0.51 and 0.13. Both periods were separately well-correlated R^2 = 0.96 and R^2 = 0.71 because they were influenced by two main advection pathways characterized by a different kind of air masses, coming from the sea (N-NW) or mainland (E-NE).

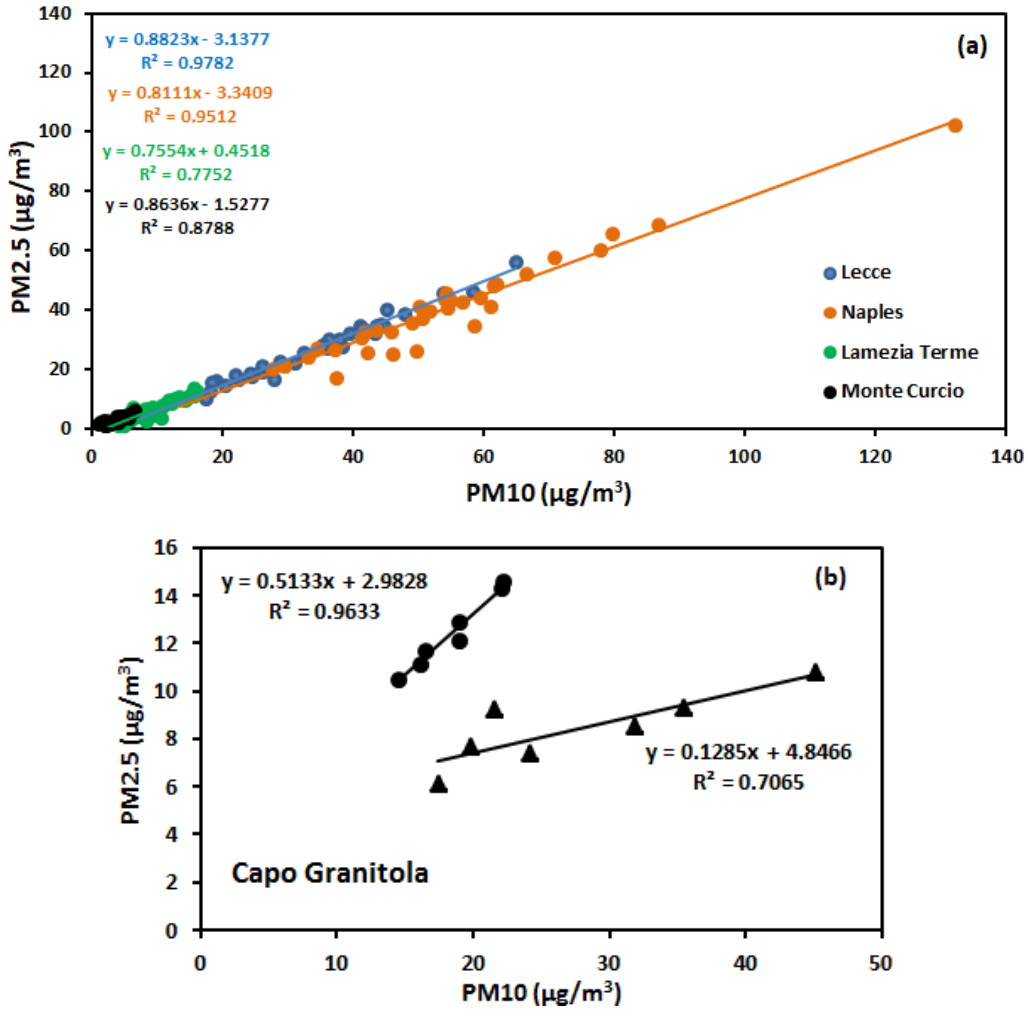

Fig. 6.14 Correlation between PM_{10} and $PM_{2.5}$ mass concentrations at (a) the Naples, Lecce, Lamezia Terme, Monte Curcio sites and (b) Capo Granitola (triangular and round points represent the samples of two distinct periods: from 25 November 2015 to 2 December 2015 and from 3 December 2015 to 9 December 2015, respectively) (Dinoi et al. 2017).

6.8.2 OC and EC levels and relationship between them

The results of statistics of TC, OC and EC concentrations show a considerable variation of average values (±standard deviation) among the sampling locations (Table 6.3 and Table 6.4). The average OC concentrations ranged from 0.9 μg m^{-3} to 12.8 μg m^{-3} in PM_{10} and from 0.9 μg m^{-3} to 11.8 μg m^{-3} in $PM_{2.5}$, increasing about 14 times from remote to urban sites. The same behavior was found also for EC concentrations, but with a larger variability, ranging from 0.06 μg m^{-3} to 2.3 μg m^{-3} (in PM_{10}) and from 0.05 μg m^{-3} to 1.8 μg m^{-3} (in $PM_{2.5}$), increasing more than 36 times from remote to urban sites. The results obtained show similar features with other studies performed in different European sites (Cavalli et al. 2016), indicating that the high spatial variability of EC, compared to OC, is due to local primary emissions (traffic, biomass burning for heating). The results obtained in the urban sites of Naples and Lecce with the highest OC and EC average values indicate that the two environments are strongly affected by anthropogenic emissions. Significantly lower values were found in Lamezia Terme and Capo Granitola, characterized by relatively limited sources, and probably influenced by sea-breeze effects that favor the pollutant's dispersion. The extremely low concentrations measured in Monte Curcio are in good agreement with free tropospheric conditions characterizing a remote site. The TC percentage in the PM fractions was mainly affected by the contribution of the OC concentration.

Sites	TC	OC	EC	TC/PM	OC/PM	EC/PM	OC/EC	SOC	SOC/OC
	(μg/m^3)	(μg/m^3)	(μg/m^3)	%	%	%	(min)	(μg/m^3)	%
Naples	15.1 ± 5.2	12.8 ± 5.1	2.3 ± 1.0	31	26	5	6.4 (2.6)	7.6 ± 5.3	52
Lecce	12.2 ± 6.4	10.7 ± 5.9	1.5 ± 0.8	35	31	5	7.3 (2.8)	6.9 ± 4.8	59
Lamezia Terme	4.9 ± 2.3	4.3 ± 2.0	0.6 ± 0.3	48	42	6	6.9 (4.1)	1.7 ± 1.1	37
Capo Granitola	2.6 ± 1.5	2.3 ± 1.2	0.3 ± 0.3	13	11	2	10.0 (4.4)	0.7 ± 0.6	41
Monte Curcio	1.0 ± 0.4	0.9 ± 0.3	0.06 ± 0.04	30	28	2	15.9 (10.0)	0.4 ± 0.1	47

Table 6.3 TC, OC, EC, and SOC concentrations in PM_{10} together with OC/EC, TC/PM, OC/PM, EC/PM and SOC/PM ratios for each observation site (Dinoi et al. 2017).

Sites	TC	OC	EC	TC/PM	OC/PM	EC/PM	OC/EC	SOC	SOC/OC
	($\mu g/m^3$)	($\mu g/m^3$)	($\mu g/m^3$)	%	%	%	(min)	($\mu g/m^3$)	%
Naples	13.7 ± 4.8	11.8 ± 4.6	1.8 ± 0.5	39	33	6	6.4 (2.6)	7.2 ± 4.4	54
Lecce	10.4 ± 5.1	9.0 ± 4.7	1.4 ± 0.7	40	34	6	6.9 (2.6)	5.7 ± 3.6	57
Lamezia Terme	4.7 ± 2.1	4.0 ± 2.0	0.6 ± 0.3	67	57	10	6.5 (3.0)	2.1 ± 1.3	47
Capo Granitola	2.0 ± 1.3	1.7 ± 1.1	0.3 ± 0.2	17	15	2	8.0 (4.0)	0.6 ± 0.4	40
Monte Curcio	0.9 ± 0.3	0.9 ± 0.3	0.05 ± 0.03	33	31	2	15.5 (10.0)	0.4 ± 0.2	48

Table 6.4 TC, OC, EC, and SOC concentrations in $PM_{2.5}$ together with OC/EC, TC/PM, OC/PM, EC/PM and SOC/PM ratios for each observation site (Dinoi et al. 2017).

The correlation between the OC and EC atmospheric concentrations gives qualitative information regarding the sources contributing to carbonaceous species in PM (Turpin et al. 1994). Fig. 6.15 show the scatter plots of OC versus EC concentrations, in both size fractions, using different colors for each site. Good correlations were found for the sites of Capo Granitola (R^2 = 0.80, R^2 = 0.90), Monte Curcio (R^2 = 0.76, R^2 = 0.73), and Lamezia Terme (R^2 = 0.76, R^2 = 0.67) in PM_{10} and $PM_{2.5}$, respectively (Fig. 6.15). The weaker correlation (R^2 = 0.36, R^2 = 0.37) observed in Lecce indicates that, in addition to primary sources, other emission sources contribute significantly. At Naples, on the contrary, OC and EC were not correlated in both size fractions (R^2 = 0.003, R^2 = 0.07). The result obtained in Naples has also been found in other urban areas such as Milan (Lonati et al. 2007) and Thessaloniki (Samara et al. 2014). This behavior suggests that the sources of OC are different from those of EC and/or can be the result of the presence of different emission sources, having significantly different OC/EC ratios.

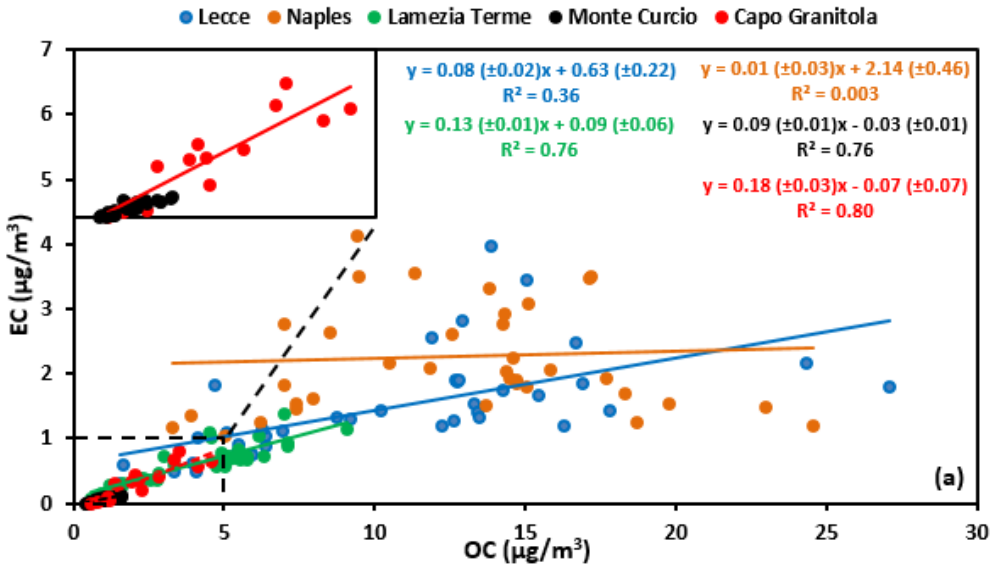

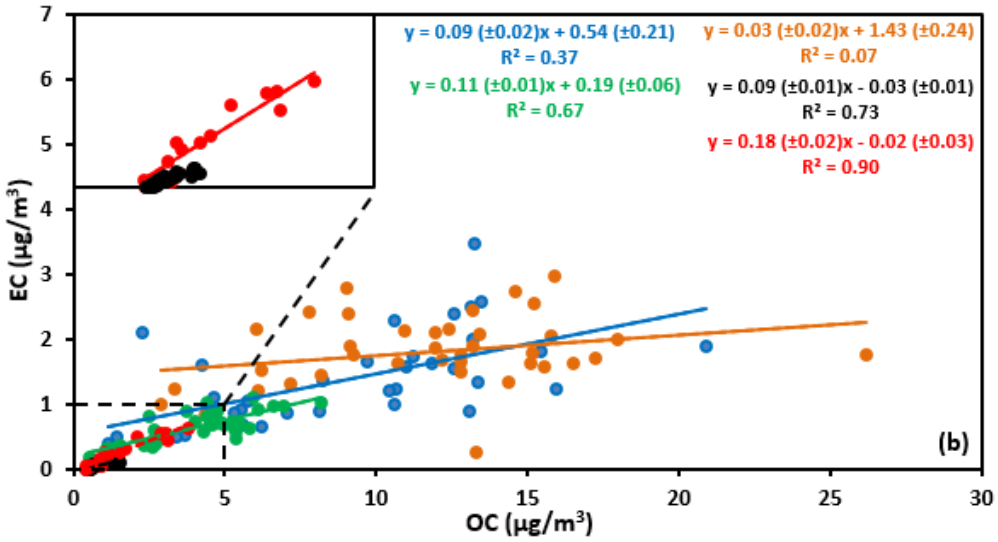

Fig. 6.15. Scatter plot of OC vs. EC in (a) PM_{10} and (b) $PM_{2.5}$ fractions at all observation sites with linear fits. The solid lines indicate the linear regressions of data. Dotted lines show in detail the scatter plot of OC vs. EC related to Monte Curcio and Capo Granitola, in both pictures (Dinoi et al. 2017).

Organic aerosol can be emitted directly into the atmosphere as primary particles or it can be of secondary origin. When volatile organic compounds (VOC) are oxidized in the atmosphere, they produce oxidized volatile organic compounds (OVOC) which condense onto pre-existing aerosol forming secondary organic aerosol (SOA). In general, the OC/EC ratio shows a seasonal variability depending on the sources influencing specific sites (e.g., road traffic, biomass burning) and also influenced by the formation of SOA that depends on atmospheric conditions (Samara et al. 2014; Sandrini et al. 2014b; Cesari et al. 2016b).

Table 6.3 and Table 6.4 show the OC/EC values obtained at the five sites in both PM fractions. These OC/EC ratios are in agreement with the other average values measured in the similar station (Sandrini et al. 2014b), ranging from 6.4 to 15.9 in PM_{10} and from 6.4 to 15.5 in and $PM_{2.5}$. From one side, the rural site of Monte Curcio was characterized by the highest OC/EC average ratios, 15.9 and 15.5, and this highlights the clear prevalence of the organic carbon species over EC. Also in clean environments, like Capo Granitola, the emissions of EC are limited, thus the OC/EC ratio tends to be higher (Kim et al. 2000). In contrast, the site of Naples (in both fractions), Lamezia Terme (in $PM_{2.5}$), and Lecce (in $PM_{2.5}$) were characterized by the lowest OC/EC average ratios, 6.4, 6.5, and 6.9 respectively. The relatively high values suggest a clear prevalence of the organic carbon contribution over EC that could be attributed to significant local sources with higher OC and lower EC emission rates. One of the local sources is the local heating systems, particularly in small

towns, are often based on biomass burning, an important OC source which leads to the increase of the amount of primary carbonaceous particles.

In this case study, the SOC concentrations were calculated according to the methodology proposed by (Castro et al. 1999). In general, the OC/EC ratio varies considerably from source to source, due to the strengths of the different emission sources, and the presence of a minimum ratio for OC/EC suggests that samples contain almost exclusively primary carbonaceous compounds (Na et al. 2004). In addition, the minimum ratios can be affected by various factors, such as meteorology, local sources and long-range aerosol transport. Under these conditions, the organic carbon may still contain small proportions of secondary OC; therefore, this calculation provides a lower limit for the SOC content. Average concentrations of secondary organic carbon and its percentage contribution to the ambient OC are summarized in Table 6.3 and Table 6.4.

Over the whole measurement campaign, the average SOC concentrations ranged from 0.4 to 7.6 μg m^{-3} in PM_{10} and from 0.4 to 7.2 μg m^{-3} in $PM_{2.5}$, accounting from 37 to 59% of the OC in PM_{10} and from 40 to 57% in $PM_{2.5}$. An interesting observation is that the spatial variability of the ratio SOC/OC is much smaller with respect to the observed variability of SOC and OC concentrations. The SOC/OC values found are comparable with those observed in other sites influenced by different sources. In central Italy, SOC/OC ratios between 44% and 54% were observed at the three sites of different typology (rural, urban background, and urban) (Cesari et al. 2016b). In Northern Italy, SOC/OC ratios between 52% (summer) and 76% (winter) were observed at different sites (Khan et al. 2016). These results show that SOC particles observed in this study were an important component of the OC mass in all sites. In particular, the higher percentage of SOC in the OC, observed at the urban and suburban sites of Naples and Lecce, can be attributed to several factors. In winter, the increased emission of volatile organic precursors, together with the stable atmospheric condition and the prolonged residence time, may strengthen atmospheric oxidation of volatile organic compounds. On the other hand, as regards the other measurement sites, the lower percentage of SOC estimated can be prevalently due to the direct emission in the atmosphere from combustion sources.

To better analyze the role of meteorology on the local aerosol and carbon concentrations, the correlations of the main meteorological parameters with measured concentrations were investigated. Although particulate mass concentrations and their components are controlled primarily by emission sources, meteorological and topographical factors also play a crucial role in their dispersion and diffusion. The average daily values of relative humidity,

temperature, and wind velocity for each sampling site during the study period are shown in Table 6.5.

The daily average values of the relative humidity (RH) ranged from 50 to 85% in Lecce and Lamezia Terme, from 30 to 100% in Monte Curcio, and from 65 to 85% in Capo Granitola (no data are available for Naples). The higher daily temperature values were measured in Lamezia Terme (9.1 ÷ 16.6 °C) and Capo Granitola (10.6 ÷ 15.2 °C) followed by Naples (8.7 ÷ 14.2 °C), Lecce (4.7 ÷ 12.5 °C), and Monte Curcio (−2.2 ÷ 8.2 °C). The results of the regression analysis revealed that relative humidity was not significantly correlated with the carbon concentrations at all sites ($R^2 \cong 0.1$). The temperature was not correlated with carbon concentrations at Monte Curcio, Naples, and Capo Granitola; instead in Lecce and Lamezia Terme, larger OC and EC concentrations at lower temperature were found with low correlations (R^2 between 0.2 and 0.3). This was observed in previous work in Lecce and was associated with the contribution of biomass burning for domestic heating (Cesari et al. 2016b).

The statistical analysis of the wind velocity versus the EC and OC data indicated that the wind velocity did not show any correlation with the carbonaceous concentrations for the Naples and Monte Curcio sites, while a slight correlation was found at the Lecce ($0.37 < R^2 < 0.51$), Lamezia Terme ($0.32 < R^2 < 0.48$) and Capo Granitola ($0.75 < R^2 < 0.86$) sites. At these sites, the correlation between the wind velocity and the OC and EC concentrations follows the form of a power law where the carbonaceous mass concentrations decrease with the increase in wind velocities. The wind velocity plays a leading role in the cleansing of the atmosphere from particulate matter in the sites influenced by local sources, affecting the turbulence near the ground.

Sites	Wind Velocity (m/s)	Temperature (°C)	Relative Humidity (%)
Naples	1.8 (0.5–5.7)	10.8 (8.7–14.2)	——
Lecce	1.5 (0.2–5.3)	10.0 (4.7–12.5)	79.3 (50.0–87.1)
Lamezia Terme	2.8 (0.8–10.2)	12.6 (9.1–16.6)	70.4 (54.3–84.8)
Capo Granitola	3.6 (0.6–13.7)	13.0 (10.6–15.2)	76.2 (64.2–85.8)
Montecurcio	3.2 (0.2–13.4)	2.8 (−2.2–8.2)	70.9 (29.9–99.0)

Table 6.5 Average values of meteorological parameters collected during the campaign: wind velocity, temperature, and relative humidity. In parentheses, the minima and maxima values are reported (Dinoi et al. 2017).

The wind-rose pictures related to each site are shown in Figure 6.16, with the wind direction used to evaluate also the possible relationship between the carbonaceous sources and

pollutant levels. The sites of Naples and Lecce showed one of the most frequent advection patterns, with the wind generally coming from the North and North-Northwest (N-NW) directions, respectively, accounting for 89% of the total observations. In the case of Lamezia Terme and Monte Curcio, the wind blows mainly from two directions: East-Northeast (E-NE) and Southwest-Northwest (SW-NW). However, the two dominant pathways were not characterized by differences in carbonaceous concentrations.

In Capo Granitola, the major prevailing wind directions during the campaign were between WNW-NW and N-NE, which was a peculiar wind distribution (generally NW and SE) at this site (Cristofanelli et al. 2017), with winds from inland generally associated with higher concentrations and more polluted events. Associated with the N-NE wind direction, the OC and EC concentrations were higher than average (43 - 59%), while the carbonaceous concentrations associated with wind from the (W-NW) direction were observed to be lower (65 - 71%), in both size fractions. As noted above, in Capo Granitola it is possible to recognize two distinct periods, the first period is characterized by WNW-NNW wind direction, indicating possible advection from the sea. The second period is characterized by air mass from the NNE-ENE sector (mainland).

To further investigate the correlation between wind direction and measured PM, OC, and EC concentrations, the concentration roses were produced for each measurement site. The unique interesting results were obtained for Capo Granitola data. Fig. 6.17 show that the two measurement periods identified are characterized by significantly different concentrations. During the first measurement period, with winds coming from the sea (WNW-NW, in blue in Fig. 6.17), PM_{10} concentrations are larger than those observed in the second period with the wind coming from the mainland (NNE-ENE, in red in Fig. 6.17). However, OC and EC concentrations in this period are smaller than those measured when wind originated from the mainland, especially for EC.

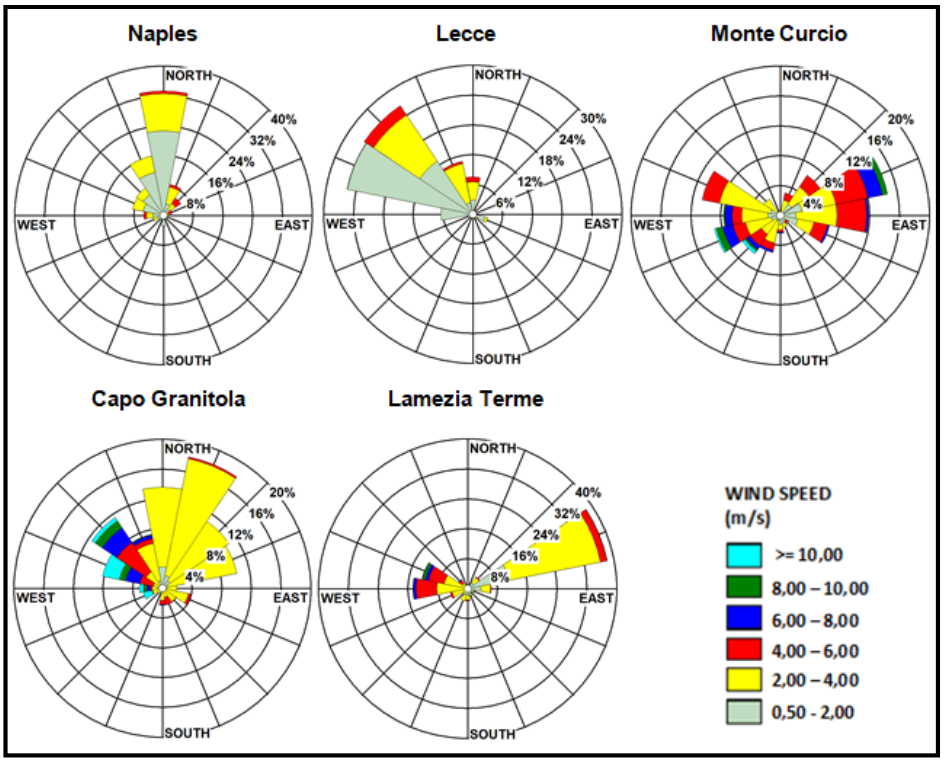

Fig. 6.16 Wind roses of the prevailing wind directions and associated speeds related to each site during the measuring campaign. (Dinoi et al. 2017)

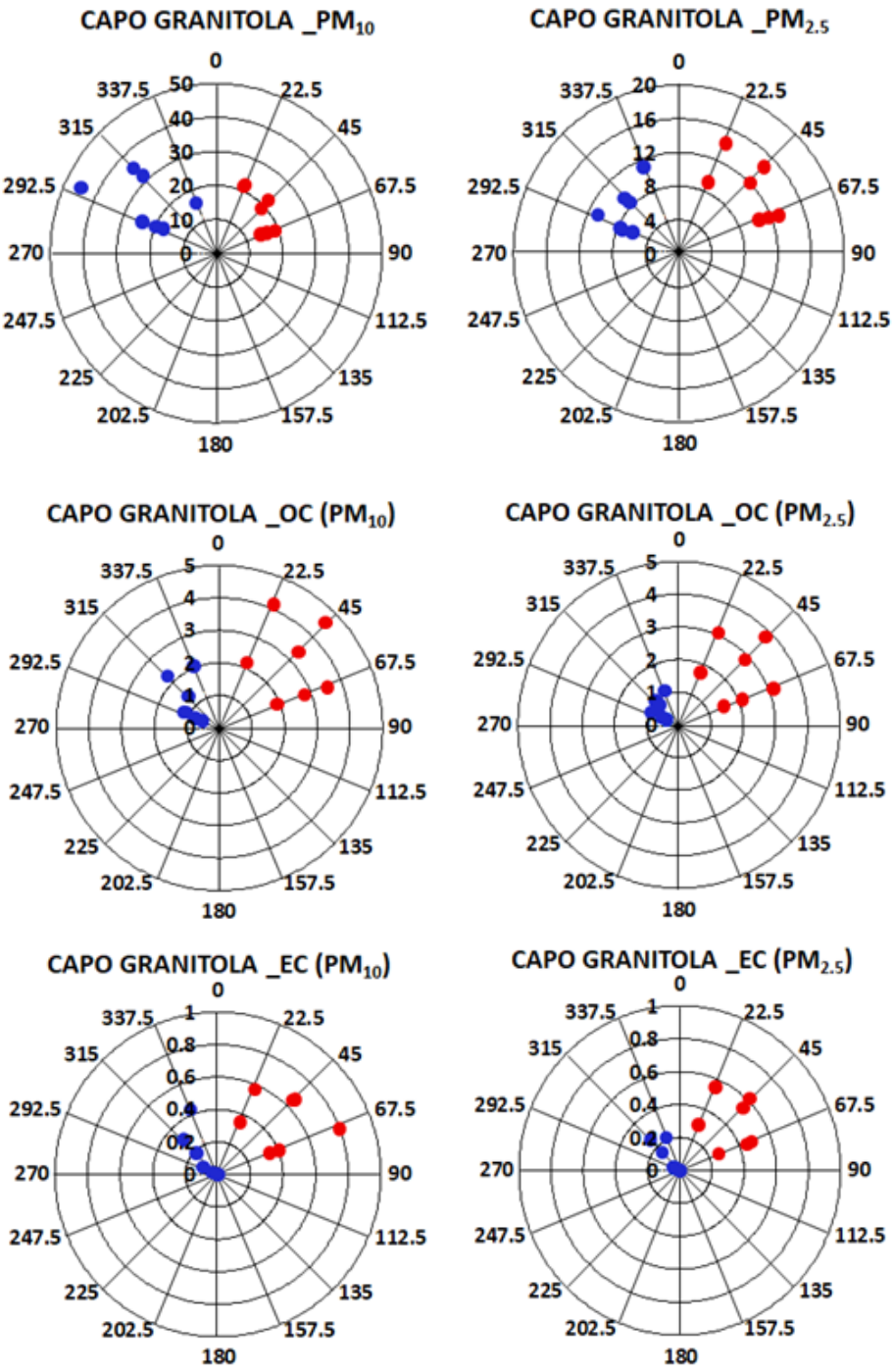

Fig. 6.17 Concentration roses of PM10, PM2.5, and associated OC and EC concentrations. Blue and red dots represent the concentrations of the two distinct periods, from 25 November 2015 to 2 December 2015 and from 3 December 2015 to 9 December 2015, respectively. (Dinoi et al. 2017)

This suggests that the first period is influenced by coarse particles with a low carbon content that may be due to a marine contribution that has these characteristics in Southern Italy (Contini et al. 2014). Daily trends of coarse particles (diameter > 2.5 μm) and fine particles (diameter < 2.5 μm) number concentrations, obtained by using the OPC and shown in Fig. 6.18, show a larger contribution of coarse particles during the first measurement period. In

the second period, air mass advected from the NNE-ENE sector and influenced by mainland and likely by anthropogenic sources, producing particles richer in carbon, may explain the higher measured $PM_{2.5}$, OC and EC concentrations, and the different correlation between $PM_{2.5}$ and PM_{10} shown in Fig. 6.18.

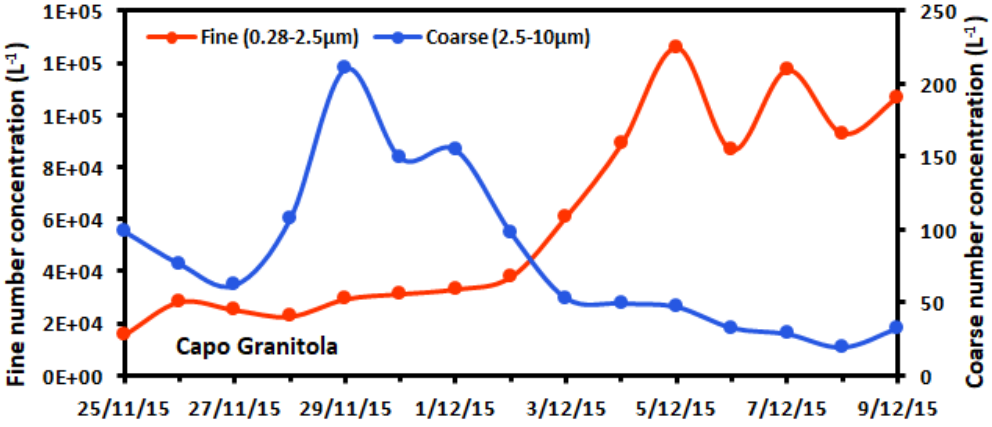

Fig. 6.18 Comparison between trends of coarse and fine daily particles number concentrations for the two size fractions at Capo Granitola during the measuring campaign (Dinoi et al. 2017).

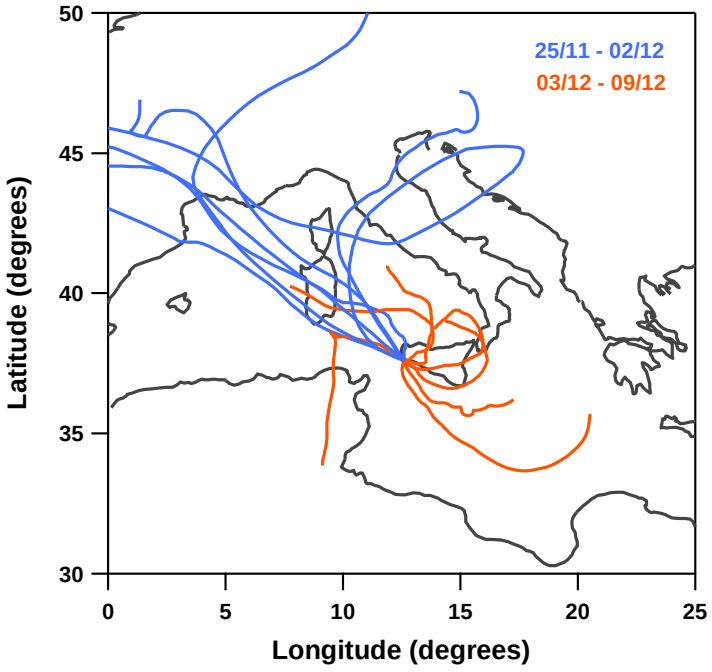

Fig. 6.19 72-h back trajectories arriving at the Capo Granitola site during the sampling campaign. Blue and red lines represent the back of the two distinct periods, from 25 November 2015 to 2 December 2015 and from 3 December 2015 to 9 December 2015, respectively. (Dinoi et al. 2017).

The advection patterns during the two measurement periods in capo Granitola were investigated using air backward trajectories analysis by the HYSPLIT (Hybrid Single-Particle Lagrangian Integrated Trajectory) model (Draxler and Rolph 2010). Trajectories were computed each day for a 72-h period, which is considered sufficient to represent the synoptic air flows. Fig. 6.19 shows that air mass arriving at Capo Granitola during the sampling campaign could be separated into two advection patterns: that from the sea relative to the first measurement period (blue lines), and that showing advection above the mainland during the second measurement period (red lines). This supports the hypothesis of the presence of a marine contribution during the first measurement period. The average wind velocity near ground level, measured at 5 m from the coastline, was relatively high (6.4 m s^{-1}) during the first period compared to the second period (2.4 m s^{-1}). Results of the meteorological model MOLOCH (MOdello LOCale in H coordinates) indicate that the wind velocities in the open sea are significantly higher during the first measurement period compared to the second one (http://www.isac.cnr.it/dinamica/projects/forecasts/moloch/). Such high wind velocity could favor the breaking of waves in the open sea and the formation of sea-spray.

7 Conclusions and Key Findings

The Mediterranean Basin still does suffer from the impact of anthropogenic pressures which lead to environmental degradation. Chemical pollution, maritime transport, and climate change are key factors causing air quality degradation at both regional and local scales. On the other hand, air pollutant dynamics and distribution in the Mediterranean region are closely related to its unique geographical characteristics and specific weather conditions that favor the enhancement of air pollutant photochemical production and accumulation.

The work developed during this Ph.D. focuses on the chemical characterization of aerosol over the Central-Southern Mediterranean region in order to investigate and improve our knowledge in term of variations of the $PM_{2.5}$ and PM_{10} levels in relation to both natural and anthropogenic sources. The experimental study was conducted following two monitoring approaches, particularly through observational measurements obtained from both land-based and over-water monitoring campaigns. Therefore, in the first approach, the PM assessment in the Mediterranean area was performed across *off-shore* sites, fixed along the routes followed during oceanographic campaigns carried out onboard the CNR- Research vessel; in the second approach, the monitoring program was developed at *on-shore* sites, in particular, at the high altitude GAW-Observatory "Monte Curcio" of the CNR-IIA and across a number of GAW stations, including Monte Curcio, as part of the Regional Network "I-AMICA" in Southern Italy. Aerosol levels and variations of its fractions were furthermore evaluated in relation to both natural and anthropogenic sources. Central-Southern Mediterranean Basin, especially in the summertime, is heavily affected by natural sources, like Saharan dust outbreaks and wildfire events, therefore, their influence on aerosol variations over the studied area was addressed and presented. All the case studies carried out in this Thesis show the obviously joint contribution of natural and anthropogenic sources on particulate matter sampled in different environmental conditions (i.e., marine, coastal and high altitude). Natural emissions are mainly represented by the sea spray, volcanic emissions and mineral dust (Saharan dust) which have a significant impact on air quality in Mediterranean country (as Cyprus, Spain, France, Greece, Malta, and Italy), and contribute to exceeding the PM daily and annual limit values. On the other hand, the anthropogenic emissions can be associated with different sources: indeed in the over-water measurements carried out on the research vessel one of the most significant contributions can be associated with the shipping emission, whereas on-land measurements performed at the ground-based monitoring stations show predominant vehicular traffic and/or biomass burning contributes.

Measurements of particulate matter in both fractions, PM_{10} and $PM_{2.5}$, were performed during an oceanographic campaign across the Tyrrhenian Sea on board the CNR- research vessel during summer 2017 within MEDOCEANOR ongoing program, in order to assess the spatial distribution and temporal variation of aerosol concentrations in Marine Boundary Layer prevalently close to natural emission sources. Furthermore, to gain more insight into the atmospheric mechanisms leading to aerosol levels across the Mediterranean Basin, the measurements performed during previous three cruise campaigns during 2011, 2012, and 2015, were synthesized, integrated and then analyzed in a coherent way. Sampling periods of each of these three cruise campaigns refer to: Fall 2011, summer 2012, and summer 2015. Elemental composition of both $PM_{2.5}$ and $PM_{2.5-10}$ collected during all cruise campaigns were determined in order to identify specific tracers for different classes of particles that can be found in the Mediterranean atmosphere. The obtained results highlight the influence of anthropogenic sources prevalently when the routes of these campaigns traveling close to harbors and industrial areas whereas natural sources influences became predominant close to natural point sources located in the Southern Mediterranean area. In particular, the natural contribution is represented by volcanic, crustal and sea spray sources, which are the main natural sources that contribute to air quality in the Mediterranean area. In particular, during the 2017 cruise campaign, the persistent enrichment of elements highly volatile as Sb, Se, and Sn, due to volcanic and fumarolic emissions has been observed. In the fumaroles area a good correlation was indeed achieved between the sulfur dioxide gas, prevalently emitted from fumaroles and used as a tracer, and sulfate ion (coming from the SO_2 reaction with water and condensation on particles), except for the Vulcano (2) sampling point where the change of the weather affected the results. In addition to natural contributions, the performed Factor Analysis highlighted a contribution from anthropogenic sources; for example, close to Campi Flegrei area, vehicular traffic and shipping emissions have been observed. Shipping emissions representing both local harbors and maritime traffic across the basin, represent one of the most important contributions found in all 2011, 2012, and 2015 cruise campaigns particularly when the route of the cruises developed across the Strait of Gibraltar and Strait of Messina. These areas are exposed to considerable naval traffic, both for tourists and for economic activities. In the Mediterranean marine environment, maritime transport became a “hot” issue in the past decade for atmospheric research and air pollution and climate policy. Despite implications on both human health and radiative budget involve an increasing interest, data referring to air pollutants directly measured on the sea are yet

relatively scarce. The results obtained during this study give a contribution to our current understanding of how and why regional air quality may change in the Mediterranean region. The "case study 2" focused on the carbonaceous aerosol components, organic carbon (OC) and elemental carbon (EC) performed at the high altitude station Monte Curcio in southern Italy. In recent years, particular attention has been paid to carbonaceous aerosols through systematic studies regarding their abundances, sources, and spatial variations. Nevertheless, the Mediterranean area is a hot spot for air pollution and climate, highly impacted by biomass burning and anthropogenic activities, emitting high concentrations of EC and OC. Only a few observations are available in this crucial area, where these emissions are able to play a significant role in climate, in an environment already highly impacted and sensitive to climate change. OC and EC are co-emitted, but in different proportions, depending on the source. Elemental carbon is directly emitted into the atmosphere from the incomplete combustion of fossil fuels, biofuels, and biomass. It has a long photochemical lifetime and this makes it a good indicator for primary anthropogenic air pollution. Organic carbon originates from a variety of processes. It can be released into the atmosphere from anthropogenic (fossil fuel combustion, domestic heating and cooking, industrial processes, biomass burning), and biogenic sources (vegetation, wind-lifted biological particles, fires, emissions from marine environments), as primary OC (POC), or produced within the atmosphere by photochemical reactions through gas-to-particle conversion of volatile organic compounds, as secondary OC (SOC). At Monte Curcio site seasonal trends of OC and EC in both PM size fractions have been observed with concentrations higher during the warm season compared to those observed during the cold season. This could be due to the height of the Planetary Boundary Layer (PBL) which during the cold season was lower respect to the height of the monitoring station, therefore this means that the measurements were representative of free troposphere conditions. The OC/EC ratio in both fraction show values in accordance with those found in other high altitude remote sites. In $PM_{2.5,}$ the ratio decreased during the warm period then go up again, in a similar way the ratio OC/EC in PM_{10} decreased during the warm period reaching the maximum in December. The major presence of OC associated at $PM_{2.5}$ is due to the decoupling from the planetary boundary layer and representative of free troposphere conditions.

The values of $EC(PM_{2.5})/EC(PM_{10})$ and $OC(PM_{2.5})/OC(PM_{10})$ ratios suggested that elemental carbon was predominantly in the fine fraction, while the organic carbon showed a trend during the campaign, with the lowest value obtained in September and October probably due to the intrusion of coarse fraction coming from wildfires or anthropogenic

sources in local area. To obtain information on SOC, the SOC/OC ratio was used, showing an important decrease during the warm period in both fractions as well as the OC/EC ratio; this means an increase in the EC contribution, therefore an increase in POC probably due to wildfire emissions, common enough in Southern Italy during summer season. The monthly average concentration of EC and eBC shows similar trends with larger concentrations during the warm period, moreover measured eBC were larger than EC of an average factor of about 3. The weekly pattern of eBC in the warm season showed higher concentrations during the weekends probably due to higher local road traffic emissions during weekends (touristic site downstream of the sampling station site). Analyzing the hourly trend of eBC concentrations during cold period show a minimum early in the morning (5 am) and grew up until 1 pm and then decrease again, following the diurnal cycle of planetary boundary-layer height. The hybrid receptor model (CWT) used showed differences in the possible sources of carbonaceous aerosol between the different seasons. Carbonaceous aerosols can be transported over long distances, potentially influencing global climate. This is in part due to highly variable temporal and spatial concentrations in the troposphere, caused by dispersion or turbulent mixing and in part due to undiscovered atmospheric transformations, such as heterogeneous oxidation or cloud seeding. At Monte Curcio station has been observed that carbonaceous aerosol mainly comes from long-range transport prevalently during the cold season, whereas during the warm season is affected by regional sources. The pattern of eBC and EC are similar in both season, this because they are both mainly primary pollutants having essentially the same sources. The pattern of OC is similar to EC only during the warm season, probably because the formation of secondary organic aerosol (SOA) is influenced also by the circulation of air masses and could induce the differences observed in the CWT of EC and OC. Complex mechanisms such as condensation, coagulation, cloud processing, and photochemical oxidation processes lead indeed to the formation of secondary aerosols. Due to the geographical location, this area of the Mediterranean basin is affected by local and long-range transport of marine, desert, and anthropogenic aerosols. Therefore, simultaneous aerosol measurements for carbonaceous characterization in the Southern Italy across different ground-based sites (e.g., coastal, mountain, and urban) distributed, thus, over the same geographical region would be a useful tool for exploring long-range transport vs. local emissions in conjunction with aerosol aging processes. In this context, and with this aim, an intensive measurement campaign was conducted (Case study 3) from November 2015 to January 2016 at five different sites of Southern Italy, to investigate and compare the characteristics and the relative contributions of carbonaceous species (OC and EC) to the

PM_{10} and $PM_{2.5}$ mass. The results obtained were related to the climatic and geographic conditions of the study areas to identify the possible factors affecting the concentrations of carbonaceous species. The carbonaceous content was investigated in daily 24-h $PM_{2.5}$ and PM_{10} samples simultaneously collected at five sites in the framework of the I-AMICA network: the suburban site of Lecce, two coastal sites (Lamezia Terme, and Capo Granitola), the remote high altitude site of Monte Curcio, and the urban site of Naples. The sites were selected based on their distance from pollution sources, according to criteria proposed by the European Environment Agency. An increasing trend from remote to urban sites was observed for the $PM_{2.5}$ and PM_{10} concentrations with higher values observed at the marine site of Capo Granitola compared to those observed at Lamezia Terme, likely because of a major contribution of sea spray in the coarse fraction considering the location of Capo Granitola site very close to the sea. The $PM_{2.5}$ and PM_{10} concentrations are highly correlated at all sites, with the exception of Capo Granitola where significantly different $PM_{2.5}/PM_{10}$ ratios were observed due to air masses coming from the sea or from inland. The increasing trend of both OC and EC average concentrations were also observed with minimal at the remote mountain site and increased in the following order: remote < coastal/marine < suburban < urban (i.e., Monte Curcio < Capo Granitola < Lamezia Terme < Lecce < Naples). This result highlights how the anthropogenic sources (vehicular traffic) are predominant in urban sites. Also, the OC and EC concentrations were well correlated at all sites, with the exclusion of the urban site of Naples in which the different trend may be due to local sources with different OC/EC ratios in primary emissions. The OC/EC ratios are generally higher in PM_{10} with respect to $PM_{2.5}$ or comparable (in Naples and Monte Curcio). In addition, the OC/EC ratios were higher at the sites minimally influenced by local combustion/pollution (Monte Curcio and Capo Granitola), and this highlights the clear prevalence of the organic carbon species over EC. Carbonaceous aerosol at Monte Curcio mainly comes from long-range transported aerosol during the cold season, finding extremely low concentrations that are in good agreement with free tropospheric conditions characterizing the remote site.

8. Recommendation for future works

As recognized by the scientific community, the complexity of air pollution phenomenology within the Mediterranean Basin, which to a large extent is influenced by regional and long-range transported pollutants, requires for a dense network of regional background monitoring sites along with measurements and data analysis. The overall goal of the research work developed during this Ph.D. has been to gain more insight into the atmospheric mechanisms influencing the aerosol levels across the Mediterranean basin. Despite the relatively short time period, the thesis work developed during the PhD provided datasets whose analysis reported here highlighted that aerosol observations conducted both on-land across monitoring sites, and over-water measurements during intensive oceanographic campaigns in the Mediterranean can provide useful information enabling better characterization of aerosol concentrations and their spatio-temporal variability in the Mediterranean sea basin, highlighting both meteorological and source location influence. However, moving from these findings, additional datasets are needed along with different approaches, such as modeling applications which include climatological variability as well as atmospheric chemistry and source emissions of key air pollutants for identifying patterns and source impacts of aerosols composition over time in the Mediterranean region, and to discriminate the different sources using other source apportionment tools (as PMF). In addition, a well-planned observation system is required to provide a consistent and standardized set of long-term observations on trace gases, particles, and physical parameters, at strategic sites that are well distributed and representative of major atmospheric transport patterns. Therefore, to fill the observation gaps in the Mediterranean basin both on-shore and off-shore measurements campaigns will be performed to measure main aerosol components as well as sulphate, nitrate, ammonium along with trace metals, crustal element, heavy metals, elemental carbon (EC), organic carbon (OC) and secondary inorganic compounds with the supporting facilities of the Institute of Atmospheric Pollution Research of the CNR and within the large number of projects in which the CNR-IIA is involved as coordinator or partner.

References

Aiuppa A, Allard P, D'Alessandro W, et al (2000) Mobility and fluxes of major, minor and trace metals during basalt weathering and groundwater transport at Mt. Etna volcano (Sicily). Geochim Cosmochim Acta 64:1827–1841. doi: 10.1016/S0016-7037(00)00345-8

Aiuppa A, Dongarrà G, Valenza M, et al (2003) Degassing of trace volatile metals during the 2001 eruption of etna. In: Geophysical Monograph Series. American Geophysical Union (AGU), pp 41–54

Aleksandropoulou V, Torseth K, Lazaridis M (2015) Contribution of natural sources to PM emissions over the metropolitan areas of athens and Thessaloniki. Aerosol Air Qual Res 15:1300–1312. doi: 10.4209/aaqr.2014.11.0278

Allard P, Aiuppa A, Loyer H, et al (2000) Acid gas and metal emission rates during long-lived basalt degassing at Stromboli volcano. Geophys Res Lett 27:1207–1210. doi: 10.1029/1999GL008413

Allen AG, Mather TA, McGonigle AJS, et al (2006) Sources, size distribution, and downwind grounding of aerosols from Mount Etna. J Geophys Res Atmos 111:n/a-n/a. doi: 10.1029/2005JD006015

Amato F, Pandolfi M, Escrig A, et al (2009) Quantifying road dust resuspension in urban environment by Multilinear Engine: A comparison with PMF2. Atmos Environ 43:2770–2780. doi: 10.1016/J.ATMOSENV.2009.02.039

And RLP, Wishinski PR, And PKH, et al (2001) Comparative application of multiple receptor methods to identify aerosol sources in northern Vermont. Environ Sci Technol 35:4622–4636. doi: 10.1021/es010588p

Anderson TW (1984) An Introduction to Multivariate Statistical Analysis. 675. doi: 10.2307/2343317

Andreae MO, Gelencsér A (2006) Black carbon or brown carbon? the nature of light-absorbing carbonaceous aerosols. Atmos Chem Phys 6:3131–3148. doi: 10.5194/acp-6-3131-2006

Anttila P, Paatero P, Tapper U, Järvinen O (1995) Source identification of bulk wet deposition in Finland by positive matrix factorization. Atmos Environ 29:1705–1718. doi: 10.1016/1352-2310(94)00367-T

Aruna K, Kumar TVL, Rao DN, et al (2013) Black carbon aerosols in a tropical semi-urban coastal environment: Effects of boundary layer dynamics and long range transport. J Atmos Solar-Terrestrial Phys 104:116–125. doi: 10.1016/J.JASTP.2013.08.020

Ashbaugh LL, Malm WC, Sadeh WZ (1985) A residence time probability analysis of sulfur concentrations at grand Canyon National Park. Atmos Environ 19:1263–1270. doi: 10.1016/0004-6981(85)90256-2

Avino P, Brocco D, Lepore L (2001) DETERMINATION OF ATMOSPHERIC ORGANIC AND ELEMENTAL CARBON PARTICLE IN ROME WITH A THERMAL METHOD. Anal Lett 34:967–974

Bagnato E, Aiuppa A, Parello F, et al (2007) Degassing of gaseous (elemental and

reactive) and particulate mercury from Mount Etna volcano (Southern Italy). Atmos Environ 41:7377–7388. doi: 10.1016/j.atmosenv.2007.05.060

Barberi F, Rosi M, Sodi A (1993) Volcanic hazard assessment at Stromboli based on review of historical data. Bull Volcanol

Becker JS (2005) Trace and ultratrace analysis in liquids by atomic spectrometry. TrAC - Trends Anal. Chem. 24:243–254

Bellinger DC (2005) Teratogen update: Lead and pregnancy. Birth Defects Res Part A - Clin Mol Teratol 73:409–420. doi: 10.1002/bdra.20127

Bencardino M, Sprovieri F, Cofone F, Pirrone N (2011) Variability of atmospheric aerosol and ozone concentrations at marine, urban, and high-altitude monitoring stations in southern Italy during the 2007 summer Saharan dust outbreaks and wildfire episodes. J Air Waste Manag Assoc 61:952–967. doi: 10.1080/10473289.2011.599279

Bencardino MM, Pirrone NN, Sprovieri FF (2014) Aerosol and ozone observations during six cruise campaigns across the Mediterranean basin: temporal, spatial, and seasonal variability. Environ Sci Pollut Res 21:4044–4062. doi: 10.1007/s11356-013-2196-6

Berndt T, Sipilä M, Stratmann F, et al (2014) Enhancement of atmospheric H2SO4/H2O nucleation: Organic oxidation products versus amines. Atmos Chem Phys 14:751–764. doi: 10.5194/acp-14-751-2014

Beuck H, Quass U, Klemm O, Kuhlbusch TAJ (2011) Assessment of sea salt and mineral dust contributions to PM10 in NW Germany using tracer models and positive matrix factorization. Atmos Environ 45:5813–5821. doi: 10.1016/j.atmosenv.2011.07.010

Bian Q, Alharbi B, Sharee MM, et al (2017) Sources of PM2.5 carbonaceous aerosol in Riyadh, Saudi Arabia. Atmos Chem Phys Discuss 1–36. doi: 10.5194/acp-2017-829

Birch ME, Cary RA (1996) Elemental Carbon-Based Method for Monitoring Occupational Exposures to Particulate Diesel Exhaust. Aerosol Sci Technol 25:221–241. doi: 10.1080/02786829608965393

Blando JD, Turpin BJ (2000) Secondary organic aerosol formation in cloud and fog droplets: A literature evaluation of plausibility. Atmos Environ 34:1623–1632. doi: 10.1016/S1352-2310(99)00392-1

Bond TC, Doherty SJ, Fahey DW, et al (2013) Bounding the role of black carbon in the climate system: A scientific assessment. J Geophys Res Atmos. doi: 10.1002/jgrd.50171

Borgese L, Zacco A, Pal S, et al (2011) A new non-destructive method for chemical analysis of particulate matter filters: The case of manganese air pollution in Vallecamonica (Italy). Talanta 84:192–198. doi: 10.1016/j.talanta.2010.12.048

Briggs NL, Long CM (2016) Critical review of black carbon and elemental carbon source apportionment in Europe and the United States. Atmos. Environ. 144:409–427

Calabrese S, Aiuppa A, Allard P, et al (2011) Atmospheric sources and sinks of volcanogenic elements in a basaltic volcano (Etna, Italy). Geochim Cosmochim Acta 75:7401–7425. doi: 10.1016/j.gca.2011.09.040

Calabrese S, Randazzo L, Daskalopoulou K, et al (2016) Mount Etna volcano (Italy) as a major “dust” point source in the Mediterranean area. Arab J Geosci 9:. doi:

10.1007/s12517-015-2165-0

Canepari S, Perrino C, Astolfi ML, et al (2009) Determination of soluble ions and elements in ambient air suspended particulate matter: Inter-technique comparison of XRF, IC and ICP for sample-by-sample quality control. Talanta 77:1821–1829. doi: 10.1016/j.talanta.2008.10.029

Caracausi A, Ditta M, Italiano F, et al (2005) Changes in fluid geochemistry and physico-chemical conditions of geothermal systems caused by magmatic input: The recent abrupt outgassing off the island of Panarea (Aeolian Islands, Italy). Geochim Cosmochim Acta 69:3045–3059. doi: 10.1016/j.gca.2005.02.011

Caratori Tontini F, Cocchi L, Muccini F, et al (2010) Potential-field modeling of collapse-prone submarine volcanoes in the southern Tyrrhenian Sea (Italy). Geophys Res Lett 37:n/a-n/a. doi: 10.1029/2009GL041757

Carslaw D (2015) The openair manual open-source tools for analysing air pollution data. King's Coll London 287

Castro LM, Pio CA, Harrison RM, Smith DJT (1999) Carbonaceous aerosol in urban and rural European atmospheres: Estimation of secondary organic carbon concentrations. Atmos Environ 33:2771–2781. doi: 10.1016/S1352-2310(98)00331-8

Cavalli F, Alastuey A, Areskoug H, et al (2016) A European aerosol phenomenology -4: Harmonized concentrations of carbonaceous aerosol at 10 regional background sites across Europe. Atmos Environ 144:133–145. doi: 10.1016/J.ATMOSENV.2016.07.050

Cavalli F, Viana M, Yttri KE, et al (2010) Toward a standardised thermal-optical protocol for measuring atmospheric organic and elemental carbon: The EUSAAR protocol. Atmos Meas Tech 3:79–89. doi: 10.5194/amt-3-79-2010

Cesari D, Amato F, Pandolfi M, et al (2016a) An inter-comparison of PM10source apportionment using PCA and PMF receptor models in three European sites. Environ Sci Pollut Res 23:15133–15148. doi: 10.1007/s11356-016-6599-z

Cesari D, Donateo A, Conte M, et al (2016b) An inter-comparison of PM2.5 at urban and urban background sites: Chemical characterization and source apportionment. Atmos Res 174–175:106–119. doi: 10.1016/j.atmosres.2016.02.004

Cesari D, Merico E, Dinoi A, et al (2018) Seasonal variability of carbonaceous aerosols in an urban background area in Southern Italy. Atmos Res 200:97–108. doi: 10.1016/j.atmosres.2017.10.004

Chalbot M, Lianou M, Vei I, et al (2013) Spatial attribution of sulfate and dust aerosol sources in an urban area using receptor modeling coupled with Lagrangian trajectories. Atmos Pollut Res 4:346–353. doi: 10.5094/APR.2013.039

Charlson RJ, Covert DS, Larson T V., Waggoner AP (1978) Chemical properties of tropospheric sulfur aerosols. Atmos Environ. doi: 10.1016/0004-6981(78)90187-7

Charlson RJ, Schwartz SE, Hales JM, et al (1992) Climate forcing by anthropogenic aerosols. Science (80-) 255:423–430. doi: 10.1126/science.255.5043.423

Cheng MD, Hopke PK, Barrie L, et al (1993a) Qualitative determination of source regions of aerosol in Canadian high Arctic. Environ Sci Technol 27:2063–2071. doi:

10.1021/es00047a011

Cheng MD, Hopke PK, Zeng Y (1993b) A receptor-oriented methodology for determining source regions of particulate sulfate observed at Dorset, Ontario. J Geophys Res 98:16839. doi: 10.2166/wst.2010.513

Chester DK, Duncan AM, Guest JE, Kilburn CRJ (1986) Mount Etna : the anatomy of a volcano. Springer Netherlands

Cheung K, Daher N, Kam W, et al (2011) Spatial and temporal variation of chemical composition and mass closure of ambient coarse particulate matter (PM10–2.5) in the Los Angeles area. Atmos Environ 45:2651–2662. doi: 10.1016/J.ATMOSENV.2011.02.066

Chiodini G, Todesco M, Caliro S, et al (2003) Magma degassing as a trigger of bradyseismic events: The case of Phlegrean Fields (Italy). Geophys Res Lett 30:. doi: 10.1029/2002GL016790

Chow JC, Watson JG, Chen L-WWA, et al (2007) The IMPROVE_A temperature protocol for thermal/optical carbon analysis: Maintaining consistency with a long-term database. J Air Waste Manag Assoc 57:1014–1023. doi: 10.3155/1047-3289.57.9.1014

Chow JC, Watson JG, Edgerton SA, Vega E (2002) Chemical composition of PM2.5 and PM10 in Mexico City during winter 1997. Sci Total Environ 287:177–201. doi: 10.1016/S0048-9697(01)00982-2

Chow JC, Watson JG, Pritchett LC, et al (1993) The dri thermal/optical reflectance carbon analysis system: description, evaluation and applications in U.S. Air quality studies. Atmos Environ Part A, Gen Top 27:1185–1201. doi: 10.1016/0960-1686(93)90245-T

Chu B, Jiang J, Lu Z, et al (2012) Effects of Inorganic Seeds on Secondary Organic Aerosol (SOA) Formation.pdf

Chueinta W, Hopke PK (2001) Beta gauge for aerosol mass measurement. Aerosol Sci Technol 35:840–843. doi: 10.1080/027868201753227398

Clements N, Eav J, Xie M, et al (2014) Concentrations and source insights for trace elements in fine and coarse particulate matter. Atmos Environ 89:373–381. doi: 10.1016/J.ATMOSENV.2014.01.011

Collins JF, Brown JP, Dawson S V., Marty MA (1991) Risk assessment for benzo[a]pyrene. Regul Toxicol Pharmacol 13:170–184. doi: 10.1016/0273-2300(91)90020-V

Contini D, Cesari D, Donateo A, et al (2014) Characterization of PM10 and PM2.5 and Their Metals Content in Different Typologies of Sites in South-Eastern Italy. Atmosphere (Basel) 5:435–453. doi: 10.3390/atmos5020435

Contini D, Genga A, Cesari D, et al (2010) Characterisation and source apportionment of PM10 in an urban background site in Lecce. Atmos Res 95:40–54. doi: 10.1016/j.atmosres.2009.07.010

Cooper JA, Watson JG (1980) Receptor oriented methods of air particulate source apportionment. J Air Pollut Control Assoc 30:1116–1125. doi: 10.1080/00022470.1980.10465157

Coulter RL (1979) A Comparison of Three Methods for Measuring Mixing-Layer Height. J. Appl. Meteorol. 18:1495–1499

Crenn V, Fronval I, Petitprez D, Riffault V (2017) Fine particles sampled at an urban background site and an industrialized coastal site in Northern France — Part 1: Seasonal variations and chemical characterization. Sci Total Environ 578:203–218. doi: 10.1016/j.scitotenv.2015.11.165

Cristofanelli P, Busetto M, Calzolari F, et al (2017) Investigation of reactive gases and methane variability in the coastal boundary layer of the central Mediterranean basin. Elem Sci Anth 5:12. doi: 10.1525/elementa.216

D'Alessandro A, D'Anna G, Luzio D, Mangano G (2009) The INGV's new OBS/H: Analysis of the signals recorded at the Marsili submarine volcano. J Volcanol Geotherm Res 183:17–29. doi: 10.1016/J.JVOLGEORES.2009.02.008

Daus B, Weiss H, Altenburger R (2009) Uptake and toxicity of hexafluoroarsenate in aquatic organisms. Chemosphere 78:307–312. doi: 10.1016/j.chemosphere.2009.10.033

De Gois JS, Almeida TS, Alves JC, et al (2016) Assessment of the Halogen Content of Brazilian Inhalable Particulate Matter (PM10) Using High Resolution Molecular Absorption Spectrometry and Electrothermal Vaporization Inductively Coupled Plasma Mass Spectrometry, with Direct Solid Sample Analysis. Environ Sci Technol 50:3031–3038. doi: 10.1021/acs.est.5b01934

De Leeuw G (1986) Vertical profiles of giant particles close above the sea surface. Tellus B 38 B:51–61. doi: 10.1111/j.1600-0889.1986.tb00087.x

Dekov VM, Kamenov GD, Savelli C, Stummeyer J (2006) Anthropogenic Pb component in hydrothermal ochres from Marsili Seamount (Tyrrhenian Sea). Mar Geol 229:199–208. doi: 10.1016/J.MARGEO.2006.03.003

Dinoi A, Cesari D, Marinoni A, et al (2017) Inter-Comparison of Carbon Content in PM2.5 and PM10 Collected at Five Measurement Sites in Southern Italy. Atmosphere (Basel) 8:243. doi: 10.3390/atmos8120243

Dinoi A, Perrone MR, Burlizzi P, et al (2010) Application of MODIS Products for Air Quality Studies Over Southeastern Italy. Remote Sens 2:1767–1796. doi: 10.3390/rs2071767

Directive 2008/50/EC D (2008) Ambient air quality and cleaner air for Europe. Off J Eur Union

Draxler RR, Rolph GD (2010) HYSPLIT (HYbrid single-particle Lagrangian integrated trajectory) model access via NOAA ARL READY. NOAA Air Resources Laboratory, Silver Spring, MD. Dostupno na http//ready. arl. noaa. gov/HYSPLIT. php (06. 06. 2010.)

Durant JL, Ash CA, Wood EC, et al (2010) Short-term variation in near-highway air pollutant gradients on a winter morning. Atmos Chem Phys 10:8341–8352. doi: 10.5194/acp-10-8341-2010

Easter RC, Peters LK (1994) Binary homogeneous nucleation: temperature and relative humidity fluctuations, nonlinearity, and aspects of new particle production in the atmosphere. J Appl Meteorol. doi: 10.1175/1520-

0450(1994)033<0775:BHNTAR>2.0.CO;2

Ebert M, Müller-Ebert D, Benker N, Weinbruch S (2012) Source apportionment of aerosol particles near a steel plant by electron microscopy. J Environ Monit 14:3257–3266. doi: 10.1039/c2em30696d

Ehn M, Thornton JA, Kleist E, et al (2014) A large source of low-volatility secondary organic aerosol. Nature 506:. doi: 10.1038/nature13032

El Haddad I, Marchand N, Dron J, et al (2009) Comprehensive primary particulate organic characterization of vehicular exhaust emissions in France. Atmos Environ 43:6190–6198. doi: 10.1016/j.atmosenv.2009.09.001

El Haddad I, Marchand N, Temime-Roussel B, et al (2011a) Insights into the secondary fraction of the organic aerosol in a Mediterranean urban area: Marseille. Atmos Chem Phys 11:2059–2079. doi: 10.5194/acp-11-2059-2011

El Haddad I, Marchand N, Wortham H, et al (2011b) Primary sources of PM2.5organic aerosol in an industrial Mediterranean city, Marseille. Atmos Chem Phys 11:2039–2058. doi: 10.5194/acp-11-2039-2011

EPA USEPA (2012) APTI Course 435, Atmospheric Sampling. BiblioGov

Escrig A, Monfort E, Celades I, et al (2009) Application of Optimally Scaled Target Factor Analysis for Assessing Source Contribution of Ambient PM $_{10}$. J Air Waste Manage Assoc 59:1296–1307. doi: 10.3155/1047-3289.59.11.1296

Escudero M, Stein A, Draxler RR, et al (2006) Determination of the contribution of northern Africa dust source areas to PM10 concentrations over the central Iberian Peninsula using the Hybrid Single-Particle Lagrangian Integrated Trajectory model (HYSPLIT) model. J Geophys Res Atmos 111:1–15. doi: 10.1029/2005JD006395

European Environment Agency. Trends and projections in Europe : tracking progress towards Europe's climate and energy targets

Falkovich AH, Rudich Y (2001) Analysis of semivolatile organic compounds in atmospheric aerosols by direct sample introduction thermal desorption GC/MS. Environ Sci Technol 35:2326–2333. doi: 10.1021/es000280i

FavalliM M, Karátson D, Mazzuoli R, et al (2005) Volcanic geomorphology and tectonics of the Aeolian archipelago (Southern Italy) based on integrated DEM data. Bull Volcanol 68:157–170. doi: 10.1007/s00445-005-0429-3

Feng Y, Ramanathan V, Kotamarthi VR (2013) Brown carbon: A significant atmospheric absorber of solar radiation. Atmos Chem Phys 13:8607–8621. doi: 10.5194/acp-13-8607-2013

Finizola A, Sortino F, Lénat JF, et al (2003) The summit hydrothermal system of Stromboli. New insights from self-potential, temperature, CO2 and fumarolic fluid measurements, with structural and monitoring implications. Bull Volcanol 65:486–504. doi: 10.1007/s00445-003-0276-z

Finlayson-Pitts BJ, Pitts JN (2000) Chemistry of the Upper and Lower Atmosphere: Theory, Experiments, and Applications

Fitzgerald JW (1991) Marine aerosols: A review. Atmos Environ Part A Gen Top 25:533–545. doi: 10.1016/0960-1686(91)90050-H

Fleming ZL, Monks PS, Manning AJ (2012) Review: Untangling the influence of air-mass history in interpreting observed atmospheric composition. Atmos Res 104–105:1–39. doi: 10.1016/J.ATMOSRES.2011.09.009

Forster, P. and Ramaswamy V (2007) Changes in Atmospheric Con- stituents and in Radiative Forcing, Climate Change 2007. In: The Physical Science Basis. pp 129–234

Francis P, Oppenheimer C, Stevenson D (1993) Endogenous growth of persistently active volcanoes. Nature 366:554–557. doi: 10.1038/366554a0

Furger M, Minguillón MC, Yadav V, et al (2017) Elemental composition of ambient aerosols measured with high temporal resolution using an online XRF spectrometer. Atmos Meas Tech 10:2061–2076. doi: 10.5194/amt-10-2061-2017

G. Pace, A. di Sarra, D. Meloni SP and PC (2006) Aerosol optical properties at Lampedusa (Central Mediterranean). 1. Influence of transport and identification of different aerosol types. Atmos Chem Phys 6:697–713. doi: 10.5194/acp-6-715-2006

Gabbianelli G, Gillot P., Lanzafame G, et al (1990) Tectonic and volcanic evolution of Panarea (Aeolian Islands, Italy). Mar Geol 92:313–326. doi: 10.1016/0025-3227(90)90011-8

Gao N, Cheng M-D, Hopke PK (1994) Receptor modeling of airborne ionic species collected in SCAQS. Atmos Environ 28:1447–1470. doi: 10.1016/1352-2310(94)90207-0

Gao N, Cheng M-D, Hopke PK (1993) Potential source contribution function analysis and source apportionment of sulfur species measured at Rubidoux, CA during the Southern California Air Quality Study, 1987

Gao N, Hopke PK, W.Reid N (1996) Possible Sources for Some Trace Elements Found in Airborne Particles and Precipitation in Dorset, Ontario. J Air Waste Manage Assoc 46:1035–1047. doi: 10.1080/10473289.1996.10467539

Gencarelli CN, De Simone F, Hedgecock IM, et al (2014) Development and application of a regional-scale atmospheric mercury model based on WRF/Chem: A Mediterranean area investigation. Environ Sci Pollut Res 21:4095–4109. doi: 10.1007/s11356-013-2162-3

Gentner DR, Isaacman G, Worton DR, et al (2012) Elucidating secondary organic aerosol from diesel and gasoline vehicles through detailed characterization of organic carbon emissions. Proc Natl Acad Sci 109:18318–18323. doi: 10.1073/pnas.1212272109

George C, Ammann M, D'Anna B, et al (2015) Heterogeneous Photochemistry in the Atmosphere. Chem. Rev. 115:4218–4258

Glasius M, Hansen AMK, Claeys M, et al (2018) Composition and sources of carbonaceous aerosols in Northern Europe during winter. Atmos Environ 173:127–141. doi: 10.1016/j.atmosenv.2017.11.005

Gleser LJ (1997) Some thoughts on chemical mass balance models. Chemom Intell Lab Syst 37:15–22. doi: 10.1016/S0169-7439(96)00060-3

Goldstein AH, Worton DR, Williams BJ, et al (2008) Thermal desorption comprehensive two-dimensional gas chromatography for in-situ measurements of organic aerosols. J Chromatogr A 1186:340–347. doi: 10.1016/j.chroma.2007.09.094

Gordon GE (1988) Receptor models Development and testing of such models has moved from the research domain into application to practical problems. Environ Sci Technol 22:1132–1142

Grantz DA, Garner JHB, Johnson DW (2003) Ecological effects of particulate matter. Environ Int 29:213–39. doi: 10.1016/S0160-4120(02)00181-2

Grimm H, Eatough DJ (2009) Aerosol measurement: The use of optical light scattering for the determination of particulate size distribution, and particulate mass, including the semi-volatile fraction. J Air Waste Manag Assoc 59:101–107. doi: 10.3155/1047-3289.59.1.101

Guenther AB, Jiang X, Heald CL, et al (2012) The model of emissions of gases and aerosols from nature version 2.1 (MEGAN2.1): An extended and updated framework for modeling biogenic emissions. Geosci Model Dev 5:1471–1492. doi: 10.5194/gmd-5-1471-2012

Hans Wedepohl K (1995) The composition of the continental crust. Geochim Cosmochim Acta 59:1217–1232. doi: 10.1016/0016-7037(95)00038-2

Harrison RM, Smith DJT, Pio CA, Castro LM (1997) Comparative receptor modelling study of airborne particulate pollutants in Birmingham (United Kingdom), Coimbra (Portugal) and Lahore (Pakistan). Atmos Environ 31:3309–3321. doi: 10.1016/S1352-2310(97)00152-0

Hatzianastassiou N, Katsoulis B, Vardavas I (2004) Sensitivity analysis of aerosol direct radiative forcing in ultraviolet-visible wavelengths and consequences for the heat budget. Tellus, Ser B Chem Phys Meteorol 56:368–381. doi: 10.1111/j.1600-0889.2004.00110.x

Hellström L, Elinder CG, Dahlberg B, et al (2001) Cadmium exposure and end-stage renal disease. Am J Kidney Dis. doi: 10.1053/ajkd.2001.28589

Henry RC (1987) Current factor analysis receptor models are ill-posed. Atmos Environ 21:1815–1820. doi: 10.1016/0004-6981(87)90122-3

Henry RC (2003) Multivariate receptor modeling by N-dimensional edge detection. Chemom Intell Lab Syst 65:179–189. doi: 10.1016/S0169-7439(02)00108-9

Henry RC, Lewis CW, Hopke PK, Williamson HJ (1984) Review of receptor model fundamentals. Atmos Environ 18:1507–1515. doi: 10.1016/0004-6981(84)90375-5

Hering SV, Friedlander SK (1982) Origins of aerosol sulfur size distributions in the Los Angeles basin. Atmos Environ 16:2647–2656. doi: 10.1016/0004-6981(82)90346-8

Hien PD, Bac VT, Thinh NTH (2005) Investigation of sulfate and nitrate formation on mineral dust particles by receptor modeling. Atmos Environ 39:7231–7239. doi: 10.1016/j.atmosenv.2005.09.003

Ho SSH, Yu JZ (2004) In-injection port thermal desorption and subsequent gas chromatography–mass spectrometric analysis of polycyclic aromatic hydrocarbons and n-alkanes in atmospheric aerosol samples. J Chromatogr A 1059:121–129. doi: 10.1016/J.CHROMA.2004.10.013

Ho SSH, Yu JZ, Chow JC, et al (2008) Evaluation of an in-injection port thermal desorption-gas chromatography/mass spectrometry method for analysis of non-polar

organic compounds in ambient aerosol samples. J Chromatogr A 1200:217–227. doi: 10.1016/j.chroma.2008.05.056

Hobbs P V., Bowdle DA, Radke LF, et al (1985) Particles in the Lower Troposphere over the High Plains of the United States. Part I: Size Distributions, Elemental Compositions and Morphologies. J Clim Appl Meteorol 24:1344–1356. doi: 10.1175/1520-0450(1985)024<1344:PITLTO>2.0.CO;2

Hodzic A, Kasibhatla PS, Jo DS, et al (2016) Rethinking the global secondary organic aerosol (SOA) budget: Stronger production, faster removal, shorter lifetime. Atmos Chem Phys 16:7917–7941. doi: 10.5194/acp-16-7917-2016

Hohaus T, Trimborn D, Kiendler-Scharr A, et al (2010) Atmospheric Measurement Techniques A new aerosol collector for quasi on-line analysis of particulate organic matter: the Aerosol Collection Module (ACM) and first applications with a GC/MS-FID. Atmos Meas Tech 3:1423–1436. doi: 10.5194/amt-3-1423-2010

Holmes NS (2007) A review of particle formation events and growth in the atmosphere in the various environments and discussion of mechanistic implications. Atmos Environ 41:2183–2201. doi: 10.1016/j.atmosenv.2006.10.058

Hopke PK (1991a) An introduction to receptor modeling. Chemom Intell Lab Syst 10:21–43. doi: 10.1016/0169-7439(91)80032-L

Hopke PK (1991b) An introduction to receptor modeling. Chemom. Intell. Lab. Syst. 10:21–43

Hopke PK (2003) Recent developments in receptor modeling. J Chemom 17:255–265. doi: 10.1002/cem.796

Hopke PK (1988) Target transformation factor analysis as an aerosol mass apportionment method: A review and sensitivity study. Atmos Environ 22:1777–1792. doi: 10.1016/0004-6981(88)90066-2

Hopke PK (2016) Review of receptor modeling methods for source apportionment. J. Air Waste Manag. Assoc. 66:237–259

Hopke PK, Gao N, Cheng MD (1993) Combining chemical and meteorological data to infer source areas of airborne pollutants. Chemom Intell Lab Syst 19:187–199. doi: 10.1016/0169-7439(93)80103-O

Hopke PK, Ito K, Mar T, et al (2006) PM source apportionment and health effects: 1. Intercomparison of source apportionment results. J Expo Sci Environ Epidemiol 16:275–286. doi: 10.1038/sj.jea.7500458

Hoppel WA, Fitzgerald JW, Frick GM, et al (1990) Aerosol size distributions and optical properties found in the marine boundary layer over the Atlantic Ocean. J Geophys Res 95:3659–3686. doi: 10.1029/JD095iD04p03659

Hsu Y-K, Holsen TM, Hopke PK (2003) Comparison of hybrid receptor models to locate PCB sources in Chicago. Atmos Environ 37:545–562. doi: 10.1016/S1352-2310(02)00886-5

Hussein T, Puustinen A, Aalto PP, et al (2004) Urban aerosol number size distributions. Atmos Chem Phys 4:391–411

IARC Working Group on the Evaluation of Carcinogenic Risks to Humans (2010) IARC

monographs on the evaluation of carcinogenic risks to humans. Ingested nitrate and nitrite, and cyanobacterial peptide toxins. IARC Monogr Eval Carcinog Risks Hum 94:v–vii, 1–412. doi: 10.1002/food.19940380335

Iezzi G, Caso C, Ventura G, et al (2014) First documented deep submarine explosive eruptions at the Marsili Seamount (Tyrrhenian Sea, Italy): A case of historical volcanism in the Mediterranean Sea. Gondwana Res 25:764–774. doi: 10.1016/J.GR.2013.11.001

Ilacqua V, Hänninen O, Saarela K, et al (2007) Source apportionment of population representative samples of PM 2.5 in three European cities using structural equation modelling. Sci Total Environ 384:77–92. doi: 10.1016/j.scitotenv.2007.06.020

IPCC (2013) Summary for Policymakers. Cambridge University Press, Cambridge

Italiano F, De Santis A, Favali P, et al (2014) The Marsili Volcanic Seamount (Southern Tyrrhenian Sea): A Potential Offshore Geothermal Resource. Energies 7:4068–4086. doi: 10.3390/en7074068

Italiano F, Nuccio PM (1991) Geochemical investigations of submarine volcanic exhalations to the east of Panarea, Aeolian Islands, Italy. J Volcanol Geotherm Res 46:125–141. doi: 10.1016/0377-0273(91)90079-F

Jacob DJ, Winner DA (2009) Effect of climate change on air quality. Atmos Environ 43:51–63. doi: 10.1016/J.ATMOSENV.2008.09.051

Jaenicke R (1993) Aerosol--cloud--climate interactions. Academic Press

Järup L (2003) Hazards of heavy metal contamination. Br Med Bull 68:167–182. doi: 10.1093/bmb/ldg032

Jenkin ME, Clemitshaw KC (2000) Ozone and other secondary photochemical pollutants: chemical processes governing their formation in the planetary boundary layer. Dev Environ Sci 2499–2527. doi: 10.1016/S1474-8177(02)80014-6

Jeong U, Kim J, Lee H, et al (2011) Estimation of the contributions of long range transported aerosol in East Asia to carbonaceous aerosol and PM concentrations in Seoul, Korea using highly time resolved measurements: A PSCF model approach. J Environ Monit 13:1905–1918. doi: 10.1039/c0em00659a

John W, Wall SM, Ondo JL, Winklmayr W (1990) Modes in the size distributions of atmospheric inorganic aerosol. Atmos Environ Part A Gen Top 24:2349–2359. doi: 10.1016/0960-1686(90)90327-J

Josse J, Husson F (2016) **missMDA** : A Package for Handling Missing Values in Multivariate Data Analysis. J Stat Softw 70:. doi: 10.18637/jss.v070.i01

Juntto S, Paatero P (1994) Analysis of daily precipitation data by positive matrix factorization. Environmetrics 5:127–144. doi: 10.1002/env.3170050204

Kalnay E, Kanamitsu M, Kistler R, et al (1996) The NCEP/NCAR 40-year reanalysis project. Bull Am Meteorol Soc 77:437–471. doi: 10.1175/1520-0477(1996)077<0437:TNYRP>2.0.CO;2

Kanaya Y, Komazaki Y, Pochanart P, et al (2008) Mass concentrations of black carbon measured by four instruments in the middle of Central East China in June 2006. Atmos Chem Phys Discuss 8:14957–14990. doi: 10.5194/acpd-8-14957-2008

Khan MB, Masiol M, Formenton G, et al (2016) Carbonaceous PM2.5and secondary organic aerosol across the Veneto region (NE Italy). Sci Total Environ 542:172–181. doi: 10.1016/j.scitotenv.2015.10.103

Kim E, Brown SG, Hafner HR, Hopke PK (2005) Characterization of non-methane volatile organic compounds sources in Houston during 2001 using positive matrix factorization. Atmos Environ 39:5934–5946. doi: 10.1016/J.ATMOSENV.2005.06.045

Kim E, Hopke PK (2007) Source Identifications of Airborne Fine Particles Using Positive Matrix Factorization and U.S. Environmental Protection Agency Positive Matrix Factorization. J Air Waste Manage Assoc 57:811–819. doi: 10.3155/1047-3289.57.7.811

Kim KH, Sekiguchi K, Kudo S, Sakamoto K (2011) Characteristics of atmospheric elemental carbon (char and soot) in ultrafine and fine particles in a roadside environment, Japan. Aerosol Air Qual Res 11:1–12. doi: 10.4209/aaqr.2010.07.0061

Kim YP, Moon KC, Hoon Lee J (2000) Organic and elemental carbon in fine particles at Kosan, Korea. Atmos Environ 34:3309–3317. doi: 10.1016/S1352-2310(99)00445-8

Klockenkämper R, von Bohlen A (2014) Total-Reflection X-Ray Fluorescence Analysis and Related Methods

Kong S, Han B, Bai Z, et al (2010) Receptor modeling of PM2.5, PM10 and TSP in different seasons and long-range transport analysis at a coastal site of Tianjin, China. Sci Total Environ 408:4681–4694. doi: 10.1016/J.SCITOTENV.2010.06.005

Kourtchev I, Ruuskanen TM, Keronen P, et al (2008) Determination of isoprene and α-/β-pinene oxidation products in boreal forest aerosols from Hyytiälä, Finland: Diel variations and possible link with particle formation events. Plant Biol 10:138–149. doi: 10.1055/s-2007-964945

Kumar AV, Patil R., Nambi KS. (2001) Source apportionment of suspended particulate matter at two traffic junctions in Mumbai, India. Atmos Environ 35:4245–4251. doi: 10.1016/S1352-2310(01)00258-8

L. Borgese, M. Salmistraro, A. Gianoncelli, A. Zacco, R. Lucchini, N. Zimmerman, L. Pisani, G. Siviero, L.E. Depero EB (2012) Airborne particulate matter (PM) filter analysis and modeling by total reflection X-ray fluorescence (TXRF) and X-ray standing wave (XSW). Talanta 89:99–104. doi: 10.1016/j.talanta.2011.11.073

Laakso L, Gagné S, Petäjä T, et al (2007) Detecting charging state of ultra-fine particles: instrumental development and ambient measurements

Lack DA, Langridge JM, Bahreini R, et al (2012) Brown carbon and internal mixing in biomass burning particles. Proc Natl Acad Sci U S A 109:14802–7. doi: 10.1073/pnas.1206575109

Lack DA, Moosmüller H, McMeeking GR, et al (2014) Characterizing elemental, equivalent black, and refractory black carbon aerosol particles: A review of techniques, their limitations and uncertainties. Anal Bioanal Chem 406:99–122. doi: 10.1007/s00216-013-7402-3

Lai AM, Shafer MM, Dibb JE, et al (2017) Elements and inorganic ions as source tracers in recent Greenland snow. Atmos Environ 164:205–215. doi:

10.1016/j.atmosenv.2017.05.048

Lawson CL, Hanson RJ (1987) Solving Least Squares Problems (Classics in Applied Mathematics)

Lê S, Josse J, Rennes A, Husson F (2008) FactoMineR: An R Package for Multivariate Analysis

Leaitch WR, Isaac GA (1991) Tropospheric aerosol size distributions from 1982 to 1988 over eastern North America. Atmos Environ Part A Gen Top 25:601–619. doi: 10.1016/0960-1686(91)90058-F

Lewis ER, Schwartz SE (Stephen E (2004) Sea salt aerosol production : mechanisms, methods, measurements and models : a critical review. American Geophysical Union

Lim YB, Tan Y, Perri MJ, et al (2010) Atmospheric Chemistry and Physics Aqueous chemistry and its role in secondary organic aerosol (SOA) formation. Atmos Chem Phys 10:10521–10539. doi: 10.5194/acp-10-10521-2010

Liora N, Poupkou A, Giannaros TM, et al (2016) Impacts of natural emission sources on particle pollution levels in Europe. Atmos Environ 137:171–185. doi: 10.1016/j.atmosenv.2016.04.040

Lonati G, Ozgen S, Giugliano M (2007) Primary and secondary carbonaceous species in PM2.5 samples in Milan (Italy). Atmos Environ 41:4599–4610. doi: 10.1016/J.ATMOSENV.2007.03.046

Long CM, Nascarella MA, Valberg PA (2013) Carbon black vs. black carbon and other airborne materials containing elemental carbon: Physical and chemical distinctions. Environ Pollut 181:271–286. doi: 10.1016/j.envpol.2013.06.009

Macias ES, Zwicker JO, Ouimette JR, et al (1981) Regional haze case studies in the southwestern U.S—I. Aerosol chemical composition. Atmos Environ 15:1971–1986. doi: 10.1016/0004-6981(81)90231-6

Massling A, Nielsen IE, Kristensen D, et al (2015) Atmospheric black carbon and sulfate concentrations in Northeast Greenland. Atmos Chem Phys 15:9681–9692. doi: 10.5194/acp-15-9681-2015

Masson O, Piga D, Gurriaran R, D'Amico D (2010) Impact of an exceptional Saharan dust outbreak in France: PM10 and artificial radionuclides concentrations in air and in dust deposit. Atmos Environ 44:2478–2486. doi: 10.1016/J.ATMOSENV.2010.03.004

Mather TA, Oppenheimer C, Allen AG, McGonigle AJS (2004) Aerosol chemistry of emissions from three contrasting volcanoes in Italy. Atmos Environ 38:5637–5649. doi: 10.1016/j.atmosenv.2004.06.017

Matsumoto K, Nagao I, Tanaka H, et al (1998) Seasonal characteristics of organic and inorganic species and their size distributions in atmospheric aerosols over the northwest Pacific Ocean. Atmos Environ. doi: 10.1016/S1352-2310(97)00499-8

Meng Z, Seinfeld JH (1994) On the Source of the Submicrometer Droplet Mode of Urban and Regional Aerosols. Aerosol Sci Technol 20:253–265. doi: 10.1080/02786829408959681

Mészáros A, Vissy K (1974) Concentration, size distribution and chemical nature of atmospheric aerosol particles in remote oceanic areas. J Aerosol Sci 5:101–109. doi:

10.1016/0021-8502(74)90011-1

Mkoma SL, Maenhaut W, Chi X, et al (2009) Characterisation of PM10 atmospheric aerosols for the wet season 2005 at two sites in East Africa. Atmos Environ 43:631–639. doi: 10.1016/J.ATMOSENV.2008.10.008

Monahan EC, Fairall CW, Davidson KL, Boyle PJ (1983) Observed inter-relations between 10m winds, ocean whitecaps and marine aerosols. Q J R Meteorol Soc 109:379–392. doi: 10.1002/qj.49710946010

Mora J, Maestre S, Hernandis V, Todolí JL (2003) Liquid-sample introduction in plasma spectrometry. TrAC - Trends Anal. Chem. 22:123–132

Moreno T, Jones TP, Richards RJ (2004) Characterisation of aerosol particulate matter from urban and industrial environments: Examples from Cardiff and Port Talbot, South Wales, UK. Sci Total Environ 334–335:337–346. doi: 10.1016/j.scitotenv.2004.04.074

Moreno T, Pérez N, Querol X, et al (2010) Physicochemical variations in atmospheric aerosols recorded at sea onboard the Atlantic-Mediterranean 2008 Scholar Ship cruise (Part II): Natural versus anthropogenic influences revealed by PM10 trace element geochemistry. Atmos Environ 44:2563–2576. doi: 10.1016/j.atmosenv.2010.04.027

Moroni B, Castellini S, Crocchianti S, et al (2015) Ground-based measurements of long-range transported aerosol at the rural regional background site of Monte Martano (Central Italy). Atmos Res 155:26–36. doi: 10.1016/J.ATMOSRES.2014.11.021

Mulik J, Puckett R, Williams D, Sawicki E (1976) Ion Chromatographic Analysis Of Sulfate And Nitrate In Ambient Aerosols. Anal Lett. doi: 10.1080/00032717608059128

Myriokefalitakis S, Vignati E, Tsigaridis K, et al (2010) Global Modeling of the Oceanic Source of Organic Aerosols. Adv Meteorol 2010:1–16. doi: 10.1155/2010/939171

Na K, Sawant AA, Song C, Cocker DR (2004) Primary and secondary carbonaceous species in the atmosphere of Western Riverside County, California. Atmos Environ 38:1345–1355. doi: 10.1016/j.atmosenv.2003.11.023

Ng NL, Kwan AJ, Surratt JD, et al (2008) Atmospheric Chemistry and Physics Secondary organic aerosol (SOA) formation from reaction of isoprene with nitrate radicals (NO 3)

Nicolás JF, Galindo N, Yubero E, et al (2009) Aerosol Inorganic Ions in a Semiarid Region on the Southeastern Spanish Mediterranean Coast. Water Air Soil Pollut 201:149–159. doi: 10.1007/s11270-008-9934-2

Nisbet ICT, LaGoy PK (1992) Toxic equivalency factors (TEFs) for polycyclic aromatic hydrocarbons (PAHs). Regul Toxicol Pharmacol 16:290–300. doi: 10.1016/0273-2300(92)90009-X

O'Dowd CD, de Leeuw G (2007) Marine aerosol production: a review of the current knowledge. Philos Trans R Soc A Math Phys Eng Sci 365:1753–1774. doi: 10.1098/rsta.2007.2043

O'Dowd CD, Smith MH (1993) Physicochemical properties of aerosols over the northeast Atlantic: Evidence for wind-speed-related submicron sea-salt aerosol production. J

Geophys Res Atmos 98:1137–1149. doi: 10.1029/92JD02302

Orsini DA, Ma Y, Sullivan A, et al (2003) Refinements to the particle-into-liquid sampler (PILS) for ground and airborne measurements of water soluble aerosol composition. Atmos Environ 37:1243–1259. doi: 10.1016/S1352-2310(02)01015-4

Öztürk F, Zararsız A, Kırmaz R, Tuncel G (2010) An approach to measure trace elements in particles collected on fiber filters using EDXRF. Talanta 83:823–831. doi: 10.1016/j.talanta.2010.10.038

Paatero P (1999) The Multilinear Engine—A Table-Driven, Least Squares Program for Solving Multilinear Problems, Including the n-Way Parallel Factor Analysis Model. J Comput Graph Stat 8:

Paatero P (1997) Least squares formulation of robust non-negative factor analysis. Chemom Intell Lab Syst 37:23–35. doi: 10.1016/S0169-7439(96)00044-5

Paatero P, Eberly S, Brown SG, Norris GA (2014) Methods for estimating uncertainty in factor analytic solutions. Atmos Meas Tech 7:781–797. doi: 10.5194/amt-7-781-2014

Paatero P, Hopke PK (2003) Discarding or downweighting high-noise variables in factor analytic models. In: Analytica Chimica Acta. pp 277–289

Paatero P, Tapper U (1993) Analysis of different modes of factor analysis as least squares fit problems. Chemom Intell Lab Syst 18:183–194. doi: 10.1016/0169-7439(93)80055-M

Pandolfi M, Gonzalez-Castanedo Y, Alastuey A, et al (2011) Source apportionment of PM10and PM2.5at multiple sites in the strait of Gibraltar by PMF: Impact of shipping emissions. Environ Sci Pollut Res 18:260–269. doi: 10.1007/s11356-010-0373-4

Parshintsev J, Kivilompolo M, Ruiz-Jimenez J, et al (2010) Particle-into-liquid sampler on-line coupled with solid-phase extraction-liquid chromatography-mass spectrometry for the determination of organic acids in atmospheric aerosols. J Chromatogr A. doi: 10.1016/j.chroma.2010.06.026

Pérez C, Nickovic S, Pejanovic G, et al (2006) Interactive dust-radiation modeling: A step to improve weather forecasts. J Geophys Res Atmos 111:. doi: 10.1029/2005JD006717

Pérez N, Moreno T, Querol X, et al (2010) Physicochemical variations in atmospheric aerosols recorded at sea onboard the Atlantic-Mediterranean 2008 Scholar Ship cruise (Part I): Particle mass concentrations, size ratios, and main chemical components. Atmos Environ 44:2552–2562. doi: 10.1016/j.atmosenv.2010.04.023

Peterson MR, Richards MH (2002) Thermal-Optical-Transmittance Analysis for Organic , Elemental , Carbonate , Total Carbon , and OCX2 in PM2 . 5 by the EPA / NIOSH Method - # 83. Symp Air Qual Meas Methods Technol 1–20

Petzold A, Ogren JA, Fiebig M, et al (2013) Sciences ess Atmospheric Chemistry and Physics Climate of the Past Geoscientific Instrumentation Methods and Data Systems Recommendations for reporting "black carbon" measurements. Atmos Chem Phys 13:8365–8379. doi: 10.5194/acp-13-8365-2013

Pey J, Alastuey A, Querol X (2013) PM10and PM2.5sources at an insular location in the western mediterranean by using source apportionment techniques. Sci Total Environ

456–457:267–277. doi: 10.1016/j.scitotenv.2013.03.084

Pietrodangelo A., Bencardino M., Cecinato A., Decesari S., Perrino C., Sprovieri F. PN and FMC (2010) Role of atmospheric pollution on harmful health effects. In: Fabrizio Bianchi, Giuseppe Cavarretta LC (ed) CNR Environment and Health Inter-departmental Project: present knowledge and prospects for future research. Consiglio Nazionale delle Ricerche – Roma © 2010

Pio C, Cerqueira M, Harrison RM, et al (2011) OC/EC ratio observations in Europe: Re-thinking the approach for apportionment between primary and secondary organic carbon. Atmos Environ 45:6121–6132. doi: 10.1016/j.atmosenv.2011.08.045

Pirrone N, Cinnirella S, Feng X, et al (2010) Global mercury emissions to the atmosphere from anthropogenic and natural sources. Atmos Chem Phys 10:5951–5964. doi: 10.5194/acp-10-5951-2010

Poirot RL, Wishinski PR (1986) Visibility, sulfate and air mass history associated with the summertime aerosol in northern vermont. Atmos Environ 20:1457–1469. doi: 10.1016/0004-6981(86)90018-1

Poirot RL, Wishinski PR, Hopke PK, Polissar A V. (2001) Comparative application of multiple receptor methods to identify aerosol sources in northern Vermont. Environ Sci Technol 35:4622–4636. doi: 10.1021/es010588p

Polissar A V., Hopke PK, Malm WC, Sisler JF (1998) Atmospheric aerosol over Alaska 1. Spatial and seasonal variability. J Geophys Res Atmos 103:19035–19044. doi: 10.1029/98JD01365

Polissar A V., Hopke PK, Poirot RL (2001) Atmospheric aerosol over Vermont: Chemical composition and sources. Environ Sci Technol 35:4604–4621. doi: 10.1021/es0105865

Polissar A V, Hopket PK, Malm WC, Sisler JF (1996) THE RATIO OF AEROSOL OPTICAL ABSORPTION COEFFICIENTS TO SULFUR CONCENTRATIONS, AS AN INDICATOR OF SMOKE FROM FOREST FIRES WHEN SAMPLING IN POLAR REGIONS. Atmos Environ 30:1157

Poster DL, Schantz MM, Sander LC, Wise SA (2006) Analysis of polycyclic aromatic hydrocarbons (PAHs) in environmental samples: a critical review of gas chromatographic (GC) methods. Anal Bioanal Chem 386:859–881. doi: 10.1007/s00216-006-0771-0

Pratt KA, Prather KA (2012) Mass spectrometry of atmospheric aerosols-Recent developments and applications. Part II: On-line mass spectrometry techniques. Mass Spectrom. Rev.

Putaud J-P, Raes F, Van Dingenen R, et al (2004) A European aerosol phenomenology-2: chemical characteristics of particulate matter at kerbside, urban, rural and background sites in Europe ARTICLE IN PRESS AE International-Europe. Atmos Environ 38:2579–2595. doi: 10.1016/j.atmosenv.2004.01.041

Putaud JP, Van Dingenen R, Alastuey A, et al (2010) A European aerosol phenomenology - 3: Physical and chemical characteristics of particulate matter from 60 rural, urban, and kerbside sites across Europe. Atmos Environ 44:1308–1320. doi: 10.1016/j.atmosenv.2009.12.011

QLD gov QLD gov. https://www.qld.gov.au/environment/pollution/monitoring/air/air-monitoring/measuring/oscillating-microbalance

Querol X, Alastuey A, Rodriguez S, et al (2001) PM10 and PM2.5 source apportionment in the Barcelona Metropolitan area, Catalonia, Spain. Atmos Environ 35:6407–6419. doi: 10.1016/S1352-2310(01)00361-2

Querol X, Alastuey A, Viana M, et al (2013) Variability of carbonaceous aerosols in remote, rural, urban and industrial environments in Spain: Implications for air quality policy. Atmos Chem Phys 13:6185–6206. doi: 10.5194/acp-13-6185-2013

Querol X, Alastuey A, Viana MM, et al (2004) Speciation and origin of PM10 and PM2.5 in Spain. J Aerosol Sci 35:1151–1172. doi: 10.1016/J.JAEROSCI.2004.04.002

Querol X, Pey J, Pandolfi M, et al (2009) African dust contributions to mean ambient PM10mass-levels across the Mediterranean Basin. Atmos Environ 43:4266–4277. doi: 10.1016/j.atmosenv.2009.06.013

Querol X, Viana M, Alastuey A, et al (2007) Source origin of trace elements in PM from regional background, urban and industrial sites of Spain. Atmos Environ 41:7219–7231. doi: 10.1016/j.atmosenv.2007.05.022

Reimann C, De Caritat P (2000) Intrinsic flaws of element enrichment factors (EFs) in environmental geochemistry. Environ Sci Technol 34:5084–5091. doi: 10.1021/es001339o

Riccobono F, Schobesberger S, Scott CE, et al (2014) Oxidation products of biogenic emissions contribute to nucleation of atmospheric particles. Science (80-). doi: 10.1126/science.1243527

Robinson AL, Grieshop AP, Donahue NM, Hunt SW (2010) Updating the Conceptual Model for Fine Particle Mass Emissions from Combustion Systems Allen L. Robinson. J Air Waste Manage Assoc 60:1204–1222. doi: 10.3155/1047-3289.60.10.1204

Rodríguez S, Querol X, Alastuey A, de la Rosa J (2007) Atmospheric particulate matter and air quality in the Mediterranean: A review. Environ. Chem. Lett.

Roscoe BA, Hopke PK, Dattner SL, Jenks JM (1982) The Use of Principal Component Factor Analysis to Interpret Particulate Compositional Data Sets. J Air Pollut Control Assoc 32:637–642. doi: 10.1080/00022470.1982.10465439

Roy AA, Wagstrom KM, Adams PJ, et al (2011) Quantification of the effects of molecular marker oxidation on source apportionment estimates for motor vehicles. Atmos Environ 45:3132–3140. doi: 10.1016/J.ATMOSENV.2011.03.020

Salako GO, Hopke PK, Cohen DD, et al (2012) Exploring the variation between EC and BC in a variety of locations. Aerosol Air Qual Res 12:1–7. doi: 10.4209/aaqr.2011.09.0150

Salvador P, Artíñano B, Pio C, et al (2010) Evaluation of aerosol sources at European high altitude background sites with trajectory statistical methods. Atmos Environ 44:2316–2329. doi: 10.1016/J.ATMOSENV.2010.03.042

Samara C, Voutsa D, Kouras A, et al (2014) Organic and elemental carbon associated to PM10 and PM2.5 at urban sites of northern Greece. Environ Sci Pollut Res 21:1769–

1785. doi: 10.1007/s11356-013-2052-8

Sandrini S, Fuzzi S, Piazzalunga A, et al (2014a) Spatial and seasonal variability of carbonaceous aerosol across Italy. Atmos Environ 99:587–598. doi: 10.1016/j.atmosenv.2014.10.032

Sandrini S, Fuzzi S, Piazzalunga A, et al (2014b) Spatial and seasonal variability of carbonaceous aerosol across Italy. Atmos Environ 99:587–598. doi: 10.1016/j.atmosenv.2014.10.032

Savoie DL, Prospero JM (1989) Comparison of oceanic and continental sources of non-sea-salt sulphate over the Pacific Ocean. Nature 339:685–687. doi: 10.1038/339685a0

Schauer JJ, Mader BT, Deminter JT, et al (2003) ACE-Asia intercomparison of a thermal-optical method for the determination of particle-phase organic and elemental carbon. Environ Sci Technol 37:993–1001. doi: 10.1021/es020622f

Schmid H, Laskus L, Jürgen Abraham H, et al (2001) Results of the "carbon conference" international aerosol carbon round robin test stage I. Atmos Environ 35:2111–2121. doi: 10.1016/S1352-2310(00)00493-3

Schneider JK, Gagosian RB (1985) Particle Size Distribution of Lipids in Aerosols off the Coast of Peru. J Geophys Res 90:7889–7898. doi: 10.1038/304429a0

Schroeder WH, Dobson M, Kane DM, Johnson ND (1987) Toxic Trace Elements Associated With Airborne Pariacnlaie Matter: A Review. J. Air Pollut. Control Assoc. 37:1267–1285

Seibert P, Kromp-Kolb H, Baltensperger U, et al (1994) Trajectory Analysis of High-Alpine Air Pollution Data. In: Air Pollution Modeling and Its Application: NATO: Challenges of Modern Society. pp 595–596

Seinfeld JH, Pandis SN (2006) Atmospheric Chemistry and Physics; From Air Pollution to Climate Change SECOND EDITION

Seung SP, Bae MS, Schauer JJ, et al (2005) Evaluation of the TMO and TOT methods for OC and EC measurements and their characteristics in PM2.5at an urban site of Korea during ACE-Asia. Atmos Environ 39:5101–5112. doi: 10.1016/j.atmosenv.2005.05.016

Shiraiwa M, Li Y, Tsimpidi AP, et al (2017) Global distribution of particle phase state in atmospheric secondary organic aerosols. Nat Commun 8:. doi: 10.1038/ncomms15002

Shotyk W, Chen B, Krachler M (2005) Lithogenic, oceanic and anthropogenic sources of atmospheric Sb to a maritime blanket bog, Myrarnar, Faroe Islands. J Environ Monit 7:1148. doi: 10.1039/b509928p

Small H, Stevens TS, Bauman WC (1975) Novel Ion Exchange Chromatographic Method Using Conductimetric Detection. Anal Chem. doi: 10.1021/ac60361a017

Sprovieri F, Hedgecock IM, Pirrone N (2010) An investigation of the origins of reactive gaseous mercury in the Mediterranean marine boundary layer. Atmos Chem Phys 10:3985–3997. doi: 10.5194/acp-10-3985-2010

Sprovieri F, Pirrone N (2008a) Spatial and temporal distribution of atmospheric mercury species over the Adriatic Sea. Environ Fluid Mech 8:117–128. doi: 10.1007/s10652-

007-9045-4

Sprovieri F, Pirrone N (2008b) Particle size distributions and elemental composition of atmospheric particulate matter in southern Italy. J Air Waste Manag Assoc 58:797–805. doi: 10.3155/1047-3289.58.6.797

Sprovieri F, Pirrone N, Gärdfeldt K, Sommar J (2003) Mercury speciation in the marine boundary layer along a 6000 km cruise path around the Mediterranean Sea. Atmos Environ 37:63–71. doi: 10.1016/S1352-2310(03)00237-1

Squizzato S, Cazzaro M, Innocente E, et al (2017) Urban air quality in a mid-size city — PM2.5 composition, sources and identification of impact areas: From local to long range contributions. Atmos Res 186:51–62. doi: 10.1016/J.ATMOSRES.2016.11.011

Sthol A (1996) Trajectory statistics - a new method to establish source-receptor relationship of air pollutants and its application to the transport of particulate sulfate in Europe. Atmos Environ 30:579–587

Stone E, Schauer J, Quraishi TA, Mahmood A (2010) Chemical characterization and source apportionment of fine and coarse particulate matter in Lahore, Pakistan. Atmos Environ 44:1062–1070. doi: 10.1016/J.ATMOSENV.2009.12.015

Suoranta T, Bokhari SNH, Meisel T, et al (2016) Elimination of Interferences in the Determination of Palladium, Platinum and Rhodium Mass Fractions in Moss Samples using ICP-MS/MS. Geostand Geoanalytical Res 40:559–569. doi: 10.1111/ggr.12116

Symonds RB, Reed MH (1993) Calculation of multicomponent chemical equilibria in gas-solid- liquid systems: calculation methods, thermochemical data, and applications to studies of high-temperature volcanic gases with examples from Mount St. Helens. Am J Sci. doi: 10.2475/ajs.293.8.758

Taiwo AM, Harrison RM, Shi Z (2014) A review of receptor modelling of industrially emitted particulate matter. Atmos. Environ. 97:109–120

Tanner SD, Baranov VI, Bandura DR (2002) Reaction cells and collision cells for ICP-MS: a tutorial review

Tasoglou A, Pandis SN (2015) Formation and chemical aging of secondary organic aerosol during the β-caryophyllene oxidation. Atmos Chem Phys 15:6035–6046. doi: 10.5194/acp-15-6035-2015

Tobias DE, Perlinger JA, Morrow PS, et al (2007) Direct thermal desorption of semivolatile organic compounds from diffusion denuders and gas chromatographic analysis for trace concentration measurement. J Chromatogr A 1140:1–12. doi: 10.1016/J.CHROMA.2006.11.045

Trua T, Serri G, Marani M, et al (2002) Volcanological and petrological evolution of Marsili Seamount (southern Tyrrhenian Sea). J Volcanol Geotherm Res 114:441–464. doi: 10.1016/S0377-0273(01)00300-6

Tsigaridis K, Kanakidou M (2003) Global modelling of secondary organic aerosol in the troposphere: A sensitivity analysis. Atmos Chem Phys 3:1849–1869. doi: 10.5194/acp-3-1849-2003

Tsimpidi AP, Karydis VA, Pandis SN, Lelieveld J (2016) Global combustion sources of organic aerosols: model comparison with 84 AMS factor-analysis data sets. Atmos

Chem Phys 16:8939–8962. doi: 10.5194/acp-16-8939-2016

Turpin BJ, Huntzicker JJ (1995) Identification of secondary organic aerosol episodes and quantitation of primary and secondary organic aerosol concentrations during SCAQS. Atmos Environ 29:3527–3544. doi: 10.1016/1352-2310(94)00276-Q

Turpin BJ, Huntzicker JJ, Hering S V. (1994) Investigation of organic aerosol sampling artifacts in the los angeles basin. Atmos Environ 28:3061–3071. doi: 10.1016/1352-2310(94)00133-6

Turpin BJ, Lim H-J (2001) Aerosol Science & Technology Species Contributions to PM2.5 Mass Concentrations: Revisiting Common Assumptions for Estimating Organic Mass Species Contributions to PM2.5 Mass Concentrations: Revisiting Common Assumptions for Estimating Organic Mass. Aerosol Sci Technol 35:602–610. doi: 10.1080/02786820119445

Tyler G (2001) ICP-OES , ICP-MS and AAS Techniques Compared. ICP Opt Spectrosc 1–11

US EPA, OAR O of AQP and S SPECIATE

US EPA, ORD N Air Research Grants

VanCuren R (Tony), Gustin MS (2015) Identification of sources contributing to PM2.5 and ozone at elevated sites in the western U.S. by receptor analysis: Lassen Volcanic National Park, California, and Great Basin National Park, Nevada. Sci Total Environ 530–531:505–518. doi: 10.1016/J.SCITOTENV.2015.03.091

Vezzoli (1988) Island of Ischia. Quad La Ric Sci

Viana M, Amato F, Alastuey A, et al (2009) Chemical Tracers of Particulate Emissions from Commercial Shipping. Environ Sci Technol 43:7472–7477. doi: 10.1021/es901558t

Viana M, Kuhlbusch TAJ, Querol X, et al (2008) Source apportionment of particulate matter in Europe: A review of methods and results. J Aerosol Sci 39:827–849. doi: 10.1016/j.jaerosci.2008.05.007

Viana M, Maenhaut W, ten Brink HM, et al (2007) Comparative analysis of organic and elemental carbon concentrations in carbonaceous aerosols in three European cities. Atmos Environ 41:5972–5983. doi: 10.1016/j.atmosenv.2007.03.035

Viana M, Pey J, Querol X, et al (2014) Natural sources of atmospheric aerosols influencing air quality across Europe. Sci Total Environ 472:825–833. doi: 10.1016/j.scitotenv.2013.11.140

Volkamer R, San Martini F, Molina LT, et al (2007) A missing sink for gas-phase glyoxal in Mexico City: Formation of secondary organic aerosol. Geophys Res Lett 34:1–5. doi: 10.1029/2007GL030752

von Glasow R (2010) Atmospheric chemistry in volcanic plumes. Proc Natl Acad Sci 107:6594–6599. doi: 10.1073/pnas.0913164107

Wåhlin P (2003) COPREM - A multivariate receptor model with a physical approach. Atmos Environ 37:4861–4867. doi: 10.1016/j.atmosenv.2003.08.032

Wang C-F, Yang J-Y, Ke C-H (1996) Multi-element analysis of airborne particulate matter

by various spectrometric methods after microwave digestion

Wang D, Hopke PK (1989) The use of constrained least-squares to solve the chemical mass balance problem. Atmos Environ 23:2143–2150. doi: 10.1016/0004-6981(89)90175-3

Wang G, Zhang R, Gomez ME, et al (2016) Persistent sulfate formation from London Fog to Chinese haze. Proc Natl Acad Sci 113:13630–13635. doi: 10.1073/pnas.1616540113

Wang ZB, Hu M, Mogensen D, et al (2013) Atmospheric Chemistry and Physics The simulations of sulfuric acid concentration and new particle formation in an urban atmosphere in China. Atmos Chem Phys 13:11157–11167. doi: 10.5194/acp-13-11157-2013

Washenfelder RA, Attwood AR, Brock CA, et al (2015) Biomass burning dominates brown carbon absorption in the rural southeastern United States. Geophys Res Lett. doi: 10.1002/2014GL062444

Watson JG, Chow JC, Wang XL, et al (2012) Overview of Real-World Emission Characterization Methods. Dev Environ Sci 11:145–170. doi: 10.1016/B978-0-08-097760-7.00007-X

Watson JG, Robinson NF, Lewis C, et al (1997) CHEMICAL MASS BALANCE RECEPTOR MODEL VERSION 8 (CMB8) USER'S MANUAL With assistance from

Watson JG, Zhu T, Chow JC, et al (2002) Receptor modeling application framework for particle source apportionment. In: Chemosphere. Pergamon, pp 1093–1136

Whitby KT, Cantrell B (1976) Atmospheric aerosols- Characteristics and measurement. In: International Conference on Environmental Sensing and Assessment, Las Vegas, Nev

WHO (2016) WHO | Mortality and burden of disease from ambient air pollution

Williams BJ, Goldstein AH, Kreisberg NM, Hering S V. (2006) An In-Situ Instrument for Speciated Organic Composition of Atmospheric Aerosols: T hermal Desorption A erosol G C/MS-FID (TAG). Aerosol Sci Technol 40:627–638. doi: 10.1080/02786820600754631

Worton DR, Goldstein AH, Farmer DK, et al (2011) Origins and composition of fine atmospheric carbonaceous aerosol in the Sierra Nevada Mountains, California. Atmos Chem Phys 11:10219–10241. doi: 10.5194/acp-11-10219-2011

Worton DR, Kreisberg NM, Isaacman G, et al (2012) Thermal desorption comprehensive two-dimensional gas chromatography: An improved instrument for in-situ speciated measurements of organic aerosols. Aerosol Sci Technol 46:380–393. doi: 10.1080/02786826.2011.634452

Wu C, Yu JZ (2016) Determination of primary combustion source organic carbon-to-elemental carbon (OC / EC) ratio using ambient OC and EC measurements: Secondary OC-EC correlation minimization method. Atmos Chem Phys 16:5453–5465. doi: 10.5194/acp-16-5453-2016

Xiao ZM, Zhang YF, Hong SM, et al (2011) Estimation of the main factors influencing haze, based on a long-term monitoring campaign in Hangzhou, China. Aerosol Air

Qual Res 11:873–882. doi: 10.4209/aaqr.2011.04.0052

Xu J, Wang Q, Deng C, et al (2017) Insights into the characteristics and sources of primary and secondary organic carbon: High time resolution observation in urban Shanghai. Environ Pollut 2:1–11. doi: 10.1016/j.envpol.2017.10.003

Yassaa N, Peeken I, Zllner E, et al (2008) Evidence for marine production of monoterpenes. Environ Chem 5:391–401. doi: 10.1071/EN08047

Yatkin S, Gerboles M, Borowiak A (2012) Evaluation of standardless EDXRF analysis for the determination of elements on PM10loaded filters. Atmos Environ 54:568–582. doi: 10.1016/j.atmosenv.2012.02.062

Yu J, Cocker Iii DR, Griffin RJ, et al (1999) Gas-Phase Ozone Oxidation of Monoterpenes: Gaseous and Particulate Products

Yu S (2000) Role of organic acids (formic, acetic, pyruvic and oxalic) in the formation of cloud condensation nuclei (CCN): a review. Atmos Res 53:185–217. doi: 10.1016/S0169-8095(00)00037-5

Zeng Y, Hopke PK (1989) A study of the sources of acid precipitation in Ontario, Canada. Atmos Environ 23:1499–1509. doi: 10.1016/0004-6981(89)90409-5

Zhang Q, Jimenez JL, Canagaratna MR, et al (2007) Ubiquity and dominance of oxygenated species in organic aerosols in anthropogenically-influenced Northern Hemisphere midlatitudes. Geophys Res Lett 34:1–6. doi: 10.1029/2007GL029979

Zhang Q, Jimenez JL, Canagaratna MR, et al (2011) Understanding atmospheric organic aerosols via factor analysis of aerosol mass spectrometry: a review. Anal Bioanal Chem 401:3045–3067. doi: 10.1007/s00216-011-5355-y

Zhang Y, Seigneur C, Seinfeld JH, et al (2000) A comparative review of inorganic aerosol thermodynamic equilibrium modules: Similarities, differences, and their likely causes. Atmos Environ. doi: 10.1016/S1352-2310(99)00236-8

Zhu Y, Hinds WC, Kim S, et al (2002) Study of ultrafine particles near a major highway with heavy-duty diesel traffic. Atmos Environ 36:4323–4335. doi: 10.1016/S1352-2310(02)00354-0

Annex 1 List of Abbreviations

AAS	Atomic Absorption Spectroscopy
AES	Atomic Emission Spectroscopy
BC	Black Carbon
BrC	Brown Carbon
BSC-DREAM	Dust Regional Atmospheric Model
bVOC	Biogenic Volatile Organic Compounds
CMB	Chemical Mass Balance
COPD	Chronic Obstructive Pulmonary Disease
CWT	Concentration Weighted Trajectory
Dp	Particles diameter
eBC	Equivalent Black Carbon
EC	Elemental Carbon
EDXRF	Energy Dispersive X-ray Fluorescence
EF	Enrichment Factor
EPA	American Environmental Protection Agency
FA	Factor Analysis
GAW	Global Atmosphere Watch
GC	Gas Chromatography
HYSPLIT	Hybrid single-particle Lagrangian integrated trajectory model
IC	Ion Chromatography
ICP	Inductively Coupled Plasma
MAAP	Multi-Angle Absorption Photometer
MAE	Microwave-assisted extraction
MBL	Marine Boundary Layer
MS	Mass Spectroscopy
NAAPS	Navy Aerosol Analysis and Prediction System
NCEP	National Centers for Environmental Prediction
NIOSH	US National Institute for Occupational Safety and Health
OA	Organic Aerosol
OC	Organic Carbon
PAH	Polycyclic Aromatic Hydrocarbons

PBL	Planetary Boundary Layer
PCA	Principal Component Analysis
PM	Particulate Matter
PMF	Positive Matrix Factorization
POA	Primary Organic Aerosol
POC	Primary Organic Carbon
PSCF	Potential source contribution function
RM	Receptor Model
RTA	Residence Time Analysis
RTWC	Residence time-weighted concentration
SIA	Secondary Inorganic Aerosol
SOA	Secondary Organic Aerosol
SOC	Secondary Organic Carbon
TEOM	Tapered Element Oscillating Microbalance
TOT	Thermal Optical Transmittance
TSP	Total Suspended Particulate matter
VOC	Volatile Organic Compounds
WHO	World Health Organization

Annex 2 Supplementary Images

a)

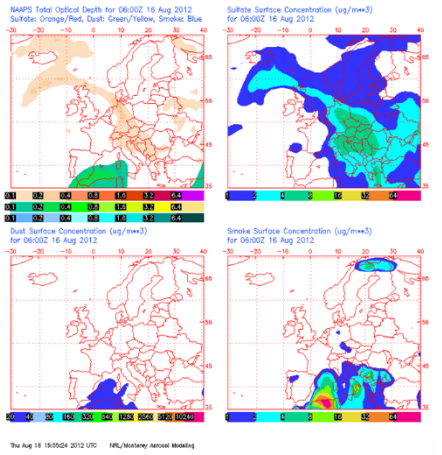

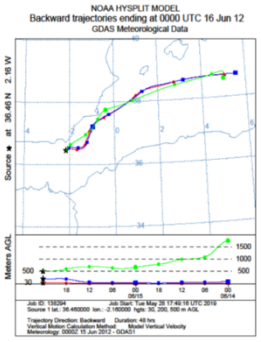

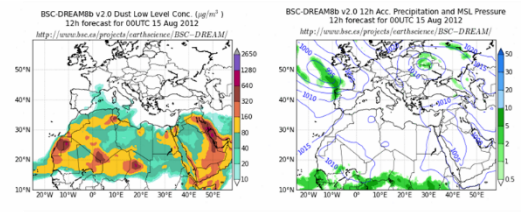

b)

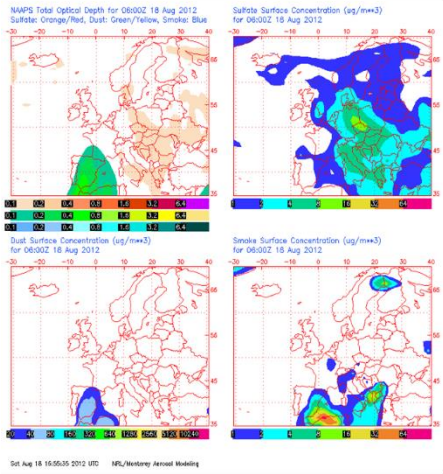

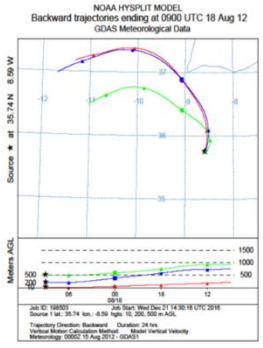

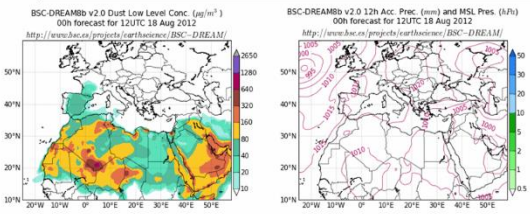

c)

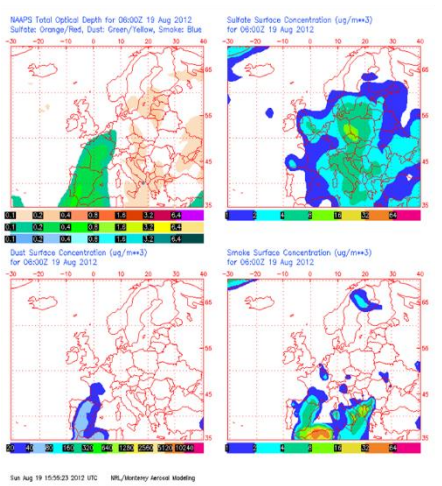

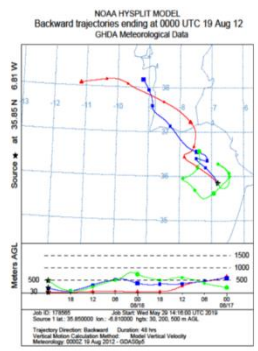

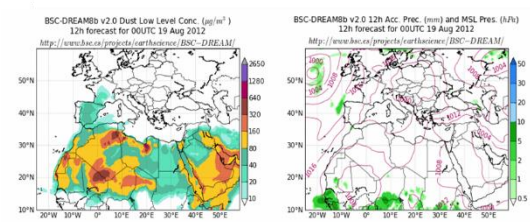

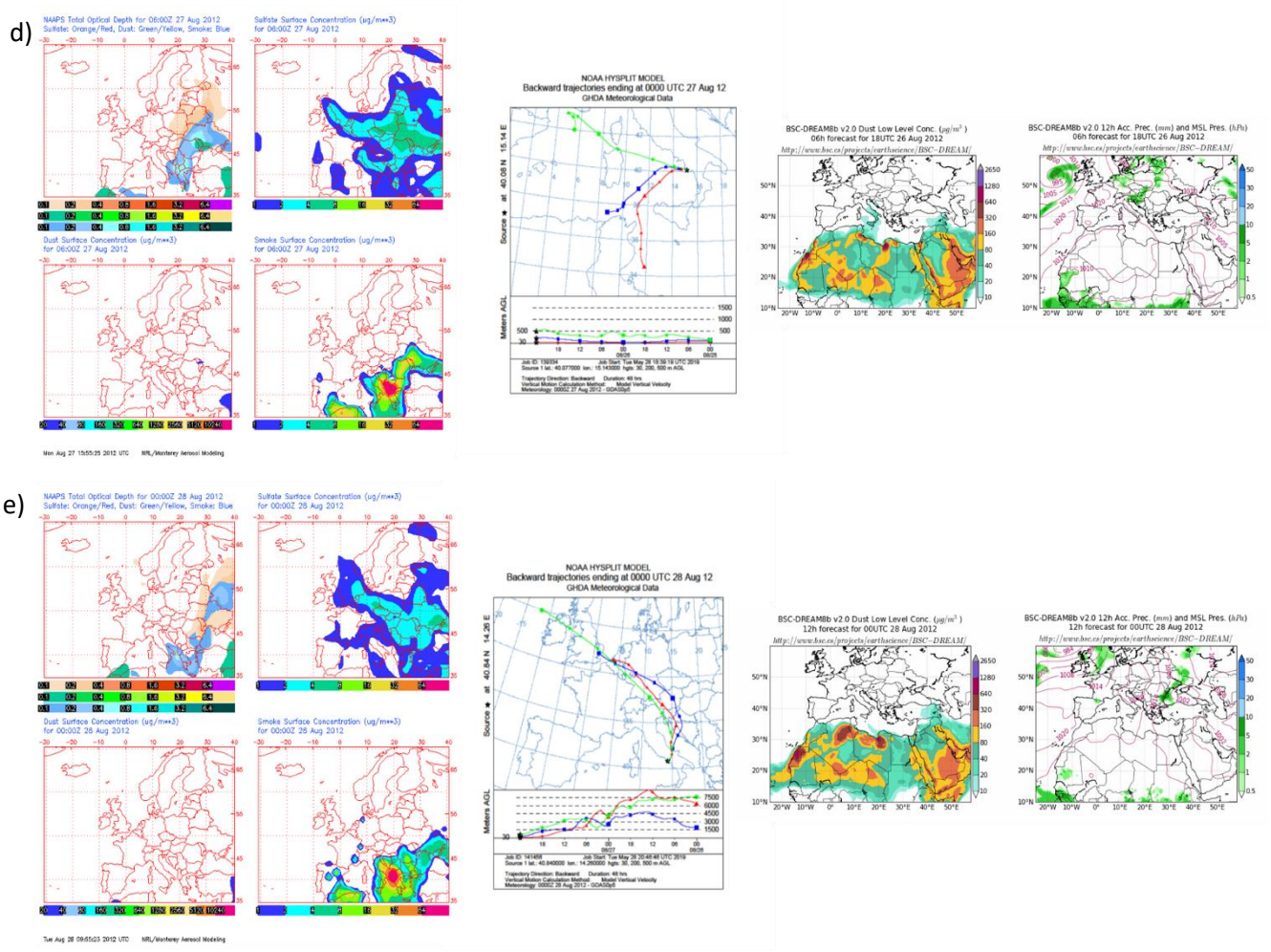

Fig. S1 NAAPS, BSC-DREAM and back trajectory maps for Fenice 2012 campaign:
a) 16 August (12s3); b) 18 August (12s5); c) 19 August (12s6); d) 27 August (12s14); e) 28 August (12s15).

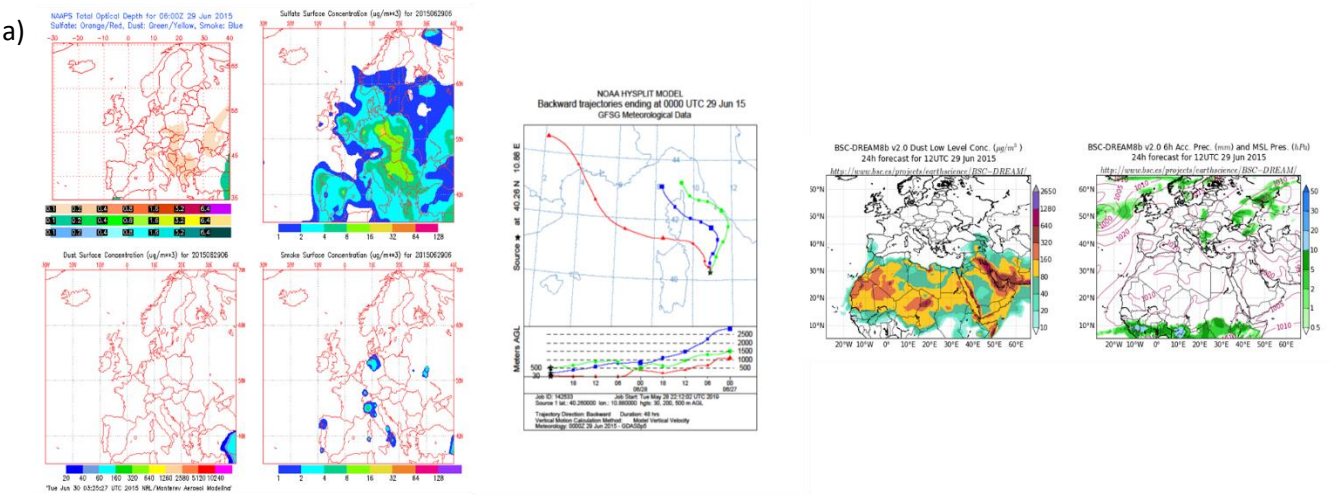

b)

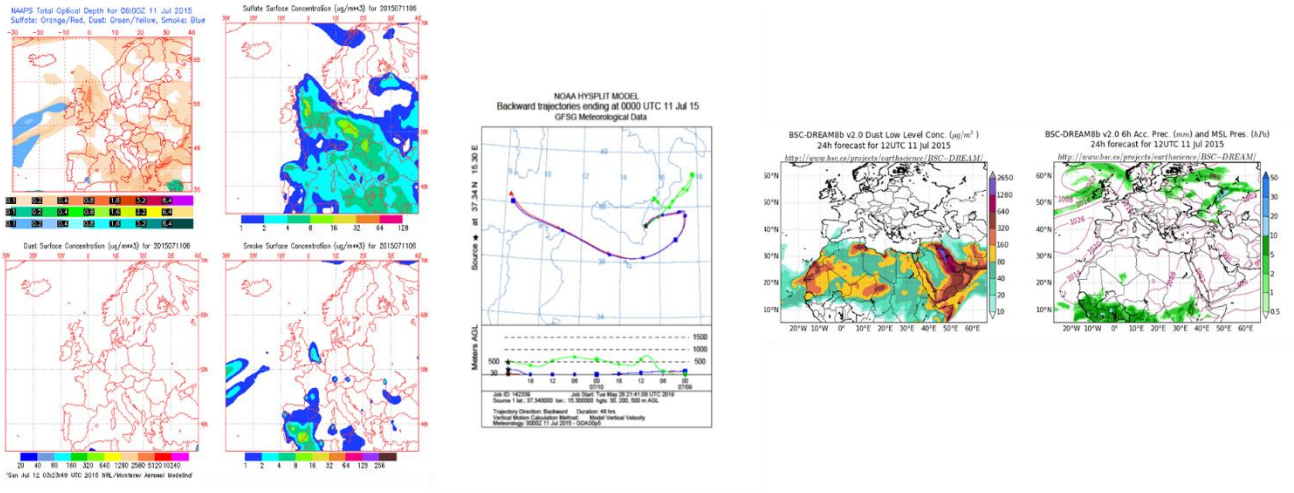

Fig. S2 NAAPS, BSC-DREAM and back trajectory maps for Minerva 2015 campaign: a) 29 June (15s2); b) 11 July (15s14)

Annex 3 List of publications, Conference proceedings of Sacha Moretti

Pubblications:

1. Adelaide Dinoi, Daniela Cesari, Angela Marinoni, Paolo Bonasoni, Angelo Riccio, Elena Chianese, Giuseppina Tirimberio, Attilio Naccarato, Francesca Sprovieri, Virginia Andreoli, Sacha Moretti, Daniel Gullì, Claudia R. Calidonna, Ivano Ammoscato and Daniele Contini ***"Inter-Comparison of Carbon Content in PM2.5 and PM10 Collected at Five Measurement Sites in Southern Italy"***. Atmosphere (**2017)**, 8, 243; DOI:10.3390/atmos8120243
2. Mariantonia Bencardino, Virginia Andreoli, Jessica Castagna, Francesco D'Amore, Valentino Mannarino, Sacha Moretti, Attilio Naccarato, Nicola Pirrone, and Francesca Sprovieri "***Airborne Particles during a Firework Festival in Belvedere M.mo, South-Western Italian Coast"***. Open Journal of Air Pollution (**2018**), 7, 156-180; DOI: 10.4236/ojap.2018.72009
3. Sacha Moretti, Apostolos Salmatonidis, Xavier Querol, Antonella Tassone, Virginia Andreoli, Mariantonia Bencardino, Nicola Pirrone, Francesca Sprovieri, Attilio Naccarato ***"Contribution of volcanic and fumarolic emission to the marine aerosol in the western Mediterranean Sea: results from Med-Oceanor 2017 cruise campaign"***. *in preparation.*

Conference Proceedings:

- Mariantonia Bencardino, Virginia Andreoli, Jessica Castagna, Francesco D'Amore, Valentino Mannarino, Moretti Sacha, Naccarato Attilio, Tassone Antonella, Sprovieri Francesca, Pirrone Nicola. **"*Seasonal patterns of Saharan dust detected over the central Mediterranean basin, at the high-altitude Monte Curcio GAW station*".** Conference Proceeding "3rd International Conference on Atmospheric Dust - DUST2018", **Bari, 29-31 May 2018**, ProScience, Vol. 5 (2018) 1-5, 10.14644/dust.2018.00
- Jessica Castagna, Mariantonia Bencardino, Marcella Capua, Francesco D'Amore, Giulio Esposito, Valentino Mannarino, Sacha Moretti, Attilio Naccarato, Jheny Orbe, Antonella Tassone, Francesca Sprovieri, Nicola Pirrone. "***The atmospheric impact of volcanic activities in the Mediterranean Sea investigated during a measurements cruise campaign***". Conference Proceeding "3rd International Conference on Atmospheric Dust - DUST2018", **Bari, 29-31 May 2018**, ProScience, Vol. 5 (2018) 13-18, 10.14644/dust.2018.003
- Attilio Naccarato, Jessica Castagna, Sacha Moretti, Mariantonia Bencardino, Francesco Carbone, Francesco D'Amore, Maria Martino, Antonella Tassone, Nicola Pirrone, Francesca Sprovieri, "***Investigation of particulate matter collected during three cruise campaigns in the Mediterranean Sea: composition and source***

apportionment". Convegno nazionale sul Particolato atmosferico "PM2018", **Matera, 23-25 May 2018**, pp. P20

- Jessica Castagna, Mariantonia Bencardino, Francesco Carbone, Attilio Naccarato, Valentino Mannarino, Sacha Moretti, Francesco D'Amore, Francesca Sprovieri, Nicola Pirrone, "***Caratterizzazione del particolato atmosferico rilevato nel corso di 10 campagne di misura off-shore nel Mar Meditteraneo***". "VII Convegno nazionale sul Particolato atmosferico", **Rome, 17-20 May 2016**; P33.
- Jessica Castagna, Francesco Carbone, Attilio Naccarato, Sacha Moretti, Giulio Esposito, Mariantonia Bencardino, Francesco D'Amore, Francesca Sprovieri, and Nicola Pirrone "***Variability of fine and coarse aerosol over the Western Mediterranean Basin during the Minerva 2015 research cruise campaign***". "European Geosciences Union 2016", **Wien, 17-22 April 2016**. (2016EGUGA..18.4022C)

Acknowledgments

First of all, I would like to thank my supervisors, Dr. Francesca Sprovieri and Dr. Attilio Naccarato for having supported and encouraged me during the PhD program.

I would like to thank the whole group of people working with me at CNR-IIA and everybody who have shared moments of laughs and chats about research topic and not only.

It is pleasure to thank those who revised my thesis, Dr. Mar Viana and Prof. Ugo Cosentini for the scientific revision and helpful comments to improve my thesis.

I owe my deepest gratitude to all the people that have been involved in my PhD during these three years: Professor Xavier Querol, for the opportunity to work with him for short period but intense and for helpful discussions. Moreover, I want like to thank the group of PhD and researcher of CSIC-IDAEA for the reception given to me and the time spent together.

Most of all, I would like to thank my parents, my sister, Noemi and all my friends. A special thank for Simona, who supported me in different ways during the whole doctoral course and in particular during writing of the thesis.